INVESTIGATING THE ROLE OF A NOVEL NUCLEAR ESCRT-III ASSEMBLY

by

Alexa Cleasby

A thesis submitted to the University of Sheffield as partial fulfilment of the requirements for the degree of Doctor of Philosophy

January 2014

Department of Chemistry (Chemical biology)

DECLARATION

The work described in this thesis was undertaken between the University of Sheffield and the University of Manchester between January 2010 and September 2013 under the supervision of Dr. B. Ciani and Prof. P. Woodman. Unless stated, all work was conducted by the author and has not been submitted, in whole or part, for any other degree at this or any other institution.

September 2013

A. Cleasby

Dept. of Chemistry,
Dainton Building,
Brook Hill,
Sheffield,
S3 7HF.

Dept. of Life Sciences,
Michael Smith Building,
Oxford Road,
Manchester,
M13 9PL.

ACKNOWLEDGMENTS

Everybody is so talented nowadays that the only people I care to honour as deserving real distinction are those who remain in obscurity.

-Thomas Hardy

Many people deserve thanks for their contribution to this project. First and foremost I'd like to thank my supervisor, Dr. Barbara Ciani, for all her enthusiasm, support and guidance throughout this project and especially during these last few months of thesis writing. I am very grateful for the coffee breaks and dog-walking therapy as well.

A huge thank you is owed to Prof. Philip Woodman at the University of Manchester, not only for letting me work in his lab and treating me like one of this own students, but also for sharing his lab bench with me and accepting my constant tidying of it. His willingness to give up his time for discussions and critiques of this research was also very much appreciated. I extend my thanks to everyone, past and present, in the Woodman group for all their help. Especially deserving of those thanks is Dr. Flavia Stefani for generously teaching me all the cell biology I know and turning me into a biologist that does a bit of chemistry rather than the other way around. Thank you to Louise Walker for always having cells waiting for me whenever I told her I'd be coming to Manchester and to Mrs Sandra Taylor for being a brilliant technician. Thank you to Dr. Vicki Jones for her assistance with the CHMP4B-myc cell line and for the kind gift of the water fleas, who sadly passed away this year (RIP). The lab was shared with Prof. Viki Allan and her group; I thank them all also for their help and kindness. I'd also like to thank Mrs Jane Kotts for her training and assistance on the Deltavision microscope. Lastly from Manchester, I thank Dr. Tamara Griffiths and Dr. Sean Woodall for giving me a place to sleep when the hours were long and for many Thai lunch dates.

Back in my home turf of Sheffield, I'd like to thank Dr. Jim Reid for his useful insights and thoughts on this work, as well as for his supervision during my master's year, which allowed me to realise my interest in biological chemistry. Thanks also go to members of his group; Dr. Ruth Davidson, who started my training in biochemistry back in my

undergrad days and also to Dr. Nate Adams for his assistance and useful ideas throughout my PhD, especially for his help with my fluorescence quenching assays. I'd also like to thank Dr. Helen Bryant for useful discussions concerning cell biology and ESCRT proteins in DNA damage.

A big thank you to everyone, past and present, from E floor for all their humour, support and friendship over the years, especially all the people in E81. I particularly thank Dr. Dave Finger from E floor for being a wealth of knowledge, better than any text book. I include each year's intake of master's students in my thanks for letting me teach them biology and in doing so allowing me to improve as a scientist.

Thank you to all my non-scientists friends, who despite not really understanding what I do, have listened, cared, celebrated and commiserated with me over the years; especially Alex, Anna, Izzy, Lara S, Laura and Martha who have been calling me a doctor since my PhD began. I'm also thanking Lara J here, because although she's a scientist, primarily she's been an excellent housemate and friend.

I also need to thank Dr. Ian Cleasby, not only for being a supportive big brother, but also for his help in proof reading this thesis and helping me understand the complex world of statistics.

Matthew Jackson, deserves a massive thank you for being a rock both at work and at home, spending hours retrieving lost work for me, feeding me whilst I was writing and generally making life better.

Finally, I'd like to take this opportunity to thank my parents, Ed and Karen, for supporting a second child through seven years of university education. They always pick up the phone when I call and they've listened to every high and low of the last three and half years, including letting me explain my project and new data to them countless times determined that they would eventually understand it. Thank you for everything!

ABSTRACT

The ESCRT machinery plays a critical role in many cellular processes involving membrane remodelling, such as multivesicular body formation, virus budding and cytokinesis. The mammalian ESCRT-III complex is made up of 11 proteins called CHMPs (Chromatin-modifying proteins), given that they were discovered associated with condensed chromatin. Depletion of individual ESCRT-III or VPS4 results in mitotic and nuclear defects indicating functions in nuclear morphology maintenance, chromosome alignment and cell cycle progression.

This thesis outlines experiments that revealed the presence of a novel nuclear ESCRT-III assembly dependent upon ESCRT-III subunit CHMP7.

CHMP7 is a largely uncharacterised ESCRT-III member, which is double the length of other CHMP proteins and contains an N-terminus domain of unknown function. *In vitro* pull-down assays show that CHMP7 interacts with VPS4 and LIP5, a positive regulator of VPS4, whereas bioinformatic analysis suggests that the N terminus of CHMP7 contains winged helix domains, generally associated with nucleic acid binding functions. CHMP7 also interacts, *in vitro*, with CHMP1A and CHMP4B. Depletion of VPS4 isoforms reveals that in contrast to other ESCRT-III subunits, CHMP7 localises exclusively to nuclear structures in HeLa M cells. Depletion of VPS4 isoforms freezes CHMP7 on nuclear structures, including CHMP4B and CHMP1B, forming an assembly exclusively dependent upon the presence of CHMP7. Taken together these data suggest that the nuclear CHMPs may form a specific functional complex.

The nuclear ESCRT-III structures localise adjacent to, and sometime within promyelocytic leukaemia (PML) nuclear bodies. PML has functions in DNA damage response, suggesting that CHMP7, 4B and 1B accumulate on chromatin structures. Indeed, CHMP7 and CHMP4B formed filaments connecting lagging chromosomes in control cells, which persisted in cells blocked in cytokinesis by VPS4 isoform depletion. Furthermore, CHMP7 localised to 70% of micronuclei -a defect arising due to the incorrect segregation of chromosomes during mitosis and cytokinesis. Overexpression of the SUMO E2 ligase, UBC9, partially recreated the nuclear phenotype for CHMP7 only, implying UBC9 acts as a nuclear import chaperone for CHMP7. *In vitro* pull-down assays showed a direct interaction between CHMP7 and both UBC9 and SUMO-1, also CHMP7 is predicted to contain a SUMO-interacting motif, but not a sumoylation site. In contrast, CHMP1B and CHMP4B did have predicted sumoylation sites.

In summary, the data presented suggest the existence of a nuclear ESCRT-III assembly that binds chromatin and plays a role in chromosome trafficking during cell division.

TABLE OF CONTENTS

LIST OF FIGURES AND TABLES

CHAPTER 1

CHAPTER 2

CHAPTER 3

CHAPTER 4

CHAPTER 5

CHAPTER 6

CHAPTER 7

CHAPTER 1 INTRODUCTION

This thesis focuses on a family of mammalian coiled coil proteins known as both chromatin modifying proteins and charged multivesicular body proteins (CHMPs). As the former name suggests these proteins have been implicated in nuclear functions, such as transcriptional regulation and nuclear signalling. Arguably, they are better known by their latter name as the majority of work in the surrounding literature covers their role in endocytosis and the multivesicular body (MVB) sorting pathway. CHMPs form the final complex in the endosomal sorting complexes required for transport (ESCRT) machinery (known as ESCRT-III).

1.1 The endosomal sorting complexes required for transport (ESCRT) machinery

The ESCRT machinery is an evolutionary conserved group of proteins that play vital roles in trafficking and membrane scission events, where fission occurs away from the cytoplasm. For example, the ESCRTs function in the MVB pathway, the final stages of cytokinesis and virus release in viral budding (figure 1)[1].

The machinery is comprised of four functionally distinct complexes; ESCRT-0, ESCRT-I, ESCRT-II and ESCRT-III[2]. Many of the proteins that form these complexes have been identified in yeast as class-E vacuolar protein-sorting (VPS) proteins, whereby defects cause aberrations in the endosome and block the MVB pathway.

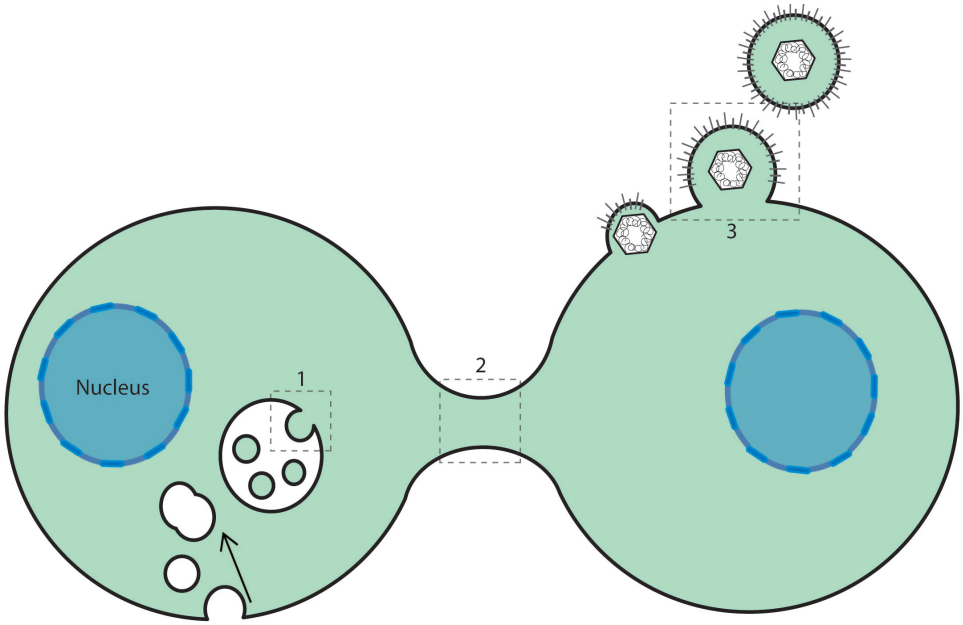

Figure 1 Established fission roles of the ESCRT complexes. The MVB pathway (1) is not the only role the ESCRT machinery is involved in. The machinery functions in other comparable membrane fission events, such as the final stages of cytokinesis (2) and viral budding (3).

ESCRT proteins are encoded from a highly conserved set of genes in eukarya. Some ESCRT-III members are also found in archea, where their membrane remodelling function is conserved[3,4]. For each ESCRT gene in yeast there often corresponds more than one mammalian homolog, reflecting a higher level of complexity in the mammalian system. For example, humans express three CHMP4 isoforms corresponding to one equivalent in yeast called SNF7. In total humans express 12 known CHMP proteins that comprise the ESCRT-III complex and these proteins fall into 1 of 8 groups termed CHMP1-7 and increased sodium tolerance 1 (IST1). CHMPs each correspond to equivalent proteins in yeast, except for CHMP7 where no homolog exists. In order to discuss CHMP proteins further, the preceding three ESCRT complexes and their role in the MVB pathway will first be introduced.

1.1.1 The MVB sorting pathway

The ESCRT machinery has largely been studied in relation to the function of the MVB pathway in endocytosis. During endocytosis, early endosomes undergo a maturation process into MVB's, whereby parts of the limiting

membrane form invaginations that separate off into the lumen of the endosome[5].

These vesicles are known as intraluminal vesicles (ILVs) and contain protein cargo selected for degradation. The early endosome can be viewed as a sorting platform, organising the selection of cargo for degradation and allowing reusable material to be recycled (figure 2). It is this organisation and selection of cargo that the early ESCRT machinery (ESCRT-0, I and II) aid in. Late ESCRT machinery (ESCRT-III and VPS4) is involved with the membrane deformation, remodelling and abscission concerned with the formation of cargo filled ILVs, i.e. MVB biogenesis[6].

The maturation of the early endosome to the late endosome or 'multivesicular body (MVB)' is preceded by the generation of a Rab7 domain. Rab GTPases function in membrane trafficking and membrane fusion. Rab7 is recruited

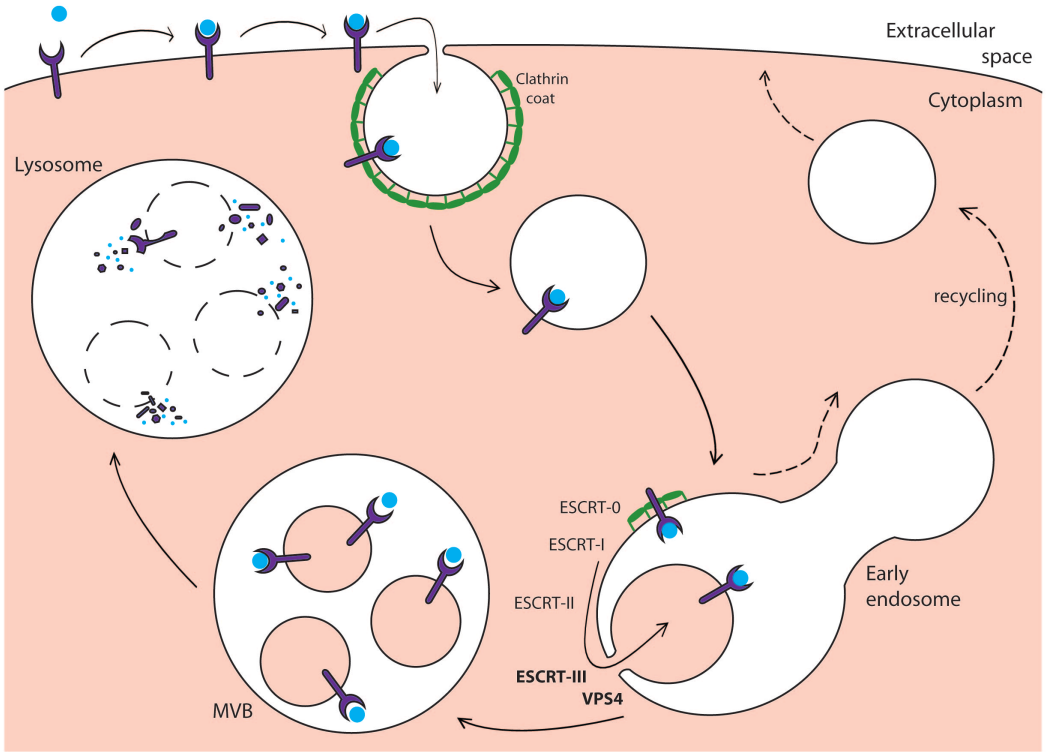

Figure 2 Brief outline of endocytic internalisation and sorting. Various membrane proteins (purple) and their ligands (blue) are internalised by endocytosis and translocated to the early endosome. Cargo is sorted for recycling or degradation resulting in the accumulation of ILVs in the lumen of the endosome. The matured endosome is known as a multivesicular body (MVB) or 'late endosome'. This MVB can then fuse with the lysosome for degradation.

to the early endosome by Rab5-GTP, which is in turn converted to the GDP-bound form. This conversion allows Rab7 to displace Rab5 and is referred to as a 'Rab switch'. The early endosome progresses through this Rab5/Rab7 hybrid state before becoming an MVB. The different composition of Rab proteins in the endosomal membrane dictates which effector proteins are recruited and couples each stage of membrane traffic[7].

Selective degradation of targeted proteins, receptors and cytoplasmic material is a method of quality control and regulation adopted by the cell. Growth factors, for example bind to their receptor on the cell surface initiating intracellular signalling. This signalling eventually requires signal termination, which is achieved by endocytosis of the activated receptor. Endocytosis allows the cell to maintain and alter its cell surface protein composition[8].

Endocytosis is an extremely important function of the cell that regulates many processes such as; receptor signalling, down-regulation, neurotransmission and cell growth and differentiation amongst others[2]. Endocytosed material is

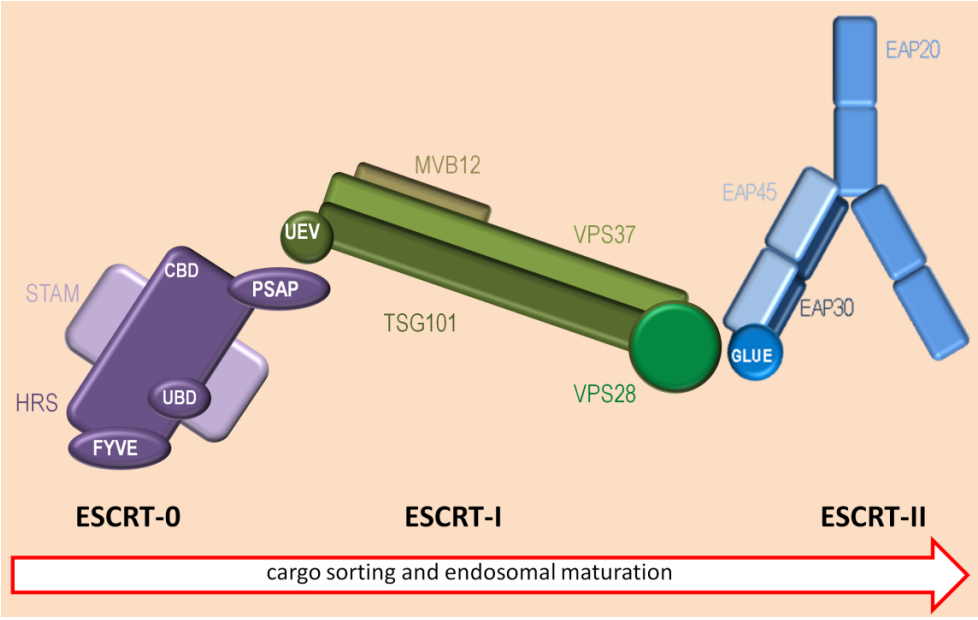

Figure 3 Molecular interactions of the early ESCRT machinery. Scheme outlining interactions of early ESCRT machinery on the endosomal membrane, and indicating the direction of cargo handover: ESCRT-0 to ESCRT-I via a PSAP-UEV interaction; ESCRT-I to ESCRT-II *via* VPS28 and the GLUE domain of EAP45 with both ESCRT-0 and ESCRT-II interacting with membrane lipids. ESCRT-II recruits (and potentially activates) myristolyated CHMP6. ESCRT-III and VPS4 are considered as 'late ESCRT machinery'.

internalised into clathrin coated pits that bud into the cytoplasm forming vesicles that are delivered to and fuse with the endosome. At this stage the MVB 'sorting' by the ESCRT machinery can begin. A ubiquitin tag acts as a molecular signal for lysosomal degradation allowing ESCRT components to recognise the appropriate cargo. This system of cell maintenance is absolutely essential to the cell, as otherwise proteins can build up to detrimental effect, potentially having such far reaching effects as neurodegenerative diseases and certain types of cancer[6].

During MVB sorting it is proposed the ESCRT complexes are recruited sequentially to the site of budding on the endosomal membrane, through both lipid and protein interactions with varying affinity and specificity (figure 3).

1.1.2 The ESCRT-0 complex

ESCRT-0 is made up of two subunits; hepatocyte *g*rowth factor (HGF)–regulated Tyr-kinase substrate known as HRS and, signal transducing acceptor molecule or STAM (figure 4).

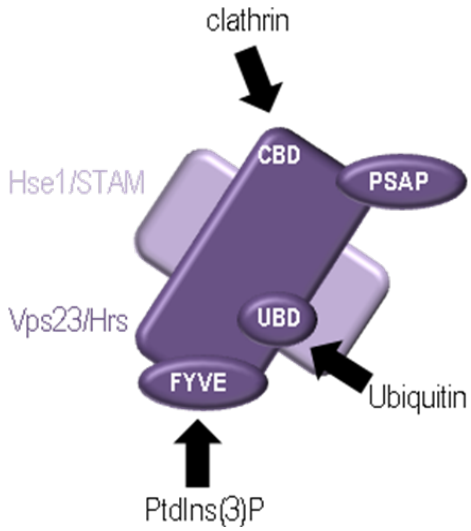

Figure 4 ESCRT-0 complex. Diagram showing the two subunits of ESCRT-0 and their main proposed binding sites. These include: Clathrin binding domain (CBD), ubiquitin binding domain (UBD), zinc finger domain (FYVE) and a PSAP-like motif (i.e. proline, serine, alanine and proline) , which is the site of ESCRT-0 – ESCRT-I interaction.

The ESCRT-0 complex is recruited to the endosomal membrane through a FYVE zinc-finger domain, which binds to the acidic membrane lipid phosphatidylinositol 3-phosphate (PtdIns(3)P)[6]. It has been proposed that ESCRT-0 is likely to concentrate ubiquitinated cargo on the endosomal membrane[9].

The ESCRT-0 complex contains two ubiquitin binding domains (UBDs) and also contains clathrin-binding domains[2]. Clathrin, a 'coat' protein surrounds endocytosed vesicles and can form a double layered flat coat on the endosomal membrane. Whilst not involved in vesicle formation, clathrin, does act to localise cargo on the membrane in conjunction with HRS[4]. Both HRS and STAM contain other UBD's and so can mediate interactions with the cargo and aid selection[10]. ESCRT-0, therefore, can collect and concentrate the ubiquitinated material in small clathrin-coated domains, ready for capture within ILVs.

ESCRT-0 is the furthest upstream component of the ESCRT machinery and interaction with it determines the fate of material. For example, in the absence of ESCRT-0 cargo is normally recycled rather than entered into the degradative MVB pathway[11].

1.1.3 The ESCRT-I complex

The ESCRT-I complex is comprised of four subunits; tumour susceptibility gene 101 known as TSG101, VPS28, VPS37 (in humans one of four isoforms A-D) and MVB12 (figure 5)[2,6]. Of these, it is TSG101 that interacts with the ESCRT-0 complex, *via* a ubiquitin E2 variant domain (UEV)[11]. Specifically this UEV domain binds to a PSAP-like motif (tetrapeptide motif, i.e. proline-serine-alanine-proline) in ESCRT-0 which allows recruitment of ESCRT-I[12]. The clathrin scaffold ensures ubiquitinated cargo encounters ESCRT-I.

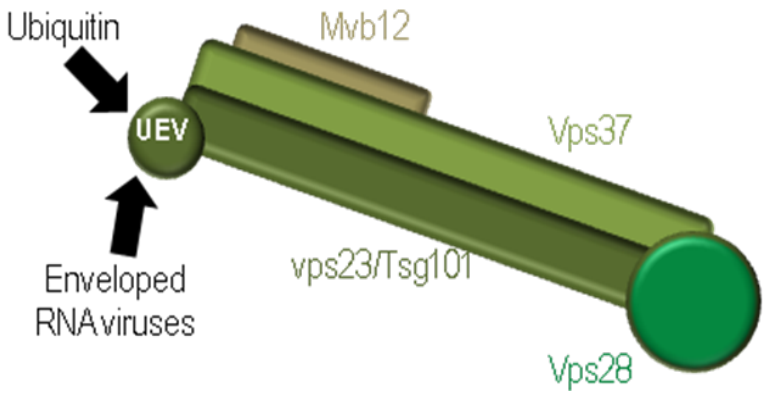

Figure 5 ESCRT-I complex. Diagram showing the four subunits of ESCRT-I; TSG101, Vps37, Vps28 and Mvb12. The ubiquitin E2 variant domain interacts with the PSAP-like motif of ESCRT-0, as well as binding to ubiquitin and various viral proteins of RNA viruses.

TSG101 is able to bind ubiquitinated cargo through its UEV domain, allowing it to displace ESCRT-0. In cells depleted of TSG101 the MVB pathway is severely disrupted, mature MVBs cannot form and in their place appear tube-like enlarged endosomes[13].

In addition TSG101 can interact, *via* the UEV domain, with some viral proteins of enveloped RNA viruses such as HIV and Ebola, thereby engaging ESCRT-I and the remaining downstream ESCRTs in viral budding, a process mechanically similar to the formation of ILVs[14]. This process is independent of ESCRT-0. Evidence has shown that in respect to HIV, TSG101 interacts with a domain of the HIV Gag protein and inhibition of this binding prevents viral budding and release[15].

TSG101 is important in midbody formation during cytokinesis as well through interactions with centrosome associated protein 55kDa (CEP55) a mitotic phospho-protein that localises to the midbody during telophase. ESCRT-III proteins and the ESCRT associated protein, Alg2-interacting protein X (ALIX) are also important here, acting in conjunction with TSG101. It has been suggested that the isoforms present in human CHMPs may reflect specialised functions, such as in midbody abscission[16].

1.1.4 The ESCRT-II complex

The ESCRT-II complex is comprised of three subunits; ELL-associated protein or EAP45, EAP30 and EAP20 in a 1:1:2 ratio respectively (figure 6). Studies in yeast have suggested ESCRT-II is essential to MVB formation by recruiting the ESCRT-III complex[17].

All three subunits of ESCRT-II contain no significant sequence homology with each other; however, they all adopt the same basic structure of two repeats of a winged helix domain[18]. In general, winged helix domains are known for their nucleic acid binding potential. To date, ESCRT-II has been connected to transcriptional regulation through interactions with RNA polymerase II elongation factor ELL[19].

EAP45 contains two zinc finger domains (NZF), where one is believed to bind ubiquitinated cargo and may participate in cargo handover[20].These zinc finger domains are found within a novel domain called GLUE (GRAM-like Ubiquitin binding in EAP45)[21]. The GLUE domain is also able to bind to PtdIns(3)P, although if this can occur at the same time as ubiquitin binding remains unclear. This interaction with PtdIns(3)P is only partially specific as the GLUE

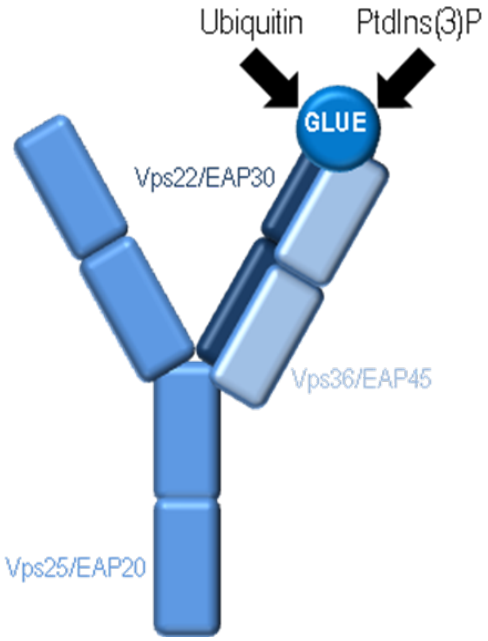

Figure 6 ESCRT-II Complex. Diagram showing composition of the four subunits of ESCRT-II. The GLUE domain of EAP45 binds to ubiquitin and can also interact with the endosomal membrane *via* PtdIns(3)P.

domain can bind to other phosphoinositides as opposed to the FYVE domain of ESCRT-0, which is highly specific for PtdIns(3)P[9]. EAP30 is also known to bind with low specificity to acidic phospholipids, which adds to ESCRT-IIs overall affinity for the membrane and aids membrane targeting[22]. It is assumed that cargo transfer into MVB's is able to occur *via* the sequential recruitment of the complexes themselves and their various affinities for ubiquitin binding. In yeast, VPS25 (EAP20 in mammals) is known to interact with a subunit of ESCRT-III, VPS20 (CHMP6 in mammals). This may be the main component responsible for recruiting ESCRT-III to the concentrated cargo as ESCRT-III is the only ESCRT complex with no UBDs[23].

1.1.5 The ESCRT-III complex

Furthest downstream, ESCRT-III and the VPS4 enzyme complex are the last complexes of the machinery recruited and termed 'late ESCRT machinery'. ESCRT-III plays a key role in the machinery; it is the only ESCRT complex conserved across both eukaryotes and prokaryotes[24]. The complex brings together such factors as upstream ESCRT-I and II and downstream components, such as de-ubiquitinating enzymes and VPS4 to regulate disassembly.

ESCRT-III contains no ubiquitin binding domains, but instead recruits de-ubiquitinating enzymes to remove mono-ubiquitin tags from cargo proteins before their enclosure within ILVs. This allows ubiquitin to be recycled for successive use[25]. The de-ubiquitinating enzymes involved in this process are; associated molecule with the SH3 domain of STAM (AMSH) and Ubiquitin-specific protease Y (UBPY)[23].

The ESCRT-III complex, along with the AAA ATPase, VPS4, is primarily involved in the final stages of membrane deformation and the eventual neck scission.

The ESCRT-III complex differs from the other ESCRT complexes in that it does not exist as a stable heteromeric complex in the cytoplasm, but as

small highly-charged subunits. i.e. CHMPs. CHMPs are transiently recruited to the endosomal membrane where they assemble into a higher order lattice-like structure and form circular filaments. The mechanism and function of this structure is unclear, but may relate to an ability to spatially restrict membrane curve-inducing factors evoking membrane buckling and ultimately budding away from the cytoplasm[6,26].

CHMPs are all approximately 190-240 amino acids in length and whilst they have varied sequences they are characterised by a small acidic region near the C terminal and a basic region at the N terminal, contained within a domain from the sucrose non-fermenting (SNF7) family[27]. This biased arrangement of acidic and basic residues is typical of CHMPs with the basic N terminal being predicted in all CHMPs as an anti-parallel coiled-coiled in the SNF7 domain. A coiled coil is a structural motif containing a heptad repeat, $[abcdefg]_n$, which typically contains hydrophobic residues at positions a and d and polar/charged residues at e and g. It is favourable to bury these hydrophobic residues and due to the pattern of the heptad repeat packing is exceptionally tight[28].

In the cytoplasm, CHMPs are rendered inactive by an autoinhibitory intramolecular interaction caused by the acidic region, at the C terminal, interacting with the basic region[27]. CHMP3 is the only subunit with a resolved crystal structure, which allows it to serve as a model for other CHMPs (figure 7)[29].

The crystal structure of CHMP3 shows a flat helical arrangement with potential sites for CHMP-CHMP interaction in the linker region between helices 1 and 2. This section also contains a large basic region for interaction with acidic lipids in the endosomal membrane. Truncated versions of CHMP3, lacking the acidic 5th alpha helix region, interact readily with the membrane suggesting this represents the active conformation[30]. This agrees with the hypothesis that the acidic C terminal region regulates CHMP activity, by blocking the basic N terminal from interacting with the membrane. This conformation keeps the CHMP subunits inactive in the cytosol until required.

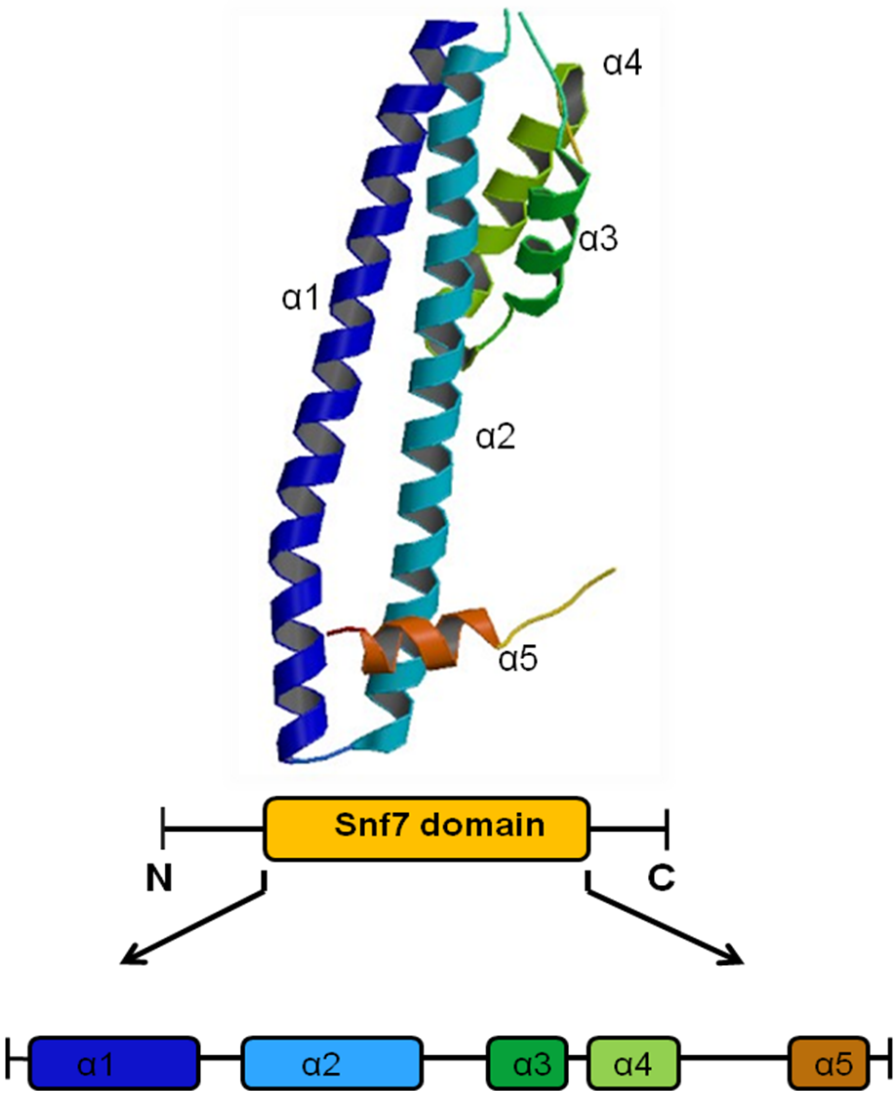

Figure 7 Crystal structure of CHMP3 (PDB 3FRT). Coiled-coil region located at the basic N terminal end spanning the 1st and 2nd alpha helices (blue). Below, scheme representing the helical regions within the SNF7 domain.

In fact, CHMP3s interaction with de-ubiquitinating enzyme, AMSH, has been proposed to be the basis of activation. This would occur by a short motif in the CHMP C terminal region interacting with AMSH *via* a microtubule interacting and trafficking (MIT) domain and thus removing the inhibition[31].

Debate still exists regarding how the CHMPs are activated (figure 8). For example, can a specific CHMP bind to the membrane in its inactive state causing a conformational change, shifting the acidic region and enabling further CHMP-CHMP interactions? Or do they require activation by AMSH and other pre-activated CHMPs in order to bind to the membrane? Another

option being that it may actually be recruitment by EAP20 (of the ESCRT-II complex) that activates these subunits initially through CHMP6[32].

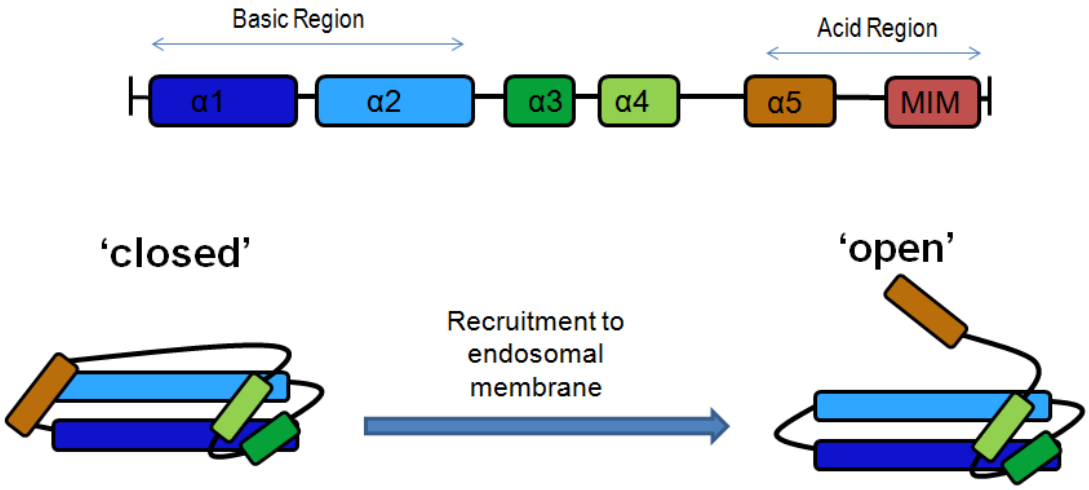

Figure 8 Auto-inhibitory intramolecular reaction. Scheme indicating the basic and acid regions of the SNF7 domain. In the cytoplasm the ESCRT-III monomers exist in an inactive 'closed' conformation. The linker region between helices 1 and 2 is a site of CHMP-CHMP interaction and becomes exposed through interaction with the endosome membrane and some accessory proteins.

The overall stoichiometry of the CHMP lattice formed on the membrane is also unclear, but formed through interactions with acidic lipids in the endosomal membrane and initiated through binding of myristolated CHMP6[32]. Although with CHMP4 being present in the highest physiological concentrations it has been suggested it forms the basis of membrane attached circular filaments, with other CHMPs acting to regulate its polymerisation[33].

CHMP subunits contain a characterised short linear motif known as a MIT interacting motif (MIM) and are able to interact with MIT-containing proteins[30]. The characteristics and binding mode of these MIMs differs between CHMPs and MIT proteins. In fact, Skalicky et al outlined five MIM motifs that mainly differ in how they bind to the MIT domain of the corresponding protein[34]. CHMP1A, 1B, 2A, 2B and 3 all contain a MIM1. This motif is located at the extreme C terminal in a helical region and is characterised by three conserved leucine residues, whereas CHMP4A, 4B, 4C and CHMP6 all contain a MIM2

The MIM2 motif is located slightly upstream of the MIM1 in a flexible random coil region and is characterised by a conserved leucine and two conserved prolines (figure 9). In comparison, CHMP5 contains a novel MIM motif termed MIM5 characterised through its binding to the VPS4 regulator protein, LIP5. It is through these MIM motifs that CHMP proteins bind to the enzyme VPS4 for disassembly, refer to figure 16 for crystal structures showing these different MIT-MIM binding modes[35].

It is also through these MIM motifs that CHMP proteins interact with many accessory proteins, such as de-ubiquitinating enzymes like AMSH and other MIT-containing proteins. For example, CHMP3 interacts with the MIT-domain of AMSH *via* a MIM4 motif that is similar to the MIM1 in sequence, but binds differently. Another example is CHMP1B with interacts with a microtubule-severing enzyme involved in cytokinesis called spastin. This interaction is through a MIM3 motif and is crucial for the correct resolution of midbodies.

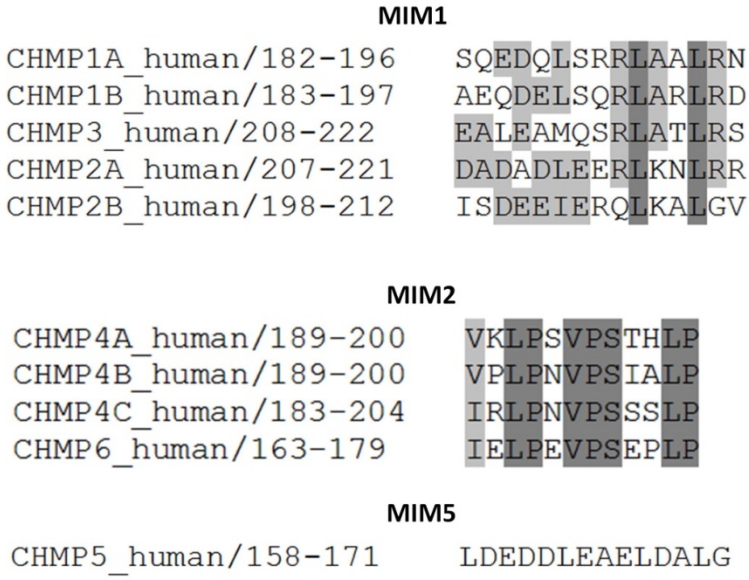

Figure 9 Sequence alignment showing the different motifs CHMP proteins have in order to bind VPS4 and other accessory proteins. CHMP1-3 plus isoforms all contain a MIM1 motif, whereas CHMP4 isoforms and CHMP6 contain a MIM2. CHMP5 contains a novel motif termed MIM5 which is known to bind tightly to a regulator of VPS4, LIP5. To date, no direct interaction has been established between VPS4 and CHMP5, which could imply the MIM5 motif is unable to bind the VPS4 MIT domain. (See section 1.4.1.1. for more about the relationship between CHMP5 and LIP5)

1.1.5.1 Core ESCRT-III complex

In yeast only core ESCRT-III components are essential, with these being the homologs of CHMP6 (VPS20), CHMP4 (SNF7), CHMP3 (VPS24) and CHMP2 (VPS2), assembling in this order. VPS20 is recruited by the ESCRT-II complex, which appears to remove auto-inhibition. VPS20 assembles on the endosome initiating polymerisation of SNF7 filaments. Wollert et al designed a C-terminal truncated VPS20 construct to remove this auto-inhibition. A mixture of truncated VPS20 with the other yeast ESCRT-III subunits was able to generate ILVs in giant unilamellar vesicles (GUVs) in the absence of ESCRT-II[5]. SNF7 filaments are capped by VPS24 and VPS2, with VPS2 being responsible for recruiting VPS4 to recycle the ESCRT subunits[36]. By fluorescently labelling subunits, Wollert et al were also able to demonstrate that VPS4 was not necessary for the actual detachment of newly formed ILVs from the membrane, but only recycling and successive rounds of ILV formation[5]. DID1 and VPS60 (CHMP1 and CHMP5) are dispensable for the generation of ILVs in yeast.

Whilst a more complex process exists in mammals comparisons can be made with the same four core proteins being implicated in humans (CHMP6, 4 isoforms, 3 and 2 isoforms). Figure 10 shows the largely agreed ESCRT-III assembly that leads to ILV formation, but the actual mechanism behind this is still unclear[2,9,25]. No significant concentration of ESCRT components is found inside these vesicles, making it likely that they dissociate from the invaginating membrane before the ILV is released[9]. ESCRT-I and II co-localise at the bud neck and appear to have a stabilising effect, effective at low physiological concentrations (approx 15nM). The recruitment of ESCRT-III subunits CHMP4 and CHMP6 initiates bud formation, at high physiological concentrations (approx 600nM)[5,37]. VPS4 disassembles the CHMP complex by interaction between MIT and MIM domains. MIM1 has a higher affinity for the MIT domain than MIM2 suggesting that MIM1-containing CHMPs be targeted first for disassembly, i.e. CHMP1, 2 and 3. The circular arrays formed by the CHMP subunits, effectively, sequesters the limiting membrane for vesicle formation capturing the attached cargo (cargo largely being membrane receptors and ligands)[38].

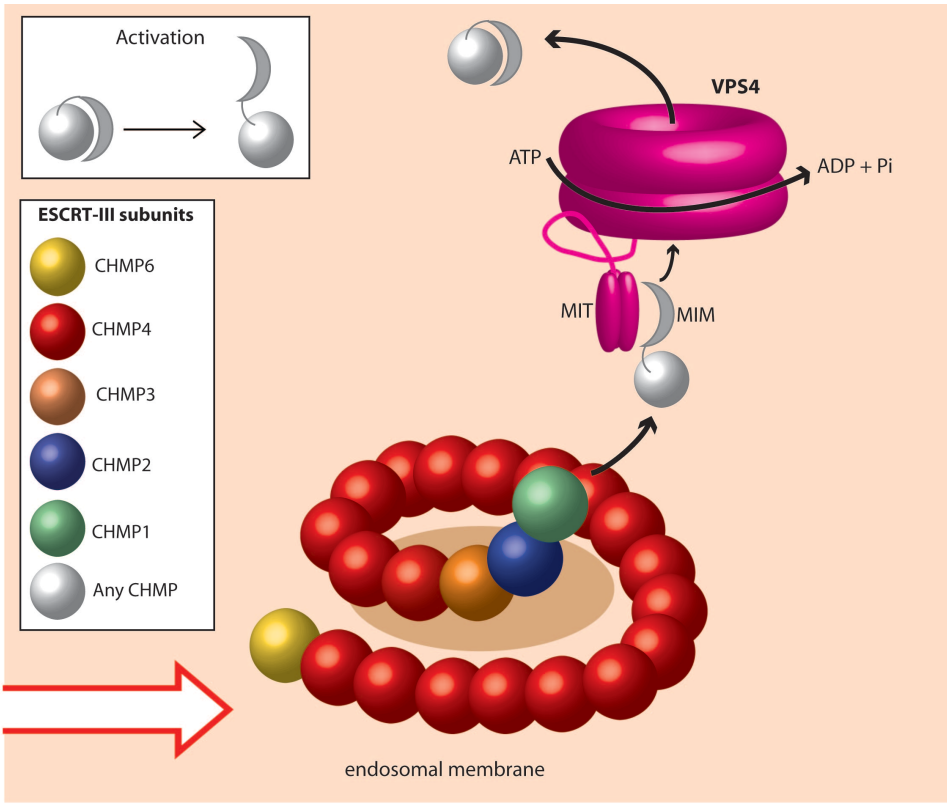

Figure 10 Molecular interactions of late ESCRT Machinery. After ESCRT-II recruits CHMP6, CHMP6 recruits further CHMPs (primarily CHMP4) to the membrane. The basic N terminal region binds to acidic membrane lipids forming circular filaments that induce inward budding. CHMP3 and 2 cap CHMP4 filaments and together with CHMP1 recruit de-ubiquitinating enzymes to remove ubiquitin. VPS4 disassembles the complex, in the presence of ATP, and returns active CHMPs back to the cytoplasm in an inactive state. Some MIM/MITs have been omitted from CHMPs and the VPS4 complex for clarity.

It has been suggested that CHMP3 and CHMP2A can form a sub-complex that acts to cap the oligomerisation of CHMP4 filaments, with Lata et al hypothesising that this CHMP2A-CHMP3 cap acts as the scaffold for the VPS4 to oligomerise and begin disassembly[39,40].The action of disassembly has been proposed as threading (MIT-MIM interaction) followed by the pulling of CHMP subunits through the central pore of oligomerised VPS4, driven by ATP hydrolysis, and released back into the cytoplasm as inactive monomers. This generalised mechanism is similar to how other AAA enzymes function. In theory, this action could draw closed the CHMP scaffold and the membrane to which they are attached thereby causing further membrane deformation and pinching of the vesicle neck[41].

Regulatory ESCRT-III subunits, such as CHMP1 and 5, are still necessary to the cell and their depletion can have serious effects. For example, CHMP1A has been classified as a tumour suppressor gene in pancreatic cancer cell lines[42].

CHMP1 has also been linked with nuclear structures called polycomb group bodies, which function in gene silencing and chromatin remodelling[43]. Deletion of CHMP5 in mice effects receptor down-regulation, leading to early embryonic lethality[44]. CHMP5 is also shown to interact strongly with LIP5 and together they promote assembly and stimulate ATPase activity of VPS4. Moreover, Morita et al found that depletion of all individual CHMP subunits (including CHMP7) caused mitotic defects in cells[45].

These findings suggest a role for ESCRT-III proteins beyond membrane scission roles such as in mitosis, cell cycle progression and tumour development. Referring back to work on CHMP1A, overexpression of this protein strongly increased the protein level of p53 and phosphorylated p53, therefore CHMP1A tumour suppression could occur *via* a p53 signalled pathway[42]. To put this into context, encoded from the gene TP53, mutated p53 is found expressed in over half of human cancers making this protein a common molecular marker for cancer.

The mammalian proteins involved in the ESCRT machinery are outlined in figure 11 alongside their equivalent yeast counterparts. A lot remains uncertain about ESCRT-III interactions and their emerging roles in other aspects of cellular events.

The ESCRT machinery

Complex	Yeast gene	Mammalian gene	Motif	Known binding partners	Role in viral budding?	Role in cyto-kinesis?
ESCRT-III	DID2	CHMP1A CHMP1B	MIM1, CC	AMSH, BMI1 *(1A only)*, CHMP2A, 2B, CHMP4A, 4B, 4C & CHMP5 *(1B only)*, LIP5, IST1, spastin *(1B only)*, UBPY *(1B only)*, VPS4A & B	All involved in viral budding and cytokinesis to varying extents	
	VPS2	CHMP2A CHMP2B		AMSH, CHMP1A, 1B, CHMP3, CHMP4A, 4B, 4C, CHMP5 *(2A only)*, MITD1 *(2A only)*, VPS4A & B		
	VPS24	CHMP3		AMSH, CHMP4A, 4B, 4C, CHMP1B, CHMP2A, STAM, VPS4A & B		
	SNF7	CHMP4A CHMP4B CHMP4C	MIM2, CC	all CHMPs, ALIX *(4B predominantly)* AMSH, Aurora B *(4C only)*, HDPTP, LIP5, UBPY, VPS4A & B		
	VPS60	CHMP5	MIM5, CC	CHMP4A, 4B, CHMP1B, CHMP2A & LIP5		
	VPS20	CHMP6	MIM2, CC	CHMP4A, 4B, 4C, ESCRT-II subunits, VPS28, VPS4A & B	NO	NO
		CHMP7	CC	CHMP4B	YES	?
VPS4	VPS4	VPS4A VPS4B	AAA, MIT, CC, CTH	all CHMPs *(not verified for CHMP5 or 7)*, IST1 & LIP5	YES	YES
ESCRT-0	VPS27	HRS	UBD, FYVE, VHS & PRD	CEP55, clathrin, PtdIns(3)P, TSG101, ubiquitin & VPS37	NO	YES
	HSE1	STAM1, 2	UBD, VHS, SH3	AMSH, ubiquitin, UBPY	NO	?
ESCRT-I	VPS23	TSG101	UEV, CC	ALIX, CEP55, EAP30, HDPTP, HRS, ub & some retroviral proteins	YES	YES
	VPS28	VPS28	CTD	CHMP6, ESCRT-II subunits, TSG101	YES	YES
	VPS37	VPS37A, B, C & D		CEP55, HRS *(37A only)*, MVB12A *(37B only* & TSG101	YES	?
	MVB12	MVB12A, B		TSG101 & VPS37B *(MVB12A only)*	YES	?
ESCRT-II	VPS22	EAP30	WH2	PtdIns(3)P	NO	?
	VPS25	EAP20	WH2	CHMP6	NO	?
	VPS36	EAP45	WH2, GLUE, NZF	PtdIns(3)P, ubiquitin & VPS28	NO	?

Accessory proteins

BRO1	ALIX	BRO1, PRD	AMSH, CEP55, CHMP4, TSG101 & UBPY
	AMSH	MIT	STAM, IST1 & some ESCRT-III subunits
IST1	IST1	MIM1, MIM2	AMSH, LIP5, spastin, VPS4A, VPS4B & UBPY
VTA1	LIP5	MIT1, MIT2, VSL	CHMP5, IST1, VPS4A, B & some other ESCRT-III subunits (MIM1 CHMPs)
DOA1	UBPY	MIT	STAM, IST1 & some ESCRT-III subunits

Figure 11 Table of all ESCRT subunits and their main accessory proteins: In alphabetical order. AAA; ATPase associated with various activity; ALIX, ALG-2 interacting protein X; AMSH, associated molecule with the SH3 domain of STAM; CC, coiled coil; CEP55, centrosomal protein of 55kD; CHMP, charged multivesicular body protein; CTH, C-terminal helix; CTD, C-terminal domain; EAP, ELL-associated protein of X kDa; ESCRT, endosomal sorting complex required for transport; FYVE, Fab1, YOTB, Vac1 and EEA1; GLUE, GRAM-like ubiquitin binding in EAP45, HRS, hepatocyte growth factor-regulated Tyr kinase substrate: IST1, increased sodium tolerance protein 1; LIP5, LYST-interacting protein 5; MIM, MIT-interacting motif; MIT, microtubule-interacting and trafficking; MITD1, MIT-domain containing protein 1; NZF, Npl4-type zinc finger; Ptd In(3)P, phosphatidylinositol 3-phosphate; PRD, proline rich domain; SH3, SRC homology 3; STAM, signal transducing acceptor molecule; UBD, ubiquitin binding domain; UBPY, ubiquitin isopeptidase Y; UEV, ubiquitin E2 variant; VHS, VPS27, HRS, STAM; VPS, vacuole sorting protein; WH2, winged helix 2.

1.1.5.2 CHMP7

CHMP7 is a unique ESCRT-III component and differs from the other CHMPs in a number of ways. For instance, it is conserved across the majority of eukaryotes, but not prokaryotes or noticeably yeast. The reason for this is unclear, but could indicate the evolution of a specialised function for CHMP7 in higher order systems such as mammalian cells. one that has been lost in yeast. Another key difference lies in the length of CHMP7; at 453 residues it is approximately double the length of all the other CHMP subunits. As yet its role in the MVB pathway and as an ESCRT-III subunit is unknown, but it does contain some important similarities to other CHMPs. The C terminal (222-453) contains a biased distribution of acidic and basic residues and based on multiple sequence alignments is predicted to contain a SNF7 domain (figure 12). This raises the possibility the C terminal half of CHMP7 could behave and interact much like the other CHMP subunits.

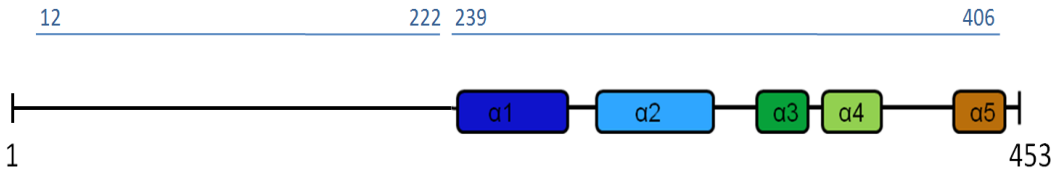

Figure 12 Diagram showing the distinct N and C terminal halves of CHMP7, with the C terminal half being similar to other CHMP subunits and containing the SNF7 coiled-coil domain.

Other CHMP-CHMP interactions have been established *via* methods such as yeast two-hybrid assays, pull down assays and immunoprecipitation experiments. Similar interaction strength is possible for CHMP7 interactions and so these methods could be employed to uncover any other CHMP7 –CHMP interactions. Interaction with CHMP4 and the CHMP7 C terminal half has been found *via* yeast two hybrid assays with all CHMP4 isoforms, but no interaction was found between CHMP4 and the CHMP7 N terminal half[46]. To date, no other CHMP7-CHMP interactions have been published. Also, it is currently uncertain whether CHMP7 contains a MIM motif. Once established, further possible binding partners could be explored, such as VPS4 and other MIT-containing proteins.

The N terminal half (1-221) displays no significant sequence homology with any known protein domain, although the possibility of a SNF7-related domain has been suggested by Horii et al[46].

Horii et al evaluated CHMP7's classification as an ESCRT-III subunit. They found that when overexpressed in HeLa cells, green fluorescent protein (GFP) tagged CHMP7 exhibited some impairment of the MVB sorting pathway[46]. This effect was defined by a slight accumulation of ubiquitinated cargo in the perinuclear area and also by the reduced disappearance of a tagged receptor, epidermal growth factor receptor (EGFR). These results indicate that CHMP7 does have an involvement in the MVB sorting pathway, as impairment of other CHMPs yields similar effects. Furthermore, they demonstrated that overexpression of a dominant negative VPS4 construct resulted in no effect upon the subcellular distribution of a GFP-tagged N terminal half CHMP7 construct, whereas GFP- C terminal CHMP7 displayed a punctate distribution and co-localised with the dominant negative VPS4. These results indicate that the CHMP7 SNF7 domain behaves similarly to other CHMPs, whereas the N terminal half is unique and not involved in MVB sorting.

Others results from Horii et al supporting CHMP7 as an ESCRT-III subunit were that overexpressed GFP-CHMP7 inhibited the release of virus like particles, which agrees with the role of the some ESCRT-III subunits in viral budding when hijacked by a virus.

1.2 ATPases associated with diverse cellular activity (AAA)

VPS4, the enzyme responsible for removing CHMP subunits from the membrane, falls into the AAA family of super proteins. AAA proteins have been identified in all organisms and are involved in such diverse processes as DNA replication, transcriptional regulation, membrane fusion, biogenesis of organelles, protein secretion and proteolysis, which demonstrates the wide range of their importance in cellular events[47-49].

Enzymes from this superfamily contain a P-loop NTPase domain and ATPase subunits of proteases, helicases or nucleic acid-stimulated ATPases[50]. These proteins share a highly conserved sequence, approximately 220 amino acids, referred to as their AAA domain or nucleotide-binding domain. This region includes the Walker A and B motifs necessary for ATP binding and hydrolysis. Enzymes in this family use the energy from ATP hydrolysis in order to drive mechanical processes such as protein unfolding and remodelling[49].

1.2.1 VPS4 enzymes

Two isoforms of VPS4 exist in humans; VPS4A and VPS4B (also known as SKD1), with 80% identity[6]. Both display approximately 60% identity to the VPS4 yeast homolog. Together with ESCRT-III, VPS4 is conserved across eukaryotes, it is essential for the regulation and normal function of the MVB pathway. For example, inhibition of VPS4 in mammals leads to impaired receptor down-regulation, arrested cytokinesis and accumulation of ESCRTs on the endosome thereby resulting in delayed vesicle formation[16,51-53].

For successive protein trafficking events, the ESCRT-III lattice needs to be removed from the endosomal membrane and recycled. The VPS4 complex is responsible for this disassembly of the CHMP subunits, recycling them back to the cytoplasm and aiding in the final stages of membrane budding and fission. VPS4 itself exists as monomers and dimers in the cytoplasm until the complex is required.

VPS4 contains a single AAA cassette (Type I ATPase) and belongs to the meiotic clade of AAA ATPases(figure 13)[54]. ATPases in this family form an oligomeric ring, generally a hexamer, where ATP typically binds at the interface between the small and large AAA domains.

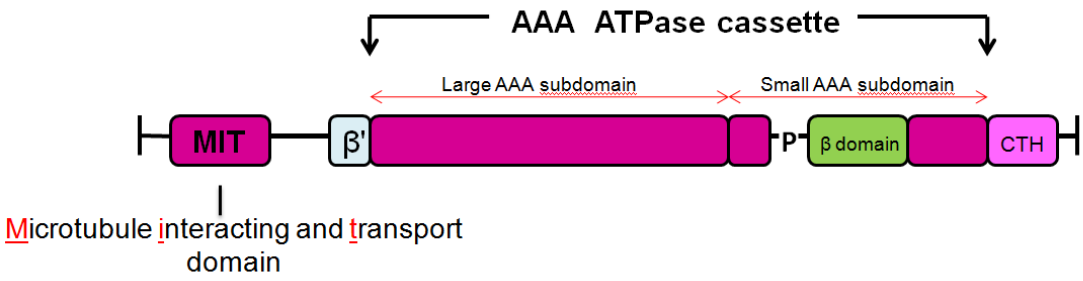

Figure 13 Cartoon representing the domains of VPS4. The AAA ATPase cassette is split into two sub-domains known as the large and small AAA sub-domains. In VPS4 the small AAA sub-domain is disrupted by a proline residue immediately followed by a β insert. CTH, C terminal helix.

Although sequence analysis classes VPS4 as an AAA protein, it does display some unique features. The AAA ATPase cassette is disrupted by a β insert, a feature seen in all VPS4 proteins, but not in any other members of the meiotic clade. Like other AAA ATPases this AAA cassette is split into two domains, a small and large AAA domain. The β insert is found within the small AAA subdomain, accommodated by a kink caused by a proline residue (that is also only found in VPS4)[54]. ClpB is the only other AAA protein that contains an insert in the same place as VPS4. In the case of ClpB, a protease, this insert is an anti-parallel coiled-coil that interacts with substrates and aids recognition[54,55]. A similar function is likely the case for the β insert of VPS4 through interaction with adaptor proteins, such as LIP5 (VTA1 in yeast)[56].

Another unique feature of VPS4 is a C terminal helical region, where the single helix packs onto the large AAA subdomain, this is also proposed to aid oligomerisation[57]. Despite these unique features, VPS4 contains all the elements of a functional ATP binding site, such as Walker A and B motifs, arginine fingers and the SRH. Active VPS4B is found in the cytosol, whereas ATPase-defective mutants of VPS4B have been found to accumulate on the endosomal membrane, impairing vesicle formation[58].

VPS4 requires ATP to initiate oligomerisation into an active complex containing 10-12 subunits, believed to form two stacked hexameric rings (although the possibility of VPS4 forming pentameric rings has not been discounted)[6]. The pore of this ring is hydrophobic and whilst mutations of this do not affect assembly of the VPS4 complex they do inhibit HIV-1 release and infectivity. This finding supports the earlier theory that, after initial capture by the MIT domain, ESCRT

subunits are pulled through this pore in order to be disassembled[54]. If this were the case partial unfolding of the ESCRTs would be required for entry into the narrow central pore, which would involve breaking key interactions and it remains unclear how VPS4 would then release these ESCRT subunits.

The N terminal domains of AAA ATPases can vary considerably as they typically are involved in substrate specificity[59]. In VPS4, the MIT domain is located between residues 1-77 and VPS4B mutants lacking this region have impaired cellular function[58]. This domain forms an anti-parallel three-helical bundle, with a crevice capable of binding other motifs in a variety of modes. (figure 14)[57].

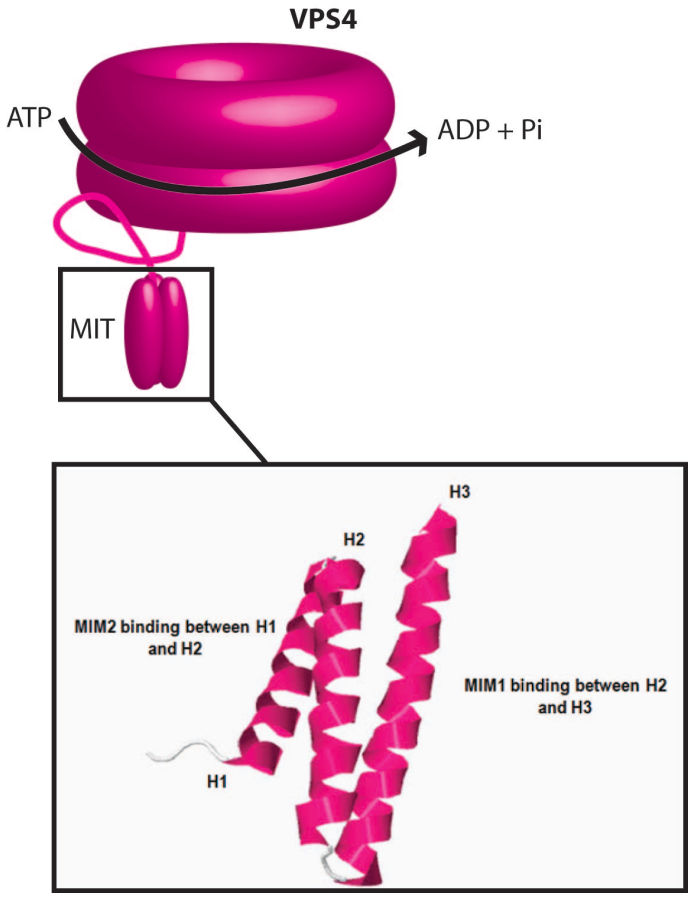

Figure 14 Cartoon of catalytically active VPS4 complex forming two stacked rings, plus the crystal structure of the MIT domain in VPS4A –further MIT domains are omitted for clarity. Structure shows the three helices of the MIT domain and the respective binding sites of MIM1 and MIM2. These binding sites appear to have no overlap and do not affect the conformation of the domain therefore the simultaneous binding of a MIM1 and MIM2 motif could occur (PDB 1YXR).

Three conserved leucine residues (or another hydrophobic residue in the case of CHMP3, Met, and CHMP2B, Ile) are critical for this binding, which occurs in the crevice between helices 2 and 3 of the MIT domain, parallel to helix 3[59]. This primary recognition is reinforced by a series of salt bridges. The MIM2 of CHMP4

isoforms and 6 lies more to the centre of the protein and is proline rich, this causes it to bind to the MIT domain in a different way, i.e. between helices 1 and 2[60,61]. The binding sites for the MIM1 and MIM2 do not overlap or alter the conformation of the MIT domain, therefore it seems VPS4 could bind MIM1 and MIM2 containing proteins simultaneously[61].

1.2.1.1 LIP5, a positive regulator of VPS4 activity

The cofactor, LIP5 promotes the oligomerisation of VPS4 into a ring from monomers and dimers in the cytoplasm. LIP5 achieves this through interactions with the β domain and C terminal region of VPS4, an interaction conserved across mammalian cells[56]. LIP5 has been established as a positive regulator of VPS4 ATPase activity and also has some association with several ESCRT-III subunits. Biochemical analysis has suggested the active VPS4-LIP5 complex comprises these proteins in a 2:1 stochiometry[62]. These observations support a model whereby LIP5 acts to assemble VPS4 hexameric rings into the active stacked form. Moreover, it is possible that the β domain interaction with LIP5 maintains communication between the rings[63,64].

LIP5 is a 307 amino acid long protein, containing two MIT domains (figure 15). A long flexible link connects these domains to the VPS4 binding VSL (VPS4, SBP1, LIP5) domain. The depletion of VTA1 in yeast and knockdown of LIP5 in mammalian cells results in cargo sorting defects, disrupted downregulation and inhibited viral budding[65].

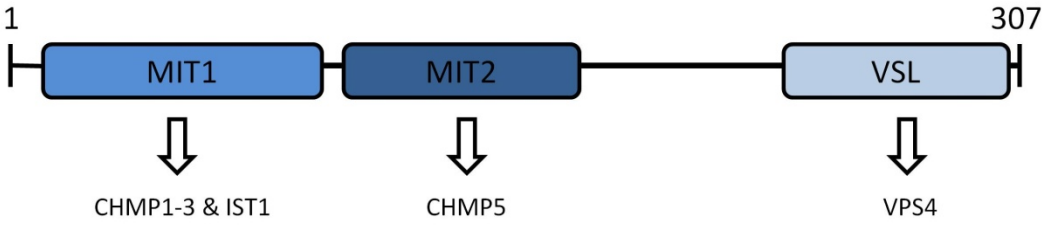

Figure 15 Cartoon representing domains of LIP5. LIP5 contains two MIT domains that both bind CHMP5 strongly, although the MIT2 appears to favour this. The MIT1 is known to interact with MIM1 CHMPs (including IST1). These MIT domains are connected to the VSL domain by a long flexible linker -this C terminal domain binds VPS4.

LIP5 binds tightly to CHMP5 (with pM affinity) and to a lesser extent MIM1 containing ESCRT-III subunits[34]. Pull down assays revealed no interaction

between LIP5 and CHMP4 isoforms or 6, although this may be due to weak interaction[66]. The strong interaction between LIP5 and CHMP5 has led to the assumption that CHMP5 may act as an adaptor for LIP5 to interact with the ESCRT-III assembly on membranes[25].

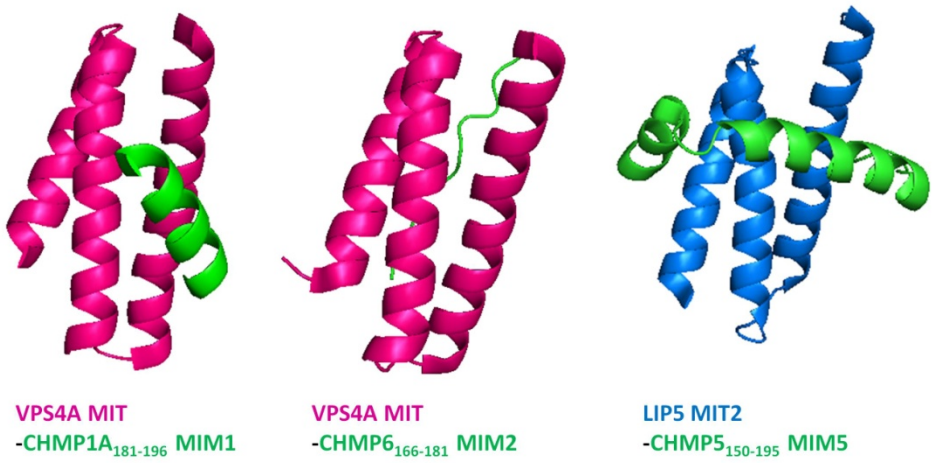

Figure 16 Comparison of MIT-MIM binding modes. Shown are structures of the following complexes: human VPS4A MIT-CHMP1A(181–199) (PDB code 2JQ9), human VPS4A MIT-CHMP6(166 –181) (PDB code 2K3W) & LIP5 MIT2-CHMP5(155–189) (code 2LXM). In each case, CHMP fragments are green, VPS4 MIT domains are pink and LIP5 MIT2 is blue.

Figure 16 shows how binding to the LIP5 MIT domain differs from both MIM2 and MIM1 binding. These different modes of binding can allow simultaneous interaction between VPS4, LIP5 and CHMPs. Evidence has also suggested the possibility of a secondary MIM binding site in some CHMPs, further extending the integrated and complex network these proteins form[65].

1.2.1.2 IST1, a negative regulator of VPS4 activity

IST1 was originally identified in yeast as an evolutionarily conserved protein that interacted with both VPS4 and DID2 (CHMP1)[67,68]. The interaction with VPS4 inhibits ATPase activity by interfering with the oligomerisation of the VPS4 complex. Therefore, IST1 acts conversely to LIP5 as a negative regulator of VPS4 rather than a positive one. This hypothesis was further compounded by experiments where overexpression of IST1 led to MVB sorting defects similar to defects displayed by cells depleted of VPS4[67]. IST1 is an example of an ESCRT protein that contains both a MIM1 and a MIM2, it is through these motifs that IST1 binds to the MIT domain in VPS4.

The human IST1 homolog was described by Agromayor et al and interactions with ESCRT components analysed by yeast two hybrid assay and co-precipitation assays[69]. The interactions observed agree with previous findings using yeast IST1. Human IST1 interacts with VPS4 (both isoforms, CHMP1 (both isoforms) and also LIP5 (figure 17).

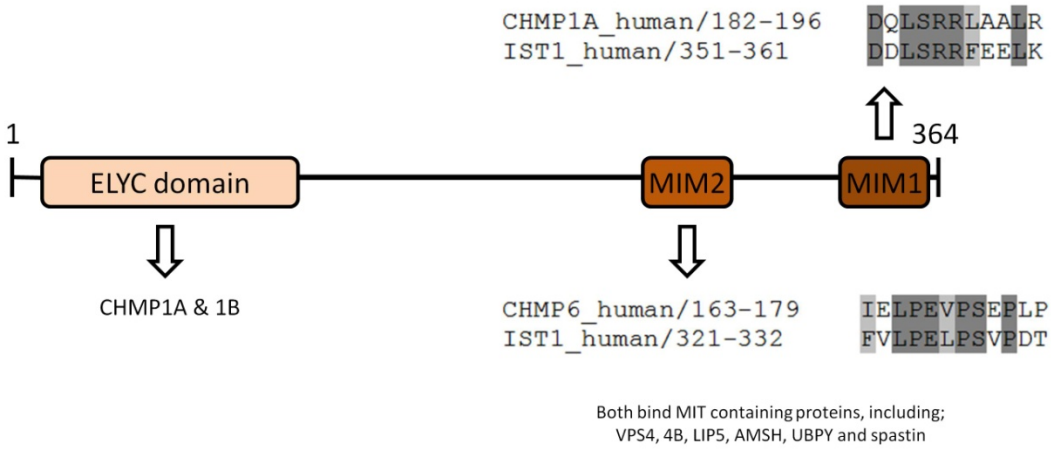

Figure 17 Cartoon representing regions and motifs of human IST1. IST1 contains two MIMs that both bind to a variety of MIT-containing proteins, including VPS4, LIP5, de-ubiquitinating enzymes (AMSH and UPBY) and also spastin. Also, shown in the MIM1 and MIM 2 sequences alignment to known MIM1 and MIM2 motifs in CHMPs. A region towards the N terminal called the ELYC (E -glutamic acid, L- leucine, Y -tyrosine and C -cysteine) domain interacts with CHMP1 isoforms.

IST1 binds CHMP1A and CHMP1B in a region found far up stream of the MIM motifs termed a ELYC domain (tetrapeptide motif). The MIMs can bind a variety of MIT domain containing proteins and having two MIMs means IST1 can bind MIT proteins simultaneously, which suggests a role for IST1 with CHMP1, alongside the LIP5:CHMP5 sub complex, in the regulation of VPS4 activity and assembly.

In terms of non-endosomal ESCRT functions, studies into virus budding and release have shown that IST1 is not required for this process. In contrast, IST1 is essential for cytokinesis. Its depletion resulted in an accumulation of multinucleated cells, a similar phenotype was observed upon depletion of proteins crucial for cytokinesis such as CEP55 or ALIX[69]. Immunofluorescence has also revealed that IST localises to the midbody during the late stages of cytokinesis. Moreover, IST1 interacts through a MIM to spastin, an enzyme involved in late cytokinesis, which itself binds CHMP1B[70]. It has been proposed

that IST1 function at the midbody in humans may be as a platform to recruit MIT containing proteins required for cytokinesis.

1.3 ESCRT complexes in viral budding

Enveloped viruses have developed the ability to hijack the ESCRT machinery to facilitate their own budding from the plasma membrane. By mimicking factors and protein domains that the cell uses during formation of ILVs, the virus can acquire an envelope by budding through the host membrane bilayer[63].

Retroviral late-budding (L) domains are generally required for efficient release of nascent virions. These late domains bind to TSG101 (ESCRT-I), *via* a PTAP motif and thereafter are treated like normal cargo. Whilst this PTAP motif is found in viruses like HIV-1, other motifs exist that also bind to TSG101. In the absence of TSG101 successful budding of virions often cannot occur[71]. Other studies have demonstrated, however, motifs that cannot bind to TSG101 and yet are still successful at hijacking the ESCRT machinery further downstream[71]. It is interesting to note that irrespective of late-budding domain motif, viral budding is blocked efficiently by dominant negative mutants of VPS4[72]. This implies that all budding viruses require the action of VPS4, but not necessarily TSG101 as well.

The role of the ESCRT-III subunits and VPS4 is to cut the neck of the budding virion, thereby releasing it from the host cell. For the HIV virus, ESCRT-0 and II are dispensable, but CHMP4 interaction with ALIX may serve as the recruiting factor and activate other ESCRT-III subunits and VPS4[25]. Recent studies have attempted to determine the extent each CHMP subunit is required for virus budding by depleting each subunit in turn and measuring the resultant virion release. The results indicate that only co-depletion of CHMP4 isoforms or CHMP2 isoforms disrupted virus budding. Depletion of CHMP5, 6, 7 and IST1 had little effect on viral budding[73]. In contrast, Horii et al found that overexpression of CHMP7 did inhibit the release of virus-like particles[46]. Therefore this is likely not a direct effect of CHMP7, but rather indirectly caused by an interaction between CHMP7 and CHMP4B (which could be important in virus budding).

1.4 ESCRT complexes in autophagy

A further function for ESCRT complexes that has not previously been mentioned is in autophagy. Autophagy is a mechanism used by eukaryotes to remove and degrade unnecessary or dysfunctional cellular components such as in organelle turn over, protein aggregates and other cytoplasmic constituents. During this process targeted material is isolated within autophagosomes, which later fuse with lysosomes for degradation. Impairment of autophagy causes developmental defects, the accumulation of protein aggregates, neuronal degradation and cell death[74]. Autophagy protects against cancer and neurodegenerative diseases.

Although there is some overlap between the endocytic and the autophagic pathways the link between autophagy and ESCRT proteins was noticed by an accumulation of autophagosomes upon ESCRT machinery inactivation[75,76]. ESCRT mutations have also been associated with inherited neurodegenerative diseases in humans. In particular a rare mutation in CHMP2B is the cause of CHMP2B-related frontotemperol dementia. Many age-related neurodegenerative disorders are associated with the accumulation of ubiquitin-containing aggregates in affected brain regions. Reduced ESCRT function is implicated in aggravating polyglutamine aggregates, which is linked to neurodegenerative disorders such as Huntington's disease[76].

Little is known about the exact function of ESCRTs in this area, but the most recent and favoured proposals are that the ESCRT machinery aids recruitment and delivery of fusion machinery to autophagosome, potentially through association with Rab7 and its activator complex HOPS (homolytic fusion and vacuole protein sorting)[76].

1.5 ESCRT complexes in cytokinesis

Cytokinesis occurs towards the end of mitosis (and meiosis) resulting in two physically separated cells. Cytokinesis begins once the separation of genetic material has successfully occurred, so can start as early as anaphase. The

process can be broken down into four stages; specification of cleavage site, formation of cleavage furrow and midbody, microtubule severing and abscission (figure 18). This is a highly regulated process and incorrect separation of genetic material or abscission occurring too early can have severe consequences. Most noticeable this can lead to tumour development and cancer[77,78].

The chromosomal passenger complex (CPC) regulates many key events in mitosis such as chromosome-microtubule attachment and activation of the spindle assembly checkpoint. This complex is comprised of aurora B kinase, inner centromere protein (INCENP), borealin and survivin. In particular, an aurora B-mediated abscission checkpoint has been identified that delays abscission. Aurora B activity is sustained by persisting chromosome bridges and its depletion was found to promote abscission[79]. Aurora B is proposed to act as a sensor of non-segregated chromatin in the midzone and abscission site[80]. Interestingly, recent findings of Carlton et al show that CHMP4C is involved in aurora B-mediated abscission timing *via* interaction with borealin. They suggest CHMP4C can inhibit abscission upon phosphorylation by aurora B[80].

Primarily, ESCRT-III complex function in cytokinesis is believed to be in abscission of the thin membrane neck by a similar mechanism as ILV formation and the CHMPs involved can be seen localising to the midbody of dividing cells. The midbody (also known as a Flemming body) is a dense microtubule-rich structure that is the final tether connecting daughter cells. CEP55, a coiled-coil phosphoprotein that translocates to the midbody ring during cytokinesis, recruits proteins containing a $GPPX_3Y$ motif, such as TSG101 (ESCRT-I) and ALIX.

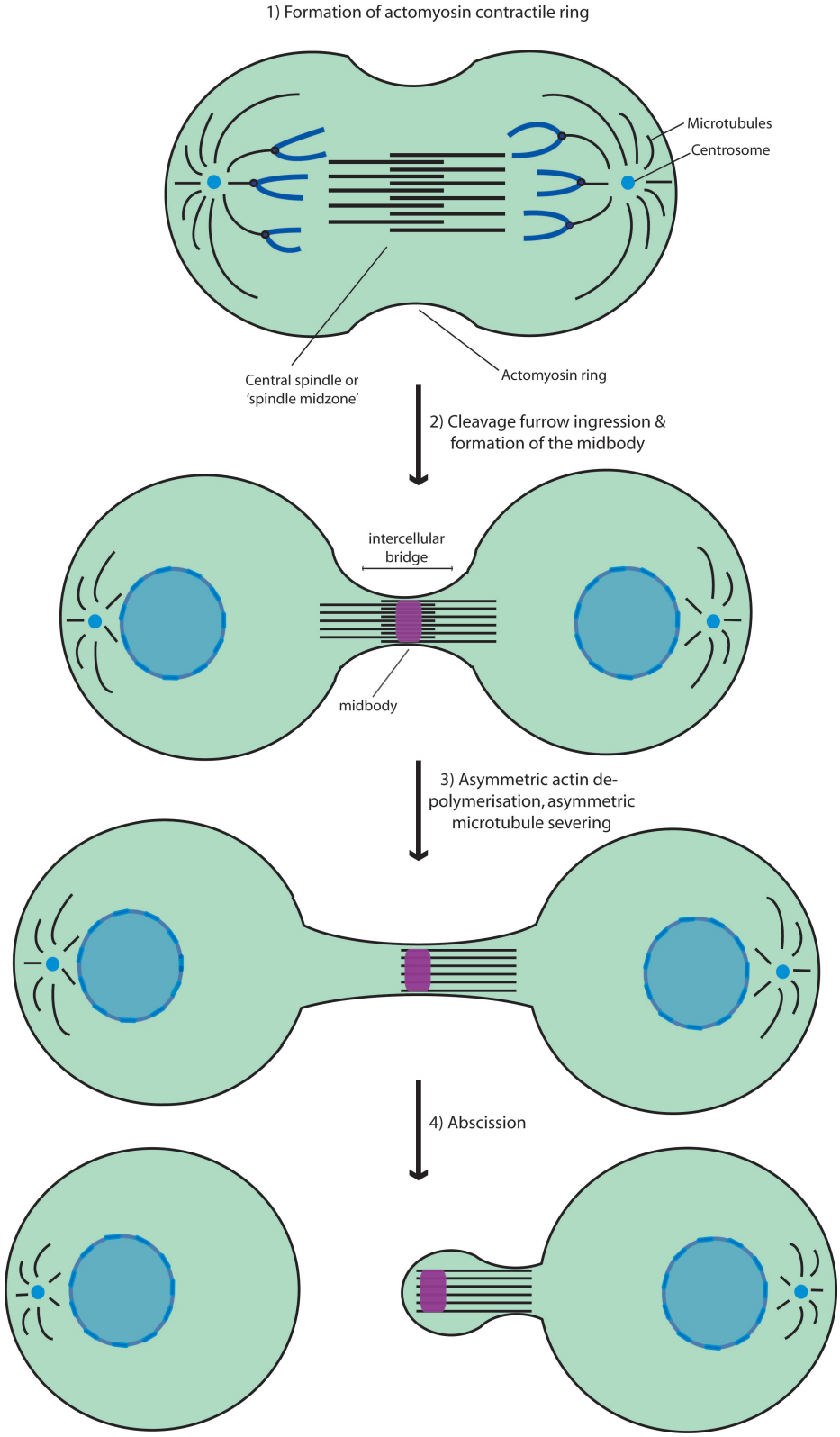

Figure 18 Scheme outlining the stages of cytokinesis. This can begin during anaphase as actomyosin ring forms, at this site the cleavage furrow can then occur and the midbody forms. Next the actin ring breaks down and asymmetric microtubule severing occurs which with the aid of ESCRT-III components leads to abscission.

The $GPPX_3Y$ motif in ESCRT-I appears to be located in an unstructured linker region between the UEV domain and the region that makes up the core complex[81]. In turn, ALIX, and probably ESCRT-I, are responsible for recruiting ESCRT-III subunits to close the membrane neck and complete cytokinesis[9]. Point mutations in ALIX blocking either CEP55 or CHMP4 binding, severely inhibits abscission[53]. The coiled-coil region of CEP55 is separated by a ‘hinge’ and it is in this region that ALIX and TSG101 of ESCRT-I bind.

For abscission to occur a functional midbody is required in order for the correct downstream protein recruitment and signalling to occur. ALIX and TSG101 are proposed to 'follow' CEP55 by first localising to centrosomes where CEP55 is found at prophase. CEP55 translocates to the midzone and then the midbody through a series of phosphorylation steps during mitosis. At the midbody both ALIX and TSG101 interact with an array of other proteins involved in cytokinesis. Elia et al investigated the spatial organisation of ESCRTs at the midbody using super resolution microscopy and found that TSG101 and CHMPs assembled into ring-like structures around the midbody centre[82]. VPS4 also localises to the midbody and is essential for abscission. Another ESCRT of particular importance is CHMP1B, which recruits spastin to the midbody. Spastin is a MIT domain containing microtubule severing enzyme which binds to the CHMP1B MIM[83,84]. Spastin is essential for cytokinesis and mutations in the gene are the most common cause of hereditary spastic paraplegia. Depletion of spastin or other proteins essential to cytokinesis, such as VPS4 leads to severe cytokinesis failure, evidenced by an increase of multinucleated cells.

The roles of ESCRT-III and VPS4 are conserved down to archea, the genome of which encodes orthologues of these proteins, but is not conserved for ESCRT-0, I or II[85]. Studies show ESCRT-III and VPS4 are vital for membrane scission, and ESCRT-I and ALIX only to varying extents[16,53,81,86].

Current evidence suggests the ESCRT-III and the VPS4 complex are important in proper functioning of both centrosomes and midbodies. Therefore, it seems likely they may mediate a number of steps in mitosis prior to membrane abscission.

CHMP1A supports the theory of a role for CHMPs during mitosis. CHMP1A regulates a nuclear protein called ataxia telangiectasia mutated (ATM). ATM is a protein kinase recruited to DNA double strand breaks, which itself activates proteins that initiate DNA damage response and cell cycle arrest. Overexpression of CHMP1A induced chromatin condensation and inhibited growth by promoting cell cycle arrest through over activation of ATM[87]. It is partly through this ATM signalling pathway that CHMP1A is proposed to act as a tumour suppressor protein[42,88]. CHMP1A is also suggested to regulate chromatin structure through its interaction with BMI-1. BMI-1 is a protein associated with polycomb group nuclear bodies and is implicated in DNA damage repair and gene silencing[89].

1.6 Project aims

The ESCRT machinery is essential for a variety of physiological and pathological processes. The VPS4 complex is particularly important in recycling CHMPs and allowing successive rounds of activity. However, their function has predominantly been studied in the context of their membrane scission role. Recent evidence suggests ESCRT-III plays a larger role in mitosis and cell cycle regulation than previously thought[1-4].

We aimed to further explore the nuclear role of CHMPs and how membrane trafficking proteins can function in mitosis. Further to this, and in comparison to the other subunits, very little is known about CHMP7 -the newest member of the ESCRT-III complex. Therefore, a second aim was to uncover new interactions between CHMP7 and other ESCRT proteins. We had reason to believe CHMP7 in particular may have some nuclear function, therefore these aims tied well together.

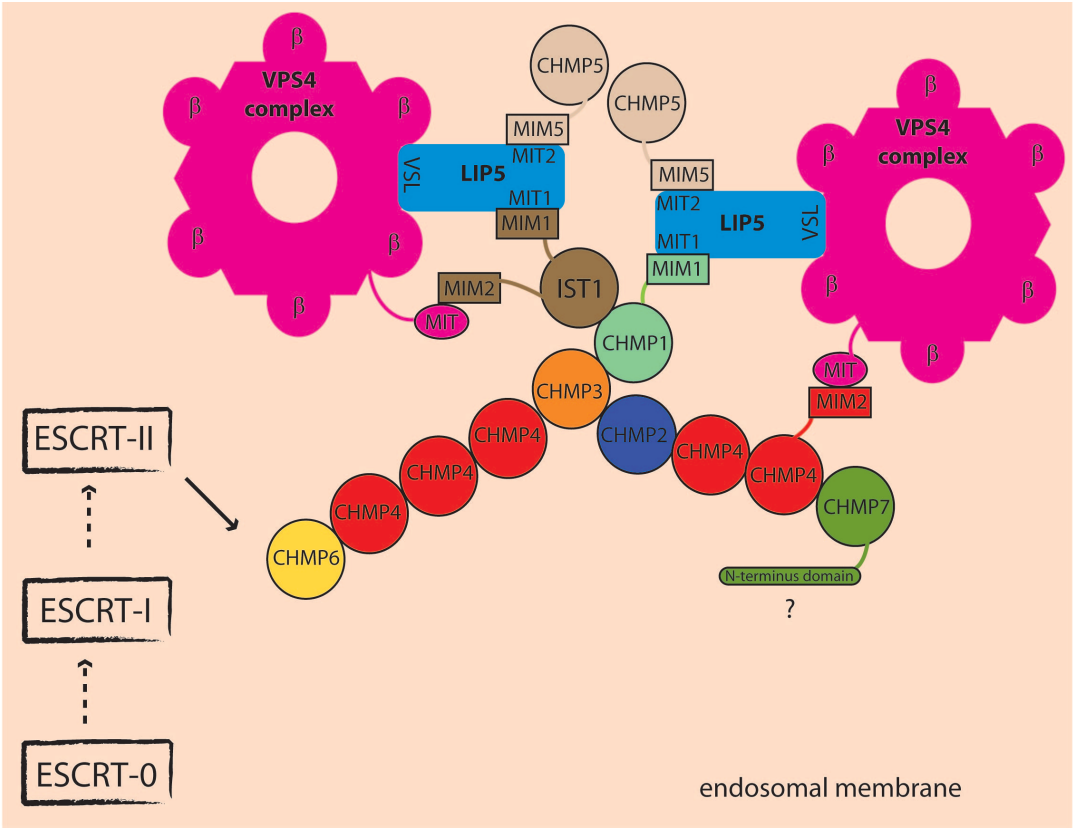

Figure 19 Scheme of ESCRT-III complexes. Scheme includes known interactions between CHMP subunits, VPS4 complex, LIP5 and IST1. For clarity not all MIT domains, MIM motifs etc are shown.

Chapter three focuses on CHMP7 with an analysis of sequence, structure and interactions. As a starting point the only known interaction for CHMP7 was between its C terminal half and CHMP4B, for this reason we wanted to provide some context for CHMP7 within the ESCRT machinery (figure 20). Chapter four studies CHMP behaviour in vivo using immunofluorescence microscopy and builds upon the interactions observed in chapter three to reveal a CHMP7-dependant nuclear ESCRT-III assembly. Chapter five follows on from this to ascertain to what nuclear structures this ESCRT-III assembly localises to as well as insights into the cause of this nuclear phenotype. Finally, chapter six focuses on the nuclear defects and phenotypes resulting from specific protein depletions and the implications these have on ESCRT-III functions during mitosis and cytokinesis.

CHAPTER 2 METHODS AND MATERIALS

2.1 Materials

2.1.1 Bacterial strains and cells

2.1.1.1 Bacterial cells

For all biochemistry DNA/cloning work, *E. coli* strain JM109 (DE3) (Promega) or DH5alpha (Promega) were used and either BL21 (DE3) (Promega) or Rosetta (DE3) (Millipore) were used for protein expression.

2.1.1.2 Eukaroytic cells

Human cervix carcinoma cells (HeLa), or a derived cell line, HeLaM, were used for all experiments. Cells were grown in DMEM (Invitrogen) and supplemented with 10% fetal bovine serum (Hyclone), 1% penicillin streptomycin solution (Invitrogen) and 1% MEAA (Lonza).

2.1.2 DNA

2.1.2.1. Plasmids

Vectors used for protein expression in bacteria were; pHis, containing a six histidine tag, pHis.Trx2, a pET-32a derived vector with a six histidine and thioredoxin tag[90] and pGEX 4t-2 with a glutatione S-transferase (GST) tag. See appendices 1 and 2 for the vector maps of modified plasmids.

GST-CHMP4B (pGEX 4t-1), GST-CHMP5 (pGEX 4t-1) and His-CHMP1A (pHis) were kindly gifted by Prof. P. Woodman, University of Manchester. His-VPS4B (pPROEX HTb)[40] was kindly gifted by Prof. W. Weissenhorn, Grenoble. His-UBC9 (pET23a) and SUMO1 G97 (pET30) were obtained from Addgene (Addgene, 8651). Lastly, GST protein control (pGEX 6p-1) was kindly gifted by Prof. C Smythe, University of Sheffield.

pGEX 4t-2	DNA insert base pairs	approx kDa of expressed protein	Extinction coefficient $M^{-1}cm^{-1}$
cDNA			
CHMP7	1359	76	87820
CHMP7 228-453	678	50	44600
CHMP7 372-438	210	36	40130
CHMP7 233-315	249	36	43110
CHMP5 116-179	192	36	43110
CHMP4B 13-100	264	36	41620
CHMP7 MIM1	81	28	40130
CHMP7 MIM2	84	28	40130

pHis.Trx2	DNA insert base pairs	approx kDa of expressed protein	Extinction coefficient $M^{-1}cm^{-1}$
cDNA			
CHMP7	1359	64	64750
CHMP7 372-438	210	24	17060
CHMP4B 13-100	264	24	18550
LIP5	921	48	41930

Table 1 Constructs designed in the duration of this project. The full length CHMP7 was cloned in order to insert it in different vectors to improve the purification process. CHMP7 228-453 contains the entire SNF7 domain of CHMP7. CHMP7 372-438 is the acidic 4th and 5th alpha helical region. CHMP7 233-315 encompasses the basic 1st and 2nd alpha helical region. CHMP5116-179 encompasses the 4th and 5th alpha helical region of the SNF7 domain. CHMP4B 13-100 encompasses the 1st and 2nd alpha helical region of the SNF7 domain. CHMP7 MIM1 and CHMP7 MIM2 span 412-438 and 389-416 respectively. Refer to appendices 5 and 6 for location of these fragments in CHMP7. LIP5 was obtained from Origene's Trueclone collection of cDNA and moved into the pHis.Trx2 vector.

All cloned plasmids (table 1) were verified by DNA sequencing at the Core Genomic Facility in the medical school of Sheffield University. For pET vectors, T7 primers were used and for the pGEX vectors, GST primers were used. Sequences were viewed and checked against mRNA sequences and vector maps using FinchTV and NCBI nucleotide BLAST. Extinction coefficients were estimated at 280nm (measured in water, in reducing conditions) using Expasy Bioinformatic Resource Portal and the Protein Knowledgebase (UniProtKB).

Vectors used for mammalian expression in HeLa M cells were; GFP-SUMO1, kindly gifted by Prof. A Sharrocks, University of Manchester; Myc-tagged versions of all 11 CHMPs (pcDNA 3) for the in vitro translations and CHMP7-myc, CHMP4B-myc (pcDNA 5) and GFP-VPS4B E235Q, GFP-VPS4A E228Q

(eGFP from Clontech) for the transient transfections -from Prof. P Woodman; and UBC9-HA wildtype and UBC9-HA C93S (pCMV4) for transient transfections from Addgene (14438 and 14439).

2.1.2.2 Synthetic oligonucleotides

Table 2, below, displays the designed oligonucleotide primers used in PCR reactions in order to make truncated CHMP DNA constructs, as well as LIP5 and CHMP7 full length cDNA.

Name	Sequence (5'-3')
CHMP7 FWD (Bam H1)	CTCGTC GGATCC ATGTGGTCCCCGGAGC
CHMP7 REV (EcoR1)	CTCGTC GAATTC CTACAATGGCTTTAGAGTCGGTTC
CHMP7 238-316 FWD (Bam H1)	CTCGTC GGATCC CCAGTCAATGACGTAGATGTTG
CHMP7 238-316 REV (EcoR1)	CTCGTC GAATTC GGAGGCATAGATCCGGTCC
CHMP7 372-438 FWD (BamH1)	CTCGTC GGATCC GGCTTAGATTTTGACAGTGAAG
CHMP7 372-438 REV (EcoR1)	CTCGTC GAATTC GCTTGGGACCAAACCTCC
CHMP4B 15-99 FWD (BamH1)	CTCGTC GGATCC GGTAAGGCCGGCAAG
CHMP4B 15-99 REV (EcoR1)	CTCGTC GAATTC GTTGGCATTCTCCAGGG
CHMP5 116-178 FWD (BamH1)	CTCGTC GGATCC ATGAAGAAGGCATACAAG
CHMP5 116-178 REV (EcoR1)	CTCGTC GAATTC GTCTTCATCAGCCAGAAG
LIP5 FWD (Bam H1)	CTCGTC GGATCC ATGGCCGCGCTTGCACCG
LIP5 REV (Eco R1)	CTCGTC GAATTC TCATTCTCTGCCTGTCGT

Table 2 Oligonucleotides used in PCR reactions. These were designed according to set parameters, i.e. between 50-65% G/C content, between 58-64°C melting temperature and between 14-29 base pairs, plus starting with G or C. The melt temperatures were estimated by attributing 4°C to every G/C and 2°C to every T/A. Primers were aimed to closely match their corresponding primer in particular within these conditions.

Recursive PCR, sometimes referred to as assembly PCR requires no DNA template. Instead, four overlapping primers that encompassed the desired region are mixed in one reaction that allows the inner primers to anneal first and the outer two second.

MIM1 -1 /FWD (Bam H1)	CTCGTC GGATCC CCGAACCCGAACCCGAGGATCTCAGAC
MIM1 -2 /FWD (inner)	GAACCCGAGGATCTCAGACGCTGAACTGGAAGCTGAACTGGAGAAACTGTC
MIM1 -3 /REV (inner)	GGTACCAGACCTTCAGACAGGGACAGTTTCTCCAGTTCAGCTTCCAG7
MIM1 -4 /REV (Eco R1)	CTCGTC GAATTC TTATTAAGACGGTACCAGACCACCTTCAG
MIM2 -1 /FWD (Bam H1)	CTGGTC GGATTC CAAGACACCACCAAAGAACCGCTGGAC
MIM2 -2 /FWD (inner)	CACCAAAGAACCGCTGGACCTGCCGGACAACCCGCGCAACCGTCATTTC
MIM2 -3 /REV (inner)	CGTGGGTTTGGAACGGAGGAGAAGGAGAAATGACGGTTGCGCGGGTTGTCC
MIM3 -4 /REV (Eco R1)	CTGGTC GAATCC TTATTAGATACGTGGGTTTGGAACGGAG

Table 3 Primers for the CHMP7 MIM1 and MIM2, these primers encompass the regions 412-438 and 389-416 of CHMP7 respectively (5' to 3'). They were designed based on short sequence predicted to bind to MIT containing proteins. These primers are designed so that the inner two primers anneal first through the complimentary section coloured blue. The outer primers containing to Bam H1 and Eco R1 site anneal second creating a PCR product that can be digested ready for ligation into an appropriate vector.

BamH1 and EcoR1 (Roche, 10 U/ µl) was used for DNA digestion and T4 DNA ligase (Roche, 1 U/µl) was used for ligation reactions (generally carried out for 16 hours at 15 °C. Taq DNA polymerase was used for PCR and recursive PCR reactions –which included PCR buffer and a master mix of dNTPs (Clontech) was made with 5 µM of each. Alternatively PCR beads (GE Healthcare) were used according to the protocol provided. In the case of PCR for use in transcription, high fidelity PWO polymerase (Roche) was used. All primers were ordered from Life Technologies. Following PCR using PWO, DPN1 was used to degrade the template DNA.

For the transcription reactions; DTT, 5x transcription buffer, T7 RNA polymerase and RNasin were all supplied by Promega, the RNase-free water was from Stratagene and the 7GG RNA cap was from New Engand Biolabs (NEB)

2.1.3 Antibodies

The primary antibodies used to detect different cell structures and proteins by immunofluorescence (IF) and Western blotting (WB) are listed in table 4 with their respective dilutions.

Antibody	Species	Source	Antigen	IF	WB	Cat. No.
anti-ALIX	rabbit	house generated	ALIX	1/100	n/a	n/a
anti-CENPF	mouse	Abcam	CENPF	1/100	n/a	ab90
anti-CHMP1A	rabbit	Proteintech	CHMP1A	1/200	1/1500	15761-1-AP
anti-CHMP1B	rabbit	Proteintech	CHMP1B	1/200	1/1500	14639-1-AP
anti-CHMP4B	rabbit	Proteintech	CHMP4B	1/200	1/1500	13683-1-AP
anti-CHMP4C	rabbit	Proteintech	CHMP4C	1/200	1/1500	16256-1-AP
anti-CHMP7 (C)	rabbit	Proteintech	CHMP7	1/200	1/150	16424-1-AP
anti-CHMP7 (N)	sheep	house generated	CHMP7	1/800	1/4000	n/a
DM1A	mouse	Millipore	alpha-tubulins	1/400	n/a	05-829
anti-EEA1	rabbit	Cell Signalling Tech.	early endosomes	1/100	n/a	3288
FK2	mouse	Millipore	ubiquitinated protein	1/800	n/a	ST1200
anti-ɣH2AX	mouse	Millipore	phosphorylated H2AX	1/50	n/a	05-464
anti-HA	rat	Santa Cruz Biotech	HA tag	1/100	n/a	sc-53516
anti-importin β	mouse	Millipore	importin β 1	n/a	1/2000	05-1530
anti-IST1	rabbit	Proteintech	IST1	1/200	n/a	51002-1-AP
anti-LAMP1	mouse	Dev. Bio. Hydridoma Bank	late endosomes	1/1000	n/a	1D4B
MS110	mouse	Millipore	BRCA1	1/100	n/a	MABC199
anti-MYC 4A6	mouse	Millipore	MYC tag	1/200	1/1500	05-724
anti-PML	rabbit	Abcam	PML	1/200	n/a	ab53773
anti-SUMO1	rabbit	Cell Signalling Tech.	SUMO1	1/100	n/a	4930
anti-TAT1	mouse	house generated	TAT1	n/a	1/5000	n/a
anti-VPS4B	rabbit	Proteintech	VPS4B	n/a	1/1000	17673-1-AP

Table 4 List of primary antibodies used, indicating the antigen and dilutions used. Thanks go to Prof. C Smythe for the anti-BRCA1 and anti-ɣH2AX and to Prof. V Allen, University of Manchester, for the anti-TAT1 and anti-CENPF.

All secondary antibodies used for IF were anti-mouse, anti-rabbit or anti-sheep and either conjugated to Cy3, Cy2 or ALEXA 488 nm (Jackson Immuno Research Laboratories, raised in donkey). Secondary antibodies used for WB were anti-goat*, anti-mouse or anti-rabbit and conjugated to IRDye 800CW or IRDye 700DX (LICOR, raised in donkey). In the case of IF, a bandpass filter was fitted to the microscope to avoid fluorophore emission bleed-through between channels (caused by the broad bandwidth of some fluorophores)

*the anti-goat antibody cross-reacted with sheep and was used to probe for the anti-CHMP7 sheep antibody.

Also, 4',6-diamidino-2-phenylindole (DAPI), a fluorescence marker that binds strongly to A-T rich regions in DNA was used to target the nucleus.

2.1.4 Molecular weight markers

Protein markers were from Biorad (Dual Colour Precision Plus) and NEB (Prestained broad range marker 10-230 kDa). All DNA markers (50bp, 100bp and 1kb) were sourced from New England Biolabs.

2.1.5 Antibiotics

Ampicillin, to a final concentration of 100µg/ml, was used for constructs transformed and expressed in *E. coli* cells. Kanamycin, to a final concentration of 50 µg/ml, was generally used for constructs designed for mammalian expression (HeLaM cells). Antibiotic used was according to the appropriate resistance highlighted in the vector map each construct. Puromycin was used in the wheat germ in vitro translation experiment to 1.6 mM.

2.1.6 Protocol kits

Name	Source
BCA Protein Assay kit	Thermo Scientific
DNA purification kit	Zymo Research Corp.
Gel Extraction kit	Qiagen
Mini-prep kit	Qiagen
Midi-prep kit	Macherey-Nagel
NucleoSpin Gel & PCR clean up kit	Macherery Nagel
RNA Extraction & Retrosynthesis cDNA kit	Agilent Technologies
RNeasy Mini kit	Qiagen
Wheat germ extract kit	Promega

All other chemical reagents were supplied by Sigma-Aldrich or Fisher Scientific, unless otherwise stated.

2.2 Methods

2.2.1 Molecular biology

2.2.1.1 Plasmids and cloning

DNA encoding CHMP7 (453 a.a) and LIP5 were PCR amplified from full length cDNA clones. CHMP7 and LIP5 (*Trueclones, Origene*) were cloned into the BamH1/EcoR1 sites of a modified pET32a vector (with a thioredoxin insert after the His_6-tag) and pGEX 4T-2 vector. From the CHMP7 cDNA different regions were amplified *via* PCR in order to create truncated versions of CHMP7. These include, CHMP7 228-453 (C terminal half), 233-315 (basic 1st and 2nd alpha helices), 372-438 (acidic 4th and 5th alpha helices). Similar regions containing only the 1st and 2nd alpha helices of the SNF7 domain were made for CHMP4B and also the acidic 4th and 5th alpha helices of CHMP5.

PCR fragments of these truncations obtained were run on a TAE 1% agarose gel, gel extracted and purified (according to the Gel Extraction kit protocol). Post digestion (section 2.2.1.3) these fragments were ligated in the above vectors, transformed into bacteria in either competent cells for expression (DE3 containing plasmid) or for further cloning and DNA work (DH5alpha). Cell cultures (5-10 ml) were grown in order to extract more DNA for further use (according to the mini or midi prep protocols), concentration determination (Nanodrop 2000) and sequencing.

The potential sites of CHMP7 MIM1 and MIM2 were generated using the recursive PCR method with codon modifications to improve amino acid expression levels in *E. coli*. These PCR products were incubated with Bam H1 and Eco R1 for one hour at 37°C in order for ligation into the required vector. Alternatively, ligation at 15°C overnight was also used with similar success.

The oligonucleotides designed for CHMP fragments did not contain a stop codon. Therefore, fragments ligated into the pHis or pHis.trx contain an extra 3 residues and fragments ligated into the GST vector contain an extra 13 residues.

2.2.1.2 DNA amplification by the Polymerase Chain Reaction (PCR) and recursive PCR

PCR allows the amplification of a specific region within a DNA sequence defined by the design of 3' and 5' primers. Primers were designed to be between14-29 base pairs long, 50-65% GC% content, between 58-64°C melting temperature and always starting and finishing with either a G or a C. The amount of DNA added to each PCR reaction varied across constructs and the volume of water adjusted accordingly. All PCR and recursive PCR was performed using a Techne Genius Thermal Cycler. For each PCR and recursive PCR reaction the following found in table 5 was prepared.

PCR reaction			Recursive PCR reaction		
X µl 2-5ng DNA 1 µl primer 3' (100pMol/ µl) 1 µl primer 5' (100pMol/ul) 8 µl dNTP mix (each 5 µM) 5 µl PCR buffer Y µl MilliQ H_2O 0.5 µl Taq DNA polymerase			1 µl per inner primers (50ng) 1 µl Outer primer 3' (100pMol/µl) 1 µl Outer primer 5' (100pMol/µl) 8 µl dNTP mix (each 5 µM) 10 µl PCR buffer 77.5 µl MilliQ H_2O 0.5µl Taq DNA polymerase		
50 µl total volume			**100 µl total volume**		
Temp (°C)	Time (min)	Cycles	Temp (°C)	Time (min)	Cycles
95	0.30	25	96	1.00	1
55	1.00		96	0.15	25
68	6.00		60	0.15	
68	3.00	1	72	0.15	
4	hold		4	hold	

Table 5 Outline of the PCR and recursive PCR reactions used, plus the general programmes used on the thermal cycler. For normal PCR the final step of the cycle (68°C for 6 minutes) is a variable step depending on the fragment to be amplified. The temperature varied to suit the polymerase enzyme used, usually between 68-72°C and the time varied according to 1 minute per kb of product.

Codon optimisation was carried out by changing codons in the sequence to those seen by Dong et al to increase expression in *E. coli* over 3 hours[91]. (see appendix 5 for codon optimisations)

2.2.1.3 DNA digestion and extraction

DNA fragments were treated for a ligation reaction by first digesting with restriction enzymes, BamH1 (GGATCC) and EcoR1 (GAATTC) for 1 hour at 37°C.

DNA digestion
X µl 1-3 µg DNA 10 µl reaction buffer (specific to enzyme used) 3 µl Bam H1 3 µl Eco R1 Y µl MilliQ H_2O
100 µl total volume

The products of the digestion reaction were analysed and separated using a TAE- 1% agarose gel (plus 8 µl ethidium bromide per 10 ml) and run in 1x TAE (40 mM Tris-Acetate, 1 mM EDTA).

Samples were mixed with DNA loading buffer before loading. Electrophoresis was conducted using constant voltage between 50-100V (Biorad). The gel was visualised under UV light (UVP Bio-imaging) and correct weight bands extracted from the gel using a sterile scalpel cleaned between incisions with 70% ethanol. The extracted gel sections were then put through a gel extraction kit, following the protocol provided by Qiagen. An aliquot of the extracted DNA was run on a second TAE-agarose gel to determine purity and the concentration determined using the Nanodrop 2000 spectrophotometer.

2.2.1.4 Ligation of DNA insert into vectors

BamH1/EcoR1 digested and purified DNA was inserted into an appropriate vector by overnight incubation at 15°C using the following reaction mix, with a 4:1 molar ratio of insert:vector.

DNA ligation
X µl insert DNA Y µl vector DNA 2.5 µl ligation buffer (supplied with enzyme) Z µl MilliQ H_2O 1.5 µl T4 DNA ligase
25 µl total volume

2.2.1.5 Preparation of competent cells

Competent cells were prepared *via* the Inoue method for 'Ultra-competent cells' laid out by Sambrook and Russell[92] (Molecular Cloning Vol.1). JM109(DE3) cells were streaked onto an agar plate free from antibiotic and incubated over night at 37°C. From this plate, a single colony was selected and grown in 25ml of SOB medium for 6-8 hours at 37°C with shaking (200rpm). Between 2 and 4ml of this culture was used to inoculate 250 ml of SOB and incubated overnight at 18°C with shaking (150rpm). When the OD at 600nm reached approximately 0.55 the culture was transferred to an ice bath for 10 minutes. The cooled culture was then centrifuged at 4°C with 4000rpm (5810R centrifuge, eppendorf). The supernatant was discarded and the resulting pellet resuspended gently in 80ml ice-cold Inoue buffer. The cells were centrifuged again under the same conditions and the resulting pellet resuspended gently in 20ml ice-cold Inoue buffer. To this, 1.5ml of dimethyl sulfoxide (DMSO) was added and mixed by swirling and left in and ice bath for a further 10 minutes. The bacterial suspension was snap frozen in liquid nitrogen using sterile pre-chilled eppendorfs. The frozen aliquots, of 100µl, were immediately stored at -80°C.

Inoue buffer	SOB medium /L
55 mM $MnCl.4H_2O$ 15 mM $CaCl_2.2H_2O$ 250 mM KCl 10 mM PIPES* (0.5M pH 6.7) MilliQ H_2O	20g Tryptone 5g Yeast Extract 0.59g NaCl 2g $MgCl.6H_2O$ 0.2 KCl 10 ml $MgSO_4$ (1M)

*Piperazine-1, 2-bis[2-ethansulfonic acid

2.2.1.6 Transformations

An aliquot of competent cells were thawed by hand and transferred to an ice bath for 10 minutes. 1 µl of DNA was added and the contents mixed and left on ice for 30 minutes. When using DNA from a ligation reaction, 10-20 µl was used for the transformation. The cells were then heat shocked for 60 seconds at 42°C and immediately transferred back to an ice bath for 2 minutes. The cells underwent a recovery step (only kanamycin resistant cells) whereby 700 µl **SOC was mixed with the aliquot of cells and the incubated for 1 hr at 37°C. The cells were than centrifuged for 2 minutes at 3000rpm and the pellet resuspended in 100 µl SOC and transferred to an LB agar plate containing ampicillin. The suspension was spread on the plate using an ethanol sterilised glass spreader and the plate left to incubate inverted at 37°C overnight.

**SOC medium is the same as SOB, but with 20mM glucose added.

LB medium /L	2xYT medium /L
10g Tryptone 5g Yeast Extract 10g NaCl	20g Tryptone 5g Yeast Extract 2.5g NaCl

LB agar plates were made by the addition of 3.75 g agar to 250 ml LB media. Agar LB media was autoclaved (121°C, 15 minutes) and allowed to cool below 50°C before the addition of ampicillin or kanamycin as appropriate. Plates were then poured and allowed to set. Once set, plates were stored inverted in the dark at 4°C.

2.2.1.7 Mini and midi preparation of DNA

For mini-preparation of DNA, a single colony was selected from an agar plate and grown up in 10ml of LB or 2xYT media with antibiotic overnight at 37°C with shaking (200rpm). The bacteria were centrifuged at 4°C/4000rpm for 12 minutes and the supernatant discarded and the pellet put onto ice. From this point the protocol provided in the Qiagen Mini-prep kit was followed.

For midi-preparation of DNA, a single colony was selected from an agar plate and grown up in 100ml of LB or 2xYT media with antibiotic 37°C with shaking (200rpm). The bacteria were centrifuged at 4°C/4000rpm for 20 minutes and the supernatant discarded and the pellet put onto ice. From this point the protocol provided in the Macherey-Nagel Midi-prep kit was followed.

2.2.1.8 Glycerol stocks

In order to store transformed *E. coli* for longer than the shelf life of an agar plate, 20% glycerol stocks were made of each construct. 800µl from an overnight 10ml culture was mixed with 200µl of sterilised glycerol and stored at -80°C. Glycerol stocks were kept for no longer than one year and new ones made at this point.

2.2.2 Protein expression and purifications

A single colony was selected from an agar plate and grown up in 10 ml of LB or 2xYT media with antibiotic overnight at 37°C with shaking (200 rpm). This started culture was added to a 500 ml of sterile LB or 2xYT media and either grown at 37°C (reaching the correct OD between 4-6 hours) or 18°C (reaching the correct OD between 12-16 hours). Once at an OD_{600} of 0.8-1 the media was brought to

0.8mM IPTG (Calbiochem) for 3-6 hours in order to induce expression. Progress of this expression was monitored using SDS-PAGE. Cultures were harvested by centrifugation for 30 minutes at 8000 rpm, 4°C (rotor ID JLA 9.1, Beckman Coulter). Cell pellets were stored at -80°C.

Auto-inducing media was to improve protein expression yields and solubility. The media is based on Studier's medium ZYM-5052[93].

Auto-Induction Medium /L
5g Yeast Extract 50 mM Na_2HPO_4 50 mM KH_2PO_4 50 mM NH_4Cl 5 mM Na_2SO_4 2 mM $MgSO_4$ (sterile filtered) 1M $CaCl_2$ 0.05 % glucose (sterile filtered) 0.5 % glycerol (sterile filtered) 1 % lactose (sterile filtered) trace metals (1000x stock) MIlliQ H_2O

Auto-inducing medium was used with a final concentration of 200 µg/ml ampicillin. This medium was used for constructs that expressed well under IPTG-expression and where a higher yield of protein was desirable. Protein expressions in auto-inducing medium were left over 24 hours (200 rpm, 18°C).

2.2.2.1 Mini-detergent screening

A detergent screening was necessary to determine a method of improving the solubility of CHMP7. Detergents tested were 0.5% Brij-35, Tween-20, X-100 Triton, DDM (non ionic) and 0.6% Na NLS and 0.5% Na Cholate (ionic). 5mg/ml lysozyme was also tested. Protein present in pellet (insoluble) and supernatant (soluble) was determined by SDS PAGE. 0.5% X-100 Triton was chosen for use in successive buffers.

2.2.2.2 His_6 and His_6.Trx tagged protein purification

pET vector cell pellets were re-suspended in Buffer A.

Buffer A (p.H 7.9)	CHMP buffer A (p.H 7.9)
20 mM TRIS 500 mM NaCl 5 mM imidazole	20 mM TRIS 500 mM NaCl 5mM imidazole 6M urea 0.5% Triton X-100

Buffer B (p.H 7.9)	Buffer C (p.H 7.9)
20 mM TRIS 500 mM NaCl 60 mM imidazole	10 mM TRIS 250 mM NaCl 1M imidazole

For CHMP7 and other full length CHMP constructs (apart from CHMP1A), 6M urea and 0.5% X-100 Triton* was added to Buffer A with protease inhibitor (Roche). Re-suspended pellets were lysed by sonication on ice (15 second bursts with 1 minute cooling four times). Bacterial lysates were centrifuged at 40,000g for 25 minutes. Clarified bacterial lysate were bound to chelating sepharose charged with 50 mM $NiSO_4$ for 30 min-1 hour at RT (4°C for VPS4B) (Amersham BioScience, GE healthcare). For the charged Ni^{2+} column, unbound material was removed with washes of Buffer A followed by further washes in Buffer B. Mixtures of buffer A, buffer B and buffer C were made to form the gradient washes –equating to 20 mM, 30 mM and 100 mM imidazole.

Proteins were eluted in buffer C (a final elution of Buffer C plus 6M urea was used for CHMP-based constructs –full length and the C terminus). Fractions containing protein were analysed by SDS PAGE. If present in the urea elution fraction, consecutive rounds of dialysis at 4°C (each with a lower concentration of urea) were carried out to remove the urea. Protein concentration was determined using UV-Vis A_{280} (Cary spectrometer) and the protein's extinction coefficient (see table 1). Protein was further purified with anion exchange chromatography

(Q Sepharose, 1ml/min, AKTA prime) using Low Salt (10 mM TRIS, pH 7.9) to High Salt Buffers (10 mM TRIS, 1M NaCl, pH 7.9). VPS4B was further purified instead with gel filtration chromatography, G25 Sephadex, 0.5ml/min, AKTA prime.

A circular dichroism (CD) spectrum was also conducted between 190-260nm at 25 °C to determine if the protein was still correctly folded (JASCO J-810 spectropolarimeter) -His tagged or untagged proteins only. See appendix 6 for these conditions.

The His_6 thioredoxin tag was removed by incubation at RT with 20 U Thrombin (1 U/1µL, Merck) and 2.5mM $CaCl_2$ in 2ml of tagged protein sample. This reaction was monitored by SDS PAGE for optimum incubation time (approx. 75 minutes for CHMP7 full length and C term, but generally variable) before scaling up the digestion. Thrombin was removed by incubation with 1 ml benzamidine beads (Amersham BioScience, GE Healthcare) for 30 minutes with shaking. This mixture was centrifuged and the supernatant loaded onto a second Ni^{2+}-charged chelating column to separate the protein from the cleaved tag. Protease inhibitor was added after cleavage of the affinity tag.

2.2.2.3 GST tagged protein purification

GST proteins, from pGEX vector cell pellets, were re-suspended in lysis buffer.

PBS (p.H 7.4)	Lysis buffer (pH 7.4)
140 mM NaCl 2.7 mM KCl 10 mM Na_2HPO_4 1.8 mM KH_2PO_4	PBS 5% glycerol 2 mM $CaCl_2$ 0.5% Triton X-100 5 mM BME*

*β-mercaptoenthanol

Re-suspended protein was incubated for 20 minutes at 4°C with 0.2 mg/ml lysozyme and 7.5µl benzonase per 10ml of lysis Buffer. This was next lysed on ice under mild sonification conditions (5 second bursts with 1 minute cooling two

times). The mixture was then centrifuged for 30 minutes at 40000g, 4°C and the supernatant left on ice until needed. At this point, protease inhibitor was also added. The protein was loaded slowly to the column and left to bind to the glutathione sepharose (Amersham Biosciences, GE healthcare) for 30 minutes at RT. Unbound material was removed with extensive washes of PBS. The protein was eluted with GST-elution buffer (20 mM TRIS, 30 mM L-glutathione, 150 mM NaCl, ph 7.4). At this point, protein was either purified by further anion exchange chromatography (AEC, see for His-tagged proteins) or buffered exchanged to remove the glutathione and bound back to the glutathione sepharose in order to perform investigative GST and His pull down assays.

2.2.2.4 Pull down assays

To establish initial protein-protein interactions between CHMP7 and other members of the ESCRT machinery, assays were performed using 100 µl of either a Nickel-NTA agarose (Qiagen) or glutathione sepharose slurry depending on the tag of the bait protein. Purified protein was incubated with the resin at RT with rocking for 30- 60 minutes. These assays occurred in the buffer the protein was purified in, normally 20 mM TRIS, 150 mM NaCl, 5% glycerol, 2 mM $CaCl_2$ pH 7.4 or PBS. In the case of VPS4B, these crude assays were performed in the presence and absence of 10 mM ATP and 4 mM $MgCl_2$ in a total volume of 400 µl. The resin was then washed three times with the appropriate buffer (PBS or buffer A) and between 20 and 60 µM of a purified prey protein was added and incubated for a further 60 minutes with rocking. This mix was washed again three times. All washes and a sample of the resin was added to 2x SDS-PAGE sample buffer and boiled at 96°C for 10 minutes and analysed by SDS-PAGE.

ATP was prepared by dissolving 0.3g of adenosine 5'-triphosphate (ATP) disodium salt in 10ml of sterile Milli-Q water and the pH made up to 7 using 1M KOH. The exact concentration was determined using 15400 $M^{-1}cm^{-1}$ as the extinction coefficient at 260 nm.

2.2.2.5 SDS-polyacrylamide gel electrophoresis (SDS-PAGE)

Protein samples were separated for analysis *via* SDS-PAGE using the buffer system of Laemmli and the protocol described by Sambrook and Russell using BioRad apparatus[94]. Gels were generally made as 5% stacking layer and between 10-15% separating layer, in less otherwise stated, and ran at 200V for between 30-60 minutes in a TRIS-Glycine-SDS buffer (National Diagnostics). All samples were boiled for 2-5 minutes prior to loading in 2x sample buffer[92]. Protein was visualised with Coomassie blue stain (50% methanol, 10 % glacial acetic acid and 0.1% Coomassie brilliant blue R-250) and destained with a solution of 10% glacial acetic acid and 30% methanol.

2.2.3 Cell biology

2.2.3.1 Culture of eukaryotic cells

All cell lines used were grown in 75 cm^2 flasks in 10 ml of supplemented DMEM (as described in the materials section) at 37°C with 5% CO_2.

Cells were sub-cultured between 60-80% confluency, for this the medium was removed and the cells washed three times with PBS. The cells were lysed by incubation with 1-3 ml trypsin EDTA-free for 5 minutes at RT and re-suspended with 10 ml of prepared DMEM medium and mixed. Cells were then diluted accordingly to a new flask with fresh media (1:5-1:20).

For experiments, cells were counted using a haemocytometer (Beckmen Coulter) with 0.25-0.5x10^4 cells per 1 ml used a standard. This plating density was chosen to give a final degree of confluency that allowed recognition of small structures such as midbodies and nuclear bodies by IF. For the purpose of western blotting and qPCR a higher cell number could be used. An antibiotic-free version of the DMEM media was used for transient transfection and RNAi experiments. When using a 12-well plate, 1 ml was added per well (i.e. 0.5x10^4 cell density). 2 ml was

added to a 6-well plate (i.e. $1x10^4$ cell density) and 5 ml to a 10 cm diameter dish (i.e. $2.5x10^4$ cell density).

2.2.3.2 Transient transfection of eukaryotic cells

Cells were transfected with DNA and JetPEI (Polyplus transfection) for 24 hours. These cells were plated 12-16 hours before transfection either on 12 mM cover slips (1 coverslip per well, 12-well plate) or in a 6-well plate (2-3 coverslips per well) or 10 cm dishes. Before transfection the medium was changed for fresh antibiotic free DMEM. For each transfection, a total of 2µg DNA was used and a carrier bacterial plasmid (pBluescript, pBS) was used to ensure the total DNA content was always the same.

Solution one	Solution two
X µl DNA Y µl pBS* (empty vector) 100 µl NaCl (150 mM)	4 µl jetPEI** 50µl NaCl (150 mM)

*amount used dependent on DNA concentration -made up to 2 µg

** linear polyethylenimine

Both solutions were mixed well before being added together. This solution was incubated for 30 minutes at RT in order to allow jetPEI-DNA complexes to form. These positive complexes interact at the cell surface and are internalised by endocytosis and delivered to endosomes. The jetPEI protects the DNA from degradation allowing it to eventually be transported to the nucleus to begin transcription of the desired DNA. 100 µl per 1 ml of this jetPEI/DNA solution was added to cells and mixed gently. Cells were fixed after 24 hours. The same protocol was used for all standard transfections, and also in the case of double transfections and transfections that followed RNAi knockdown.

Cell lines that stably expressed CHMP7-myc and CHMP4B-myc (pcDNA 5/FRT from the FlpIn system, Invitrogen) were also used, kindly gifted by Prof. P. Woodman (appendix 3). Protein expression is controlled by tetracycline activation. Doxycyclin, as a derivative of tetracycline, was used to induce expression. Between 20 and 200 ng doxycyclin was used. Hygromycin B is the

selection agent for the pcDNA5/FRT (Flp recombination target) expression plasmid, upon each cell passage 500 µg/ml was added to the fresh cell media.

2.2.3.3 RNAi depletion in eukaryotic cells

Cells to undergo RNAi knockdown were plated 16-24 hours before knockdown. These cells were treated with interferin (optimised to 1µl/ml, Polyplus) and 5nM siRNA pre-mixed in opti-mem solution. To knockdown a particular protein, 'On-Target Plus' oligos (Dharmacon) targeting the appropriate RNA was reconstituted as 20 µM stocks (made up with siRNA buffer and RNase free water, Dharmacon). A random 'non-targeting' oligo was used as negative control, with either TSG101 siRNA or VPS4A and B siRNA acting as a positive control (see appendix 4 for RNAi oligos).

Treated cells were incubated for 10 minutes at RT before returning to the incubator and left between 48 and 72 hours. Cells were analysed for the presence of phenotypes by IF and cell scoring and the efficacy of the knockdown checked by qPCR or western blotting.

RNAi knockdowns were carried out using 5nM of each oligo –including all isoforms, unless stated otherwise. VPS4A and B were initially depleted with 5 nM also. However, using 3 nM appeared to improve the number of surviving cells. Also, in the case of the VPS4A and B knockdown, it was found that giving cells longer to grow before knockdown improved the number of surviving cells (allowing easier scoring).

2.2.3.4 Cell cycle synchronisation

Cells were synchronised in S phase *via* a double thymidine block[95] (2mM) whereby cells were first blocked for 12 hours, released for 9 hours in antibiotic free DMEM and blocked a second time with 2 mM thymidine for 12 hours and released again. Cells were then fixed at intervals from 0 hours up to 10hours after the second release -with cell progressing through G2 and mitotic phase around 6 hours after the second release.

2.2.3.5 Immunofluorescence

Cells were cultured on 12-mM diameter cover slips for between 48 and 72 hours. Fixation was done with either 3% paraformaldehyde for 20 minutes at RT or in methanol at -20°C for 10 minutes. The cover slips were washed with cold PBS three times before being placed in a quencher solution to quench the aldehyde groups. This solution was 5 drops of a stock solution (50 mM Tris, 1 M glycine, pH 7.5) in PBS. The cover slips were washed again 3 times with cold PBS before being placed in PBS with 0.1% X-100 Triton for permeabilisation. The cover slips remained in this solution for approximately 3 minutes before being washed 3 times in PBS. New antibodies were trialed for the appropriate fixation method to yield the best IF images, this included trying different detergents in the permeabilisation step.

Cover slips were incubated with primary antibody for 20 minutes at RT in the dark. Cover slips were washed in PBS three or more times over a 15 minute interval and then incubated with the appropriate secondary antibody and DAPI for 20 minutes at RT in the dark. The slips were washed with PBS repeatedly over a 15 minute interval and finally washed in distilled water. Cover slips were mounted to slides with ProLong® gold (Invitrogen). Images and observations were viewed and made using an Olympus BX-61 microscope (x60 objective, pixel to micron ratio 0.1075, oil) and images acquired using a CoolSNAP HQ CCD camera (Photometrics, Tucson with *MetaMorph* software). Also, an Olympus DeltaVision microscope (x60 or x40 objective, oil) was used, with images acquired and deconvoluted using DeltaVision SoftWoRx software. Deltavision files retain all scaling and acquisition parameters in the file properties. A minimum of 100 cells was scored per treatment, with each treatment being repeated and scored three times (unless otherwise stated). Cells were quantified for nuclear defects by staining with DAPI and scored as having multiple, crescent, micro or abnormal nuclei. The presence of midbodies was scored using an anti-tubulin antibody (DM1A). The occurrence of nuclear CHMPs was scored using the custom anti-CHMP7 sheep antibody and Proteintech rabbit anti-CHMP antibodies for CHMP4B and CHMP1B. DAPI was used in order locate nuclei, by focusing through all planes of the DAPI channel nuclear CHMPs would be counted.

2.2.3.6 Western blotting

Cells cultured on the surface of a 10cm dish were washed with PBS and lysed by incubation in PBS with 1% x-100 Triton for 15 minutes at 4°C.The contents were removed from the surface of the dish, using a cell scraper, and pipetted into a sterile eppendorf and protease inhibitor added. This was centrifuged at 2000g for 30 minutes at 4°C. The supernatant was saved and frozen at -20°C. The concentration of this protein was measured using a BCA protein assay kit (Thermo Scientific). Protein samples were run on an SDS PAGE gel at 300V and 30 amps for 40 minutes. Once run, this gel was placed in transfer buffer. (25mM Tris-HCl, 0.1% SDS)

A polyvinylidene fluoride (PVDF) membrane (Millipore) was prepared by 30 second activation in methanol and then placed in transfer buffer. This membrane and the gel were sandwiched between 4 sections of filter paper and the air removed with a roller before enclosing in the western blot cartridge and submerged with transfer buffer and run at 350mA for 1 hour with tubing attached for cooling with cold water (Amersham Biosciences). The PVDF membrane was incubated overnight at 4°C with rocking in TBS with 10% blocking solution, 0.5% Tween-20 and primary antibody. The membrane was washed with TBS-Tween blocking solution for 15-30 minutes and also a 10 minute wash with water. The membrane was then incubated with rocking in the TBS-Tween blocking solution with the secondary antibody (between 1/2000-1/8000) and 0.002% SDS at RT for 1 hour in the dark. The membrane was washed extensively with TBS-Tween block and water for 30-60 minutes before scanning using a LICOR scanner with Odyssey Sa software. A mouse anti-importin beta antibody (Millipore) or mouse anti-TAT1 antibody (house generated) was used as a loading control for each blot.

2.2.3.7 Quantitative PCR

Probes for qPCR were designed using Roche Applied Science's universal probe library assay design centre and checked using nucleotide BLAST on NCBI. RNA was extracted from cultured cells by the protocol laid out by Agilent Technologies under sterile conditions, this was stored at -20°C for up to one month. First strand

cDNA synthesis, using random primers, was carried out with AffinityScript qPCR cDNA synthesis kit with protocol provided (Agilent Technogies, Stratagene). The samples of cDNA were stored at -20°C for further use.

The cDNA samples were prepared for qPCR with the addition of the appropriate primers and SYBR® Green JumpStart™ *Taq* ReadyMix™. Primer mix was prepared by 1/100 dilution of both primers in nuclease free water. Samples were covered with optical tape and DNA amplification measured using Opticon monitor software (Biorad). Protocol for PCR used were: initial denaturation at 94°C for 2 minutes, followed by 40 cycles of denaturation at 94°C for 15 seconds, annealing at 53.7°C for 1 min, 72°C for 60 sec. Tata Binding Protein (TBP) was used as a loading control for the qPCR. Designed primer pairs were supplied by Eurgentec.

2.2.3.8 Tryptophan fluorescence quenching titrations

The fluorescence emission spectrum of 100 nM His_6-UBC9 in PBS was measured using an excitation wavelength at 270nm (Spex FluoroMax) using FluorEssence software. The excitation and emission slit widths were set at 1 mm, giving a spectral bandwidth of 4.25 nm. The data interval was 0.5 nm and the integration time was 2.0 seconds. Samples were prepared in a 1 cm path length quartz cuvette (Hellma) and the emission measured at 348 nm. Synthetic CHMP4B peptide* (Ac-PNVPSIALPSKPAKKKEEED-COOH, Genscript) corresponding to resides 192-211 was added sequentially to the UBC9 sample from 1 nM to 200 nm. These titrations were conducted at RT and repeated three times in PBS. As a control the peptide was also titrated against GST with no effect on the fluorescence emission.

*The synthetic peptide was resuspended in water with 5% methanol and 10% DMSO.

2.2.3.9 Wheat germ *in-vitro* translation

In order to verify the specificity of the CHMP antibodies used in all western blotting and IF, all the CHMP isoforms were expressed by in vitro translation. This method uses wheat germ extract (a solution that contains all the cellular

components for protein synthesis, with the rest of the cell debris and components removed).

This protocol requires the addition of suitable mRNA to begin translation. In order to obtain mRNA, myc-tagged CHMP constructs underwent PCR to isolate the myc-CHMP fragment from the vector –this was achieved using the PCR protocol below. 1-2 ng of template DNA is required, but generally 0.5 µl of template DNA is enough without needing to calculate exact amounts.

PCR
0.5 µl template DNA 10 µl PCR buffer (+Mg) 10 µl dNTPs (2.5mM) 5 µl FWD CMV primer (10µM) 0.5 REV primer (100p/mol) 72 µl MilliQ H2O 2 µl PWO polymerase
100 µl total volume

Use of the FWD CMV primer allows a region upstream of the template to be included in the PCR. This region includes a T7 promoter sequence required for transcription. This added 300bp to all fragments, allowing appropriate extension times to be calculated for the PCR cycle (myc tag -500bp, CHMP7 -1200bp and the rest of the CHMPs -600bp), allowing 2 minutes of extension time per Kb. The PCR was carried out for 30 cycles of 95°C for 1 minute followed by 55°C annealing for the calculated extension time (annealing and extension were combined due to high efficiency of the polymerase used). The PCR product was treated with DPN1 (to remove template DNA) for 2-3 hours at 37°C. This was followed by PCR clean up using the kit supplied by Machery-Nagel, following their protocol. At this stage the DNA was checked on a 1% agarose gel to determine the success of the PCR reaction. The mRNA was synthesized using the clean DNA by incubating for 2 hours at 37°C degrees in the following transcription reaction.

Transcription
45 µl RNase free H_2O 20 µl 5xtranscription buffer 10 µl DTT (10 mM) 5 µl 7GG RNA cap (10 mM) 4 µl rNTPs (25 mM) 9.5 µl DNA 2.5 µl RNasin 4 µl T7 RNA polymerase
100 µl total volume

Isolated RNA was purified using the RNeasy mini kit (Quigen) using the protocol provided. RNA was stored at -20°C until needed.

The *in-vitro* translation (Promega, kit stored at -80°C) was carried out at 25°C for 1-2 hours using the following translation reaction.

Translation
2 µl RNase free H_2O 12.5 µl wheat germ extract 2 µl amino acids (-methionine) 1mM 2 µl [35S] methionine (1000Ci/mmol) 1.5 µl Potassium acetate(1M) 2 µl mRNA
22 µl total volume

Translation was stopped by the addition of 2 µl puromycin (20 mM) and left for 10 minutes before adding 1.1 µl RNase A (10mg/ml) and incubated at 37°C for a further 5 minutes. This was centrifuged for 2 minutes at 12 000g and the supernatant made up with SDS loading buffer. From this point the protocol for western blotting (from the SDS PAGE step) was followed.

CHAPTER 3 STRUCTURE AND FUNCTION OF CHMP7

3.1 Introduction

3.1.1 Background

Since the inclusion of CHMP7 in the ESCRT family in 2006, little evidence has followed to resolve its function within the ESCRT-III complex or as an auxiliary protein in ESCRT action[46]. This chapter focuses on using a combination of bioinformatics tools and biochemical methods to identify functional motifs within CHMP7 and reveal potential interaction partners.

The ESCRT family of complexes is still relatively 'young', only being discovered in 2001[25]. Yet after more than a decade of interest and research, the ESCRTs are still largely shrouded in ambiguity.

3.1.1.1 Established CHMP7 interaction partners:

CHMP4 isoforms

CHMP7 is routinely regarded as an ESCRT-III subunit, yet its only established interaction in this family of proteins is with CHMP4.

CHMP4 is the core component of the ESCRT-III complex and is vital in the MVB pathway and cytokinesis. In mammals there are three isoforms of CHMP4: - CHMP4A, B and C. These isoforms correspond to one CHMP4 in yeast referred as VPS32 or SNF7. Mammalian CHMP4 isoforms are the most abundant physiologically and interact with all the other CHMP subunits, plus a wide range

of accessory proteins. In yeast, the CHMP4 homolog is the only ESCRT-III subunit absolutely required for severing of the ILV from the membrane[96].

These isoforms also display specificity by interacting exclusively with different accessory proteins. For example, CHMP4B interacts with ALIX, a key protein involved in viral budding and cytokinesis. CHMP4B also interacts with CEP55 a protein involved in cytokinesis, whereas CHMP4C interacts with borealin, a subunit of the chromosomal passenger complex (CPC)[96,97,98]. This interaction requires the phosphorylation of CHMP4 to inhibit abscission, adding a role in protection against genetic damage to the growing list of activities involving ESCRT proteins.

Evidence suggests that of these isoforms, CHMP4B is dominant. This was demonstrated by Carlton and Martin-Serrano who found that depletion of individual CHMP isoforms, 4A or 4C, did not inhibit HIV- release whereas 4B depletion did inhibit viral budding. In addition CHMP4A and 4C were dispensable for cytokinesis completion. Depletion of CHMP4C resulted in fewer observed midbodies though, which agrees with its interaction with the CPC and abscission timing[86].

The interaction between CHMP7 and CHMP4 isoforms occurs via the SNF7-like C terminal half of CHMP7[46]. As CHMP4 is the core component of the ESCRT-III complex it is perhaps unsurprising that CHMP7 would interact it. Due to the array of functions CHMP4 has been implicated in, this interaction wouldn't allow us to immediately narrow down or make any further assumptions regarding the function(s) of CHMP7. We hope to learn more about where CHMP7 fits in within the ESCRT machinery by establishing a network of protein-protein interactions centred around CHMP7.

3.1.2 Bioinformatic analysis

Similar amino acid sequences often result in similar structures for proteins and in turn related functions. This observation allows the design of algorithms that can draw upon masses of collated protein data to make comparisons and

predictions to a relatively high accuracy. In order to make predictions on the secondary structure of CHMP7 I made use of Jpred, a server that works by generating multiple sequence alignments as 'input data' for a standardised combination of six different structure prediction algorithms[99,100]. The program assigns each amino acid in the given sequence a letter representing secondary structure, either alpha helix, beta sheet or random coil.

Since CHMP proteins are known for their coiled-coil content; I used a further algorithm known as COILS to predict the probability of coiled coil formation. COILS works by comparing a sequence to a large database of known two-stranded coiled coils and calculates a similarity score. This score is compared against the scores obtained by non-coiled coil and coiled-coil proteins in order to derive a probability[101]. Lastly, protein threading or 'fold threading' was used to make predictions on tertiary structure –primarily for the N terminal of CHMP7 (1-232), which contains no homology or sequence similarity with any known protein domain. Protein threading is a method of protein modelling based on protein structure predictions. It is used mainly for proteins that have no homologous protein structure deposited in the protein data bank (PDB), such as CHMP7. These programs statistically evaluate and compare the structures in the data bank with the protein sequence to be modelled. The program can then align each amino acid of the sequence to structural templates until it finds the 'best fit'. To some extent this method relies on the fact that relatively few 'new' structural folds have been added to the PDB in recent years with most being added similar to existing ones.

3.2 Results

3.2.1 Secondary and tertiary structure predictions

Horii et al hypothesised that CHMP7 structure is comprised of tandem SNF7 domains, where the N terminal half domain was suggested as a 'SNF7-related' domain. The C terminal SNF7 has the highest homology with CHMP6, whereas the SNF7-related domain in the N terminal has low homology to

CHMP4B. Whilst the C terminal domain is necessary for CHMP4 binding there is no known interaction between any ESCRT subunit and the proposed SNF7-related N terminal domain[46]. The results of the Jpred prediction (figure 1) indicate that the presence of an SNF7-related domain in the N terminal half is unlikely. The N terminal domain contains a mixture of short beta sheets and alpha helices and is not predicted to contain any coiled coil regions. Taken together, these data indicate that the role of the N terminal lies away from the classical functions of an ESCRT protein and may act as a bridge between a new subset of proteins and the ESCRT machinery. CHMP7 is highly conserved across eukaryotes, but unlike the other CHMPs it has no known equivalent in prokaryotes. This could indicate that CHMP7 has evolved to provide a function not necessary in prokarya and likely to involve the N terminal domain. CHMP7 may play more of a regulatory role (such as CHMP1 and 5) given that in yeast only the proteins equivalent to CHMP2, 3, 4 and 6 are critical for the MVB pathway to function. The presence of isoforms (in the case of CHMP1, 2 and 4) already indicates the processes and functions of the ESCRT-III complex in mammals is far more complex than in simpler organisms.

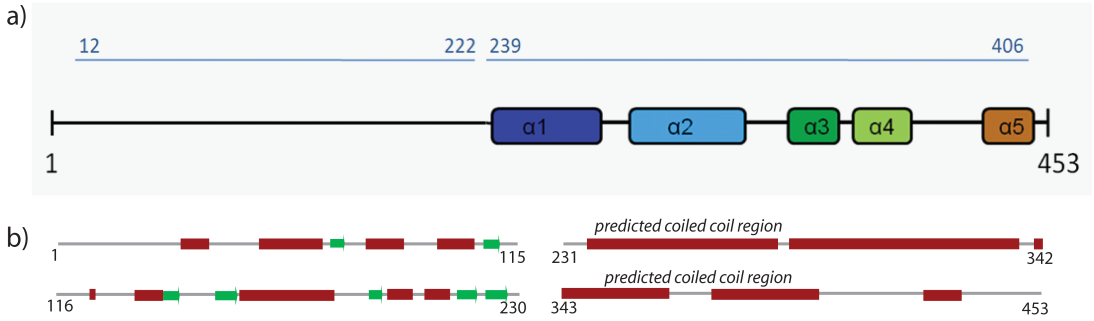

Figure 1 a) predicted schematic of CHMP7 containing the helical regions that form the SNF7 domain. b) secondary structure predicted by Jpred. The green arrows indicate regions of beta sheets, whilst the red blocks represent regions of alpha helices. The grey line represents flexible areas of random coil. Regions with a high probability of forming coiled coils are labeled –these were found only in the 'SNF7' C terminal half of CHMP7 between residues 240-300 and 350-400. Amino acid sequence used was from UniProtKB (accession number Q8WUX9).

Based on the secondary structure predictions, the tertiary structure of the CHMP7 N terminal should differ greatly from a SNF7-like domain. The SNF7 domain of CHMP3 is the only ESCRT-III with a crystal structure determined and this allows it to serve as a template (see figure 7 from chapter one, PDB 3FRT). The tertiary structure was predicted using a combination of two protein threading servers for comparison purposes, Phyre and LOMETS[102, 103]. In both cases, only the N terminal sequence of CHMP7 was run through the servers in order to generate a model unbiased by the presence of the C terminal SNF7 domain. To correctly identify the boundary between the N and C terminal CHMP7 domains, a combination of two experimental observations were used. Firstly, CHMP7 position 232 contains a serine residue flanked by a proline -this sequence is highly predicted to be phosphorylated by NetPhos v2.0[104]. Secondly, the first predicted helix of the C terminal SNF7 domain begins from residue 240. Therefore, we define the N-terminal domain of CHMP7 to run between residues 1 and 232, while the C terminal SNF7 is comprised between residues 240 and 453.

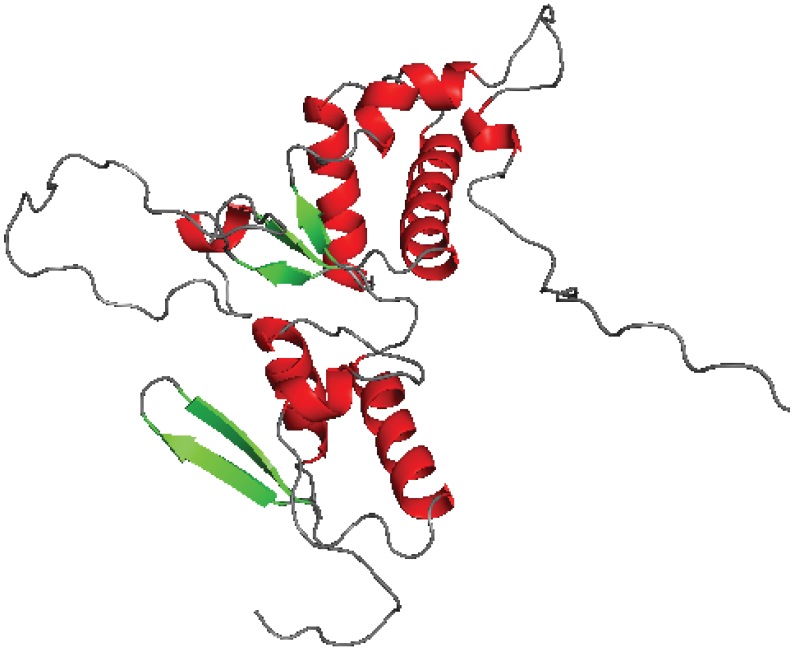

Figure 2 Predicted 3D model of the CHMP7 N terminal half using protein threading from MUSTER through the LOMETS server -showing a double winged helix motif. The green arrows represent beta sheets and the red represent alpha helixes.

Protein threading results indicated that CHMP7 1-232 may adopt a double winged helix domain, i.e. two smaller winged motifs that emulate each other roughly between 1-110 and 110-220 (figure 2). The LOMETS prediction is also supported by Phyre, which predicts two winged helix domains in this region. These winged helix domains are similar to ones found in the ESCRT-II subunits VPS36 (EAP45), VPS22 (EAP30) and VPS25 (EAP20)[20]. In fact, the entire core of the ESCRT-II complex is comprised of repeating winged-helices (8 in total). It is through these winged helices that the ESCRT-II subunits interact with each other. The recruitment of ESCRT-III by ESCRT-II in yeast is through VPS25 and VPS20 (CHMP6). This interaction increases both of their affinities for the membrane, providing a stable site for further recruitment of ESCRT-III subunits. These observed interactions (by pull down assays) have been replicated in humans (EAP20/CHMP6 interaction) by yeast two hybrid assay and immunoprecipitation[32, 105]. CHMP7 could act as a second means of communication between the ESCRT-II and -III complexes. The winged helices of the ESCRT-II subunits are all occupied in the formation of the ESCRT-II complex. Therefore CHMP7 could act as a signal to initiate disassembly of the ESCRT-II complex once the ESCRT-III lattice is fully dismantled.

By multiple sequence alignment Horii et al concluded that the SNF7 domain of CHMP7 was most similar to CHMP6[46]. For this reason they included EAP20 in their yeast two hybrid assays, but found no interaction between CHMP7 and any of the three subunits –the positive interaction between CHMP6 and ESCRT-II subunits acted as a positive control. A drawback of yeast two hybrid assays, which may mask positive interactions, is that some interactions rely on posttranslational modifications which do not occur in yeast cells. Phosphorylation is a common example of this and, as previously mentioned, is predicted in CHMP7 at serine residues most notably at position 232. Another noteworthy point is that the conditions used in their assays were based on those yielding a positive interaction between CHMP6 and EAP20. Here, we are proposing a potential interaction between CHMP7 with an ESCRT-II subunit through their winged helix domains. This is a different mode of binding than between CHMP6 (which binds through a motif found in the

coiled coil region of the 1st and 2nd alpha helix) and may require different conditions.

The winged-helix domain is a common feature of transcription factors[106]. The domain contains three helices that form next to a small beta sheet comprised of three anti-parallel beta strands. This domain is a common DNA binding domain, where normally the 3rd helix fits into the minor groove of DNA. Another common feature of a winged helix domain is an exposed patch of hydrophobic residues that is often the site of protein-protein interactions. The possibility of a DNA binding domain in the N terminal, suggests CHMP7 may have some function within the nucleus or during mitosis before the nuclear envelope reforms. This could align the function of CHMP7 closer to that of regulatory CHMP1 (which plays a minor role in ILV formation).

CHMP1 contains a nuclear localisation signal (NLS) and has been implicated in gene silencing and cell cycle regulation[43,87]. The alternative, and lesser used, name for the CHMPs (Chromatin modifying proteins) comes from results observing CHMP1 encapsulating regions of chromatin. Multiple sequence alignment from the Clustal Omega program[107] was used to compare the NLS from the CHMP1 with CHMP7. No localisation signal was found in

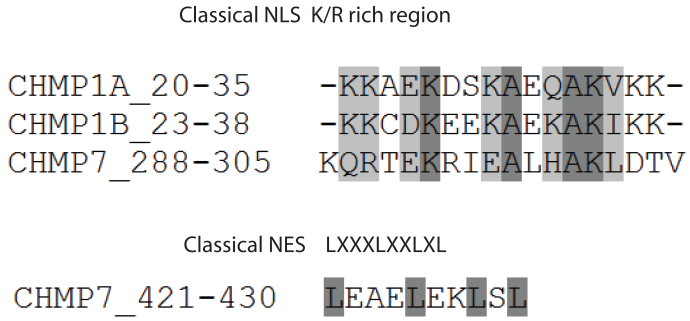

Figure 3 Multiple sequence alignment of the nuclear localisation signal (NLS) sequences from CHMP1A and CHMP1B with CHMP7. Below; the classical nuclear export signal motif, where X is any residue. A potential NES was found in the CHMP7 C terminal domain also.

the N terminal domain, but a potential one was found in the C terminal (figure 3).

NLS sequences normally contain short regions of positively charged residues, often lysine or arginine, whilst a classical NES sequence is leucine rich[108, 109, 110]. The CHMP7 C terminal could serve as a means for nuclear localisation. The presence of a double winged helix, a known DNA binding domain, could indicate some level of transcriptional control or function within the nucleus. The ability to maintain and adapt the levels of protein expression across different cell types would agree with CHMP7 being present in higher order cells, i.e. not prokaryotes, where this level of control is necessary.

Potential CHMP7 activity in the nucleus will be continued in the following chapters.

3.2.2 Interactions between CHMP7 and ESCRT-III subunits

To firmly establish CHMP7 as a member of the ESCRT-III family, the possibility of interactions with other ESCRT-III subunits was explored. The interaction between the CHMP7 SNF7 domain and CHMP4 is the starting point from which to build this network (figure 4).

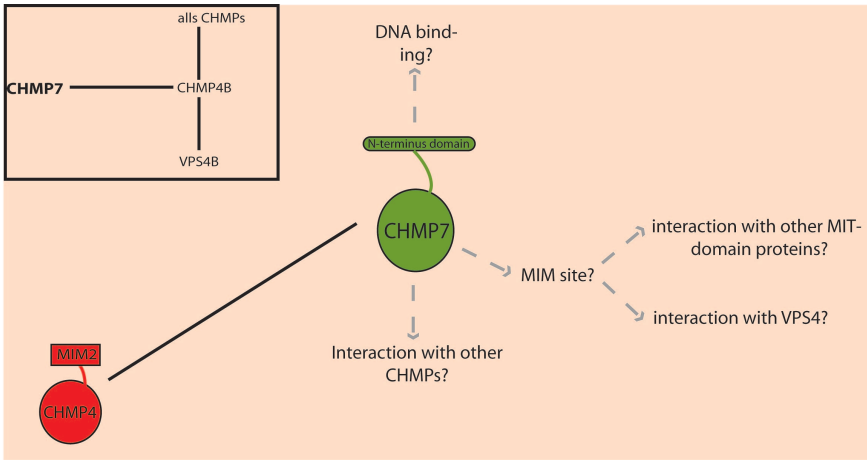

Figure 4 Basic scheme illustrating potential interaction partners for CHMP7 and the only established interaction with CHMP4

3.2.2.1 Optimisation of CHMP7 purification

CHMPs have proven difficult to purify, both across the literature and in this work. This is in part due to their tendency to interact with each other if present in high concentrations. If in their 'open' conformation they form filaments in solution and can aggregate heavily. In order to keep them from interacting high concentrations of NaCl can be used in the buffer –the salt ions disrupt interactions between the basic and acidic regions of SNF7 domain. Another issue can arise with the use of bacterial cells to overexpress a human protein, posttranslational modifications are absent and in this case, high concentrations of CHMP proteins are detrimental to bacterial cell growth. A compromise was reached between the temperature, concentration of IPTG used for induction and time left inducing. Low temperatures with a low concentration/ long induction period appeared most successful. Solubility tags, such as thioredoxin served to improve the solubility of CHMP7, together with ensuring the protein was kept dilute in all steps of the purification. Despite taking these measures, a thioredoxin tagged version of CHMP7 was largely insoluble. Protein purification in denaturing conditions was therefore the logical strategy to adopt, however protein was unable to be refolded on the column as it stuck to the resin. Consecutive rounds of dialysis, lowering the urea content gradually, allowed CHMP7 to refold slowly. At this stage, aggregation of the protein still occurred on occasion if the protein became too concentrated. Further problems with this construct also included long term storage as upon thawing (after snap freezing with liquid nitrogen) CHMP7 would aggregate. However, if experiments are able to be carried out directly after purification this full length CHMP7 construct remained soluble (<10 μM) for around 48 hours. Figure 5 shows that CHMP7 was able to refold correctly. The spectrum is characteristic of a protein containing alpha helices signified by the peaks at 208 nm and 222 nm.

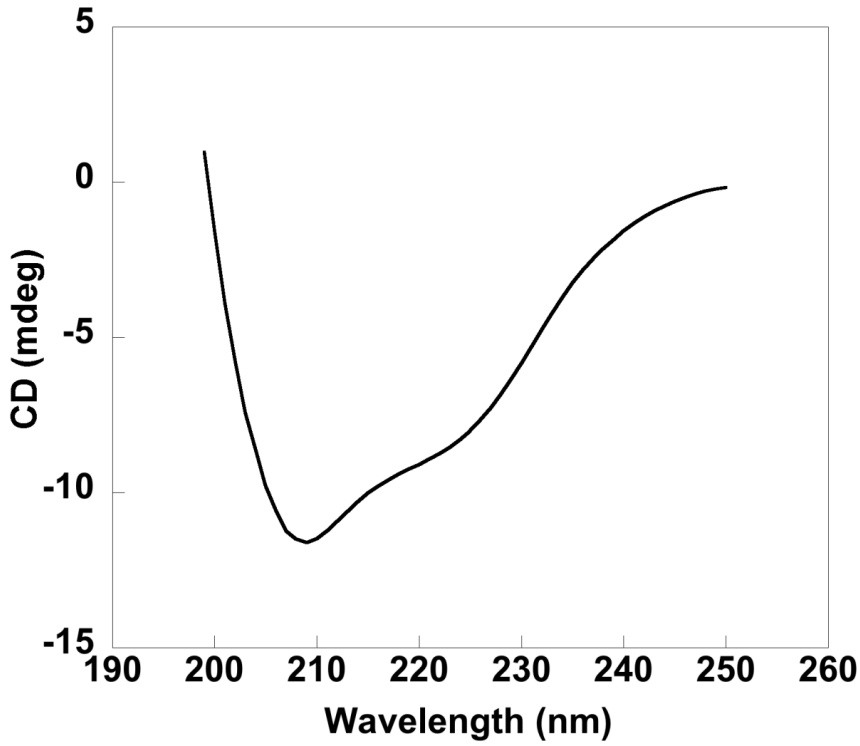

Figure 5 CD spectrum of His_6-CHMP7 displaying characteristic peaks indicative of alpha helical regions. Spectrum recorded at 25 ^{o}C using protein direct from buffer exchange in PBS, pH 7.4 (2-3 hours post purification). His-tagged protein sample was 9.45μM post buffer exchange and approximately 0.25 mg/ml was used for each CD spectrum. Spectrum collected between 260 to 190 nm.

A GST tagged CHMP7 construct was also tested for solubility, but the protein accumulated in inclusion bodies and required purification in non-denaturing conditions. A detergent screening showed a range of standard detergents improved solubility and 0.5% triton X 1-00 was selected for routine use, due largely to availability and expense compared to other detergents tested. The purification of GST-CHMP7 was also improved by the addition of 5% glycerol, 5 mM beta mercaptoethanol.

Since full length CHMP7 and CHMP4B showed a tendency to stick to resin in most of the tested purification conditions, we refrained from using them in pull down assays in order to avoid false positive results. To conduct pull down assays we decided to use fragments of CHMP proteins in order to avoid these issues. This also avoids the issue of the autoinhibitory conformation that CHMPs can adopt, which could mask interactions.

CHMP7 peptide fragments were designed based on regions of CHMP-CHMP interactions and VPS4 interaction, based on homology to motifs identified in other CHMPs. Literature indicates that CHMPs interact with each other in more than one location in order to form chains of filaments. One site of interaction is the flexible region between alpha helices 1 and 2, others are less well defined. Using the CHMP7 fragments shown in figure 6 greatly improved the purification process. The fragments were observed to overexpress in bacterial cells to a much higher extent than full length CHMP constructs.

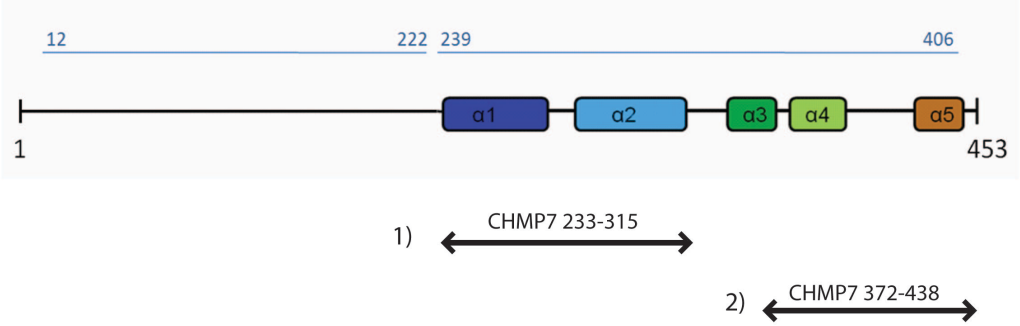

Figure 6 Sequence of CHMP7 with the two CHMP7 fragments below labelled (1) and (2). CHMP7 233-315 encompasses the 1st and 2nd alpha helical regions and is a proposed site of CHMP-CHMP interaction. CHMP7 372-438 encompasses the 4th and 5th alpha helices; this a potential second site of CHMP-CHMP interactions. This fragment was also selected as it covers the region corresponding to CHMP MIM interaction with MIT domain proteins.

As shown in figure 7, a higher concentration of soluble protein was obtained when purifying CHMP7 fragments (figure 7a) when compared to the purification of His_6.trx CHMP7 228-453 (figure 7b). Looking at lane 3 (figure 7b), it seems likely the aggregating nature of the CHMP7 C terminal affects the affinity to which it binds to the nickel charged resin as the protein appears in the flow through. The samples for these gels are taken from fractions of the same volume and prepared with SDS-PAGE loading buffer to the same dilution.

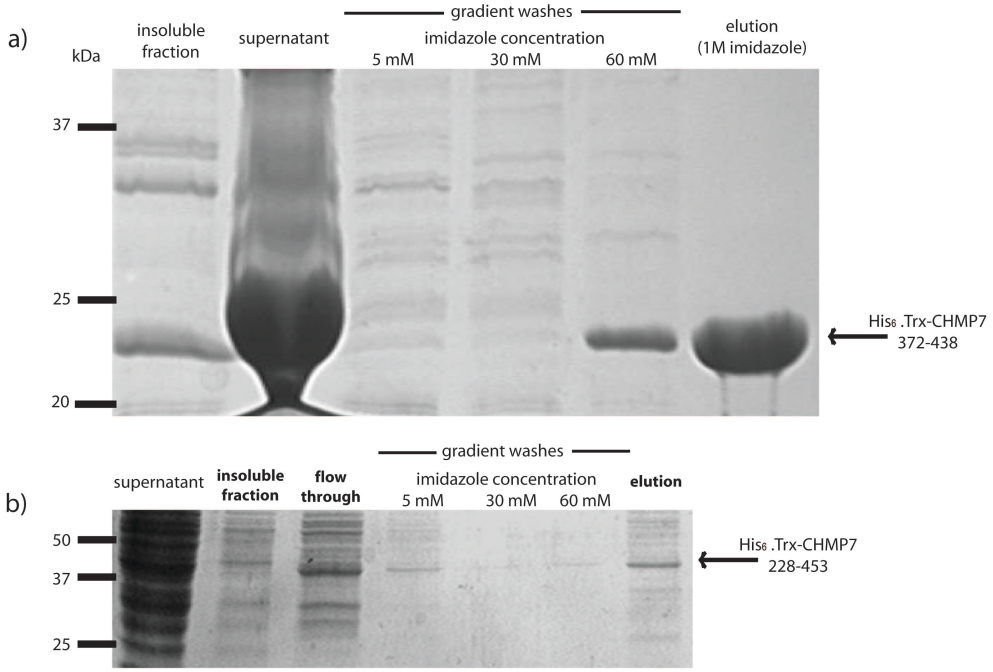

Figure 7 (a) Example of purification of a CHMP7 fragment; purification of His_6.Trx-CHMP7 372-438 (24kDa) –the acidic 4th and 5th helices of the SNF7 domain in the C terminus half. No detergent or urea was required for this purification. (b) Example of purification of His_6.trx CHMP7 228-453 (50kDa), which spans the entire SNF7 domain of CHMP7. The bacterial pellet was resuspended in the presence of 6M urea. The flow through is the supernatant passed over the resin. The elution fraction was using 1M imidazole plus 6M urea.

No detergent or urea was required for purification of the CHMP7 fragments, plus no adverse reaction to snap freeze and thawing cycles was observed (although samples were only frozen and thawed once before deposal). The fragments were designed based on potential interactions and sites of interest. CHMP7 233-315 covers the 1st and 2nd alpha helices of the C terminal, which is the proposed site of CHMP-CHMP interactions. This is also the heavily basic region known in other CHMPs to bind to the endosomal membranes through interaction with acidic lipids, specifically PtdIns(3)P^5. The absence of the 4th and 5th alpha helices means this peptide is effectively stuck in an ‘open’ conformation therefore positive interactions should also be easier to establish. In vivo the majority of these interactions would take place whilst bound to the endosomal membrane. Theoretically this could make interactions in solution less favourable, however, pull down assays (amongst other interaction detection methods) have already been used successfully in determining interactions between other CHMPs and their accessory proteins. The second CHMP7 fragment, CHMP7 372-438 was

selected as it covers the region that could contain MIMs and allow CHMP7 to interaction with MIT-domain containing proteins, such as VPS4. This fragment could also reveal a second site of CHMP-CHMP interaction.

3.2.2.2 CHMP7 interacts with CHMP4B and CHMP1A

Pull downs were conducted with CHMP7 fragments against CHMP4B and CHMP1A. A cDNA encoding fragment encompassing the 1st and 2nd alpha helices of the SNF7 domain (basic region) was cloned from full length CHMP4B cDNA. The resulting truncated CHMP4B protein was used in these assays (His_6.trx-CHMP4B 13-100). CHMP1A proved a rather more straightforward purification and so for this reason the full length protein was used in pull downs. The approach of using peptide fragments of CHMP proteins was used previously to circumvent aggregation problems and reveal interaction partners between ESCRT-III proteins by Zamborlini et al[31].

Pull down assays, using a CHMP7 372-428 fragment (acidic region), revealed an interaction with CHMP1A (figure 8). As proposed, this interaction suggests a second site of CHMP-CHMP interaction does reside in the acidic half of the C terminal. CHMP1A is known to partially function in the nucleus and evidence indicates it acts as a tumour suppressor[43]. It can be proposed that CHMP1 and CHMP7 could likely act together in the nucleus as predictive tools suggest they both contain NLS motifs; with the possibility of a DNA binding region explaining the presence of the extra N terminal domain in CHMP7. To further explore this interaction, these proteins need to be monitored in cells, see chapter four for this.

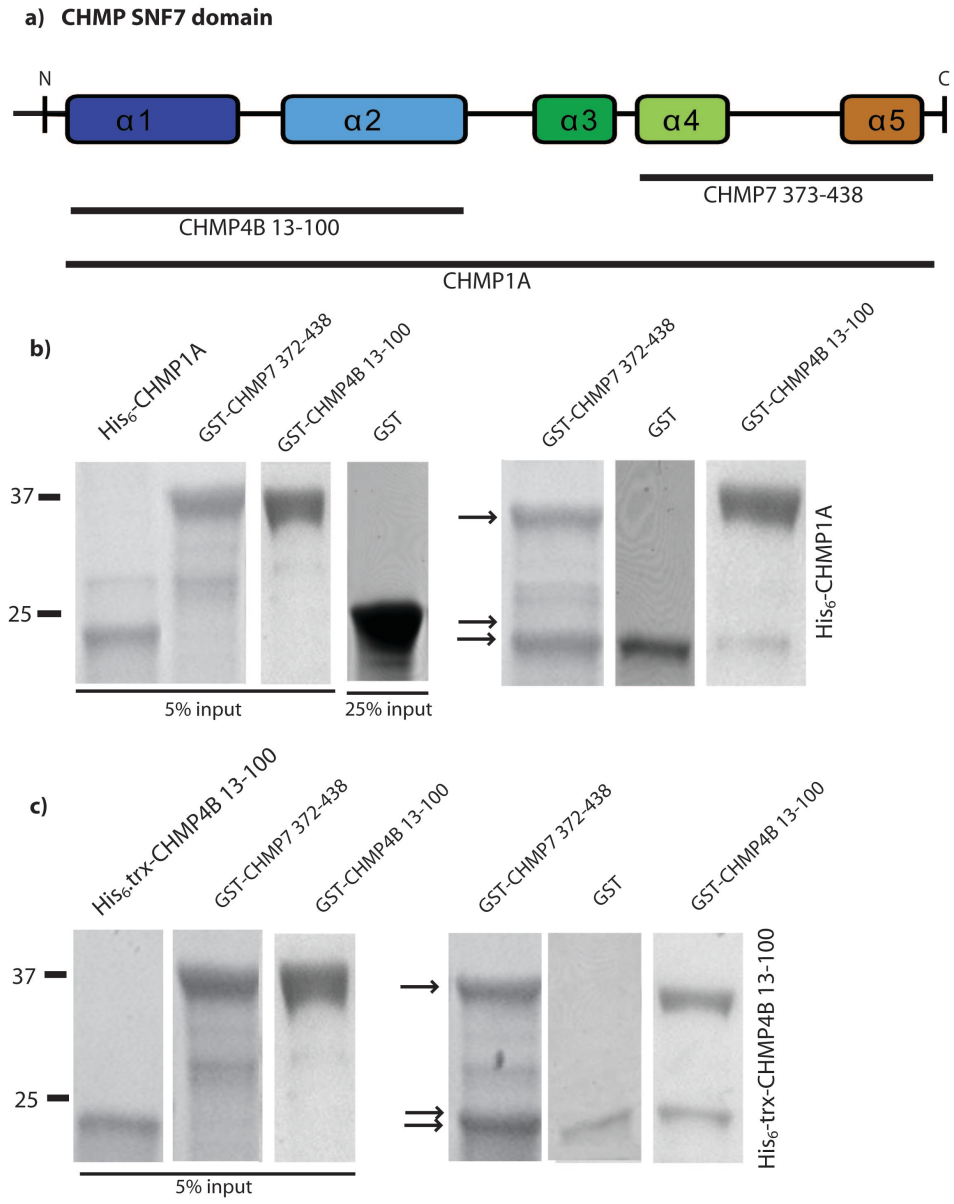

Figure 8 a) CHMP SNF7 domain illustrating the position of CHMP4B and CHMP7 fragments, full length CHMP1A was used. Pull down assays using his-tagged CHMP1A (b) and CHMP4B 13-100 (c), where arrows indicate the mass where GST-tagged CHMP fragments (35 kda) and GST (26 kda) are expected. The bottom arrow indicates his-tagged constructs, where CHMP1A full length and the his.trx tagged CHMP4B fragment are roughly both 24-25 kda. CHMP7 and CHMP4B fragments were incubated at room temperature with Ni-charged NTA agarose beads preloaded with his-tagged CHMP1A or CHMP4B 13-100 – conducted in 20 mM TRIS, 150 mM NaCl, 5% glycerol, 2 mM $CaCl_2$ pH 7.4. After binding, samples were analysed by SDS-PAGE and Coomassie staining.

Due to the basic-acidic biased nature of the amino acid sequence of the SNF7 domain, it could be argued that CHMP7 372-438 (an acidic fragment) is only interacting with CHMP1A in a fashion similar to how the domain naturally folds (the C terminal end folds over the basic N terminal end). Working with fragments rather than the full length protein allows the validity of these results to be more

heavily scrutinised. Previous unpublished work conducted by a colleague also saw a positive interaction between CHMP7 and CHMP1A *via* pull down assays using full length CHMP1A and the CHMP7 228-453 (figure 9).

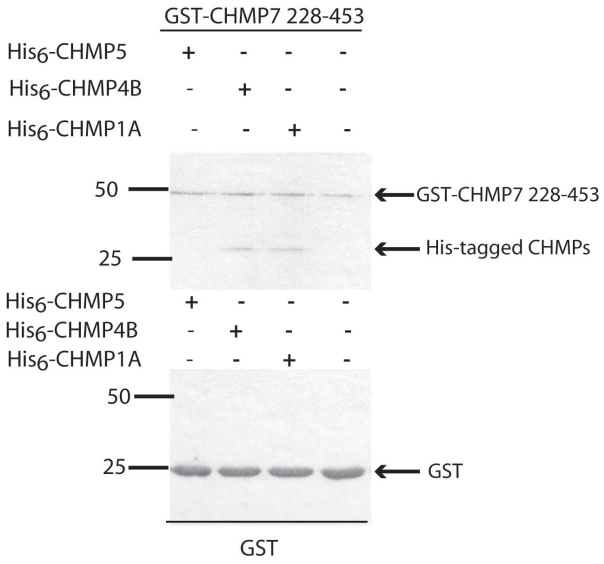

Figure 9 Pull down assays showing the positive interactions between GST-CHMP7 C terminal half (228-453) and full length CHMP4B and CHMP1A reproduced courtesy of Dr. E McKenzie (University of Manchester) using in vitro translated proteins. Assay also shows no interaction between CHMP5 and the CHMP7 228-453 and no interaction between His-tagged CHMPs and GST.

The assays in figure 8 and 9 support previous literature demonstrating CHMP4B and CHMP7 interact[46]. Furthermore, this interaction is between the 1st and 2nd alpha helical region of CHMP4B and the 4th and 5th helical region of CHMP7. This may imply that CHMP-CHMP interactions could occur in multiple sites (figure 10)[29].

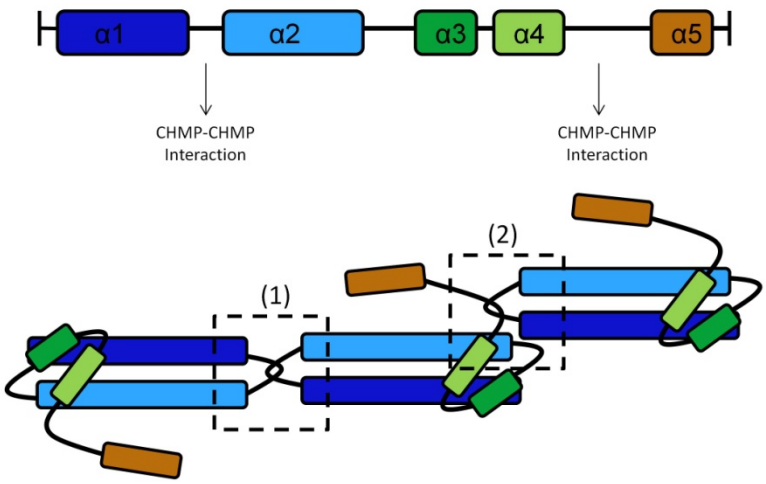

Figure 10 Cartoon of the SNF7 domain, which is crucial for CHMP polymerisation. In order to form filaments CHMPs require more than one site for CHMP-CHMP interaction. We propose a second site lies in the region between helices 4 and 5. Furthermore, we propose that these CHMP interactions are not specific with regards to which CHMP binding region they interact with i.e. either (1) or (2).

Established interactions were used as positive controls in these assays, i.e. the known interaction of CHMP4B with CHMP1A and also CHMP4B with itself[111]. Using the same CHMP4B fragment, but with different tags an interaction between these similar basic regions was seen (figure 8c) GST was used as a negative control, moreover this control shows that the presence of the large GST tag (26kda) did not interact with any of the prey protein and therefore did not contribute to any false positives. The pull downs in figure 8 are from His-tagged proteins bound to Ni-NTA agarose. All pull downs, including the GST controls, were repeated using glutathione sepharose with the GST protein as the bait in order to provide further confidence in the results (see appendix 8). A further control of resin only was added due to the possibility of the tagged protein interacting with or 'sticking' to the wrong resin. The his-tagged CHMP fragments and CHMP1A showed no affinity for the glutathione sepharose.

3.2.2.3 CHMP7 interacts with VPS4B

VPS4B interacts with ESCRT-III subunits *via* a MIT domain located towards the N terminal. This interaction has been demonstrated for all the CHMPs apart from CHMP7 and CHMP5.

VPS4 represents an important interaction partner as it recycles the ESCRT-III complex from membranes back to the cytoplasm as monomers. VPS4B was

determined correctly folded by CD (see appendix 7). Studies from the literature indicate interactions between CHMPs and VPS4 do not require ATP or LIP5 and in some cases have been carried out with just the MIT domain fragment of VPS4[54,59].

Pull down assays revealed that CHMP7 did interact with VPS4B (figure 11c), which is expected for ESCRT-III subunits. No interaction was seen with CHMP4B 13-100, in agreement with literature that places the MIM of CHMP4B (MIM2) outside this region (figure 11e).

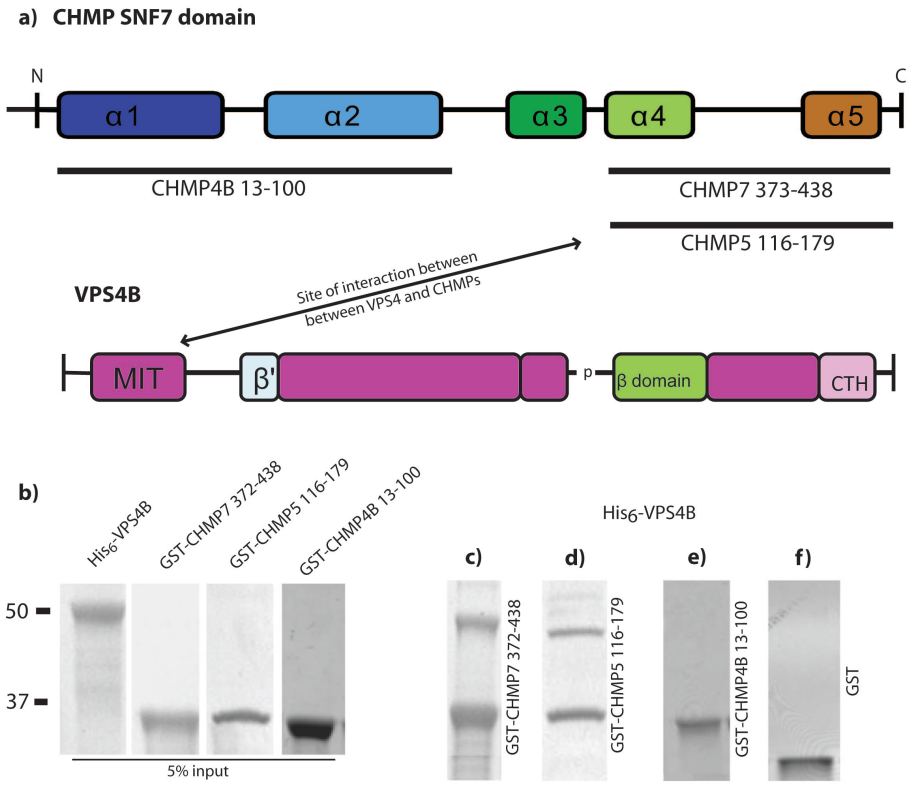

Figure 11 a) CHMP SNF7 domain illustrating the position of CHMP4B, CHMP7 and CHMP5 fragments. Below shows the domains of VPS4, where the MIT domain interacts with a MIM found towards the acidic C terminal end of CHMPs. Pull down assays were conducted using glutathione sepharose beads preloaded with either GST (f), GST-tagged CHMP7 fragment (c), GST-tagged CHMP5 fragment (d) or GST-tagged CHMP4B fragment (e). His tagged VPS4B was incubated with the preloaded GST beads in PBS, pH 7.4 at room temperature. After binding, samples were analysed by SDS-PAGE and Coomassie staining.

A further novel interaction revealed in these assays was the interaction between VPS4B and CHMP5 (figure 11d). It has previously been assumed that CHMP5 interacts with only the VPS4 regulator, LIP5, and not VPS4 itself[65].

Next, the aim was to determine through which motif CHMP7 interacted with VPS4B. CHMPs have been shown to interact with the MIT domain of VPS4 through either a MIM1 or MIM2 motif (except for CHMP5). CHMPs 1 to 3 contain a MIM1, where the presence of three hydrophobic residues (typically leucine) appears critical. In contrast, the CHMP4 isoforms and 6 interact *via* a MIM2 which is dependent upon two proline residues. Figure 12 shows proposed regions in CHMP7 for a both a MIM1, MIM2 and also a MIM5 (found in CHMP5). Interestingly, the MIM1 contains also a predicted NES sequence. This could indicate some regulatory function for VPS4 –if by binding to CHMP7 in this region it blocks the NES and effectively can trap CHMP7 in the nucleus (until its ATPase activity returns the protein to its monomer state.)

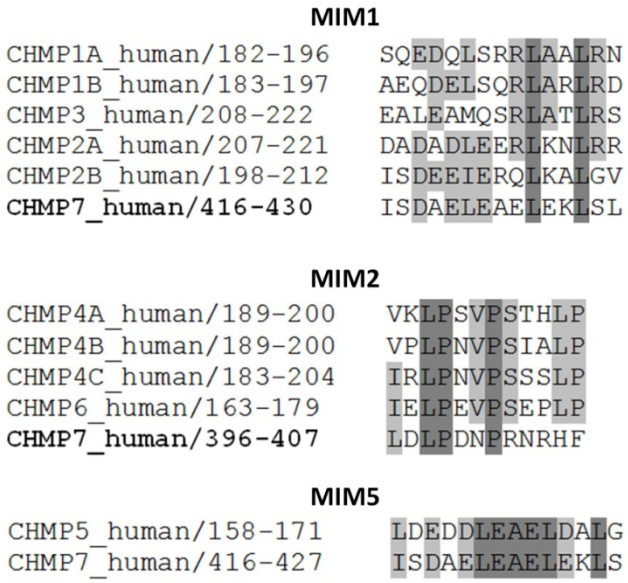

Figure 12 Sequence alignment showing a potential MIM1, MIM2 and MIM5 in CHMP7. Classically a MIM1 is at the C terminal of the protein and relies on the leucine residues. MIM2 is found further away from the C terminal where the presence of two proline residues are important. CHMP5 contains a MIM5, which is similar to a MIM1 but differs it how it binds to the MIT domain.

The SNF7 domain of CHMP7 is most similar to CHMP6, this supports the likelihood of CHMP7 containing a MIM2 rather than a MIM1. Short peptides encompassing these proposed MIM1/5 and MIM2 sites were designed and synthesised by recursive PCR. This method doesn't require a CHMP7 template, codons were optimised for expression in *E. coli* based on work by Dong et al[91].

Figure 13 reveals that CHMP7 contains either a MIM1 or MIM5. Pull down assays do not allow us to ascertain the binding mode, but interaction with the MIM

domain of VPS4 is usually through a MIM1-MIT binding mode, whereas MIM5-MIT binding is found interactions with the second MIT domain of LIP5. CHMP7 binds the VPS4B MIT domain and likely in the same way as CHMP1, which is perhaps due to them providing a similar function and therefore requiring the same regions free for interaction.

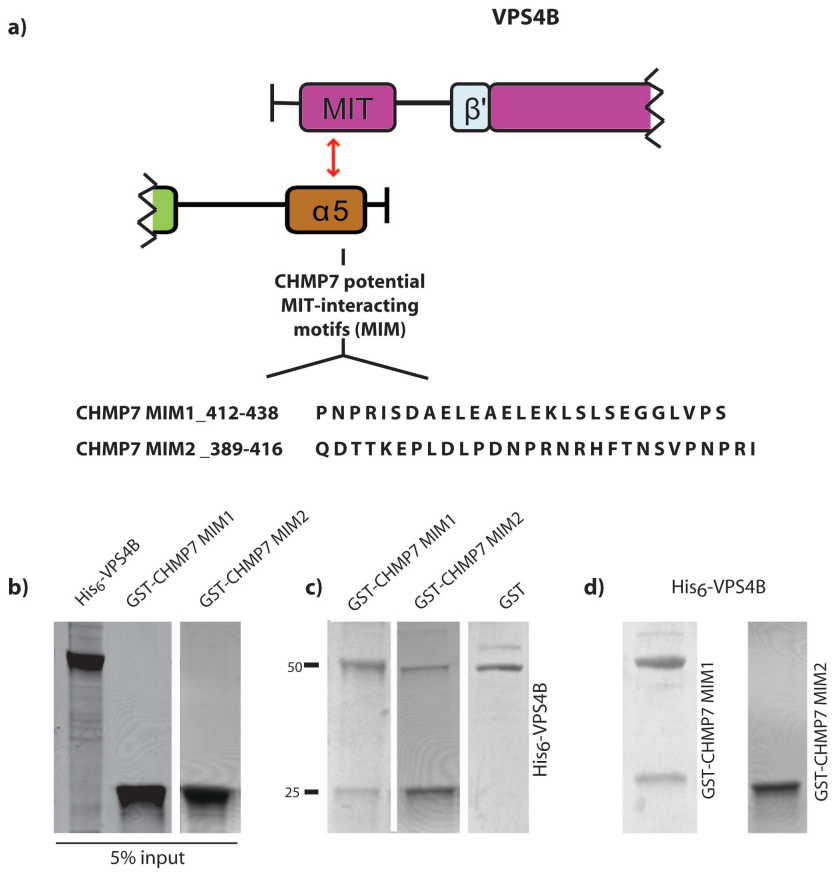

Figure 13 a) VPS4B MIT domain and the 5th CHMP7 alpha helices region, illustrating the position of proposed MIM-MIT interaction and the position of both MIM1 and MIM2 CHMP7 peptides. b) shows the purified proteins (5% of total amount used in pull down assays). c) Pull down assays were conducted using nickel charged chelating sepharose beads preloaded with His-tagged VPS4B. d) Pull down assays were conducted using glutathione sepharose beads preloaded with either GST-tagged CHMP7 MIM1 or MIM2. All assays were conducted at room temperature in either PBS, pH 7.4 (GST beads) or 20 mM TRIS, 150 mM NaCl, 5% glycerol, 2 mM $CaCl_2$ pH 7.4 (chelating sepharose beads). After binding, samples were analysed by SDS-PAGE and Coomassie staining.

The idea that CHMP7 contains a MIM2 motif also cannot entirely be discounted. In the pull down assays where GST-MIM2 was used as prey (washed over VPS4B-bound nickel chelating sepharose) a positive interaction was found (figure 13c). The reverse pulldown (with GST-MIM2 bound to glutathione sepharose) there was no observed interaction (figure 13d). One possibility is that the size of the tag (GST =26kda) could have affected this pull down by blocking access to

the MIM2 (less than 2kda). However, this should be less of a problem when the GST tag is immobilised to the resin and also would have affected the corresponding GST-MIM1 pull down assay. Potentially CHMP7 contains both a MIM1 and a MIM2, but because VPS4B has a higher affinity for MIM1s over MIM2s (seen in other CHMPs) these assays are not sensitive enough to reliably reproduce the weaker interaction between the MIM2 and VPS4B[61]. The two MIM motifs bind to the MIT domain in different regions so potentially could interact with VPS4B simultaneously. If CHMP7 did contain both motifs it could act to recruit VPS4B and then pass the enzyme over to CHMPs less accessible or bound to a membrane. By binding to VPS4B in two different ways CHMP7 could have the ability to pass the enzyme to either a MIM1 or MIM2 containing CHMP.

We decided to check the likelihood of a CHMP7 MIM2 and MIM1 using protein homology modelling. Crystal structures of MIT-MIM1 and MIT-MIM2 binding from the PDB and Swiss PDB-Viewer were used as templates to model the equivalent MIMs of CHMP7 MIM from figure 12, in complex with the MIT domains of VPS4A and VPS4B (figure 14 & 15)[112]. This method allows us to determine potential destabilising and stabilising interactions that may occur in such complexes. Figure 14 shows the alignments used for this modelling, with the level of sequence identity between VPS4A and B MIT domains.

Figure 14 a) sequence alignment showing CHMP7 sequence similarity to both CHMP6 MIM2 (166-181) and CHMP2B MIM (198-213). Ideally modelling to investigate CHMP7 MIM domains would be based on a VPS4B template -as in our assays VPS4B was used. However, no crystal structures of a VPS4B MIT -MIM2 interaction exists on the PDB. For this reason b) shows the alignment between the MIT domains of VPS4A and VPS4B to highlight their similarity.

Using Swiss PDB viewer, the amino acids of CHMP2B an CHMP6 can be mutated to match the proposed MIM sequence in CHMP7 and provide a theoretical model of the interaction between CHMP7 and VPS4B. This type of modelling can also highlight unfavourable steric clashes and also whether residues important for interaction are orientated correctly. Figure 15a shows a model of the CHMP7 MIM1-VPS4B MIT interaction. The model shows the three conserved hydrophobic leucine residues are all orientated towards corresponding leucine residues in the MIT domain. The salt bridge formed between aspartic acid (CHMP7 ASP418/CHMP2B ASP200) and arginine (VPS4B ARG59) is still present. Additionally, mutation of glutamine (CHMP2B GLN206) to glutamic acid (CHMP7 GLU224) may not decrease significantly the strength of the interaction between glutamine (GLN206) and glutamic acid (GLU70) present in the CHMP2B/VPS4 crystal structure. Finally, the mutation of a lysine residue (CHMP2B LYS208) to glutamic acid could possibly decrease the stability of the complex, however the lysine here is orientated into the solvent and not involved in the interaction between the two proteins.

The reduced stability of a CHMP7-VPS4B complex, in comparison to a complex with CHMP2B, would indicate that VPS4B may bind preferentially to CHMP2B over CHMP7. Taken together with data from the pull down assays we propose that CHMP7 interacts with VPS4B *via* a MIM1 and that this interaction is weaker than that between CHMP2B and VPS4B. It can also be noted that all important residues mentioned here in the VPS4B MIT are conserved in the VPS4A MIT. This suggests CHMP7 likely also can interact with VPS4A *via* the same motif.

Figure 15b shows a model of the CHMP7 MIM2-VPS4A MIT interaction. CHMP7 only contains two conserved prolines, unlike other MIM2 CHMPs that contain three or four. However, only the two prolines that CHMP7 contains actually interact with the MIT domain of VPS4A. Of the two extra prolines that CHMP6 contains, one is too far from the MIT domain and the other is oriented into the solvent. A salt bridge formed between VPS4A lysine (LYS55) and CHMP6 glutamic acid (GLU171) is disrupted when it is mutated to asparagine (CHMP7 ASN404), howver a hydrogen bond can form between the lysine and the asparagine so some stabilisation remains.

a) CHMP7 MIM1 -VPS4B MIT

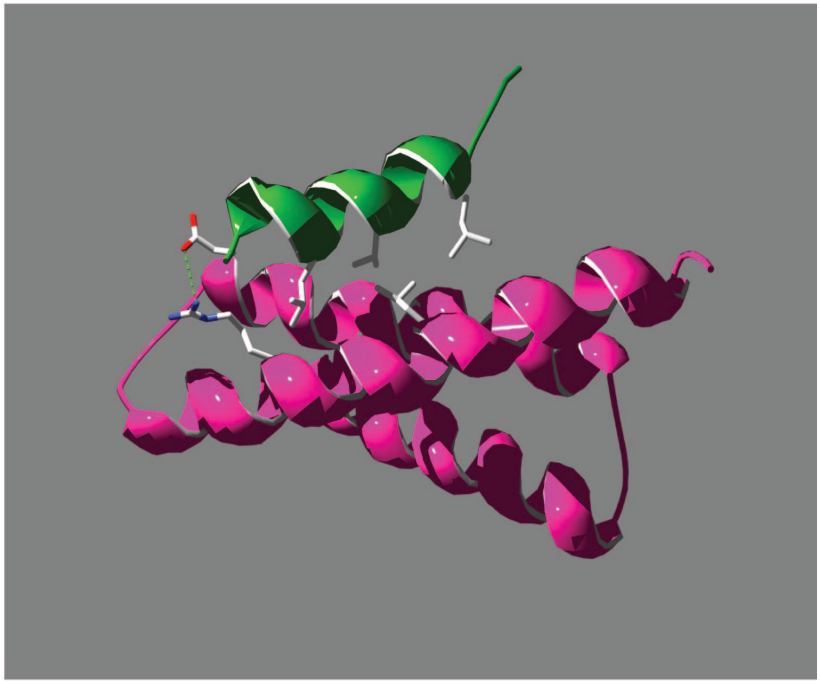

b) CHMP7 MIM2 -VPS4A MIT

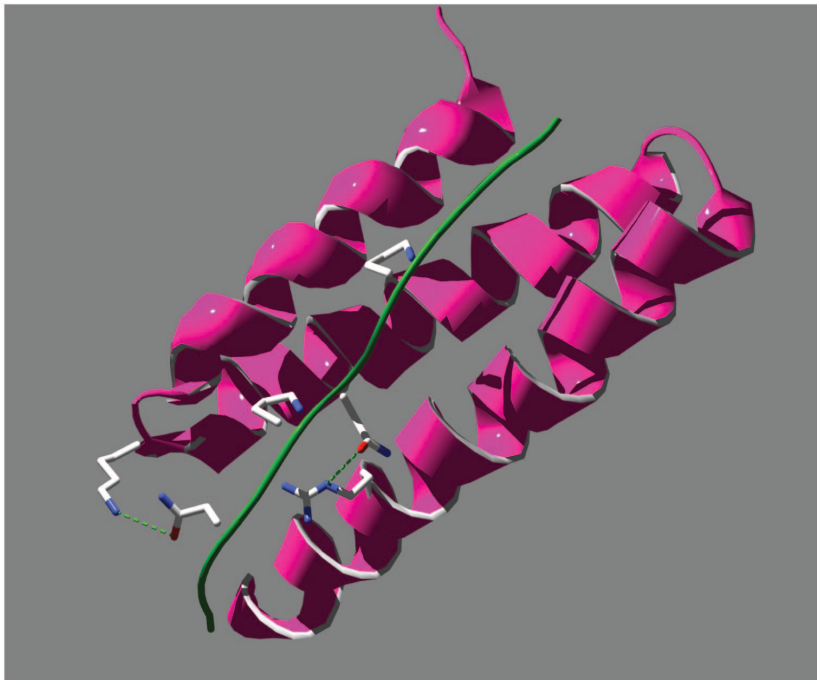

Figure 15 a) Modelled interaction of CHMP7 MIM1(green) with the VPS4B MIT domain (pink); the three conserved leucine residues from CHMP7 and leucine residues in the MIT domain are orientated toward each other and buried. Furthermore, a candidate salt bridge CHMP7 ASP418-VPS4B ARG59 stabilises the interaction. b) modelled interaction of CHMP7 MIM2 (green) with VPS4A MIT domain (pink). Conserved proline residues are orientated the same towards the MIT domain. Furthermore, this interaction can be stabilised by hydrogen bonding (shown by green dotted line). Modelled using Swiss-PDB Viewer 4.1.0 and templates from the PDB, 2JQK and 2K3W respectively.

Further hydrogen bonding occurs between arginine (VPS4A ARG67) and asparagine (CHMP7 ASN401) -this stabilisation does not occur between VPS4A and CHMP6. No steric clashes were observed in this model and all important VPS4A residues are conserved in VPS4B. This model supports pull down data indicating CHMP7 can interact with VPS4B *via* a MIM2, such as in the IST1-VPS4 complex. IST1 is an example of an ESCRT-III protein that contains both a MIM1 and a MIM2 -this allows IST1 to interact with a variety of MIT domain-containing proteins, whilst interacting with VPS4.

3.2.2.4 CHMP7 interacts with the accessory protein, LIP5

LIP5 contains two MIT domains, both of which are available for interaction whilst LIP5 is bound to VPS4. LIP5 binds to MIM1-containing ESCRT-III subunits through a MIT1 domain located at its N terminal and also binds CHMP5 through its MIT2 domain with unusually high, pM, affinity[65]. The high affinity of this interaction is attributed to CHMP5 binding *via* a novel MIM5. Pull down assays from the literature have found no visible interaction between LIP5 and any MIM2 containing CHMP (CHMP4 isoforms or CHMP6)[9].

Conditions for these pull downs were established using the known interactions between some CHMPs and LIP5. The sequence alignment in figure 16a demonstrates the stronger likelihood that CHMP7 372-438 will interact with LIP5 over CHMP7 233-315. This is expected as both MIM motifs are found in the former fragment. The pull down assays (figure 16b) agreed with this confirming an interaction with the MIM-containing CHMP7 fragment and little or no interaction between LIP5 and the fragment based on the 1st and 2nd helices of the SNF7 domain. GST acts as a negative control (figure 16c). LIP5 interacts with VPS4B *via* the beta sheet insert found in the AAA domain of VPS4. This interaction aids the oligomerisation of the VPS4 ring complex –this interaction possibly also allows communication between VPS4 rings across a surface[56,113]. In this respect CHMP5/LIP5 function as a sub-complex regulating VPS4 activity. Recently nuclear functions of CHMPs have emerged; CHMP7 may also have a nuclear role determined by its winged helix domains and putative NLS/NES

motifs. CHMPs require recycling back to their monomeric and cytoplasmic state through disassembly by VPS4B and LIP5. In the environment of the nucleus CHMP7 could effectively takes on the role of CHMP5 and regulate the interaction between LIP5 and VPS4B in order to allow the release of nuclear ESCRT-III components when necessary.

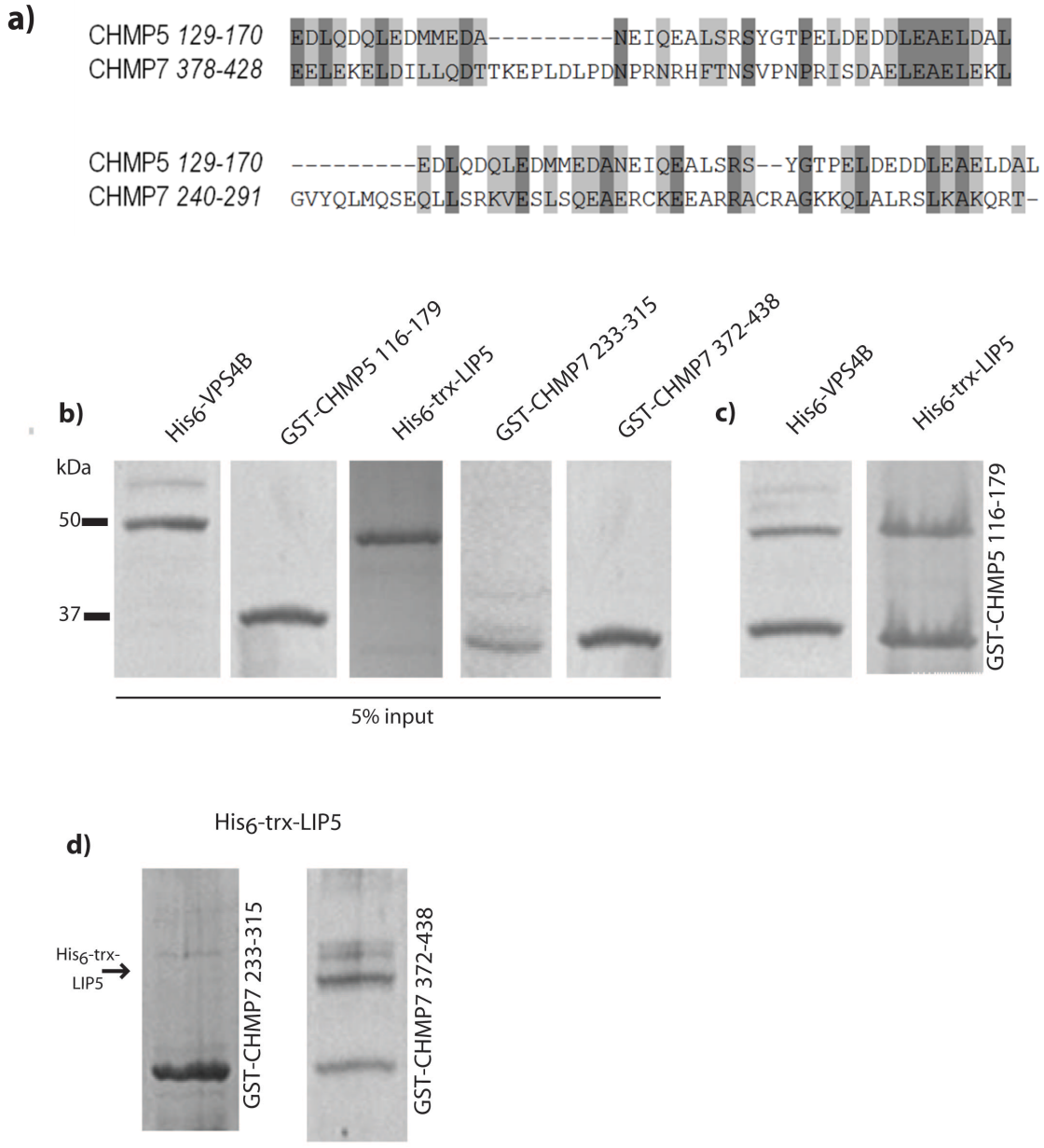

Figure 16 a) Sequence alignment comparing the CHMP5 region that interacts with LIP5 and the regions of CHMP7 (encompassed within the designed fragments). The alignment looks stronger between CHMP5 and CHMP7 372-438 -this is expected since it is this region that contains the MIM1 and also potentially the ability to bind like a MIM5 b) shows the purified proteins (5% of total amount used in pull down assays). c) Pull down assays were conducted using GST beads preloaded with GST tagged CHMP5 116-179 and incubated with His tagged LIP5 in PBS, pH 7.4 d) Pull down assays were conducted using GST beads preloaded with either GST tagged CHMP7 233-315 or 372-438 and then incubated with His tagged LIP5 in PBS, pH 7.4. See appendix 8c for controls.

The initiation of disassembly has previously been attributed to VPS2 in yeast (equivalent to CHMP2)[5]. The process and function of the human ESCRT-III subunits is more intricate and may require additional factors. No interaction between CHMP5 and VPS4 had been detected (previously attempted with yeast two hybrid), but figure 16b shows a positive interaction. Interestingly, the strong binding observed between CHMP5 and LIP5 is only *via* the MIT2 domain and not the MIT1. This implies it is the MIT domain protein that determines the type of binding and not the MIM itself and in the case of CHMP5 and CHMP7 we suspect the MIM can behave as either a MIM1 or a MIM5 depending on the interaction partner.

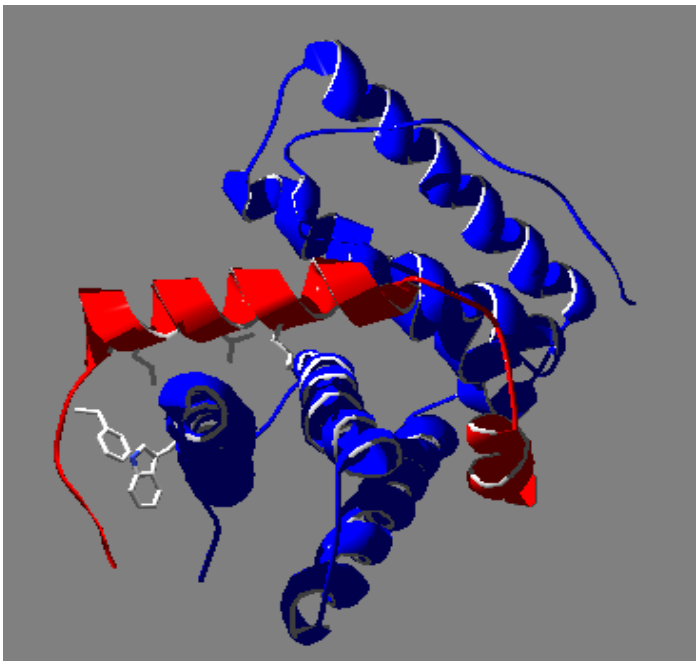

Figure 17 Modelled interaction between CHMP7 (red) and LIP5$(MIT)_2$ (blue) based on the template of LIP5(MIT)2-$CHMP5_{123\text{-}195}$(2LXM). CHMP7 interacts with the lower MIT domain (MIT2). For clarity only residues shown are the CHMP7 leucine collar residues, PHE375 and on LIP5(MIT)2 TRP-147 residue which is important for CHMP5-LIP5 binding, the phenylalanine (CHMP7 PHE375) residue if in the correct rotomer may contribute to some stability through Pi stacking interactions (this residue is ASP127 in CHMP5). Of the six candidate salt bridges outlined by Skalicky et al between $CHMP5_{123\text{-}195}$ and $LIP5(MIT)_2$ four remain, plus one new salt bridge: LIP5 LYS15-CHMP7 ASP385, LIP5 ARG146-CHMP7 GLU381, LIP5 HIS153-CHMP7 ASP390, LIP5 LYS157-CHMP7 ASP390 and the new one, LIP5 GLU26-CHMP7 ARG403. Of the two salt bridges lost these now potential could form hydrogen bonds: LIP5 ARG55-CHMP7 ASN402 and LIP5 ARG30-CHMP7 THR408.

Containing two MIMs (MIM1/5 and MIM2) that differ in affinity, interaction partner and binding mode suggests an ordered disassembly of the CHMP complex from membranes. This disassembly could occur via a serial handover mechanism with VPS4 moving from higher affinity MIM motifs (MIM1) to lower affinity motifs

(MIM2) as CHMPs are recycled back to their closed state (blocking further MIM interaction). This process can be aided by the CHMP5/LIP5 sub-complex, IST1 and a novel CHMP7/LIP5 sub-complex. The interaction between CHMP7 and LIP5 is modelled in figure 17 based on a template of the CHMP5-LIP5 interaction.

No steric hindrances were observed and in terms of stability only one salt bridge out of six was lost, but the mutations causing this could provide hydrogen bonding interactions instead.

3.3 Discussion

The observations in this chapter allow us to begin to build a protein-protein interaction network with CHMP7. Our starting point was the interaction between CHMP4 and CHMP7. The results in this chapter build upon this starting point and provide evidence that CHMP7 contains both a MIM1 and a MIM2, moreover that the MIM1 may behave similarly to a MIM5 with certain proteins. CHMP7 and CHMP5 interact with VPS4 likely through a MIM1/5 domain. In the case of CHMP7 we also observed an interaction with LIP5. This could occur either through a MIM1-MIT1, a MIM5-MIT2 interaction, or even both. Modelling of the LIP5 MIT2-CHMP7 MIM5 supported the MIM5-MIT2 binding, showing there was little loss of stability and the most important residues were conserved and orientated correctly. Our findings regarding a MIM2 are less convincing, due to inconclusive pull down assay data, although they are supported by protein modelling.

These findings open up new avenues of investigation between the interactions of CHMP7 and a host of MIT domain containing proteins, such as spastin (involved in microtubule function) and UBPY (a de-ubiquitinating enzyme). Previous literature has reported no interaction between CHMP7 and UBPY[114]. However, no published work has looked at spastin and CHMP7. Spastin is known to interact with CHMP1B through its MIT domain which requires the same conservation of leucine residues[83,84].

It also seems likely that CHMP7 contains a NLS, like CHMP1, and may be involved in activity in the nucleus. The prediction of winged helix domains in the N

terminal of CHMP7 is congruent with both theories that CHMP7 has nuclear functions and represents a hybrid ESCRT-II/ESCRT-III. Additionally, the human ESCRT-II subunits do have a role in the nucleus since they bind to transcriptional repressor ELL[20,115].

We were able to recreate the conditions to observe the CHMP4B-CHMP7 C terminal domain binding using peptide fragments of both CHMP7 and CHMP4B. These assays also revealed an interaction between CHMP1A and CHMP7, which supports the idea of a nuclear role for CHMP7 since we already know CHMP1A functions in the nucleus in gene silencing. Moreover, this interaction suggests an ESCRT-III complex could be initiated in the nucleus rather than subunits acting independently. Recent work by Morita et al demonstrated that depletion of any CHMP affected nuclear morphology and spindle maintenance[45]. Therefore, CHMP7 and CHMP1A could aid nuclear localisation of other CHMPs. Furthermore, the putative DNA binding domain in CHMP7 could direct ESCRT-III assembly to chromatin.

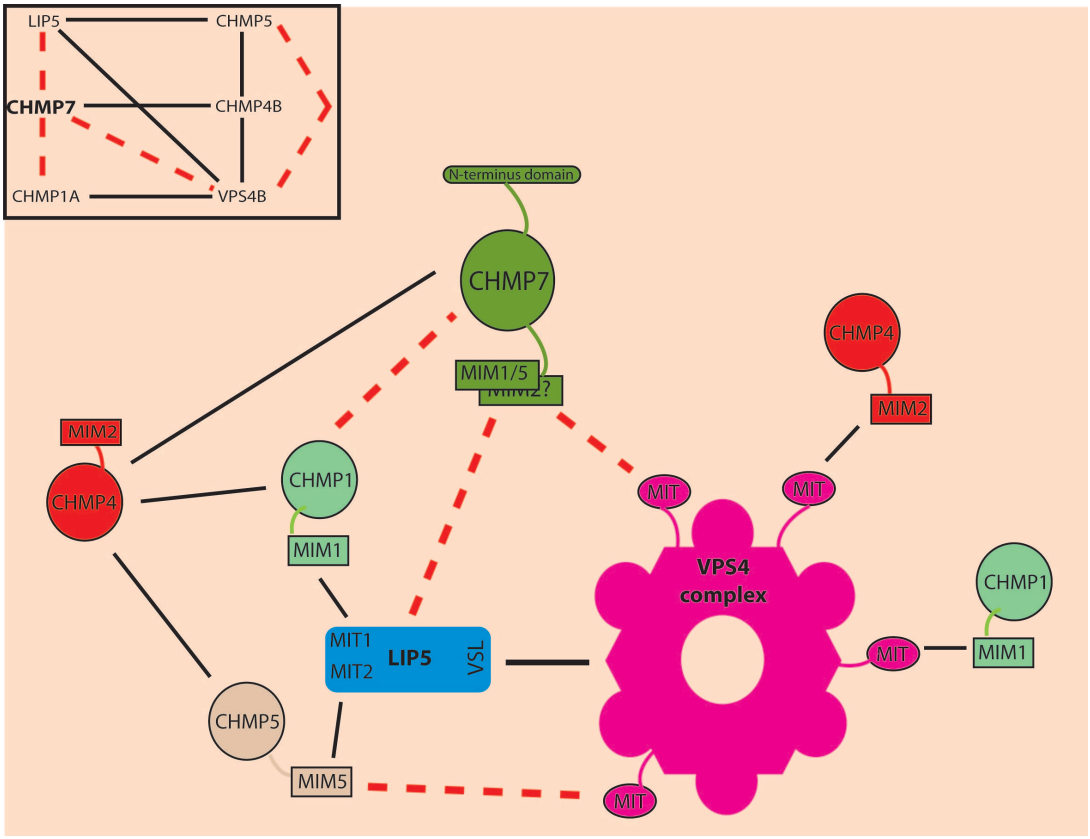

Figure 18 Scheme demonstrating all the interactions highlighted in this chapter. The dashed red lines show new interactions, whilst solid black lines indicate established interactions. This scheme also shows the two indicated MIM motifs in CHMP7.

Figure 18 shows a scheme of all new interactions introduced in this chapter (dashed red line) alongside pre-established ones (solid black line). To consolidate this network, ideally experiments would include all the CHMPs, including isoforms. This could reveal any isoform specific interactions, such as between CHMP1A and 1B, whilst also providing a fuller picture of CHMP7 activity as part of a complex. The presence of CHMP isoforms is only found in eukaryotic cells, and although anticipated to indicate specialised functions the exact role of each is unknown.

In summary, the results displayed in this chapter firmly support the ESCRT-III-like traits of CHMP7, with similarities being largely observed between CHMP7 and CHMP1, 5 and IST1. These three proteins have a regulatory role in the MVB pathway and for CHMP7 to also function in this manner agrees with the literature. For example, work by Hurley et al demonstrates that in yeast only the core ESCRT-III subunits are necessary -corresponding to CHMP6, 4A-C, 3, 2A-B and VPS4[5]. CHMP1A-B, CHMP5 and IST1 are not strictly essential in normal yeast endosomal function.

The results have also allowed us to narrow down some potential leads for CHMP7 function. These will be explored in the following chapters. Primarily, the strongest lead is the hypothesis that CHMP7 functions in the nucleus and is perhaps more 'chromatin modifying protein' than 'charged multivesicular protein'.

CHAPTER 4 A SPECIFIC ESCRT-III ASSEMBLY EXISTS IN THE NUCLEUS

4.1 Introduction

This chapter aims to expand upon the CHMP-CHMP interactions uncovered in the previous chapter by observing these proteins in vivo. This can enlighten us to their location and behaviour at different stages of the cell cycle (which can be determined by the appearance of the nucleus).

The experiments in this chapter aim to reveal functions of CHMP proteins by either depleting or overexpressing a protein of interest, i.e. VPS4 or even certain CHMPs themselves. Overexpression of a protein can promote its natural function in the cell and highlight the involvement of other proteins. By depleting a protein any possible disruption to other proteins can be observed. The correct function of CHMPs requires the action of VPS4 –therefore one crucial question is; what happens when this enzyme is depleted? This depletion is particularly revealing for the function of CHMP7, together with in-vitro pull down assays that tie it to VPS4 and other CHMPs. Furthermore, a series of epistasis experiments were conducted where a different CHMP was systematically depleted alongside VPS4 in order to reveal the level of dependence between CHMP proteins –specifically between CHMP7, CHMP4B and CHMP1B. At the end of this chapter, some preliminary cell cycle synchronisation experiments are also shown (other than this section no other cell populations were synchronised). Observing the cell at different stages of the cell cycle allows the determination of events where CHMPs are densely populated in specific regions. Specifically, we are interested if CHMP7 localises at the midbody or nucleus. Other ESCRT-III components are

known to function in cytokinesis and in events preceding the final abscission step such as chromosome segregation and spindle formation[45].

A strain from a human cell line taken from cervical cancer, HeLa M, was used for these experiments. HeLa cells have been widely used for over sixty years and are very useful due to their quick cell cycle (24 hours) and their size (20-25 microns) -which allows clear visualisation of discrete organelles under a fluorescence microscope. Proteins were observed by immuno-fluorescence microscopy (IF).

4.1.1 Using immuno-fluorescence

IF works by combining the specificity of antibodies for their antigen with fluorescence. Specific sites of interest (antigens) can be targeted such as certain peptide sequences within the chosen protein or from an attached fusion tag. A fluorophore conjugated to an antibody acts as the reporter molecule resulting in a fluorescent signal when viewed under a microscope at the correct wavelength. More than one organelle/protein can be viewed in the cell by using two primary antibodies raised in different species followed by using two secondary antibodies specific to the appropriate primary species and conjugated to different fluorophores, thereby resulting in emission at different wavelengths (figure 1). Alternatively, a fluorescent protein domain (i.e. green fluorescent protein, GFP) can be attached to the protein of interest and requires no antibody labelling to visualise. The benefits of using a tagged protein, either with a fluorescent protein domain or not, allows cells to be transfected with mutant protein DNA. The expression of this mutant protein can then be tracked by the tag to determine its effect upon the cell.

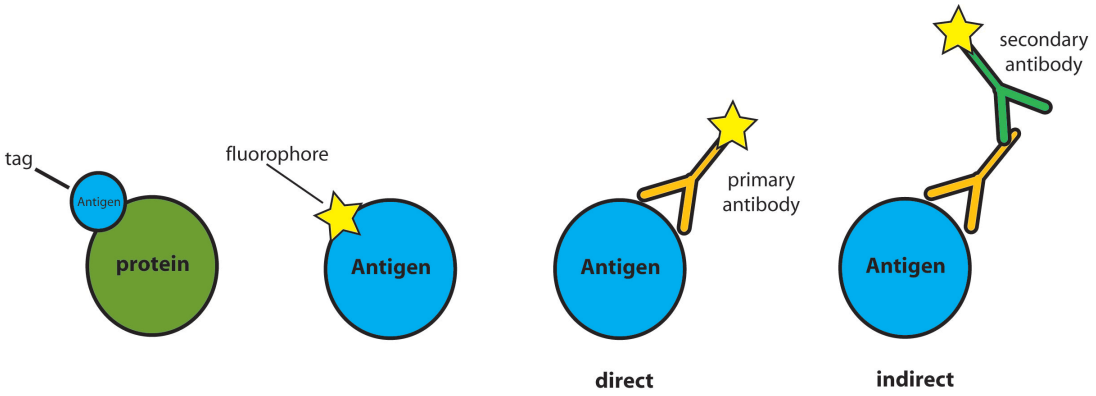

Figure 1 Examples of different methods of monitoring fluorescence. Adding a tag to the protein of interest, this tag can be fluorescent itself or detected with antibodies. Direct immunofluorescence uses a primary antibody with the fluorophore attached. Indirect immunofluoresence is more flexible and uses a secondary antibody with an attached fluorophore. The fluorophores themselves can be selected for their different emission wavelength.

4.2 Results

4.2.1 Optimisation and specificity of CHMP antibodies

Anti-CHMP antibodies (all rabbit) were tested for specificity. This is important so that any claims made, based on observations and analysis of the IF data, can be confidently verified, i.e. proof that each anti-CHMP antibody does not cross react with another. All the CHMP isoforms (with an N terminal myc tag) were in vitro translated and tested by western blot (figure 2a). Western blotting was used to determine efficacy of all protein depletions (section 4.2.6).

A second anti-CHMP7 antibody was obtained from the Scottish National Blood Transfusion Service (raised in sheep rather than rabbit). This antibody differed in that it was raised against an N terminal epitope using a GST tagged CHMP7 fragment (1-222) rather than one found in the C terminal like the rabbit antibody. The specificity of these anti-CHMP7 antibodies was also

determined by transfecting cells with a CHMP7-myc construct at different concentrations to provide samples with different levels of CHMP7-myc expression. Detection by the anti-CHMP7 antibodies reflects the gradient of increasing CHMP7-myc concentration and indicates the antibodies are recognising the same protein (figure 2b).

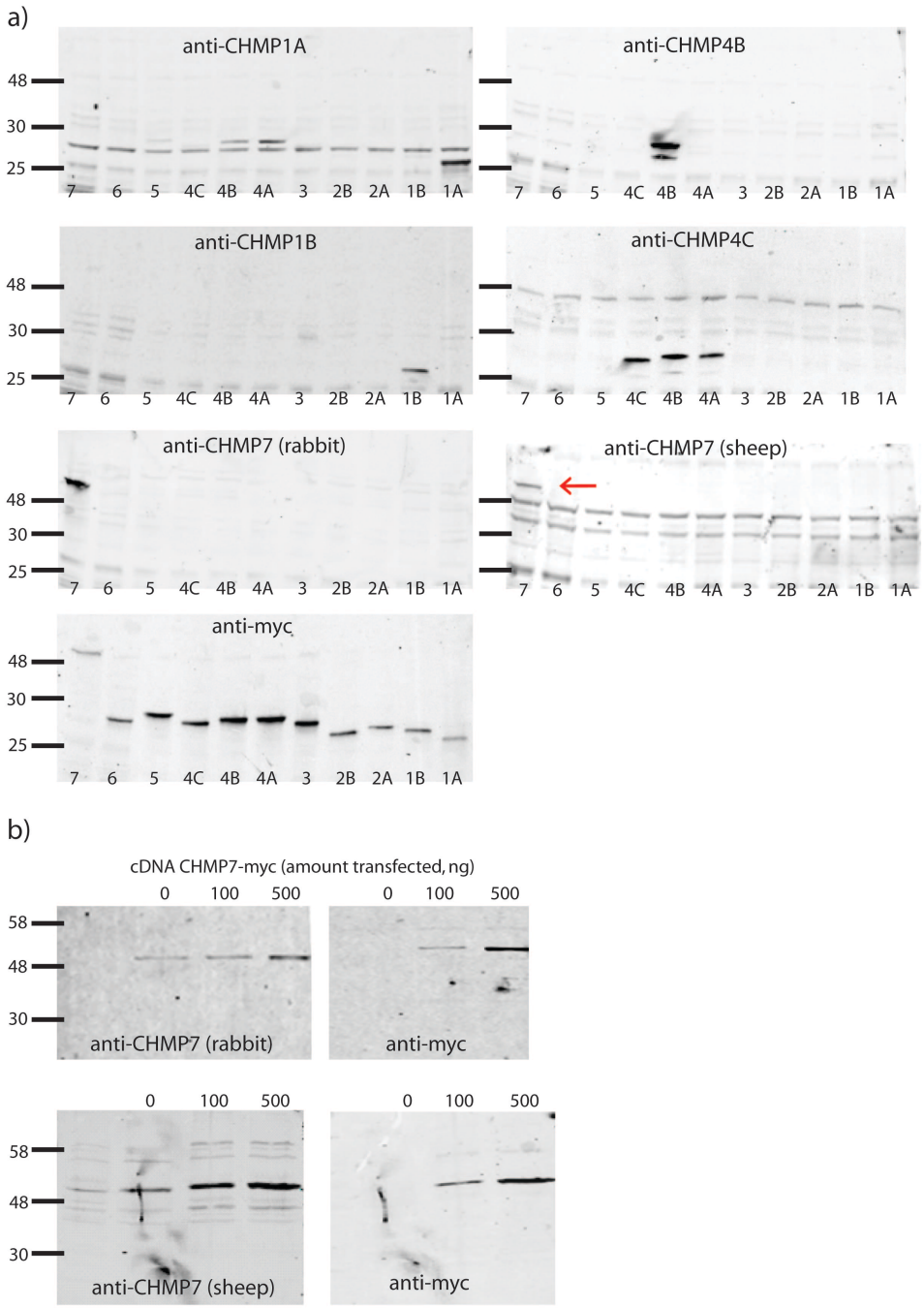

Figure 2 a) A series of western blots using in vitro translated myc-CHMP proteins in order to test the specificity of the following antibodies; anti-CHMP1A, anti-CHMP1B, anti-CHMP4B, anti-CHMP4C, anti-CHMP7 (rabbit) and anti-CHMP7 (sheep). Except for the custom made anti-CHMP7 (sheep), these antibodies were all newly available from Proteintech and had not been tested for cross reactivity. These blots show that anti-CHMP1A cross reacted with CHMP4A and CHMP4B. Anti-CHMP4C also cross reacted with other CHMP4 isoforms. Anti-CHMP1B, anti-CHMP4B and both anti-CHMP7 antibodies didn't recognise other CHMPs. The house generated anti-CHMP7 is indicated by the red arrow. b) Hela M cells were transfected with increasing concentrations of a CHMP7-myc encoding construct to demonstrate further that the custom anti-CHMP7 and Proteintech version both recognised CHMP7.

As figure 2a shows, the anti-CHMP4C and anti-CHMP1A antibodies cross-reacted with CHMP4 isoforms, therefore these antibodies cannot be used to distinguish between proteins in the CHMP family reliably. For this reason, further work looking at interactions in vivo was conducted using the anti-CHMP1B and anti-CHMP4B antibodies. A CHMP1A construct was used in the previous chapter to reveal an interaction with CHMP7 by pull down assay. Figure 3 shows the sequence alignment of the CHMP1 isoforms to demonstrate their similarity.

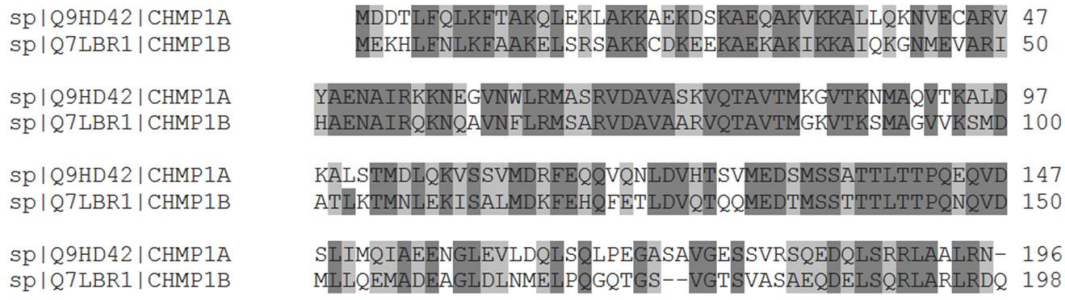

Figure 3 Sequence alignment (Clustal Omega[107]) of CHMP1A and CHMP1B. Dark grey indicates identical amino acids and light grey indicates amino acids which are similar. 60% of their sequence is identical and they share 82% similarity in terms of amino acid properties.

Antibodies for both CHMP1A and CHMP1B were raised against the full length GST-tagged protein. CHMP1A and CHMP1B contain the same motifs, such as the MIM1 and NLS, located in the same regions and both contain the coiled coil SNF7 domain. It is likely, based on this alignment that CHMP7 interacts with CHMP1B, as well as CHMP1A. CHMP1B and CHMP1A do display some key differences in the cell though, so any observations made concerning CHMP1B and CHMP7 does not necessarily hold for CHMP1A and will be treated with the appropriate caution.

The custom anti-CHMP7 antibody required optimisation by trialling different fixation methods and dilutions for visualisation. 4% PFA and methanol fixation were compared, plus 0.1% Triton X-100, 0.5% saponin and 0.1% SDS detergents (required to permeabilise the cell membrane). PFA and 0.1% Triton X-100 was chosen as the combination that gave the cleanest signal repeatedly. The staining indicated that in untreated cells CHMP7 is distributed throughout the cytoplasm and nucleus, with a stronger localisation in the peri-nuclear area (see appendix 9). Both anti-CHMP7 antibodies showed this distribution, however the custom

anti-CHMP7 did display a higher level of background staining. The sheep antibody was used straight from the unpurified bleed, which may account for the background bands in the western blot. The custom anti-CHMP7 was primarily used to co-stain with other anti-CHMP antibodies (all rabbit) for comparative purposes and analysis of co-localisation. Phenotypes observed using the custom sheep anti-CHMP7, were tested with the rabbit anti-CHMP7 antibody to look for agreement in behaviour.

4.2.2 CHMP behaviour in presence of GFP-VPS4B E235Q

CHMP subunits are known to localise on aberrant endosomes around the nucleus in the presence of a defective VPS4B, GFP-VPS4B E235Q. This VPS4B mutant contains a mutation in the Walker B motif of the AAA domain, impairing the ATPase activity since the enzyme can bind, but not hydrolyse ATP efficiently. This mutant acts as a dominant negative protein and produces sorting defects in cells. Furthermore, the ESCRT-III complex is no longer recycled and is effectively trapped on endosomes[51]. The endosomes themselves become abnormal and enlarged as cargo for sorting builds up creating a 'bottle neck' in the MVB pathway An example of this is shown in figure 4 using CHMP4B, which accumulates in the perinuclear area on endosomes. The mutant VPS4B is still able to bind to CHMPs through its MIT domain and so it too accumulates wherever CHMPs are clustered.

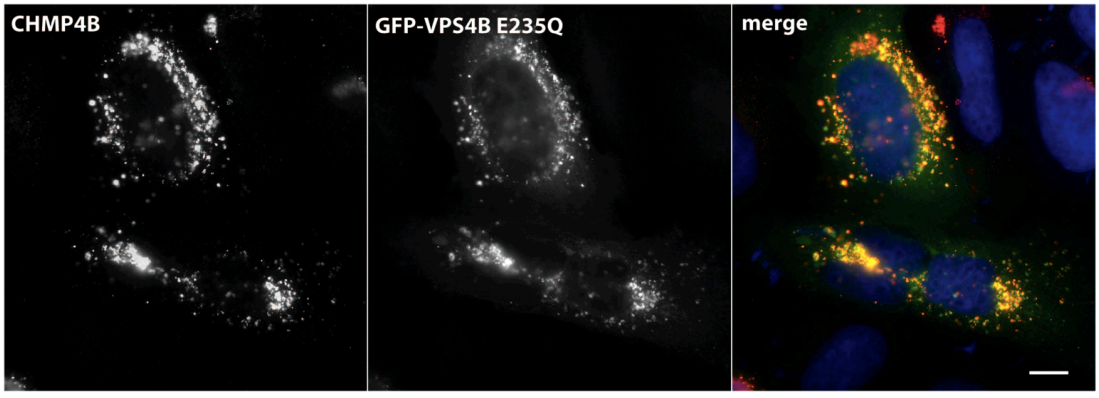

Figure 4 HeLa M cells transfected with 1µg/ml GFP-VPS4B E235Q. Cells were fixed twenty-four hours after transfection and stained with anti-CHMP4B (red, Cy3). The merge image shows co-localisation, in yellow, where the mutant VPS4B (green) and CHMP4B (red) are accumulated on endosomes. Scale bar equals 10 µm.

Both isoforms of VPS4, A and B, are responsible for removing CHMP subunits from the endosomal membrane and recycling them back to the cytoplasm in their monomeric state.

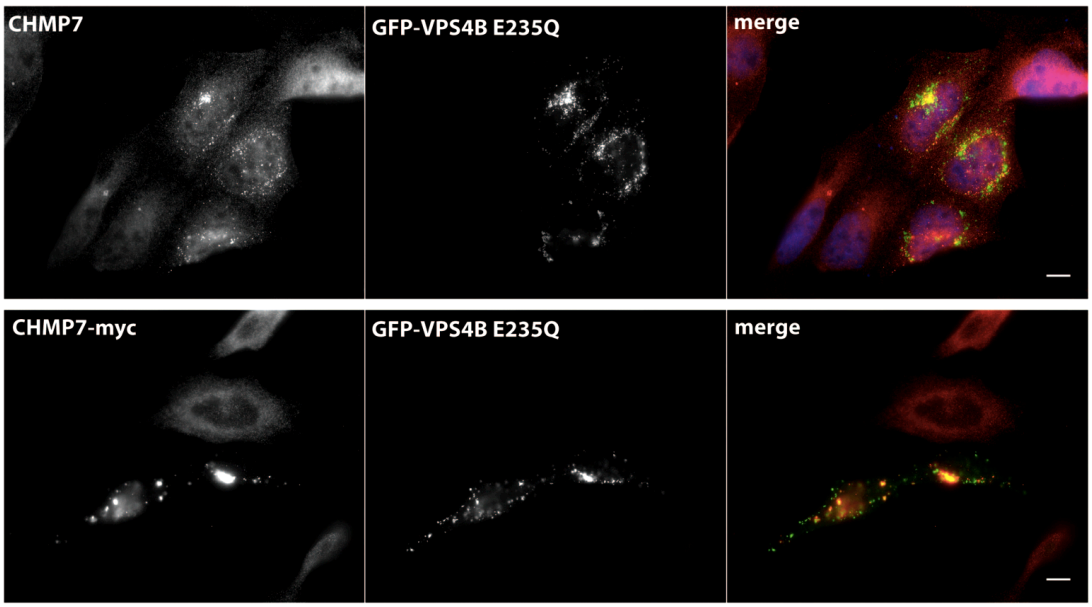

Figure 5 Effect of GFP-VPS4 E235Q transfection on endogenous CHMP7 in HeLaM cells (upper panel) and overexpressed CHMP7-myc in FRT cells (lower panel). Cells were transfected with 1µg/ml of a GFP-VPS4 E235Q plasmid and fixed after twenty-four hours. In the case of the CHMP7-myc inducible FRT stable cell line, cells were induced with 100ng/ml doxycyclin at the same time as transfection and fixed twenty-four hours later. In the case of the top panel, the custom anti-CHMP7 antibody was used and an anti-myc antibody in the bottom panel, with a Cy3 secondary antibody for both. Scale bars equal 10 µm.

CHMP7 displayed similar behaviour in cells transfected with 1ug/ml of a GFP-VPS4B E235Q construct. This demonstrates CHMP7 accumulating on aberrant MVBs, at least partially, like CHMP4B. The transfection of this VPS4 mutant does not seem to affect CHMP7 distribution as much as it has effected CHMP4B distribution. This correlates with the knowledge that CHMP4B is the most critical and abundant CHMP in the ESCRT-III complex and plays a larger part in the MVB pathway than CHMP7. For this reason CHMP4B is more greatly affected by a mutant VPS4.

It can be noted looking at figure 5 that the CHMP7-myc and endogenous CHMP7 do not behave similarly. Endogenous CHMP7 displays an even distribution across the nucleus and cytoplasm –this can be seen in cells in figure 5 (upper panel) where the level of transfection of GFP-VPS4 (EQ) is low. In contrast, overexpressed CHMP7-myc is absent from the nucleus. It is possible that the myc tag is affecting CHMP7 solubility and causing it to aggregate in the

cytoplasm, displaying a more speckled pattern. The myc-tag is located on the C terminal of CHMP7, a region critical for CHMP auto-inhibition in the cytoplasm, hence the tag itself could generate a mild dominant negative effect. On the other hand, myc tags are small and generally considered unlikely to affect the biochemical properties of a protein. The ability to simulate the effect seen by an endogenous CHMP in cells with a tagged construct, such as CHMP7-myc, is an important step towards mutagenesis studies. Titration of doxycyclin in inducible cell lines overexpressing CHMP4B-myc or CHMP7-myc allowed the identification of concentrations yielding the cleanest images by IF and with the most similar appearance to endogenous protein (20 ng/ml and 50-100 ng/ml respectively).

4.2.3 CHMP behaviour upon depletion of VPS4 isoforms

The MVB pathway is severely impaired by depletion of the VPS4 isoforms. Inward vesicle budding cannot occur and so along with CHMP subunits, ubiquitinated receptors for degradation build up on the endosome, with no means of being delivered to the lysosome.

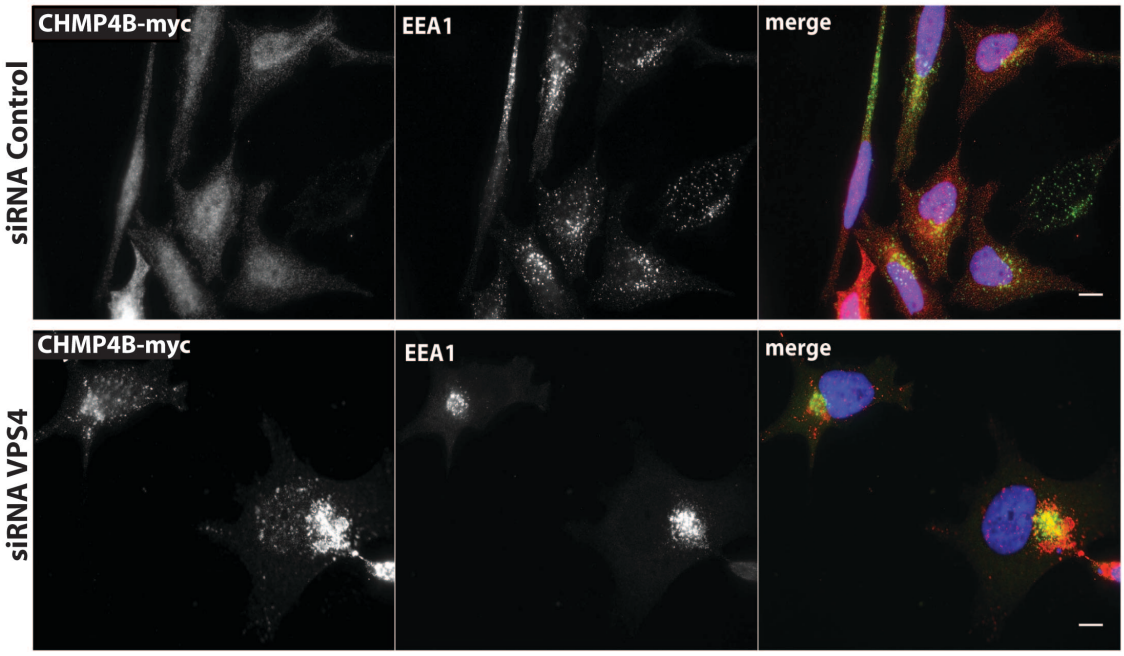

Figure 6 VPS4 depletion in FRT cells expressing CHMP4B-myc. Cells were incubated with RNAi for seventy-two hours and induced with doxycyclin (20ng/ml) twenty-four hours before fixing. The control represents where random non-targeting siRNA was used. These images use an anti-myc antibody and Cy3 secondary antibody. EEA1 (green, ALEXA488 secondary antibody) is a marker for the early endosome. Scale bar equals 10 μm.

A similar phenotype as seen by CHMP4B-myc in figure 6 would be expected for other CHMP subunits as they form a complex on the endosomal membrane and become trapped in that complex. Figure 6 also shows CHMP4B-myc localising to the midbody of a cell undergoing cytokinesis (bottom panel). This phenotype is typical due to the established role of CHMP4B in cytokinesis and demonstrates that the exogenous CHMP4B-myc construct displays the same behaviour. Similar phenotypes were observed for endogenous CHMP4B in HeLa M cells (figure 7a). CHMP4B also accumulates on midbodies (figure 7b), which are more frequent upon VPS4 depletion since cells stall in the final abscission step of cytokinesis. RNAi depletion of VPS4 blocked abscission, determined by an increased frequency of observed midbodies and the amount of cells displaying failed cytokinesis defects. Scoring for the presence of midbodies across a cell population can be an indicator of whether protein depletion is affecting cytokinesis (figure 7c).

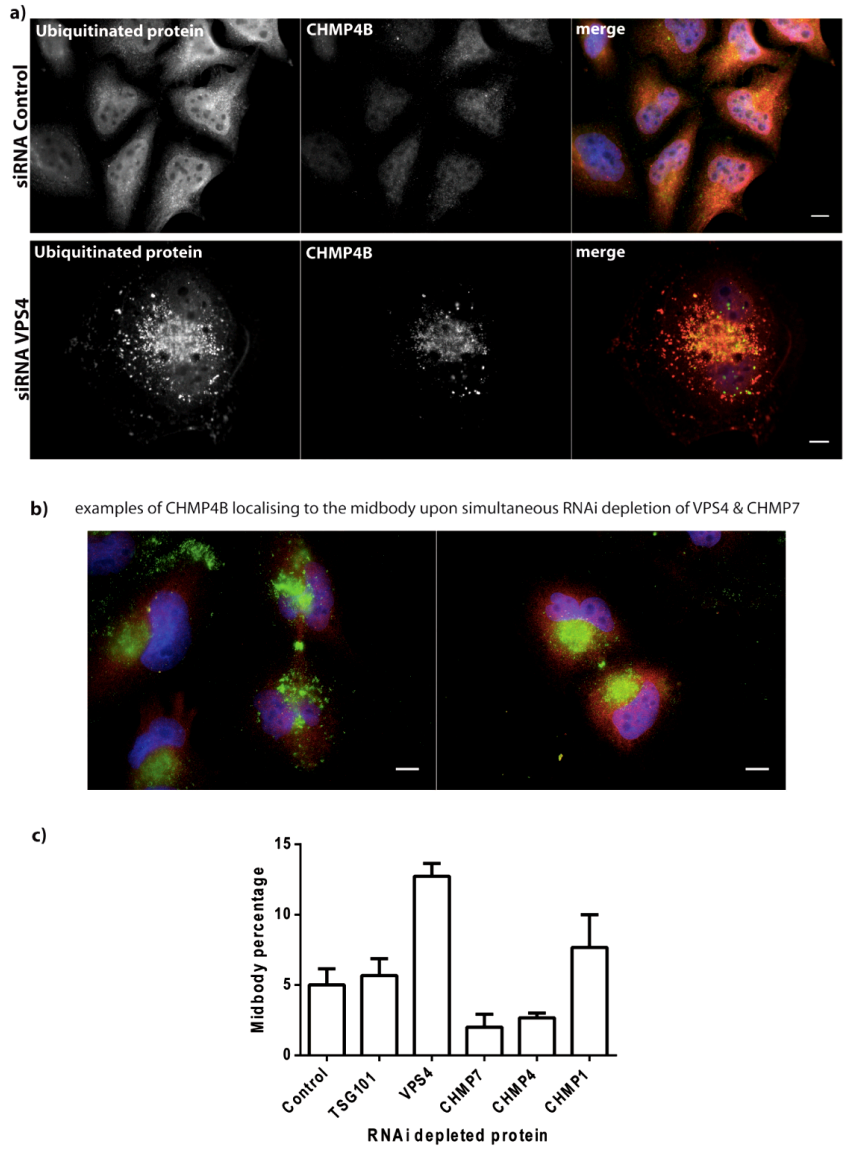

Figure 7 a) Control and VPS4 depleted HeLa M cells. Cells were treated with siRNA for seventy-two hours and stained for FK2 (red) and CHMP4B (green), with Cy3 and ALEXA 488 as secondary's. Image shows typical phenotype for a CHMP subunit by accumulating to endosomes upon depletion of VPS4 isoforms. Ubiquitinated cargo (FK2 antibody) also accumulates as the deubiquitinating enzymes that recycle ubiquitin are recruited with the aid of VPS4. (b) examples of cells with a visible midbody.. Scale bars equal 10 μm. (c) Graph showing the percentage of midbodies observed after seventy-two hours RNAi depletion of different proteins involved (or potentially involved) in cytokinesis. This analysis is based on over 300 scored cells from 3 or moreexperimental repeats, displaying the standard error of the mean (SEM). P values were calculated for each variable using a one-way anova (Tukey multiple comparisons test). The difference between the control and VPS4 depletion was statistical significant ($p \leq 0.01$), whilst comparisons between the other condition and the control were not statistically significant ($p \geq 0.5$). See figure 20 for the efficacy of these siRNA depletions.

The percentage of midbodies observed between control and VPS4 depleted cells shows a statistically significant increase caused by cytokinesis failure. TSG101, a component of the ESCRT-I complex, is recruited to midbodies by ALIX. Depleting TSG101 made no difference to the frequency of midbodies, which agrees with previous studies (figure 7c)[53]. It could still be argued that the depletion was not

effective. However, other phenotypes observed in the IF strongly indicate that the TSG101 RNAi depletion was effective, i.e. CHMPs and ubiquitinated cargo accumulating on endosomes and an increase in nuclear defects (see figure 11). This indicates that VPS4 plays a more dominant role in cytokinesis and the organisation of CHMP assemblies during this abscission.

All isoforms of CHMPs were targeted in multiple simultaneous RNA interference (CHMP4A, 4B and 4C or CHMP1A and 1B) to eliminate the possibility of functional redundancy. The frequency of midbodies is reduced in cells depleted of CHMP7 or CHMP4, however, after statistical analysis this difference was not statistically significant (based on 300 cells). A decrease in the number of midbodies in CHMP4 depleted cells would agree with the role of CHMP4 in delaying abscission, with CHMP4C binding subunits of the chromosomal passenger complex (CPC). Similar to CHMP4 function, the small decrease in observed midbodies in the cell population could be evidence that the abscission checkpoint is being bypassed in the absence of CHMP7 also. If this were the case, we would expect to see an increase in nuclear defects, especially defects relating to incorrect or incomplete chromosome segregation. The results of this analysis are presented and further discussed in chapter 6.

Depletion of the CHMP1 proteins resulted in a small increase in observed midbodies. This difference was not statistically significant, but indicates CHMP1 is involved in cytokinesis. As previously mentioned CHMP1B recruits spastin to the midbody towards the end of cytokinesis to sever microtubules; without this recruitment cytokinesis is slower and more midbodies observed. Bajorek et al found that CHMP1 depletion induced cytokinesis arrest and the accumulation of multinuclear cells[116].

The occurrences of CHMPs localisation to midbodies were examined based on the total number of midbodies found in 1000 VPS4 depleted cells (130 midbodies) (figure 8). CHMP4B was observed at 98% of these midbodies (i.e 127 midbodies), whilst CHMP1B was observed at 75% (i.e. 98 midbodies).This indicates the more dominant role played by CHMP4B in cytokinesis. In comparison, CHMP7 was only observed at 13% (i.e. 17 midbodies).

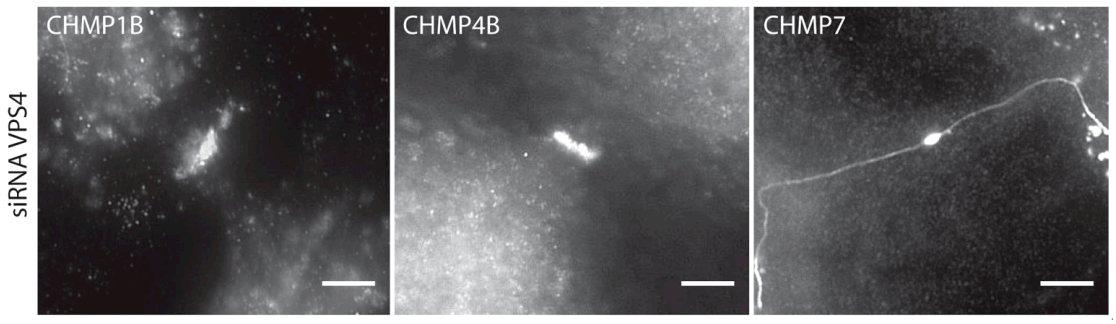

Figure 8 CHMPs localising to midbodies in VPS4 depleted cells. CHMP1B and CHMP4B localise to a larger midbody indicating an earlier stage of cytokinesis, where CHMP7 localisation is smaller and narrower indicating a midbody in a late stage of cytokinesis. All CHMP7 observed at the midbody was connected to daughter cells by a CHMP7 filament. Scale bars equal 5 μm.

However, the decrease of observed midbodies in CHMP7 depleted cells implies it does play some role in abscission. VPS4 depletion could be inhibiting CHMP7 involvement at the midbody by preventing later stages of cytokinesis where CHMP7 is required. CHMP7 appears at the midbody when it is smaller and the cells further apart, which indicates a late stage of cytokinesis. In comparison, CHMP1B and CHMP4B localise earlier to a bigger midbody at an earlier stage of cytokinesis. Figure 9 proposes an order of recruitment to the midbody, including the timing and duration of this localisation. These same issues of 'timing', i.e. the stage at which VPS4 stalls cytokinesis could also affect the amount of CHMP1B observed at midbodies. Hurley et al found that CHMP4B was one of the first ESCRT-III subunits to localise to the midbody following TSG101 and ALIX[82]. This agrees with the high level of co-localisation observed between midbodies and CHMP4B as the defects caused by VPS4 depletion don't stop cytokinesis early enough to stop ALIX recruiting CHMP4B.

CHMP1B was observed trapped at the midbody and on aberrant endosomes when VPS4 was depleted (figure 10). The general distribution of CHMP1B upon depletion of VPS4 (and transfection of a dominant negative mutant VPS4B) matches that of CHMP4B.

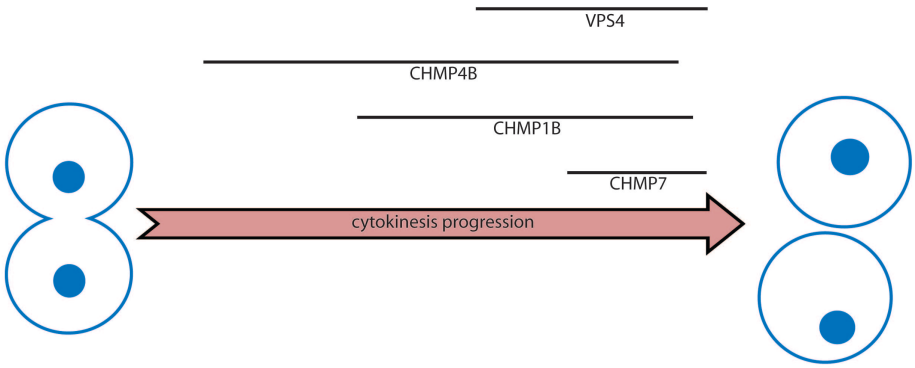

Figure 9 Cartoon illustrating recruitment and duration of ESCRTs at the midbody. CHMP4 isoforms are the first ESCRT-III to localise to the midbody recruited by ALIX. CHMP1B is recruited later and recruits spastin, which initiates microtubule disassembly. We propose that CHMP7 could be recruited at the late stages of cytokinesis and the potential reasons for this are discussed in chapter 6.

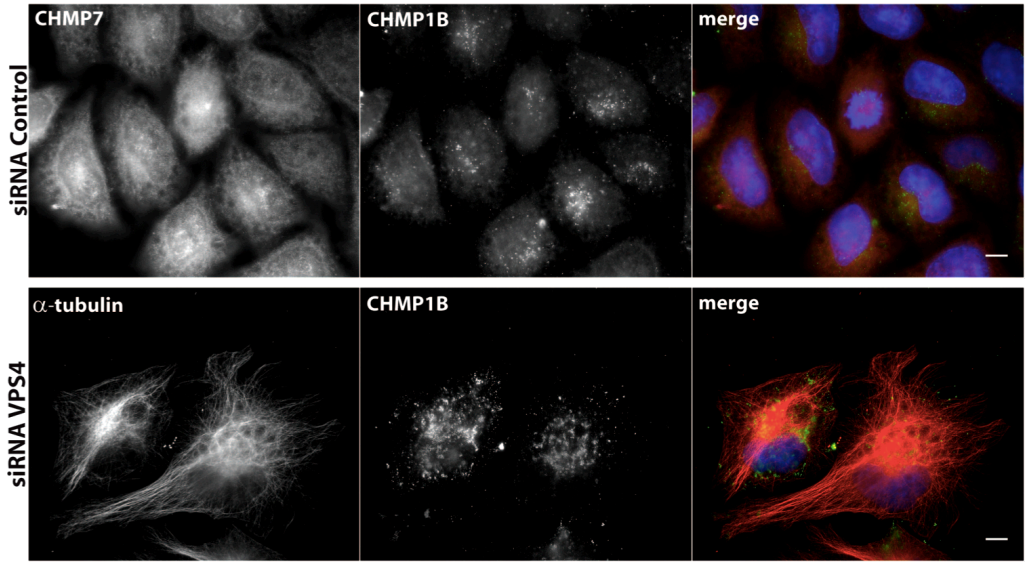

Figure 10 Control and VPS4 depleted HeLa M cells. Cells were treated with RNAi for seventy hours and probed with anti-CHMP7 (red, Cy3) in the control and anti-alpha-tubulin (DM1A, red, Cy3) in the VPS4 depletion. Both cell populations were stained with CHMP1B (green, ALEXA 488 nm). Image shows typical distribution for a CHMP subunit by accumulating to endosomes upon depletion of VPS4 isoforms. The DM1A antibody was used in order to score for the presence of midbodies where microtubules are dense. CHMP1B accumulates on midbodies in the absence of VPS4 isoforms. Scale bars equal10 μm.

Interestingly, CHMP7 did not display a similar localisation to the other CHMP proteins. Instead, upon depletion of VPS4, CHMP7 was found completely re-localised in the nucleus (figure 11b).

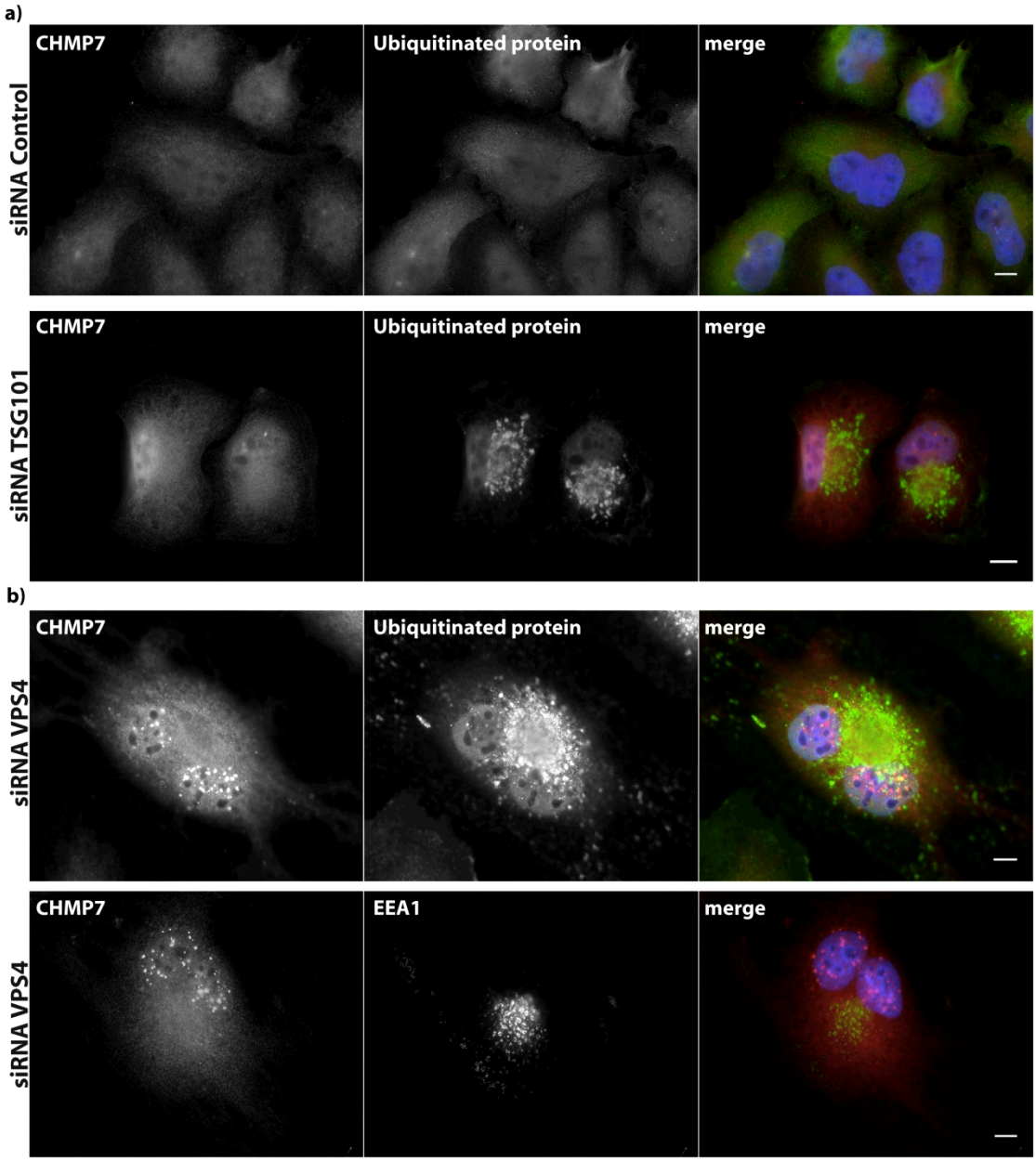

Figure 11 TSG101 and VPS4 siRNA treatment in HeLa M cells. (a) Cells treated with non-targeting RNAi are labelled as control. ESCRT-I component, TSG101 depletion, acted as positive control as its depletion is known to impair the MVB pathway. (b) Two examples of VPS4A + B knockdown cells. All images show CHMP7 (red, Cy3) and either ubiquitinated protein (FK2, green, ALEXA 488 nm) or EEA1, the marker for early endosomes. Scale bars equal10 µm.

Figure 11 shows little localisation between CHMP7 and both the early endosome and ubiquitinated cargo in VPS4 depleted cells, which suggests CHMP7's primary function is not in the MVB pathway. CHMP7 is predominantly nuclear with no endosomal clustering. This is in contrast with the behaviour displayed by CHMP7 upon transfection of the mutant GFP-VPS4B construct, where some endosomal clustering and partial VPS4B co-localisation was observed. To summarise this, the absence of both VPS4 isoforms leads to CHMP7

accumulating exclusively in the nucleus, whereas an inactive form of VPS4B results in endosomal clustering. Potentially VPS4A plays a more dominant role in recycling CHMP7 from nuclear structures, and can function in the presence of the inactive VPS4B, resulting in no observed nuclear CHMP7 spots in the transfection. The general idea of ESCRT recruitment is that the CHMPs bind to the endosomal membrane first and form spiralling filaments, before VPS4 is recruited for their disassembly[63]. It could be the case that CHMP7 is actually recruited to the endosomal membrane last, possibly by VPS4B itself. This would explain why no CHMP7 is observed on the endosome when both VPS4 isoforms are absent, but is clustered here when endogenous VPS4 is present and consequently appears 'trapped' due to the excess of inactive VPS4B. The hypothesis implies that CHMP7 recruitment to nuclear structures is independent of VPS4; making sense if we assume that CHMP7 only plays a minor role in the MVB pathway and its main role lies in the nucleus. A nuclear role is further supported by the putative DNA binding N terminal domain and nuclear localisation sequence suggested in chapter 3.

RNAi depletion of VPS4A and VPS4B separately did not have any noticeable effect on CHMP7 distribution or cell viability suggesting that VPS4 isoforms are functionally redundant; whilst the level of their involvement across different functions may vary, both isoforms are capable of 'taking over' if the other is absent.

4.2.4 Existence of a nuclear ESCRT-III complex

Both anti-CHMP7 antibodies are able to reliably reproduce staining that reveals the protein nuclear speckled phenotype observed upon VPS4 depletion (figure 12). The custom anti-CHMP7 antibody (sheep) was used for the ensuing data scoring. This was mainly because the majority of other antibodies were raised in rabbit.

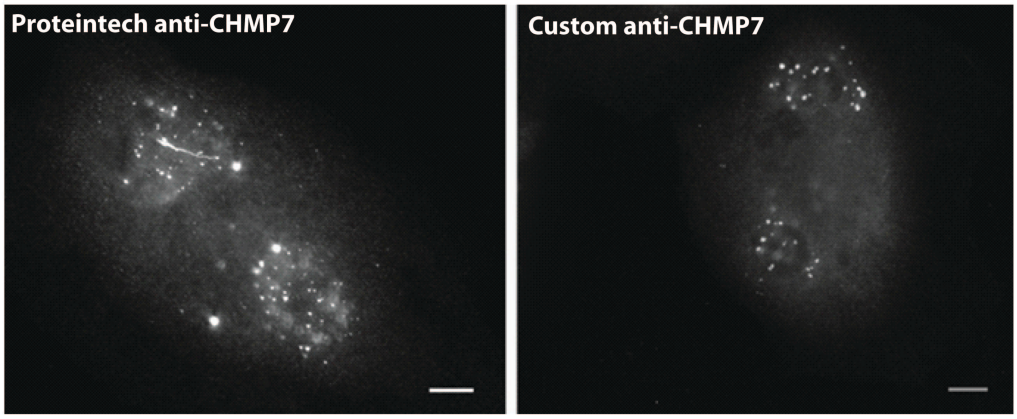

Figure 12 RNAi VPS4 depleted cells probed with each anti-CHMP7 antibody (with Cy3 secondary antibody). This demonstrates that these antibodies behave and recognise the same features, in this case the CHMP7 clusters observed when VPS4 is depleted. Scale bars equal 10 μm.

CHMP7 accumulation to nuclear structures was only seen in RNAi depletion of VPS4 isoforms and was observed in over 98% of treated cells (based on over 300 cells and scored for '1 or more nuclear spots'). In comparison, nuclear CHMP7 spots were observed in 34% of control cells. Figure 13b shows the average number of spots observed per cell, which further clarifies the difference between the control and VPS4 depletion. The 98% of VPS4 depleted cells contained approximately 15 CHMP7 spots per cell, whereas control cells contained on average less than 1 spot per cell. The 1 or 2 spots observed in the 34% of control cells, were quite diffuse in comparison to spots observed in VPS4 depleted cells (figure 13a).

TSG101 depletion acts as a positive control as it is an ESCRT-I component known to severely impair the MVB pathway and effect CHMP distribution[117]. TSG101 depletion had no significant effect on CHMP7 distribution. This observation distances it from the idea that it behaves like an ESCRT-II component (winged-helices domain containing) which interact with TSG101.

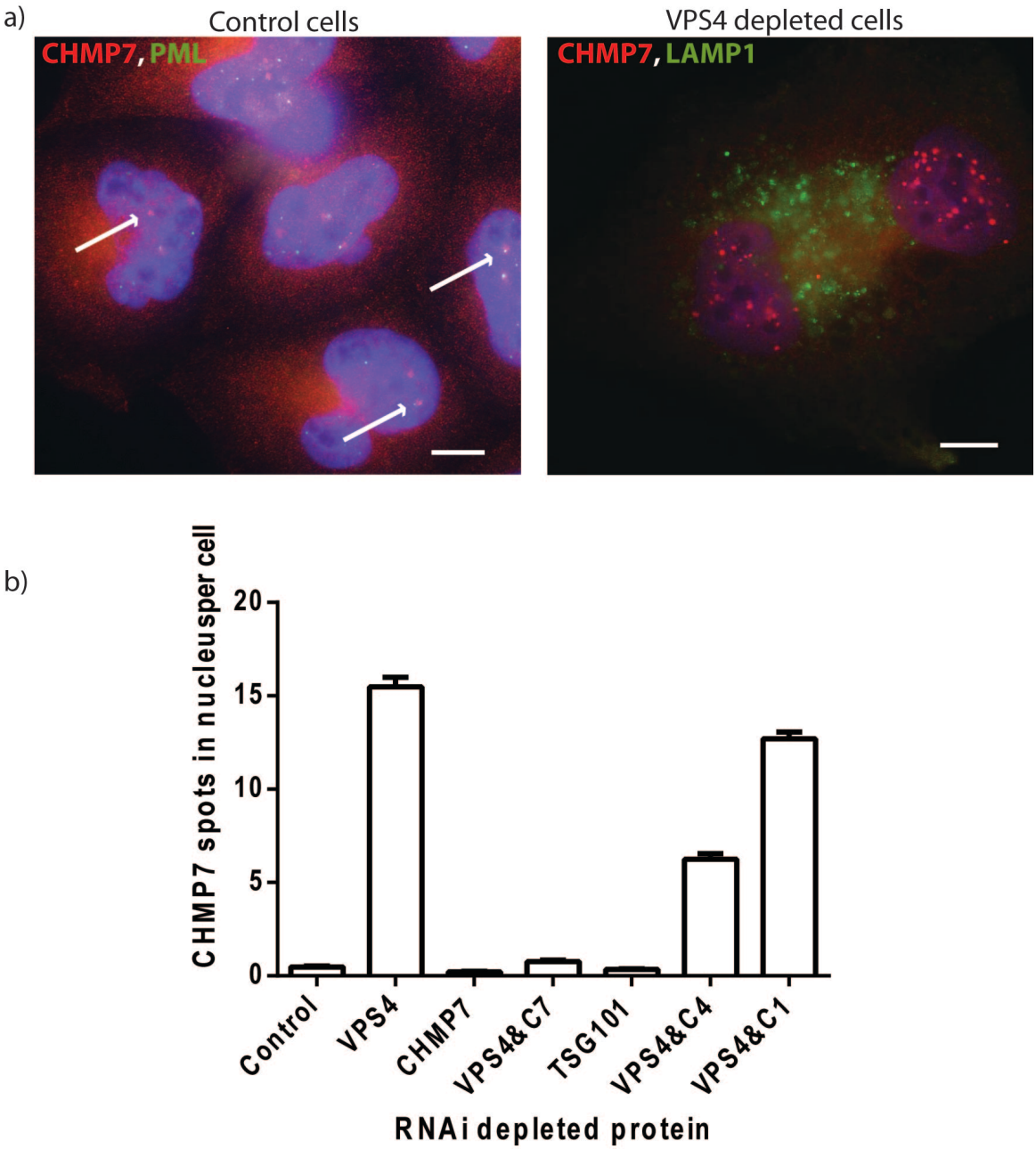

Figure 13 a) Cells treated for seventy-two hours with either 'control' non-targeting siRNA or siRNA specific to both VPS4 isoforms. Control cell image provides an example of the CHMP7 under 'normal' conditions- probed with anti-PML and anti-CHMP7, whereas the VPS4 depletion was probed using anti-CHMP7 and anti-LAMP1 (plus Cy3 and ALEXA 488 nm secondary antibodies). The white arrows indicate some of the nuclear CHMP7 clusters in control cells b) Graph shows the average number of CHMP7 spots per cell under different depletions. Scoring based on over 300 cells from at least 3 independent experiments. Control represents the use of non-targeting siRNA. VPS4&C7, VPS4&C4 and VPS4&C1 represent double RNAi treatment with VPS4 and the respective CHMP isoform(s) and based on images using the custom anti-CHMP7 antibody (sheep). Error bars represent standard error of the mean. The number of CHMP7 spots in all VPS4 depletions was statistically significantly compared to the control ($p \leq 0.0001$)

Depleting cells of both VPS4 and all the isoforms of another CHMP (4 or 1) lowered the number of nuclear CHMP7 bodies, indicating that CHMP7 relies on CHMP4 and CHMP1 for its nuclear re-localisation.

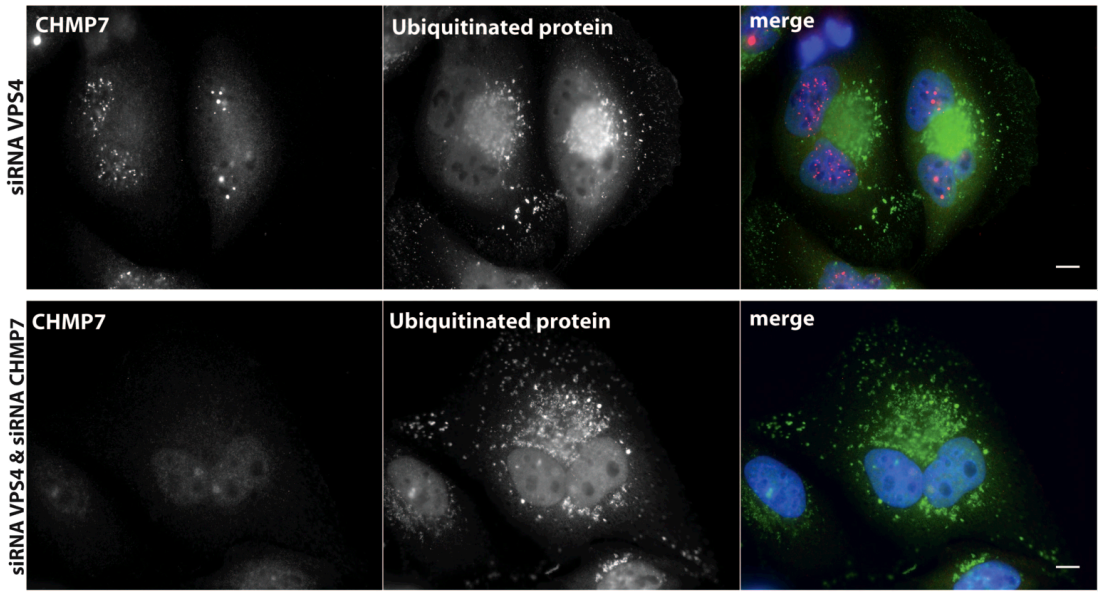

Figure 14 Cells depleted of VPS4 for seventy-two hours causes a re-distribution of CHMP7 to the nucleus. Depleting cells of both VPS4 and CHMP7 shows little extra effect on ubiquitinated cargo (FK2, green), but does indicate the RNAi knockdown is working as CHMP7 (red) is absent from the nucleus and only faint background staining is detected in the red channel. Scale bars equal10 μm.

Due to the dispersed nature of CHMP4B and CHMP1B around the nucleus (upon VPS4 depletion), nuclear spots of CHMP4B and CHMP1B are partly obscured. They are not clearly visible when focusing outside of nuclear planes, i.e. on endosomes etc. However, IF revealed that when we focussed in the DAPI focal plane, CHMP4B and CHMP1B were partially nuclear and were located at the same nuclear structures as CHMP7 (figure 15a & b). Co-staining with CHMP7 made apparent this co-localisation between CHMP7 and CHMP4B. This was also seen between CHMP1B and CHMP7, but to a lesser extent. We could not check co-localisation between CHMP4B and CHMP1B since both antibodies were rabbit. Taken together, these findings suggest that an ESCRT-III nuclear complex exists, consisting of CHMP4B, 1B and 7.

Much as the simultaneous depletion of CHMP4 or CHMP1 with VPS4 affected the number of nuclear CHMP7 –the same was observed for CHMP4B and CHMP1B. In fact, when VPS4 and CHMP7 were co-depleted no nuclear

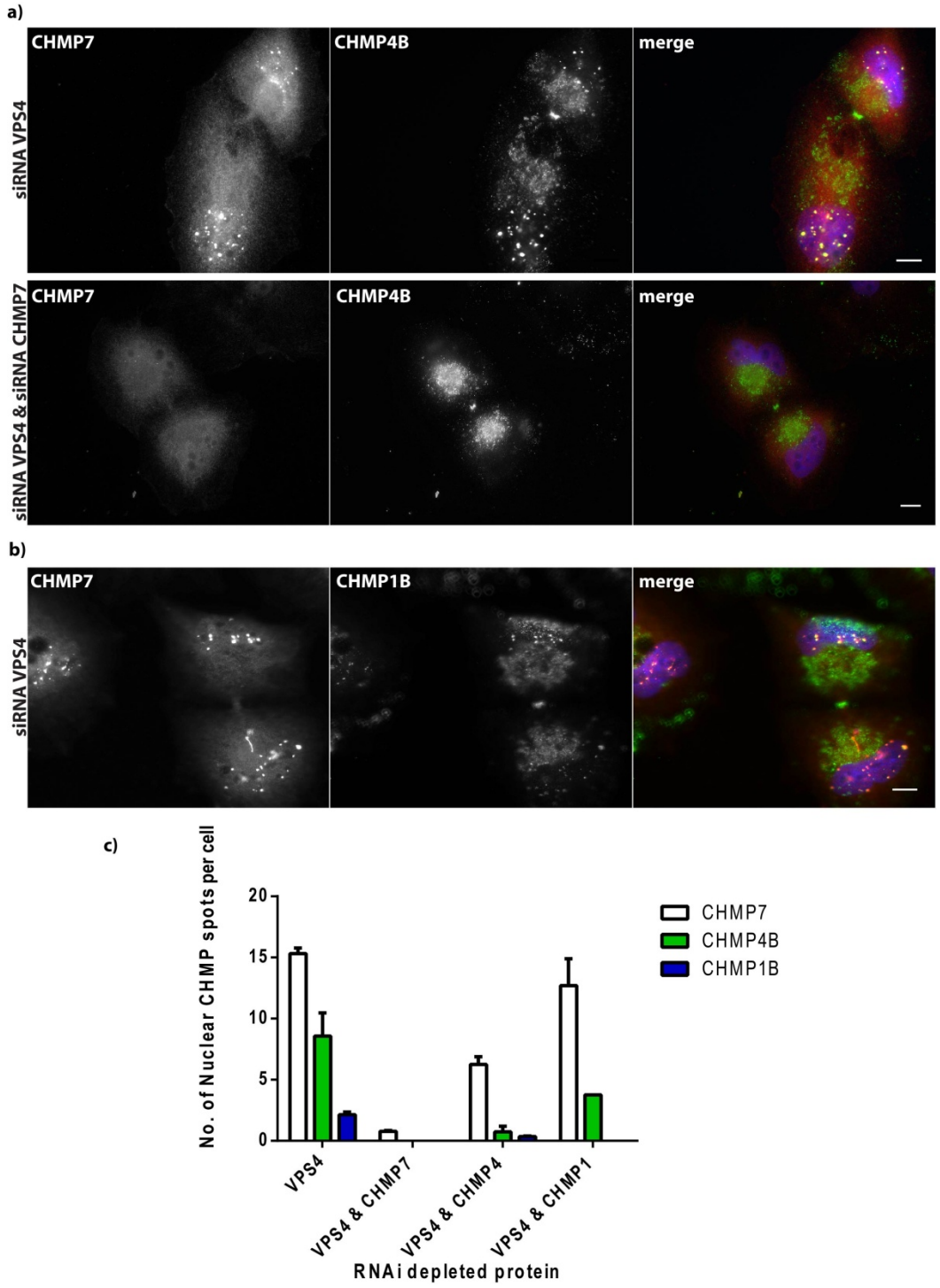

Figure 15 Examples of CHMP4B (a) and CHMP1B (b) displaying partial nuclear localisation upon RNAi depletion of VPS4. Simultaneous depletion of VPS4 and CHMP7 removes any CHMP4B/1B nuclear localisation. Scale bars equal 10 μm. c) Graph shows number of nuclear CHMP spots under various RNAi depletions, where white corresponds to CHMP7, green corresponds to CHMP4B and blue corresponds to CHMP1B. Error bars show standard error of the mean. A two way Anova test with multiple comparisons was calculated using Graphpad Prism (Turkey method) to determine P values. There is significantly more nuclear CHMP7 than CHMP4B or CHMP1B in all depletions, except for the VPS4/CHMP7 co-depletion ($P \leq 0.0001$). Co-depletion of VPS4 and CHMP4 significantly reduces the number of nuclear CHMP7 spots (($P \leq 0.0001$), but co-depletion of VPS4 and CHMP1 does not significantly affect CHMP7. In comparison, CHMP4B is significantly reduced by depletion of both CHMP7 ($P \leq 0.0001$) or CHMP1 ($P \leq 0.05$) with VPS4 compared to VPS4 alone.

CHMPs were observed at all (figure 15c). This indicates that CHMP7 is largely important for the formation or localisation of this nuclear complex. The number of CHMP7 nuclear spots is significantly reduced by co-depletion of CHMP4, but not CHMP1 simultaneously with VPS4, compared to VPS4 alone. The formation of this nuclear complex appears partially dependent upon CHMP4B. CHMP7 may aid the localisation of CHMP4B and CHMP1B to nuclear structures through the putative NLS signal. Whilst co-depletion of CHMP1 and VPS4 had no significant effect on nuclear CHMP7, it did significantly reduce nuclear CHMP4B spots ($P \leq 0.05$). Although some CHMP1B was observed displaying the nuclear spot phenotype, there was no statistically significant change in CHMP1B nuclear spots between all the depletions. These results also imply directionality in terms of recruitment to nuclear structure. CHMP7 is likely recruited first and partially requires CHMP4, but not CHMP1. CHMP4B requires CHMP7 and only partially requires CHMP1. CHMP1B is likely recruited last and requires CHMP7 and partially CHMP4 (not statistically significant). CHMP1B involvement is either partially blocked by the VPS4 depletion or it is only recruited to nuclear structures in certain cases. CHMP1B (and CHMP1A) have been shown to interact with IST1 using yeast two hybrid assays by Bajorek et al[116]. Moreover, CHMP1B has also been shown to bind LIP5 using pull down assays by Shim et al[65]. Both LIP5 and IST1 are involved in regulating VPS4 activity and oligomerisation, therefore, CHMP1B could be recruited late to these CHMP nuclear structures as part of their disassembly.

The visualisation of the CHMP nuclear body phenotype can be replicated using a myc-tagged form of CHMP4B or CHMP7. We used an inducible CHMP4B-myc HeLa stable cell line, in which the expression of CHMP4B-myc is controlled by addition of doxycyclin and the selection is maintained by addition of hygromycin B. CHMP4B-myc expression was induced twenty-four hours prior to fixation by addition of 50ng/ml doxycyclin in cells previously RNAi depleted (control and VPS4). The anti-myc antibody stain (figure 16), shows the same distribution as visualised by the anti-CHMP4B antibody. This adds further confidence that the CHMP4B co-localisation to CHMP7 in the nucleus is a real effect.

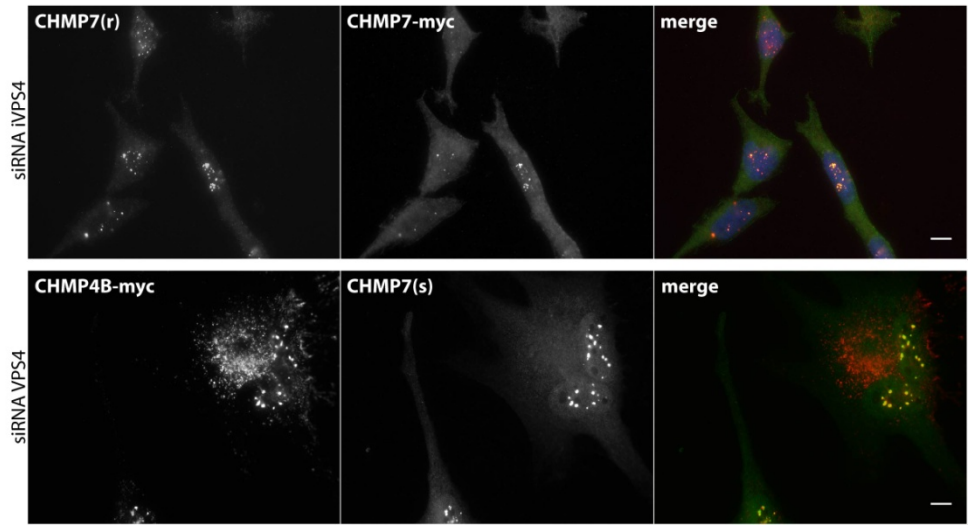

Figure 16 Top panel; VPS4 RNAi depletion in CHMP7-myc inducible cells. Cells were siRNA treated for seventy-two hours and induced twenty-four hours prior to fixing. Expression of CHMP7-myc was induced with 50ng/ml doxycyclin. The anti-CHMP7(r) antibody (rabbit, Proteintech) is red (Cy3) and the anti-myc antibody is green (ALEXA 488 nm). Bottom panel; VPS4 RNAi depletion in CHMP4B-myc inducible cells. Identical experimental to top panel except, cells were induced with 20ng/ml doxycyclin, and here myc is red (Cy3) and CHMP7 has been probed using the custom anti-CHMP7 antibody (green, ALEXA 488 nm) Scale bars equal10 µm.

The information provided by these images is limited due to the type of microscope used (Olympus BX-61 fluorescence microscope). It could be argued that the nuclear CHMP localisation could be to the outer surface of the nucleus and not necessarily inside. For this reason, VPS4 depleted cells were imaged using a confocal microscope capable of forming 3D images, by combining a number of images through the Z axis. This stack of images can be scrolled through and the point at which the CHMP spots become in focus tells us where they located. Deconvolution of this Z series can give a projected image that improves the signal to noise ratio by reallocating light to the correct pixels to give a clear image. The 3D images confirm that the CHMP7 and CHMP4B spots were inside the nucleus, figure 17 shows an example of a projected image confirming the CHMP complex is inside the nucleus.

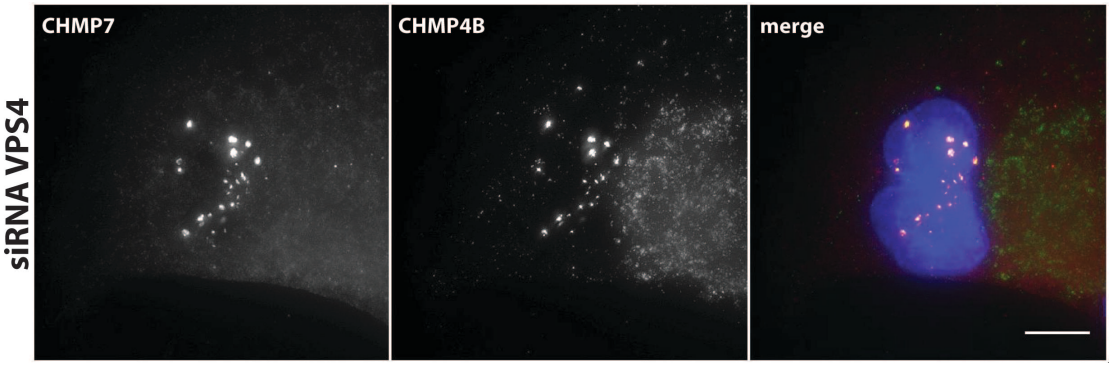

Figure 17 Confocal microscope image of VPS4 RNAi depletion in HeLaM cells. Cells were treated with siRNA for seventy-two hours, fixed as normal and probed with anti-CHMP7 and anti-CHMP4B. Cells were imaged using a deltavision deconvolution microscope to yield an XY image through a Z series. This Z series can be deconvolved resulting in one optimised image. CHMP7 (red, Cy3) and CHMP4B (green, ALEXA 488 nm) are in focus when viewing a plane in the centre of the nucleus, which means these spots are inside the nucleus. Scale bar equals 10 μm.

To investigate the timing of nuclear localisation of CHMP7, 4B and 1B in the nucleus, the effect of VPS4 depletion on cells was also analysed at twenty-four and forty-eight hours. The aim was to determine if these ESCRT-III complexes changed during successive cell cycles (one cycle being twenty-four hours). These experiments were performed in an asynchronous cell population; however, since VPS4 depletion impairs cytokinesis a large amount of multinuclear cells and cells in telophase were observed. These defects indicate attempted and failed cytokinesis.

The nuclear localisation of CHMPs sometimes resulted in the appearance of filaments (predominantly CHMP4B and CHMP7) as those shown in figure 18c. These filaments were observed in 13.7% of cells depleted of VPS4 and originated in the nucleus. CHMP4B was also seen localising with CHMP7 to filaments, but not CHMP1B. Invariably, CHMP7 filaments were observed going through midbodies or connecting nuclei in multinuclear cells. These data are further analysed and discussed in chapter 6.

The number of observed nuclear CHMP bodies increased for all three studied CHMPs over time. The first appearance of CHMPs is observed at forty-eight hours post VPS4 siRNA introduction (figure 18a). It must be noted that after twenty-four hours VPS4B is still present, indicating the RNAi is not yet in full effect (figure 18b).

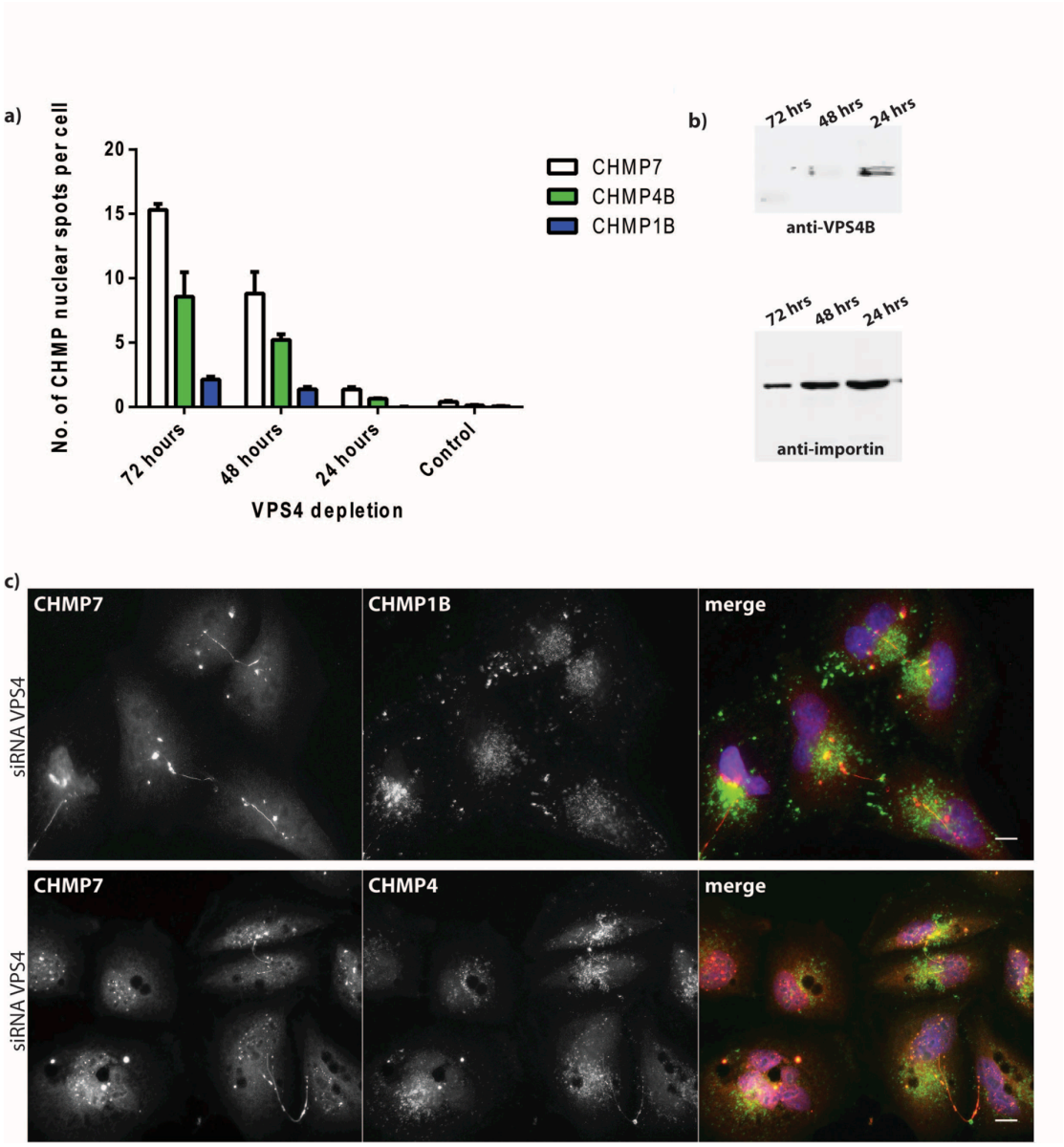

Figure 18 a) graph scoring for nuclear CHMP clusters in VPS4 depleted cells from twenty-four hours to seventy-two hours (seventy two hours being the normal knockdown duration). White shows CHMP7, green CHMP4B and blue CHMP1B. Error bars represent standard error of the mean and is based on at least 200 cells per bar. b) Western blot demonstrating VPS4B present over time, and importin beta as a loading control. c) Examples of CHMP7 filaments upon VPS4 depletion (seventy-two hour depletion). CHMP4 also localises to filaments, but CHMP1B did not. Scale bars equal 10 μm.

At twenty-four hours no CHMP7 filaments were observed, whereas at forty-eight hours 22.95% were seen per cell (average taken from 300 cells). Therefore, if we only take into account forty-eight and seventy-two hours (as VPS4 depleted populations), the number of nuclear CHMP spots increases as cells progress through the cell cycle. One must remember that many of these cells are stalled after failed cytokinesis, generating multinuclear cells. After the separation of genetic material the nuclear envelope reforms before abscission occurs[118]. When

abscission is aborted the cell ends up with both nuclei, two centrosomes and a decreased surface to volume ratio[119]. Cells that fail to complete cytokinesis often become stalled in the next phase of the cell cycle (G1 phase)[120].

A prolonged stall after failed cytokinesis appears to increase the number of nuclear ESCRT-III complexes observed. Despite this no clear relationship was observed between the number of nuclear CHMP bodies and the type of defect nuclei displayed. Specifically, there was no noticeable difference between the amount and size of CHMP bodies in a multinuclear cell compared to a 'normal' nuclei cell. This indicates the complex is not a response to failed cytokinesis and does not accumulate further when cytokinesis fails. CHMP localisation to the nucleus therefore must predate cytokinesis attempts. This agrees with previous work by Morita et al where cells depleted of CHMPs (particularly CHMP7, CHMP1 isoforms and CHMP4B) was found to exhibit mitotic defects[45]. Depletion of VPS4A and VPS4B also displayed mitotic defects, indicating a role for the nuclear ESCRT-III complex in mitotic events.

4.2.5 CHMP7 and CHMP1 play minor roles in MVB sorting

Depletion of individual ESCRT-III subunits has been shown to delay EGF receptor degradation and disrupt the MVB pathway[121]. Depletion of CHMP7 and CHMP1 had little effect on the distribution of early/late endosomes or ubiquitinated cargo. In contrast, CHMP4 depletion resulted in enlarged endosomes (EEA1 antibody) seen in figure 19a. CHMP7 and CHMP1 play only minor roles in the MVB sorting pathway and have little direct effect on endosome localisation or morphology, demonstrated by their respective depletions (figure 19a). CHMP4 is well established as having major role in the ESCRT-III endosomal complex and in vesicle formation[6].

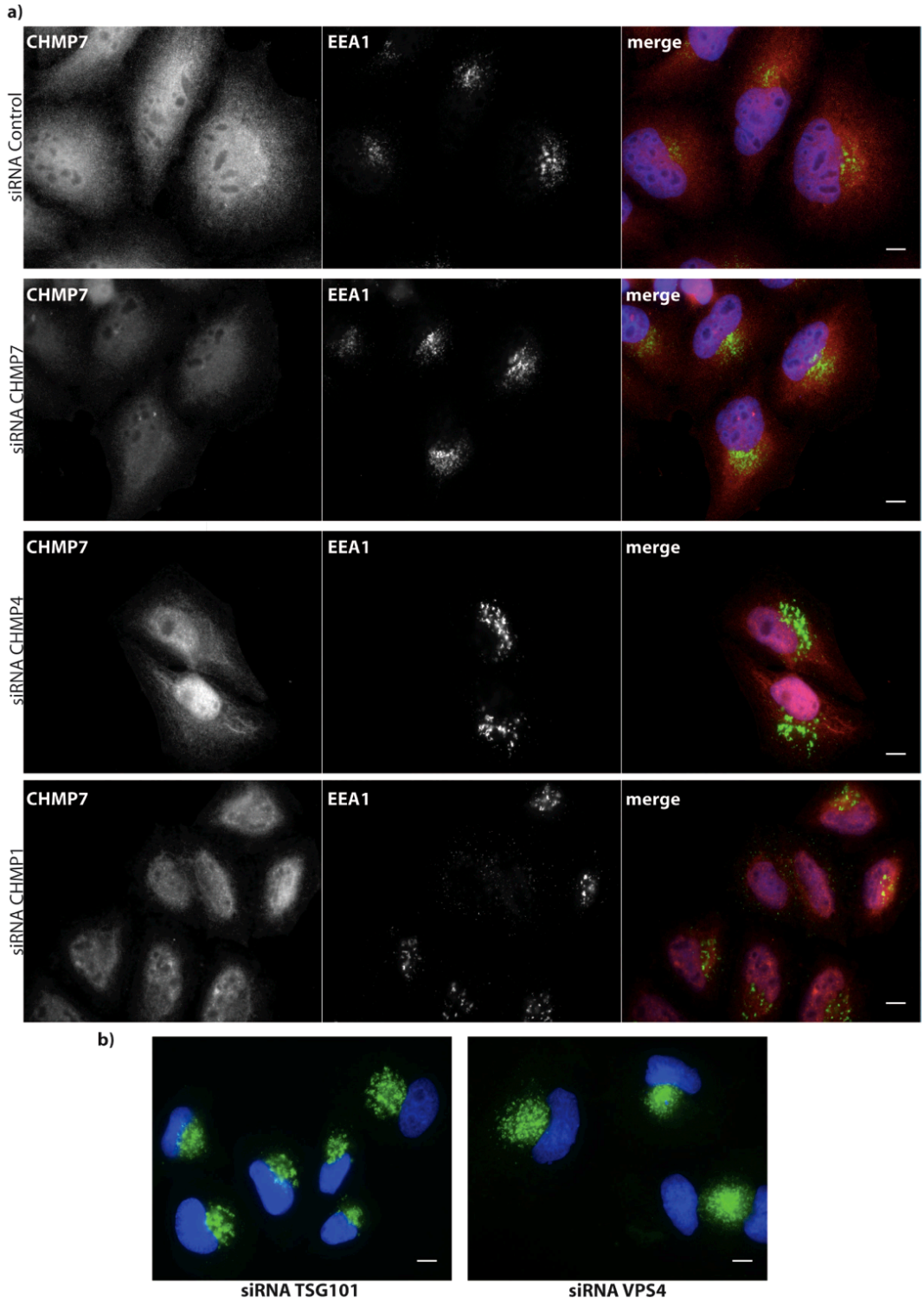

Figure 19 a) Effect on early endosomes (EEA1, green, ALEXA 488 nm) and CHMP7 (red,Cy3) upon depletion of ESCRT-III subunits, CHMP7, CHMP4 or CHMP1 (all isoforms). Depletion of CHMP4 results in the appearance of clustered aberrant endosomes, similar to the affect created by TSG101 or VPS4 depletion (b).TSG101 or VPS4 depletion is known to severely impair the MVB pathway and delay degradation. Early endosomes appear enlarged and clustered in the peri nuclear area. Scale bars equal 10 µm.

Figure 19b provides an example of abnormal endosomes (after TSG101 or VPS4 RNAi depletion). It was observed that CHMP7 appeared more nuclear (but diffuse) upon CHMP4 RNAi depletion. This could indicate some regulation of CHMP7 localisation by CHMP4. This possibility is reflected by CHMP7s partial dependence on CHMP4B for nuclear localisation.

4.2.6 Efficacy of RNAi depletions

The efficacy of all knockdowns was determined by western blot (figure 20). There was no commercial antibody available for VPS4A, therefore, the VPS4A DNA content in VPS4 depleted and controls cells was determined by qPCR (see appendices 11 and 12). These experiments consolidate the results from the IF data.

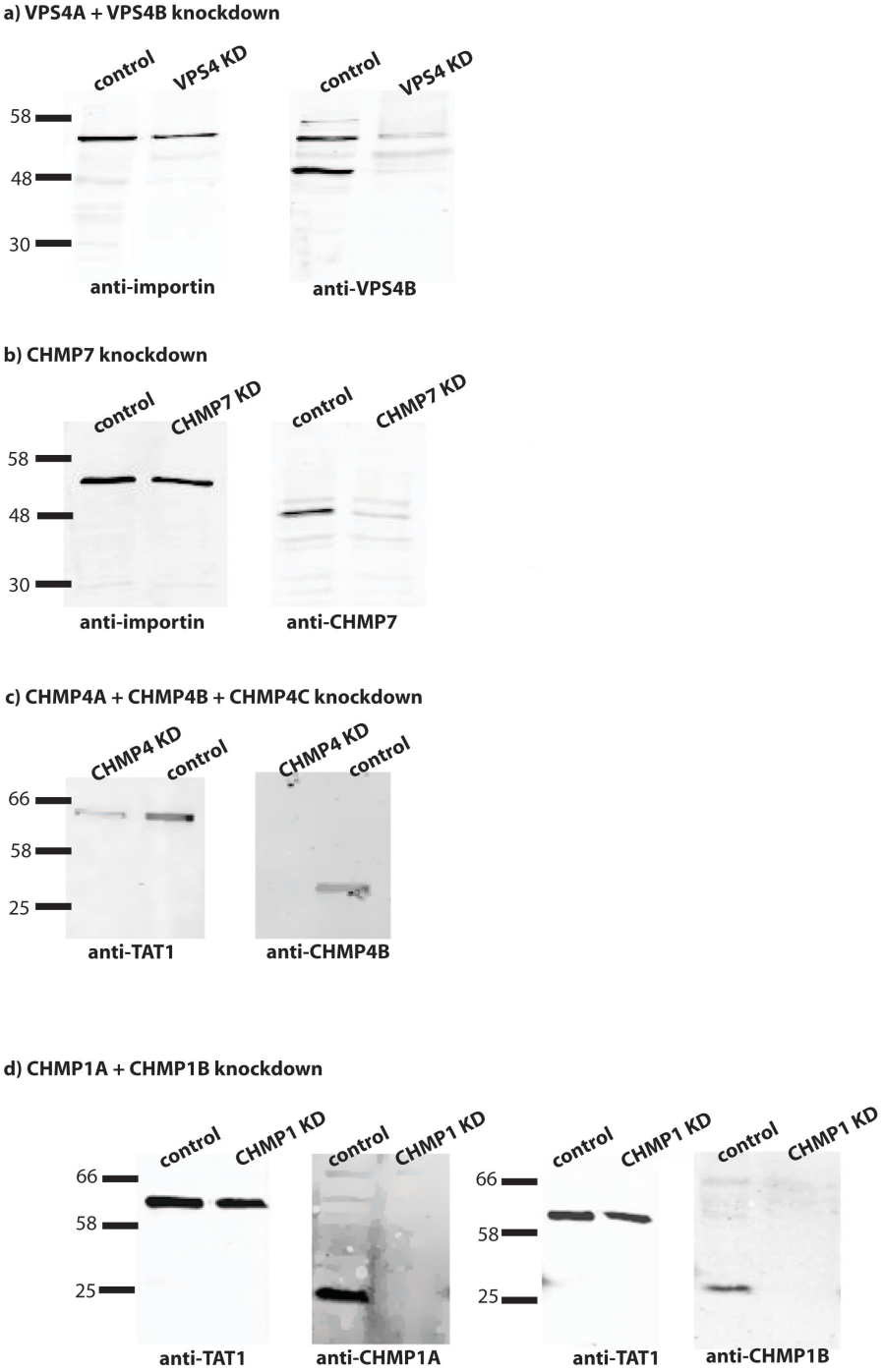

Figure 20 Western blots demonstrating the efficacy of the RNAi depletion experiments. In the case of a) VPS4 RNAi depletion, anti-VPS4B is the only commercially available antibody (Proteintech). Blots all show a loading control, either anti-importin beta (55-60kda) or anti-TAT1 (50-65kda) scanned using Odyssey Sa software from LICOR.

4.2.7 Analysis of CHMP7 subcellular localisation during the cell cycle

The cell cycle stage of cells can be determined by the appearance of the nucleus in an asynchronous population. Alternatively cells can be synchronised by blocking them at a certain stage of the cycle and then releasing them. This method allows easier and more robust scoring of a population.

Cells were blocked at the G1/S phase border using a double thymidine block. Thymidine is a nucleotide, which interacts with the DNA in cells during S phase and results in the inhibition of DNA synthesis. Therefore, excess thymidine in the media means cells remain at the end of the G1 phase, whilst other cells already passed this phase continue through the cycle until they too reach the end of G1 and become blocked. Cells are placed in fresh media (without thymidine) for longer than S phase lasts (approx eight hours) in order to allow all cells to complete this phase. By repeating this 'block and release', a higher amount of the total cell population is captured at the G1/S phase border. Once released cells are able to progress through the cell cycle and can be fixed at different times corresponding to what stage of the cell cycle they are in. HeLa cells have a complete cell cycle of around twenty-four hours. Fixing cells at zero hours shows G1 phase, four hours shows S phase, ten hours shows G2 and twelve hours shows cytokinesis –these are approximate timings and vary across cells. We aimed to monitor CHMP7 through the cell cycle in order to determine when it was located in the nucleus and if it ever accumulated at the midbody.

Preliminary results did not reveal a clear point in the cell cycle when CHMP7 was predominantly nuclear or accumulating to nuclear structures. This suggests the ESCRT-III complex, observed upon VPS4 depletion, is highly transitory. No evidence, to date, has suggested that CHMP7 plays a role in cytokinesis. As previously mentioned, data from VPS4 depletions showed that CHMP7 localised to midbodies in only 13% of cases. The majority of cells fixed between eight-twelve hours of thymidine release were undergoing cytokinesis and visible midbodies were present. CHMP7 was not seen strongly localising to these dense microtubule structures. Figure 21 shows, however, that the distribution of CHMP7 did seem biased towards the 'midbody-side' of the cell. This could suggest that

CHMP7 has some function in cytokinesis-related events if not cytokinesis itself. For example, the correct division of genetic material occurs during mitosis and into cytokinesis. This segregation of material occurs in conjunction with machinery regulating the timing of abscission. It could be proposed that CHMP7 plays a role here due to its generalised location in this region during cytokinesis, nuclear localisation, predicted DNA binding domain and mitotic defects displayed in its absence.

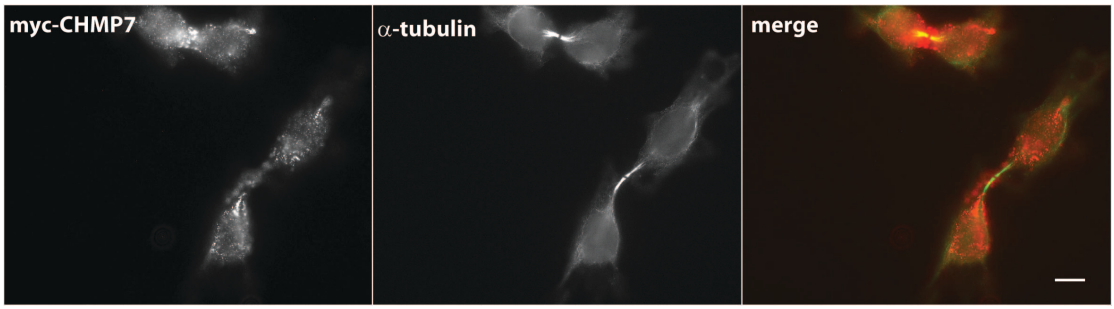

Figure 21 FRT synchronised cells, inducing CHMP7-myc, and fixed ten hours after release from double thymidine block. Induction of CHMP7-myc (red, Cy3) was induced twenty-four hours prior to the fixation of the first population of released synchronised cells. Anti-alpha-tubulin probed for microtubules (DM1A) with ALEXA 488 nm (green) secondary antibody used. At 8 hours the majority of cells should be entering cytokinesis. Scale bars equal 10 μm.

4.3 Discussion

CHMP7 displays a unique distribution upon VPS4 depletion, localising exclusively to nuclear structures (spots). CHMP4B and CHMP1B also localised partially to these structures, as well as endosomes and midbodies. The nuclear localisation of this complex seems dependent upon CHMP7. In the absence of CHMP7 no nuclear CHMPs are observed.

CHMP7 localisation itself is only partially dependent upon CHMP4, resulting in a reduction of nuclear spots when CHMP4 depletion is combined with VPS4. Pull down assays between fragments of CHMP7 and CHMP4B from chapter 3 indicated a direct interaction. The IF experiments show this interaction is not essential for CHMP7 to localise to nuclear structures though.

One working hypothesis is that CHMP7 may define a unique ESCRT-III assembly pathway onto nuclear structures, revealed upon VPS4 depletion by effectively ‘freezing’ the complex. This phenotype is not a general effect of ESCRT

machinery impairment as TSG101 depletion does not result in the same effect. Moreover, CHMP7 was not visualised localising to these nuclear structures upon any other condition than VPS4 depletion, such as monitoring its progress through the cell cycle or by depletion of other ESCRT-III subunits.

Data relying on myc-tagged CHMPs, rather than endogenous proteins, provides a route for the design and expression of mutant CHMPs in order to explore their behavior and localisation. We found that expressing CHMP7-myc and CHMP4B-myc in a stable inducible cell line, using a Tet-controlled transcription activation method, is a gentler way of introducing foreign DNA and protein expression to cells (as opposed to transient transfection). Through titration experiments, an optimum concentration of doxcyclin can also be used to express physiologically relevant concentrations of protein. Overexpression, using either CHMP7-myc or CHMP4B-myc plasmids, gave less reproducible data due to dominant negative effects.

Experimental evidence suggests CHMP7 does not play an important role in either the MVB sorting pathway or cytokinesis. However, overexpression of a dominant negative VPS4B mutant did result in partial clustering of CHMP7 on endosomes. Preliminary evidence suggests the equivalent dominant negative VPS4A mutant causes a speckled nuclear CHMP7 appearance. Interactions between VPS4A and all CHMP4 and CHMP1 isoforms are already established by Sundquist et al (biosensor binding assay)[61]. To date, no interaction between CHMP7 and VPS4A has been revealed. However, VPS4B and VPS4A share 80% sequence identity and all the other CHMPs interact with both isoforms (except for CHMP5, where this is unknown). Based on these results and observations VPS4 isoforms could specialise in separate functions and act independent of each other, whilst ultimately remaining functionally redundant. VPS4A could be involved in the nuclear disassembly of the ESCRT-III complex, whereas VPS4B is more involved in MVB sorting. Alternatively, the nuclear CHMP complex is only seen upon depletion of both isoforms simultaneously implying it is unlikely one isoform functions more in the nucleus than the other. VPS4A and B mutants appear absent from the nucleus in IF experiments, so it is possible this mutation blocks their access to the nucleus. Overexpression of wildtype VPS4 retains an even distribution between the cytoplasm and nucleus, similar to endogenous VPS4

(see appendix 10). Therefore, we suggest endogenous VPS4 is able to function unhindered in the nucleus and disassemble a CHMP complex, despite overexpression of a dominant negative VPS4 mutant. In chapter 3, it was proposed that CHMP7 might contain both a nuclear import signal implying that CHMP7 itself could act as the 'vehicle' for nuclear localisation of CHMP4B and CHMP1B. CHMPs exist as monomers in the cytoplasm so are more likely to become trapped on endosomes by VPS4 E235Q, meaning CHMP7 is unable to drive the nuclear assembly in this experiment.

VPS4 plays crucial roles in many cellular events. It could be possible the nuclear localisation of CHMPs is an indirect effect of its depletion. For example, VPS4 depletion is toxic to cells and many die. Nuclear localisation of ESCRT-III could be a reaction to cellular stress. The next chapter aims to explore what nuclear structures the ESCRT-III complex was localising to and whether this points towards a direct effect of VPS4 depletion or an indirect effect due to cell stress.

CHAPTER 5 ESCRT-III COMPLEX LOCALISES TO PML NUCLEAR BODIES

5.1 Introduction

The nucleus of eukaryotic cells is compartmentalised into diverse sub-nuclear domains. Several nuclear body (NB) structures exist in highly differentiated cell nuclei, such as the nucleoli, Cajal bodies, nuclear speckles, polycomb group (PcG) bodies and promyelocytic leukemia (PML) bodies (figure 1). This chapter describes experiments that unveil a potential link between PML NBs and that of nuclear ESCRT-III assemblies.

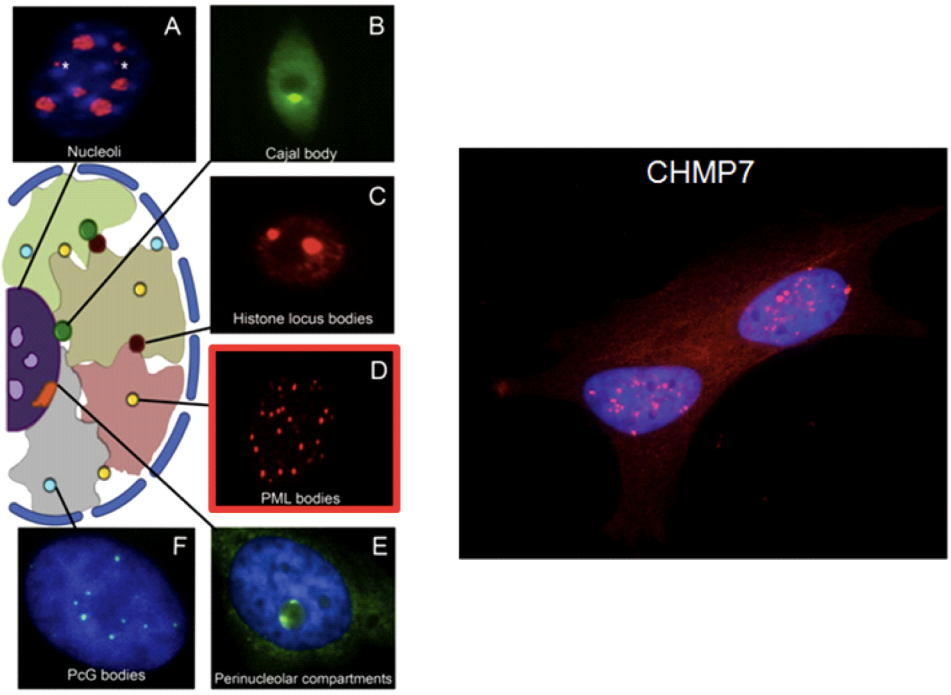

Figure 1 Cartoon illustrating the different types of nuclear structure, their localisations and appearance by IF[122]; A) nucleoli, B) cajal bodies, C) Histone locus bodies, D) PML bodies, E) perinucleolar compartments and F) Polycomb group (PcG) bodies. The nucleus is a highly organised structure; in addition the nuclear bodies shown, this space also contains defined chromosome territories and interchromatin compartments. CHMP7 probed with custom anti-CHMP7 antibody and Cy3 secondary antibody (right image, VPS4 RNAi depletion).

The range of functions of many of these nuclear structures remains relatively unknown. In particular, PML NBs have been implicated in a large variety of functions (figure 3) by the sheer number of interaction partners identified (over 100 proteins). These interaction partners include; proteins involved in apoptosis such as DAXX (death domain associated protein) which is repressed by sequestration into PML NBs, and many proteins implicated in neurodegenerative disorders and types of cancer such as ATAXIN and 27KIP1[123,124].

5.1.1 PML nuclear bodies

PML is a tumour suppressor protein occurring in various spliced isoforms and nucleates the assembly of PML NBs. These sub-nuclear bodies are also known as ND10, PML oncogenic domains (PODs) or Kremer bodies although PML nuclear body is the most common as the PML protein is the key organiser and recruitment site for body formation. PML NBs are present in most mammalian cells ranging from 1 to 40 per nucleus and are spherical objects with their sizes in diameter varying from 0.1μM to 1μM[125]. Typically these nuclear bodies are located in the interchromatin space and create extensive contacts with chromatin fibres, which may provide a stabilising effect. The centre of the body, which appears to differ depending on the PML isoform, is mainly proteinaceous and does not contain DNA or RNA with PML forming the outer shell[126]. PML nuclear bodies are incredibly dynamic structures, their number, size and composition changes throughout the cell cycle and also as a result of cellular stress, such as DNA damage, viral infection or oxidative stress[127].

PML belongs to the tripartite motif (TRIM) family of proteins, which consists of the following three motifs found at the N-terminal: a ring finger, one or two B box zinc fingers and a coiled coil region. This is collectively referred to as a RBCC domain (figure 2). The C terminal of PML varies across the isoforms, which may influence the morphology and biogenesis of individual PML nuclear bodies. Some PML isoforms, for example, do not contain an NLS and exist only in the cytoplasm. Like other TRIM proteins, PML is induced by interferons, a component of

pathogen resistance[128]. In the case of PML, transcription of the gene is controlled by interferons and p53.

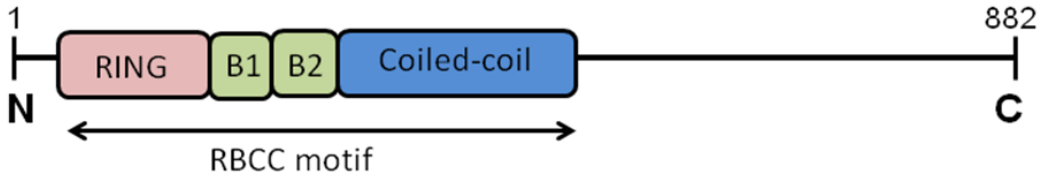

Figure 2 Cartoon representing PML, domains and motifs: The N terminal contains the RBCC motif, consisting of a ring finger, two B box zinc finger and a coiled coil region. The C terminal varies across isoforms

PML protein dimerises through the RBCC domain and these dimers can cluster together. In order to form spherical organised nuclear bodies, PML protein clusters require a post translational modification called sumoylation, which is the covalent attachment of a small ubiquitin-like modifier (SUMO) protein. At this point, sumoylated PML can recruit further proteins into the nuclear body. A common feature of proteins that localise to and interact with PML is that they too become sumoylated[127].

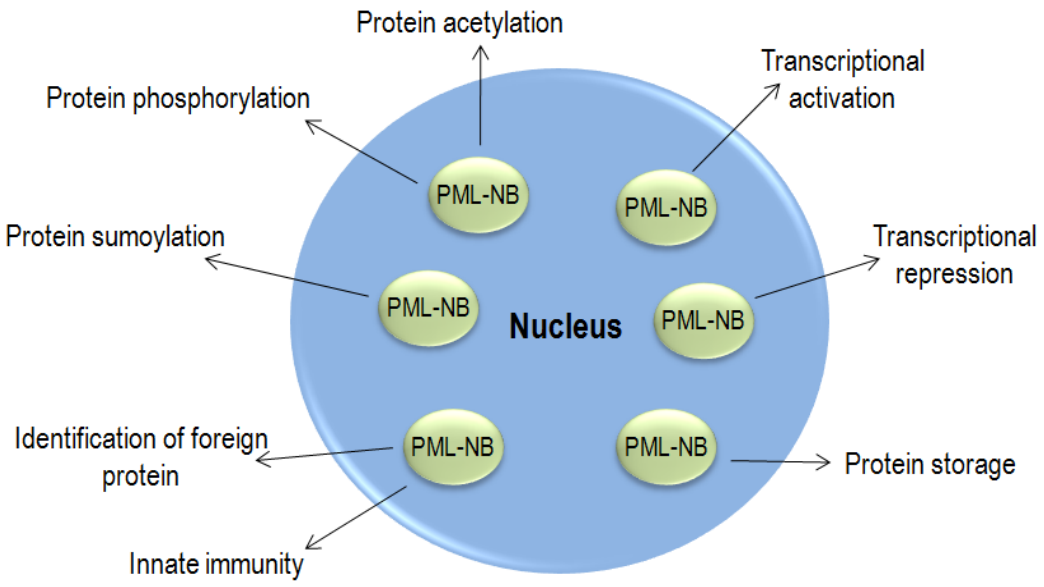

Figure 3 Implicated functions of PML nuclear bodies (PML-NB): The highly dynamic nature of PML bodies is reflective in the wide range of functions and protein partners.

The importance of sumoylation in nuclear body formation is highlighted in studies of *PML-/-* mice, which showed that PML was essential for NB formation[129]. Proper NB structure could only be restored with wildtype PML and not a sumoylation deficient PML mutant[130,124,129].

5.1.1.1 Small ubiquitin-like modifier (SUMO) protein and sumoylation

Post-translational modification by SUMO has emerged as a crucial factor for many cellular processes. This modification regulates protein-protein and protein-DNA interactions with a range of consequences. These include the regulation of diverse processes, such as nuclear-cytosolic transport, protein stability, apoptosis, transcriptional regulation and progression through the cell cycle[131,132].

Mechanistically, sumoylation and ubiquitination share many similarities and both involve a covalent attachment to their target protein. However, the end result of each is very different. Ubiquitination primarily ends in degradation of the targeted protein, whereas SUMO appears to aid solubility of its target and can alter the subcellular localisation or act as an antagonist by blocking ubiquitin binding and thereby stabilising the target protein[133].

In humans three isoforms of SUMO are expressed, SUMO1, SUMO2 and SUMO3. These small proteins range in length from 95-103 amino acids. Each isoform exists in an immature form (referred to as pro-SUMO) and requires activation by the removal of a short C terminal section. Conjugation of mature SUMO to target proteins is by an enzymatic cascade, involving activating (E1), conjugating (E2) and ligase (E3) enzymes (figure 4). Sumoylation has been extensively reviewed by Geiss-Friedlander et al and Meulmeester et al[134, 135].

The SUMO cycle is the same adopted by ubiquitin and ubiquitination. However, a vital difference lies in the E2 conjugation step. In humans, ubiquitination has, to date, thirty-five active E2 enzymes, whereas sumoylation only has one[136]. This lone sumoylation E2 enzyme, Ubiquitin-conjugating enzyme 9 (UBC9) is therefore crucial to sumoylation and in turn PML NB formation.

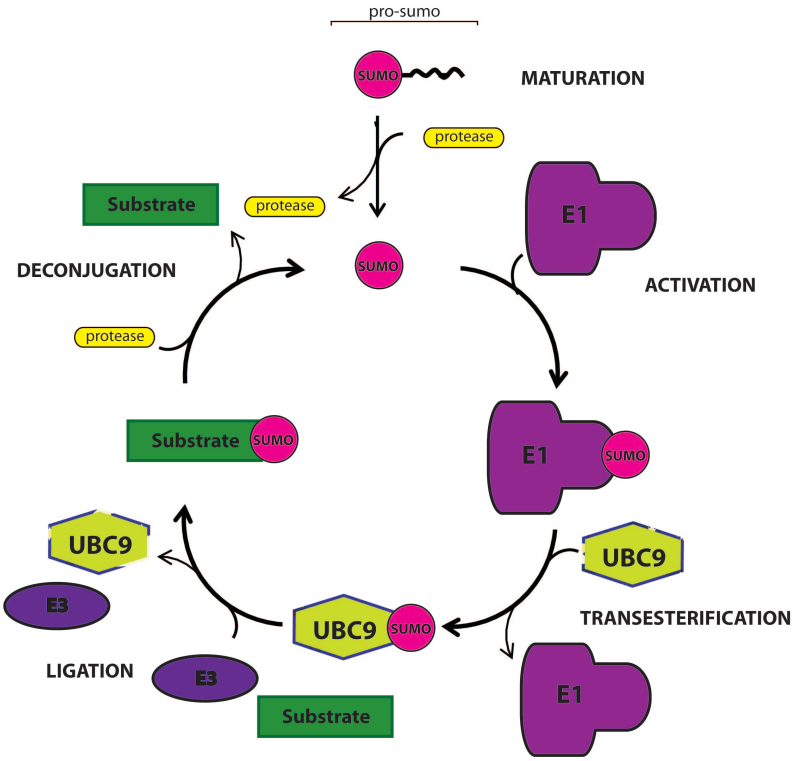

Figure 4 Cartoon illustrating the SUMO cycle. Four amino acids are cleaved from the C terminal by SUMO specific proteases revealing a diglycine motif. In an ATP-dependent manner, the C terminal forms consecutive thioester bonds with a cysteine residue in the heterodimeric E1 enzyme (ACTIVATION) and next UBC9. The SUMO-UBC9 thioester complex catalyses the formation of a isopeptide bond between SUMO and the amino group side chain of a lysine residue in the substrate. UBC9 has contact with the substrate and aids in specificity. E3 enzymes aid the sumoylation process by coordinating the SUMO-UBC9 complex into the optimal conformation for catalysis. E3 enzymes generally have little contact with the substrate, however in sumoylation through non-consensus motifs they have been implicated in substrate recognition. The same proteases involved in forming mature SUMO, also perform the deconjugation of SUMO from the substrate and SUMO is recycled.

Unlike other E2 conjugating enzymes, UBC9 has the ability to directly recognise substrates. Transesterification, aided by E1 enzymes, transfers SUMO to cysteine 93 in UBC9. This SUMO-UBC9 thioester can then catalyse interaction with the amino group of a lysine residue in the substrate. Typically lysine residues targeted for sumoylation are found within a SUMO modification consensus motif, ψ-K-x-E (where ψ is a large hydrophobic residue and x is any residue)[137]. In a minority of cases, sumoylation occurs where the sequence surrounding the target lysine residue does not conform to the consensus motif and in this case the motif is referred to as a non-consensus motif.

Sumoylation has been found in over 50 proteins, the majority of which are involved in transcription and chromatin organisation in mammalian systems[138]. A different class of SUMO binding protein exists that binds non-covalently through a SUMO-interacting motif (SIM). This SIM contains a hydrophobic core (V/I-x-V/I-

V/I, where x is any residue) flanked by either acidic residues or a serine residue[139,140]. Signalling by SUMO is proposed to rely on the recognition of these SIM binding partners. Work by Stehmeier and Muller indicated that phosphorylation of the serine residue (sometimes found in this SIM motif) dictates binding to SIM-containing proteins[141]. SUMO-mediated protein-protein interactions are sometimes regulated by the non-covalent binding of SUMO conjugates to SIMs in a binding partner, suggesting that sumoylation provides an interface for protein-protein interactions. PML is an example of a protein that is both sumoylated and interacts with SUMO *via* a SIM[142].

CHMP4B and CHMP1A interact with UBC9 in a yeast two hybrid assay[111]. This interaction links the action of our nuclear ESCRT-III complex to sumoylation and potentially PML NBs.

5.1.2 Polycomb group (PcG) bodies

PcG proteins are transcription repressor proteins that can regulate cell fate decisions. They form multiprotein complexes that bind and repress promoters for genes encoding proteins concerned with cell fate determination[89]. They are proposed to coordinate DNA accessibility throughout cell development by chromatin remodelling[143].

When first identified, CHMP1A was found localising to regions of nuclease resistant condensed chromatin and has been implicated in gene silencing[43]. This effect stems from CHMP1A's ability to recruit PcG protein, BMI1[144], providing another interesting connection between the observed nuclear ESCRT-III complex and a nuclear structure.

This chapter aims to elucidate what nuclear structures the ESCRT-III complex is localising to upon VPS4 depletion. Due to our lack of specific CHMP1A antibody, it cannot be certain that CHMP1A is localising to CHMP7, 4B and 1B in this nuclear complex and therefore makes investigating an interaction with PcG proteins more complicated. The similar appearance of PML NB's and nuclear CHMP7 by IF, plus the link between CHMP4B and UBC9, made looking at PML a logical starting point.

5.2 Results

5.2.1 VPS4 depletion affects PML number and conformation

In control cells the appearance of PML NBs was similar to that already described in the literature[145]. The NBs were small, ranging between 0.2 and 0.8 μm with an average of 9.5 bodies observed per cell (figure 5a). The PML NB number and conformation were analysed in cells either depleted of VPS4 isoforms, TSG101, individual ESCRT-III subunits (7, 4 and 1) or simultaneous depletions of VPS4 isoforms and an ESCRT subunit. Statistical analysis indicated that all RNAi depletions significantly increased the number of PML NB's (figure 5b). Knockdown conditions themselves had no noticeable effect on PML NBs. This assumption is based on a comparison of untreated HeLa cells with non-targeting RNAi control cells to ensure that the knockdown treatment itself did not cause cellular stress. Co-depletion of VPS4 and CHMP7 or depletion of TSG101 had the largest effect increasing the number of PML NBs to 28.5 and 26.25 respectively. PML bodies were larger and of less uniform shape in both TSG101 and VPS4 RNAi cells. The increase in PML NBs could be attributed to an increase in cellular stress caused by TSG101 or VPS4 depletion, which severely impairs the MVB pathway.

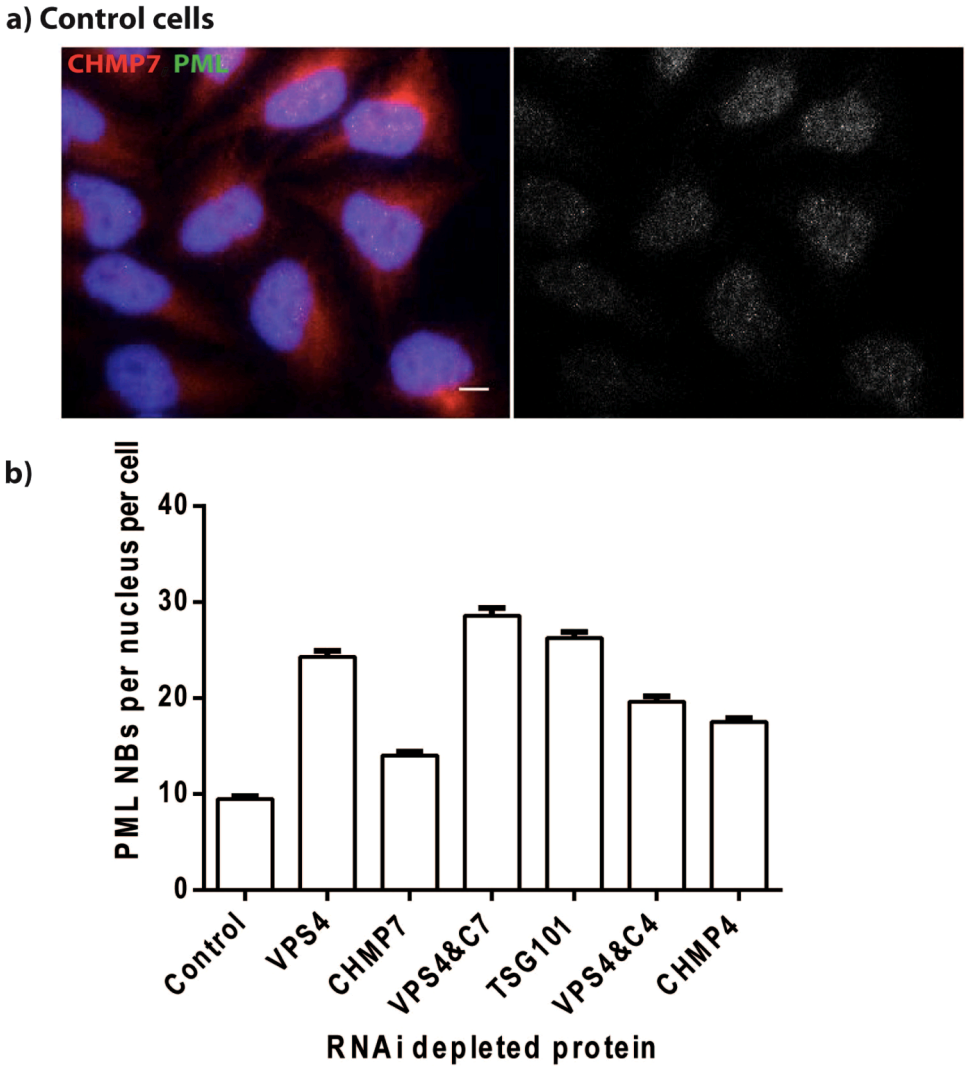

Figure 5 a) Control cells probed with anti-CHMP7 (red, Cy3) and anti-PML (green, ALEXA 488 nm), also shows the PML channel separately (right). Scale bar equal 10 µm. Compared to control (non-targeting RNAi) all the analysed depletions significantly increased the number of PML NBs. This analysis is based on over 300 scored cells from 3 independent experiments. The difference between the control and all depletions resulted in a p value of p ≤0.0001. b) Graph shows the average number of PML NBs per nucleus upon various depletions and displays the standard error of the mean (SEM). P values were calculated for each variable using a one-way anova (Tukey multiple comparisons test)

In figure 6 examples of PML appearance upon various knockdowns are shown. Interestingly, adjacent co-localisation was observed between PML structures and nuclear CHMP7. In many cases, PML NBs were observed next to or surrounding CHMP7 spots. PML NBs are sites of post translational modifications within the nucleus, with recruited proteins being either sumoylated or phosphorylated[127]. Phosphorylation has been observed in CHMP7 at serine residue 232 from high throughput mass spectrometry (figure 7) and occurs during mitosis[146]. This site marks the halfway point between the doubled winged helix N term and the SNF7-

related C terminal and could signify a specific activation of either half once CHMP7 is nuclear and mitosis is underway. In comparison both CHMP4B and CHMP1B do not contain an established phosphorylation site before the SNF7 domain and instead contain one in the centre of the SNF7 domain after the second alpha helices.

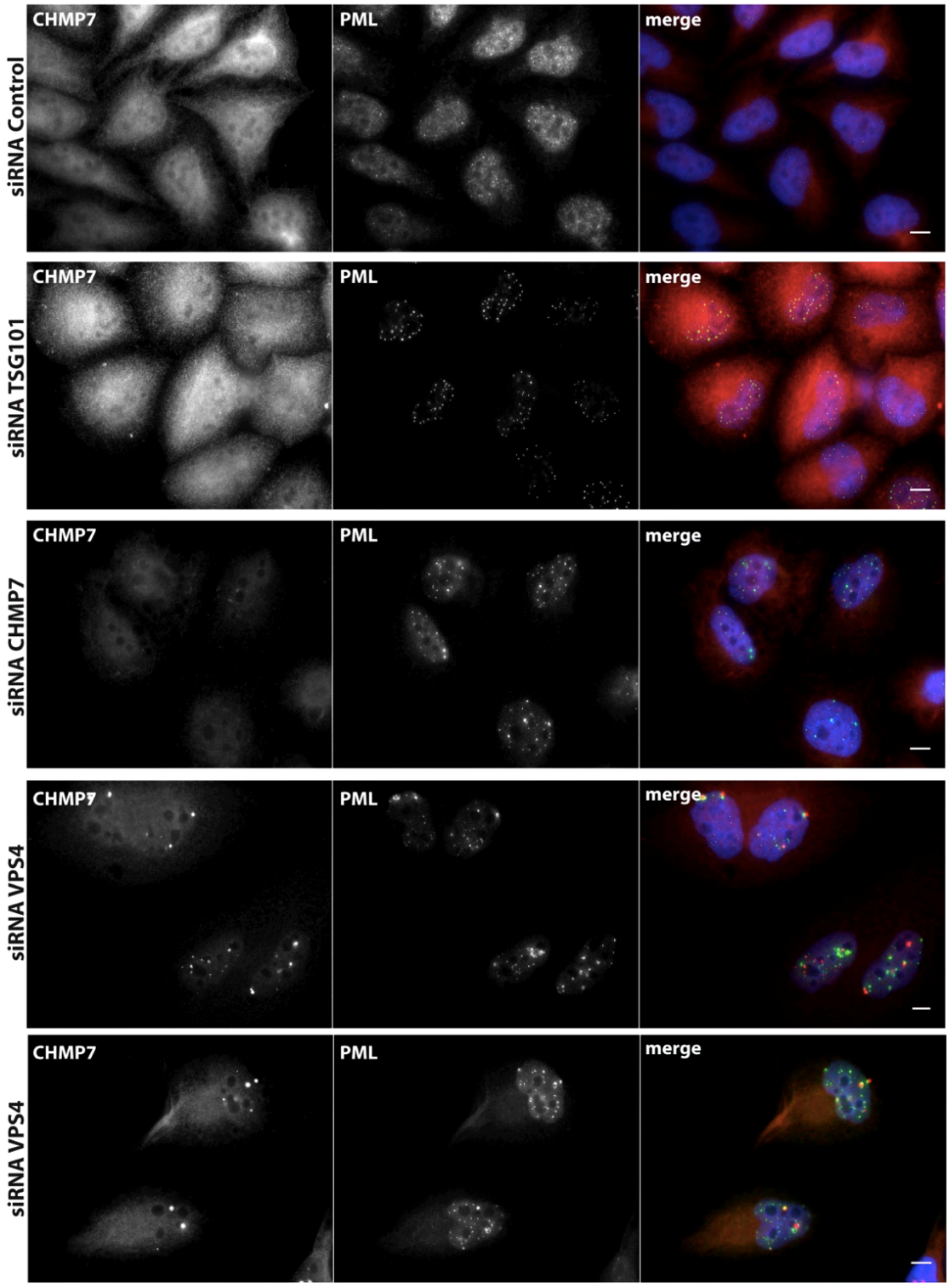

Figure 6 Effect on PML upon various RNAi seventy-two hour depletions, TSG101, CHMP7 and examples of VPS4. In control cells PML NB number is low and NB's are small and uniform. TSG101 depletion visibly increases NB number, as does CHMP7 depletion to a lesser extent. Two striking observations from VPS4 depletion were evidence of some localisation with nuclear CHMP7 (red, Cy3) and also changes in PML (green, ALEXA 488 nm) conformation and size. Scale bars equal 10 μm.

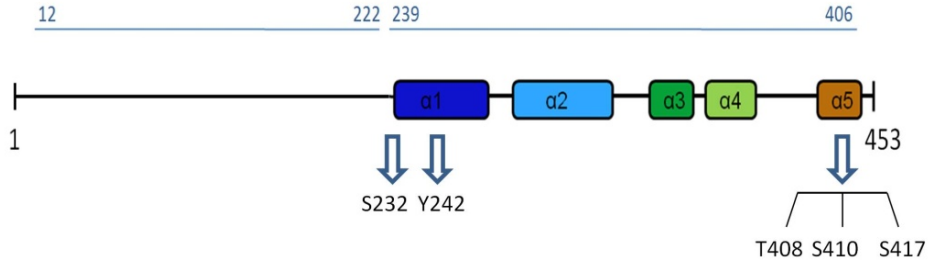

Figure 7 CHMP7 cartoon indicating the residues that were observed to be phosphorylated based on data from high throughput mass spectrometry collated by PhosphoSitePlus[147].

Confocal microscopy was additionally used to spatially locate the CHMP7 spots in relation to PML NBs (figure 8). PML NBs appear to localise in the vicinity of CHMP7 rather than directly co-localising to it. This may imply some common protein, chromatin or other nuclear structure is linking them.

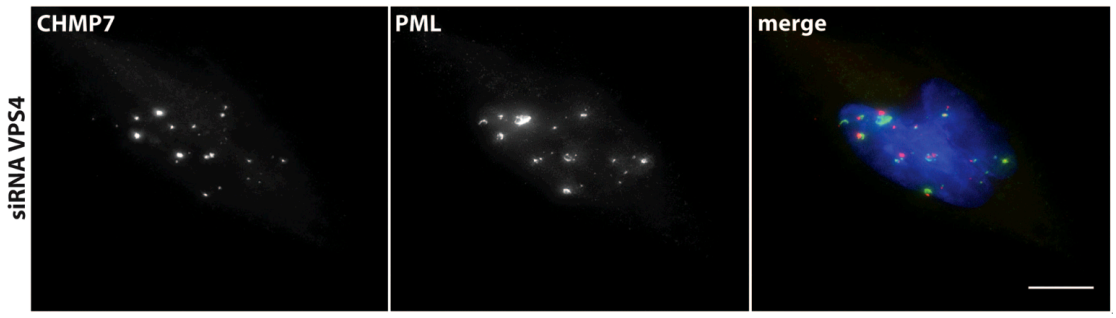

Figure 8 Confocal microscopy image of VPS4 depleted cells. Cells were imaged using a deltavision deconvolution microscope to yield an XY image through a Z series. This Z series can be deconvolved resulting in one image. CHMP7 (red, Cy3) and PML (green, ALEXA 488 nm) are adjacent inside the nucleus. Scale bar equal 10 μm

The level of co-localisation between CHMP7 and PML varied depending upon the number of nuclear CHMP7 spots. Higher co-localisation was observed in cells with fewer nuclear CHMP7 spots. In nuclei where CHMP7 spots were fewer in number, the spots tended to be larger in size (defined as >1.25μm). PML localised adjacent to CHMP7 on average in 70% of nuclei containing CHMP7 spots of 1.25 μm diameter and larger. Conversely, the co-localisation was only 25% in nuclei containing CHMP7 spots smaller than 1.25 μm (figure 9b). This co-localisation could be evidence of PML localising to large CHMP7 and using it as an anchor point to recruit proteins and form NBs. Equally, it could be the effect of PML, for example through post translational modifications, that causes larger CHMP7 bodies to form. Figure 9a shows examples of the phenotypes described

above. Where localisation is high, the PML appears to surround CHMP7 and is visible as a collection of several discrete bodies.

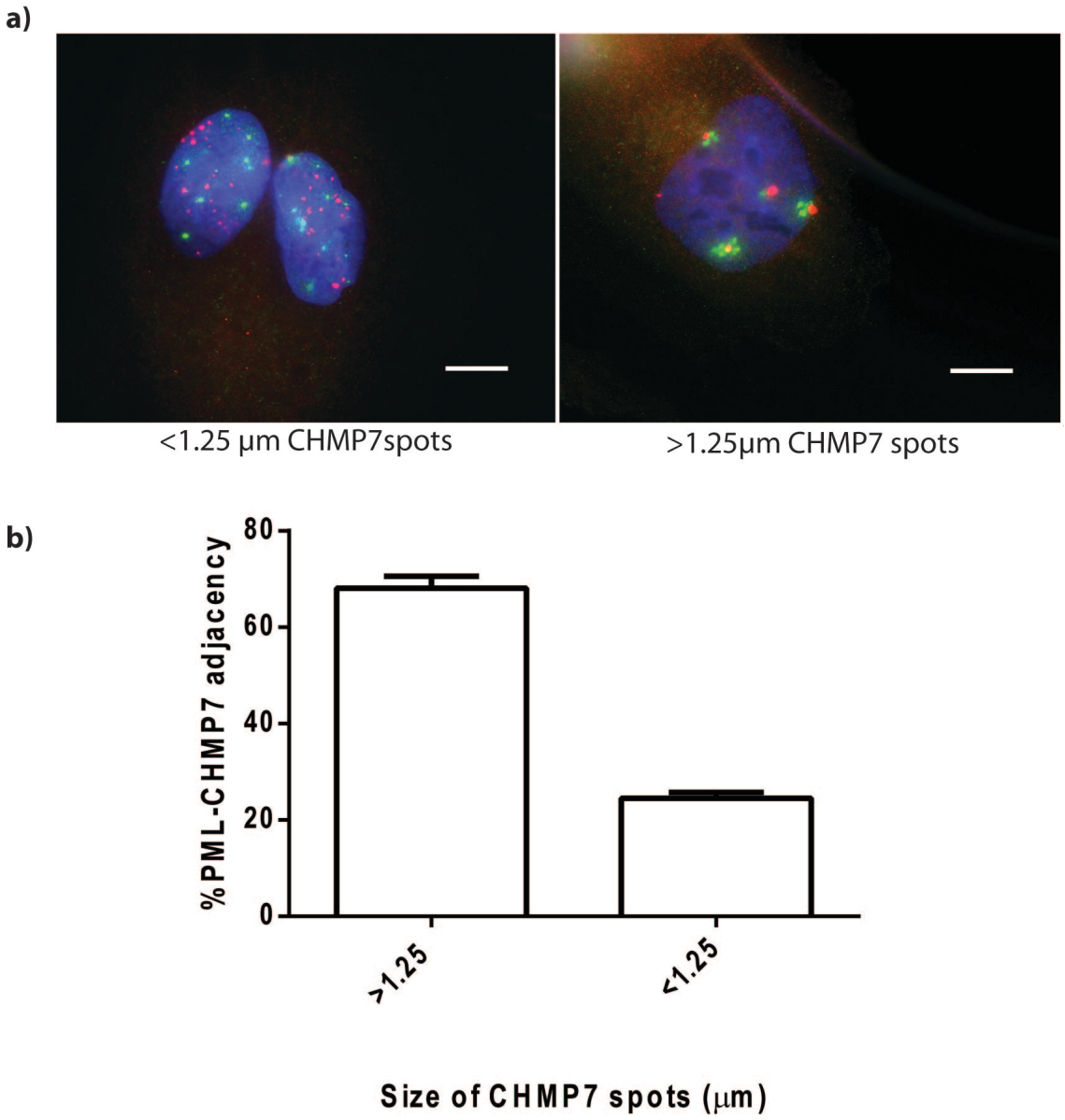

Figure 9 CHMP7 (red, Cy3) and PML (green, ALEXA 488 nm) localisation appears dependent on nuclear CHMP7 number and size. (a) IF images show high adjacency where there is fewer (and larger) CHMP7 spots compared to low adjacency in nuclei where there is more (and smaller) CHMP7 spots. Here 'small' is defined as <1.25 µm and 'larger is defined as >1.25 µm. Scale bars equal 10 µm. (b) Graph showing PML-CHMP7 adjacency in nuclei containing CHMP7 spots either <1.25 µm (typically more than 10 spots) or >1.25 µm (typically less than 10 spots). This was scored over 300 cells from 3 independent experiments and differentiated by measuring the diameter of observed spots. The standard error of the mean is shown and p value calculated using an unpaired t test ($p \leq 0.0001$).

One explanation of this phenotype could be that with PML NBs being highly dynamic structures, this could be only a snapshot of a more complicated process linking CHMP7 and PML NB formation. The formation of the ESCRT-III complex could act as a scaffold to initiate formation of large PML structures. CHMP7 is

crucial in the formation of the ESCRT-III nuclear assembly and determines the localisation of these assemblies within the nucleus. Therefore, in effect, CHMP7 determines where PML filament and ring formation occurs. Chapter 3 predicted DNA binding domains in the N terminal half of CHMP7. These DNA binding domains could be activated by phosphorylation of CHMP7 and drive ESCRT-III assemblies. In turn, this could promote large PML structures to inter-chromatin territories or chromosomes during mitosis. The link between CHMP7, chromatin and PML could lie in the DNA damage and repair function of PML bodies, since phosphorylation often acts as a signal for many DNA repair proteins to localise to DNA damage[1].

Alternatively, PML bodies have been linked with targeting damaging proteins for degradation[148]. The PML accumulating around CHMP7 upon VPS4 depletion could be a response caused by cell stress and could actually be PML orchestrating nuclear ESCRT-III sequestration. This could explain PMLs preference for targeting larger, and potentially more harmful, CHMP7 spots rather than small. In the absence of VPS4 to regulate CHMP disassembly, their affinity for each other could cause damaging CHMP aggregates to accumulate in the nucleus.

Upon certain RNAi depletions, mainly TSG101 and VPS4, PML bodies were observed changing in conformation. This was observed by the appearance of filamentous and ring like structures (figure 10). These different PML conformations were more apparent in VPS4 depleted cells. CHMP7 was seen within every PML ring observed. PML filamentous and ring-like structures are larger than 1 μm (the upper size range noted in the literature). PML ring structures larger than 1 μm, referred to as ‘PML cages’ have been observed in the literature within cells containing polyglutamine aggregates and in cells infected by certain viruses[149,150]. Therefore, this PML ring phenotype may simply represent a method employed by PML NBs to reduce cellular toxicity. There is also the intriguing possibility that this could be a mechanism for specific members of the ESCRT family to be sequestered with foreign viral machineries during an infection. Figure 10b shows PML localising to large CHMP7 nuclear spots and using the ESCRT-III assembly as a nucleation site to form filaments, in turn these filaments form ring-like structures.

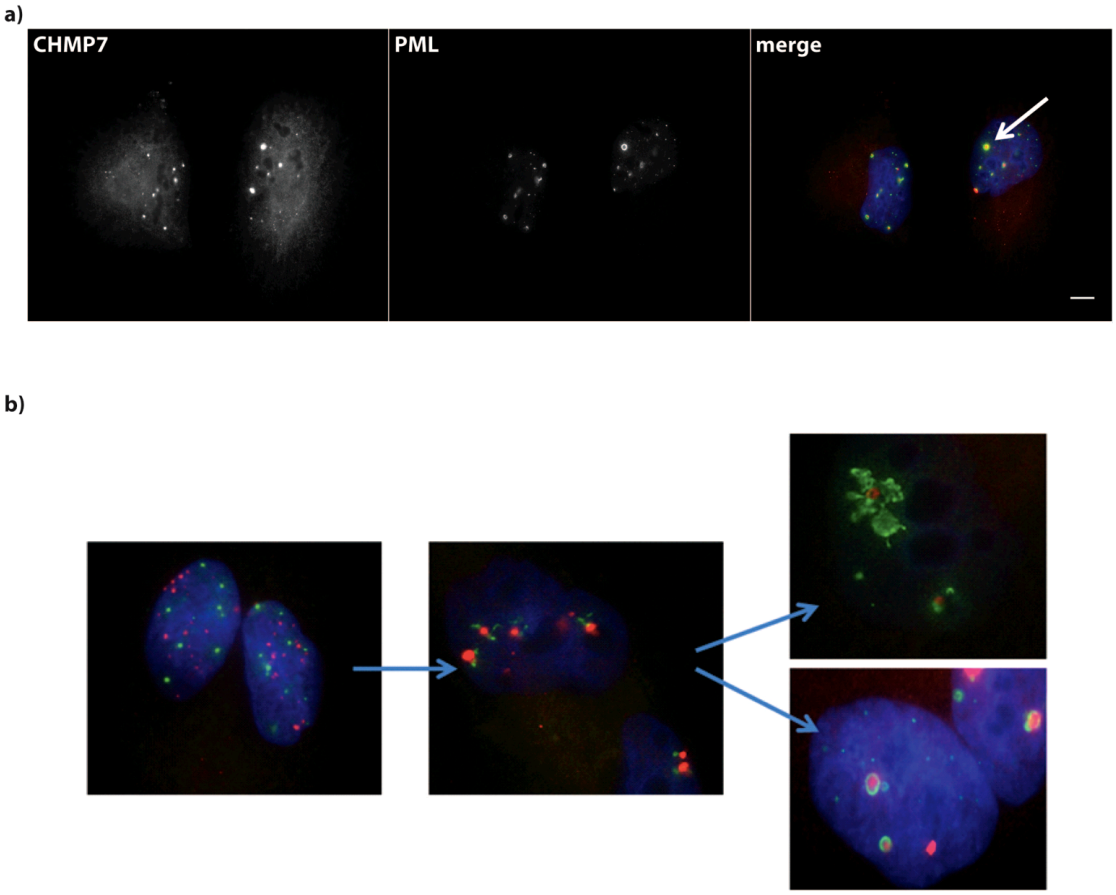

Figure 10 a) VPS4 depleted cells probed with anti-CHMP7 (red, Cy3) and anti-PML (green, ALEXA 488 nm), image shows a PML ring surrounding CHMP7, indicated by the white arrow. Scale bar equal 10 μm. PML appears to co-localise at several points around large CHMP7 spots, which leads to the formation of rings and filaments, (b) suggests a directionality to this process by showing low colocalisation when CHMP7 spots are smaller and then greater colocalisation when CHMP7 spots are larger, which several PML bodies forming around CHMP7 as potentially an intermediate step in PML filament and ring formation.

5.2.2 CHMP7 depletion inhibits PML conformational changes

The number of PML NB's per nucleus was rescored by eye to take into account the different conformations of PML, defined as dots, filaments and rings. Figure 11a illustrates examples of the PML phenotypes scored in each knockdown condition. In VPS4 depleted cells 18% of PML was in filaments and 7.5% in rings, whilst in TSG101 depleted cells only 7.3% of PML was in filaments and 1.4% in rings. No rings and less than 0.5% filaments were observed in control cells demonstrating that PML filamentous and ring-like structures are a result of from these ESCRT machinery depletions (figure 11b)

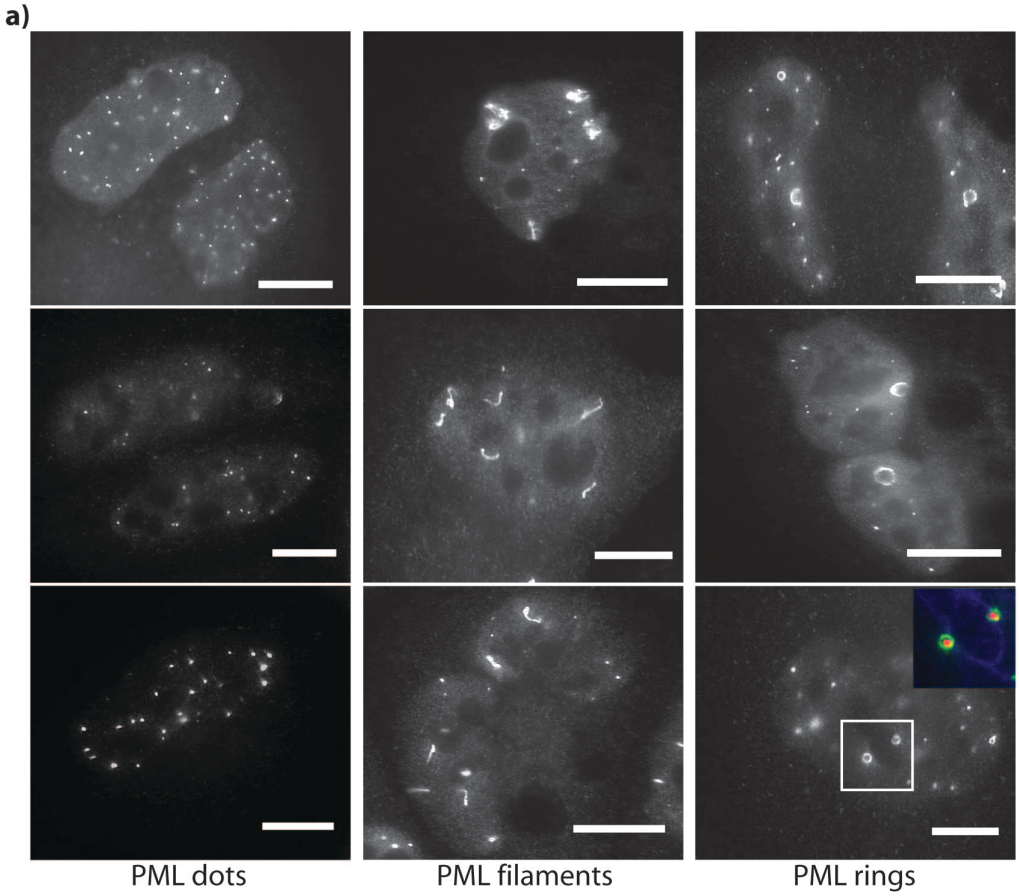

Figure 11 a) examples of differing PML conformation used as basis for scoring. Bottom left shows PML rings, inset includes anti-CHMP7 antibody. b) Total NB's per nucleus was broken down into, dots, filaments and rings. The conformation changes observed are most apparent in VPS4 depletion with 18% of PML NBs forming filaments and 7.5% forming rings. All depletions resulted in the appearance of a small amount of filaments, except for CHMP7 depletion. Standard error of the mean is shown. Scale bars equal 10 μm.

Interestingly, CHMP7 seems to be important in driving this conformational change. In cells co-depleted of VPS4 and CHMP7, rings are no longer observed and the percentage of filaments drops to 2%. In comparison, depleting CHMP4 with VPS4 shows a minor effect, with 10% filaments and 4% ring structures. Taken together these data support the hypothesis that CHMP7 is the key component of ESCRT-III nuclear assembly.

PML dots are the common form of the protein in the nucleus. Therefore it seems whilst cellular stress causes these dots to increase in size and number, it is only particular knockdowns (mainly VPS4), which influence PML conformation to form large structures.

Figure 12 shows the extent of the different PML conformations observed across different knockdowns, involving a pair of ESCRT members. This could indicate CHMP7 has an important role in initiating large PML nuclear body formation. CHMP4B interacts with UBC9, a protein crucial in the development of PML NBs *via* sumoylation[151]. Sumoylation of ESCRT components could act as the signal that initiates their localisation to nuclear structures and could induce PML conformational changes: either to fulfil a particular role such as in DNA damage response or when the nuclear CHMP concentration becomes too high and requires regulation.

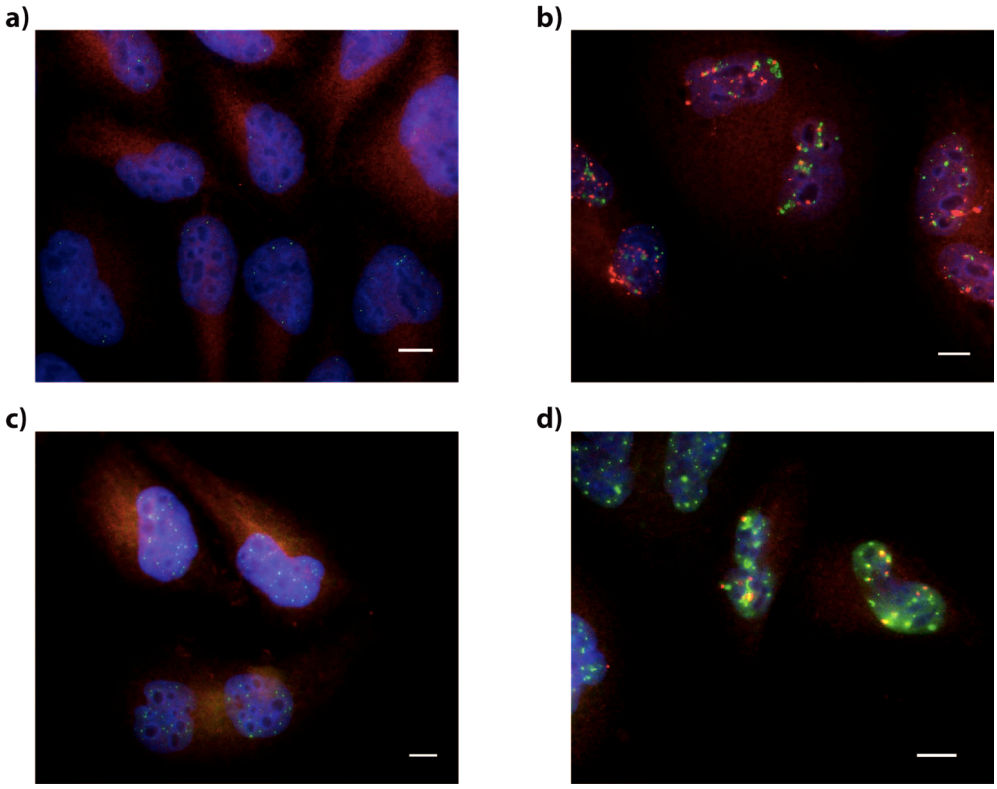

Figure 12 Comparison of RNAi depletions upon PML (green, ALEXA 488 nm) conformation in a) control cells, b) VPS4, c) VPS4 and CHMP7 and d) VPS4 and CHMP4 depleted cells, also probed for CHMP7 (red, Cy3). Scale bars equal 10 µm.

Sumoylation and de-sumoylation are already established methods of regulation employed in the DNA damage response and repair proteins and many proteins in these pathways rely on sumoylation for localisation or stability[152].

5.2.3 CHMP7 interacts with SUMO1 and UBC9

SUMO2 and SUMO3 share 96% sequence identify differing only in the addition of a few residues after the common SUMO diglycine motif –they are functionally undistinguishable and are often referred to jointly as SUMO2/3. In comparison, SUMO1 shares only 50% identity with them. SUMO2/3 is actually more abundant in its unconjugated form than SUMO1. SUMO2/3 may have a greater role in cellular response to environmental stress, such as temperature fluctuations[153].

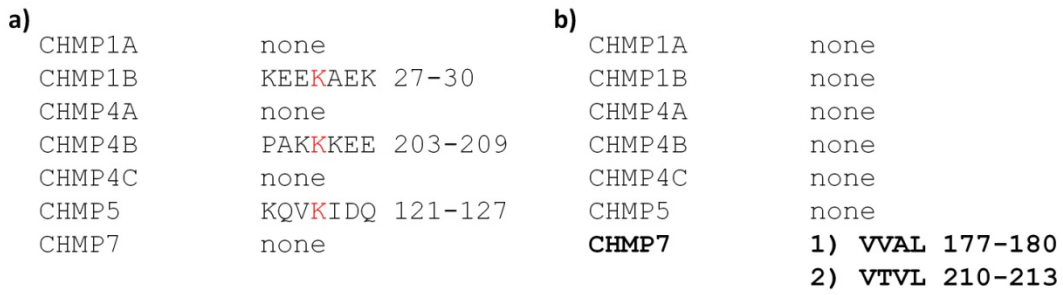

Figure 13 Prediction of a) sumoylation sites based on the ψ-K-x-E motif, but also including non-consensus lysine residues –using SUMOsp 2.0 and b) prediction of SIM's based on a repeat of hydrophobic residues – using SBM sp 1.0, where SBM stands for sumo binding motif.

ESCRT-III subunits were explored for potential sumoylation sites and SIMs *via* bioinformatic analysis[154]. Interestingly, both CHMP4B and CHMP1B contain potential sumoylation sites –two components of our nuclear assembly (figure 13a). CHMP7, however, did not contain a sumoylation site. This result could further indicate that the role of CHMP7 is largely in trafficking these subunits to specific nuclear structures. CHMP5 contained a sumoylation site, and potentially a viable antibody for this protein would reveal a nuclear localisation also upon VPS4 depletion. CHMP7 was the only ESCRT-III subunit predicted to contain SIMs (figure 13b). The potential SIMs were both found in the unique N terminal half of the protein. Literature in this area has suggested SIM binding proteins could act to target substrate specificity[155], i.e. towards CHMP4B/1B in this case.

Interaction between CHMP4B and UBC9 has already been established by yeast two hybrid assay[111,1] We made use of tryptophan fluorescence to confirm the binding between His-tagged UBC9 and a synthetic CHMP4B peptide spanning the region containing the predicted sumoylation site. This method was used as UBC9 contains four tryptophan residues, one of which is located near to the cysteine of its active site. This technique also provides a quantitative measure to support yeast two-hybrid assays from previous work. These quenching assays were conducted in triplicate and the averages are shown in figure 14.

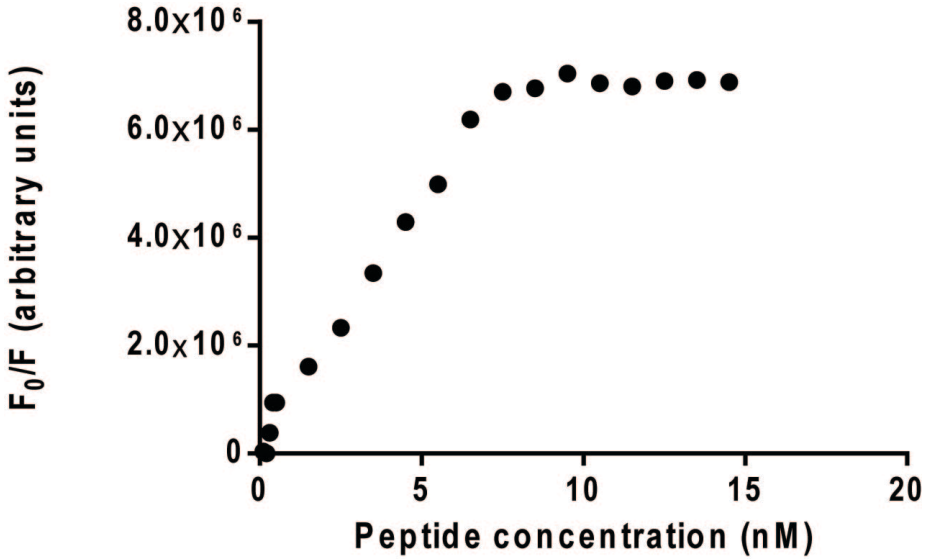

Figure 14 Fluorescence quenching titration using 100 nM histidine tagged UBC9 and 0-100 nM of CHMP4B peptide 192-211 (-PNVPSIALPSKPAKKKEEED-acetylated) UBC9 contains four tryptophan residues, one in particular resides in the active site near a cysteine crucial to sumoylation and target recognition. Emission was measured at 348 nm using FluorEssence software on a Spex FluoroMax and assays were conducted in PBS at room temperature.

The intensity of the fluorescence emission, from the tryptophan residues at 348 nm, is decreased by quenching. The accessibility of these tryptophans can be measured by the use of quenchers, i.e. the CHMP4B peptide, to perturb fluorescence. Quenching by small molecules, such as peptides, that interact with the protein in close proximity to fluorophores can greatly decrease the quantum yield of a protein. The point at which the graph plateaus indicates when UBC9 is fully quenched and the CHMP4B peptide is in excess. The graph plateaus at a very low concentration of peptide (approx 8 nM, indicating that the concentration of UBC9 is likely around ten-fold lower than expected. The concentration of UBC9 was determined by UV-Vis using an extinction coefficient of 29450 $M^{-1}cm^{-1}$ (estimated using Expasy). Salt is used in the assay buffer to screen any non-specific binding from the His tag on UBC9 by interfering with ionic interactions. The quenching is supported by the literature and likely real, but suggests some degradation of the purified UBC9 sample over time. As a control, the assay was also run using the synthetic peptide titrated against GST protein and no protein. Both of these showed no change in their fluorescent signals, which supports the interaction between His-UBC9 and the CHMP4B peptide by showing peptide specificity. Taken together with the previous yeast two hybrid data the interaction between UBC9 and the sumoylation site of CHMP4B appears likely and shows

that UBC9 does not need SUMO or other enzymes (E1 and E3) to be present in order to interact with SUMO substrates like CHMP4B.

Pull down assays were conducted using the same tagged UBC9, plus a His-tagged SUMO1 G97 construct (figure 15). This construct has the last four residues removed in order the reveal the diglycine motif.

CHMP5 116-179 did not interact with either SUMO1 G97 or UBC9 in our pull down assays, despite this region containing the predicted sumoylation site. Often sumoylation targets uncovered through *in vitro* methods require further components for a successful pull down assay including UBC9, Mg-ATP and a mixture of SUMO1, 2 and 3[156]. The substrates of SUMO1 and SUMO2/3 do not overlap completely, so CHMP5 sumoylation could be specific to SUMO2/3 or potentially not sumoylated at all[157].

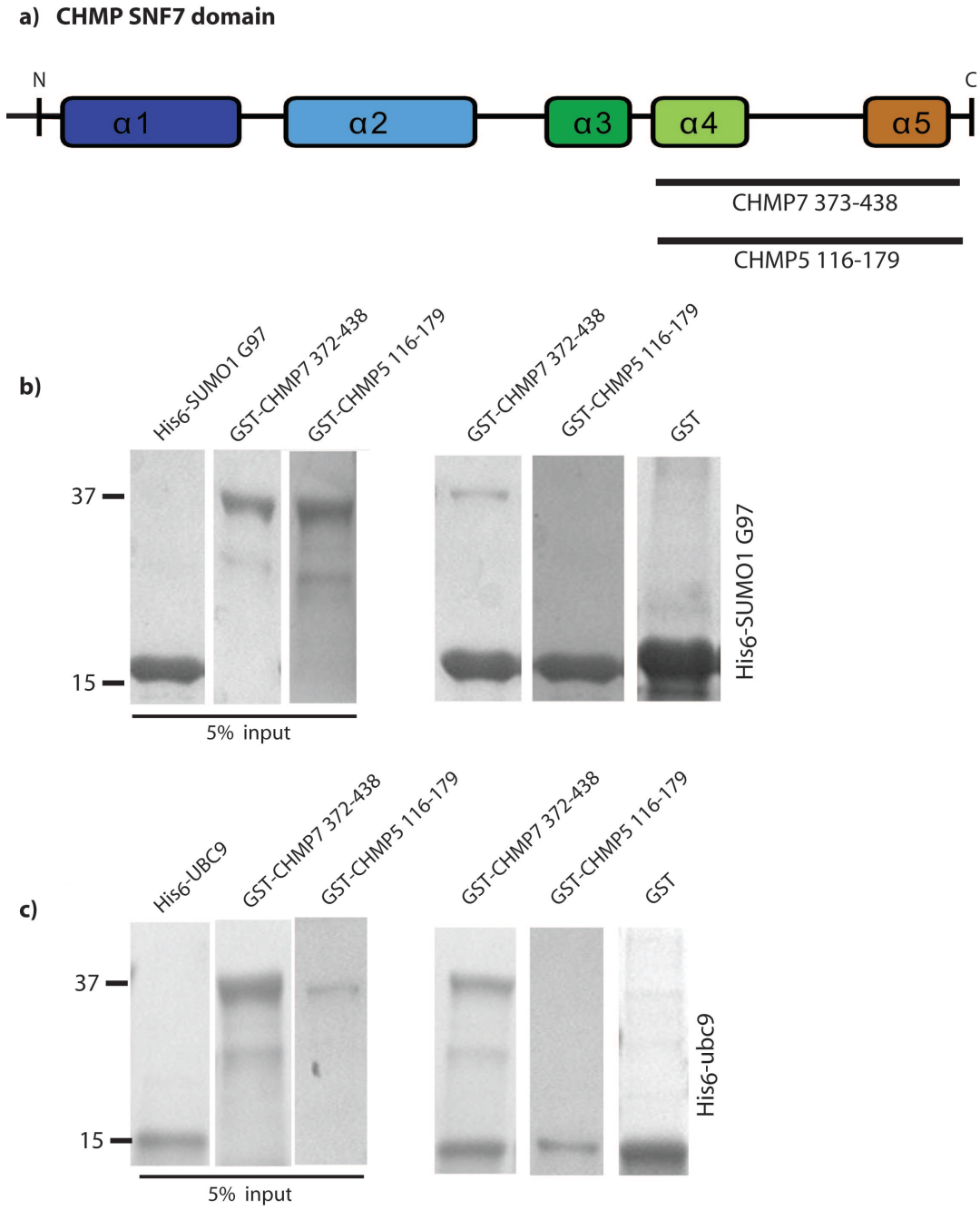

Figure 15 a) CHMP SNF7 domain illustrating the position of CHMP5 and CHMP7 fragments. Pull down assays using his-tagged SUMO1 G97 (b) and UBC9 (c). GST and GST tagged CHMP7 and CHMP5 fragments (372-438 and 116-179 respectively) were incubated at room temperature with Ni-charged NTA agarose beads preloaded with his-tagged SUMO G97 or UBC9 –conducted in 20 mM TRIS, 150 mM NaCl, 5% glycerol, 2 mM $CaCl_2$ pH 7.4. After binding, samples were analysed by SDS-PAGE and Coomassie staining.

The only difference between the pull down buffer used in this experiment and a previously successful one from the literature was the addition of 5 mM $MgCl_2$[158]. The role of $MgCl_2$ in buffers is often to screen ionic interactions. As the quenching assay shows UBC9 can interact with SUMO substrates without other enzymes or additives being present. It has been suggested that based on the number of sumolyated targets and limited substrate specificity that UBC9 can not alone orchestrate substrate specificity and targeting and therefore may not interact with all sumoylated targets[159]. This introduces the role of a SIM-containing protein in enhancing and aiding UBC9 by orchestrating substrate specificity and recognition.

Despite not containing a predicted SIM or sumoylation site, the CHMP7 fragment 372-438 interacted with SUMO1 G97 and UBC9 by pull down assay. The protein sequence was examined again for potential SUMO interacting sites. By lowering the confidence threshold on the SUMO prediction program further potential sites can be revealed. This resulted in no sumoylation sites, but two new SIM sites both located between 383-390 (ELDILL and DILLQD respectively). There are no serine residues in or flanking this motif, the nearest being upstream at position 377 (this serine is predicted to be phosphorylated by NetPhos 2.0)[104]. Phosphorylation of threonine residues near the SIM can promote binding to SUMO. There is a di-threonine motif at position 391-2 flanking the second predicted SIM and of these the first residue is highly predicted to be phosphorylated by NetPhos 2.0 (figure 16c).

The non-covalent binding site in SUMO itself is proposed to comprise aromatic/aliphatic and basic residues inside a groove between a beta sheet and alpha helical region[139]. The phosphorylation of the SIM-containing protein adds a negative charge to the motif believed to aid the SIM interaction by interacting with basic residues in the SUMO groove[160] (figure 16a and 16b).

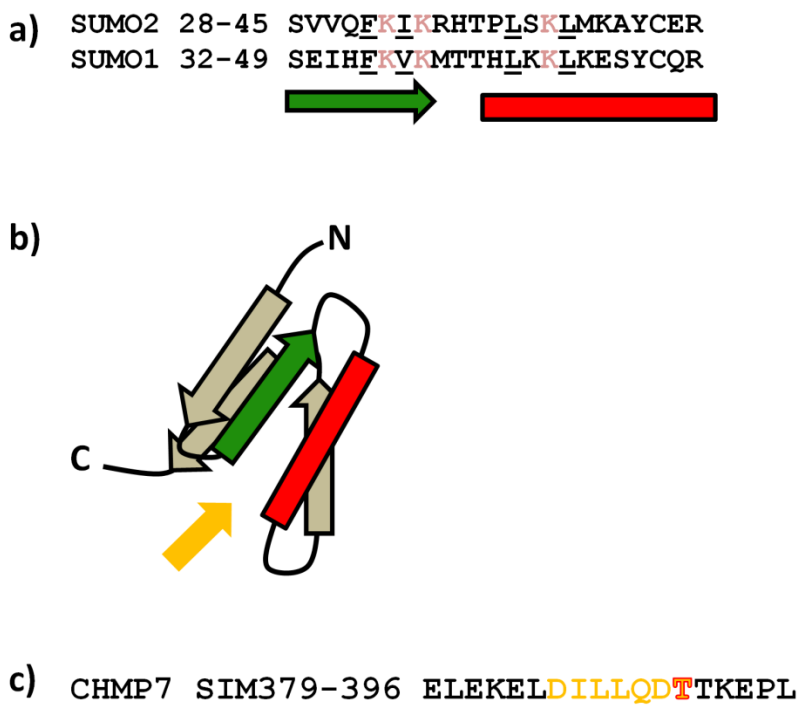

Figure 16 a) region of SUMO that forms groove in which SIM-containing partner proteins interact. Important hydrophobic residues are underlined, with important basic residues in pink. These regions correspond to a beta sheet and alpha helix secondary structure shown in (b) with unimportant secondary structure in grey. Green arrows represent beta sheets and red rectangles represent alpha helices. The yellow arrow indicates the groove in which the SIM binding site. c) Shows the predicted SIM in CHMP7, with the hydrophobic and acidic residues synonymous to this motif in yellow, plus the phosphorylated threonine highlight in red. SIMs can bind in this groove either parallel or anti- parallel in respect to the beta sheet. Differences in sequence between SUMO1 and SUMO2/3 may allow some target SIM specificity.

Interaction with UBC9 is not a requisite of SIM-containing proteins, but previous work has shown that UBC9 can interact with SIMs in proteins[155,161]. Kolesar et al showed that this interaction is important for E3-ligase independent sumoylation to occur. The interaction of CHMP7 with both SUMO1 and UBC9 could aid CHMP4B and CHMP1B sumoylation. Taken together the pull down data presented here is consistent with a mechanism whereby both sumoylation and SIM interactions regulate nuclear localisation of ESCRT-III subunits.

Sumoylation waves can be triggered by cellular stress and in response to DNA damage[160]. VPS4 depletion impairs mitosis and cytokinesis generating DNA damage in cells that progress through cell division[73]. The formation of a nuclear ESCRT-III assembly could be an indirect effect of VPS4 depletion and more specifically a direct effect of DNA damage.

5.2.4 UBC9 overexpression drives CHMP7 nuclear localisation.

Sumoylation can be difficult to monitor in cells since it is a reversible modification and only a small percentage of proteins are sumoylated at any one time. In order to probe the effect of sumoylation, the modification needs to be driven forward by overexpression of SUMO and the E2 enzyme UBC9. GFP-SUMO1 and HA-tagged UBC9 were overexpressed in HeLa M cells to probe their effect on the subcellular localisation of CHMP7.

Overexpression of GFP-SUMO1 alone had little effect on PML, but compared with overexpression of GFP demonstrated that the tag itself was not adversely affecting cells and didn't affect PML number, conformation or distribution (figure 17).

Figure 17 also shows GFP-SUMO1 partially localising to PML nuclear bodies, this is expected of SUMO since PML requires sumoylation to form NBs. Generally GFP-SUMO1 displayed a distribution across both the nucleus and cytoplasm, concentrating around the peri-nuclear area.

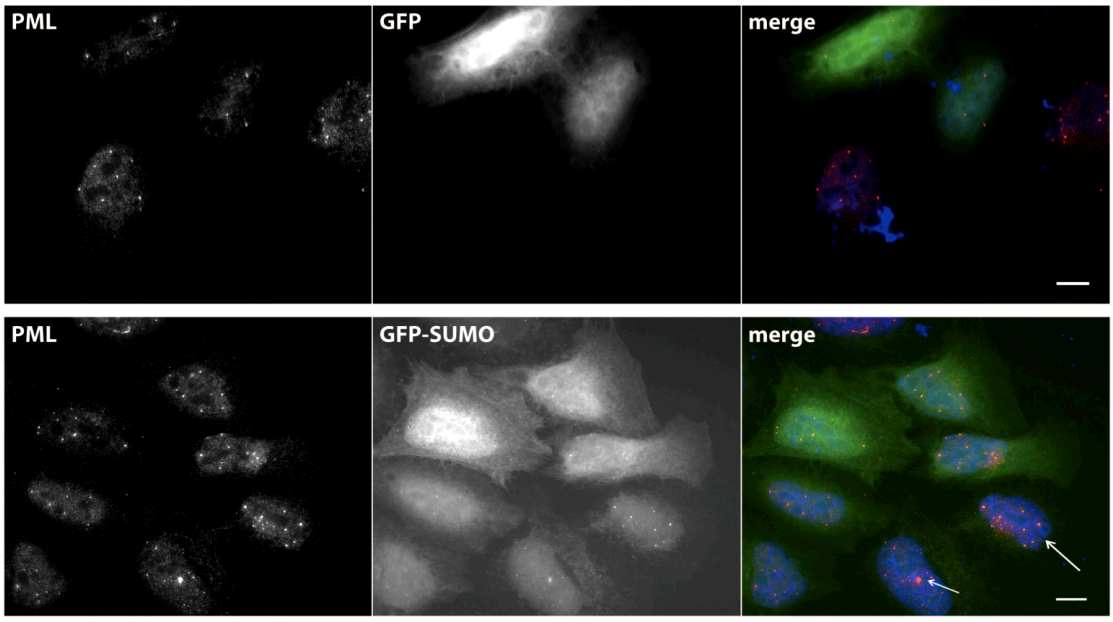

Figure 17 Cells transfected with 0.5 µg of either a GFP or GFP-SUMO1 construct for twenty four hours. GFP transfection has no effect on PML (red, Cy3) number or distribution. Overexpression of SUMO1, does not noticeably affect PML either, however, GFP-SUMO1 is seen localising with PML indicated by the white arrows. This is expected since NB formation requires sumoylated PML. Scale bars equal 10 µm

Overexpression of GFP-SUMO1 alone did not greatly alter CHMP7 distribution, even though CHMP7 was observed displaying a nuclear-speckled phenotype in a few cells (figure 18). Figure 18 shows that when UBC9-HA wildtype was overexpressed simultaneously with GFP-SUMO1 the number of cells observed with nuclear CHMP7 increased. This would imply that overexpression of both proteins is crucial to effectively push sumoylation. Work by Kolesar et al has suggested that the SUMO-UBC9 fusion protein increases the affinity of SIM-containing proteins for SUMO[161]. Observing an increase in nuclear CHMP7 when both SUMO and UBC9 are overexpressed is in agreement with biochemical data from pull downs assays indicating that CHMP7 directly interacts with both SUMO and UBC9.

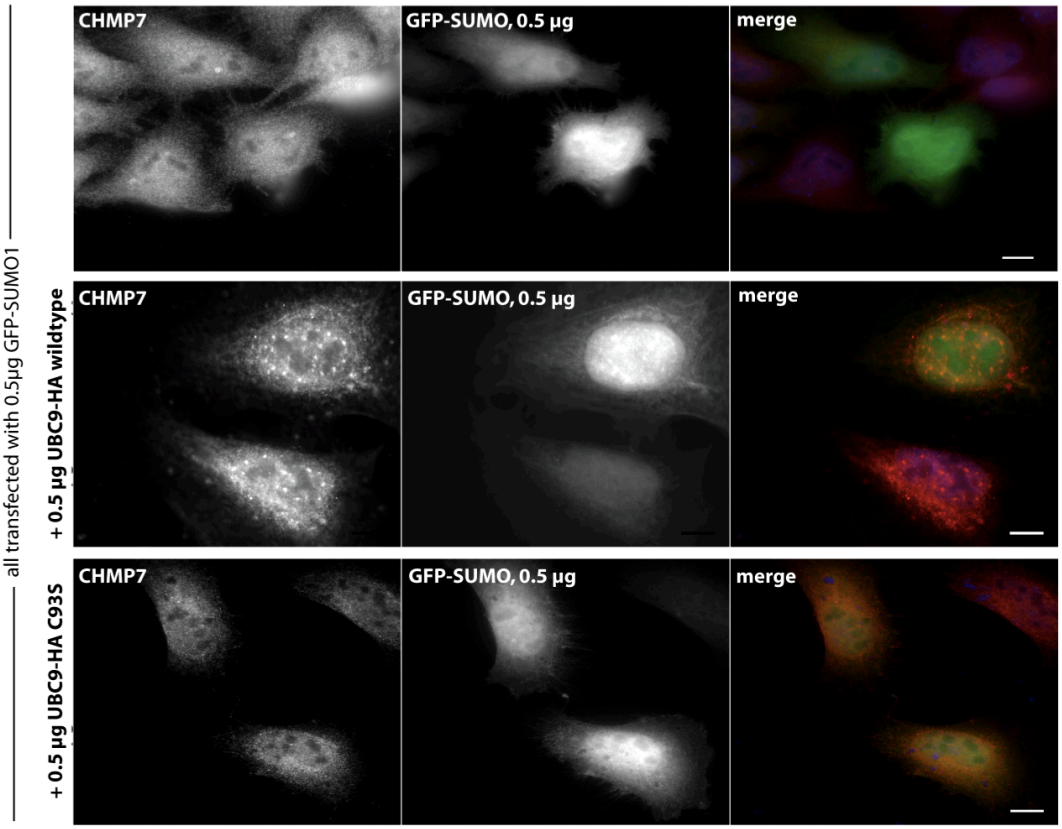

Figure 18 Cells were transfected for twenty-four hours with different combinations of cDNA constructs, these were either; 0.5 µg GFP-SUMO1, 0.5 µg GFP-SUMO1 and 0.5 µg UBC9-HA wildtype or 0.5 µg GFP-SUMO1 and 0.5 µg UBC9-HA C93S. These indicated that a combination of SUMO1 and UBC9 wildtype overexpression results in nuclear localised CHMP7 (red, Cy3). Active UBC9 appears important as overexpression of UBC9 C93S did not result in the nuclear phenotype. Scale bars equal 10 µm.

Catalytically active UBC9 is important in this increase in nuclear CHMP7, as overexpression of GFP-SUMO1 with an inactive UBC9 did not result in the nuclear CHMP7 phenotype (figure 18 bottom panel).

Overexpression of UBC9-HA wildtype (alone) resulted in nuclear-localised CHMP7 and looked similar to that displayed in RNAi VPS4 depleted cells (figure 19 top panel). In contrast, overexpression of UBC9-HA C93S (alone) not only resulted in very little CHMP7 localised to nuclear structures, but a very low level of CHMP7 in the nucleus at all. In this case, CHMP7 appeared concentrated in the peri-nuclear area. The distribution of endogenous UBC9 is generally nuclear. The appearance of the inactive UBC9 is in stark contrast appearing absent from the nucleus.

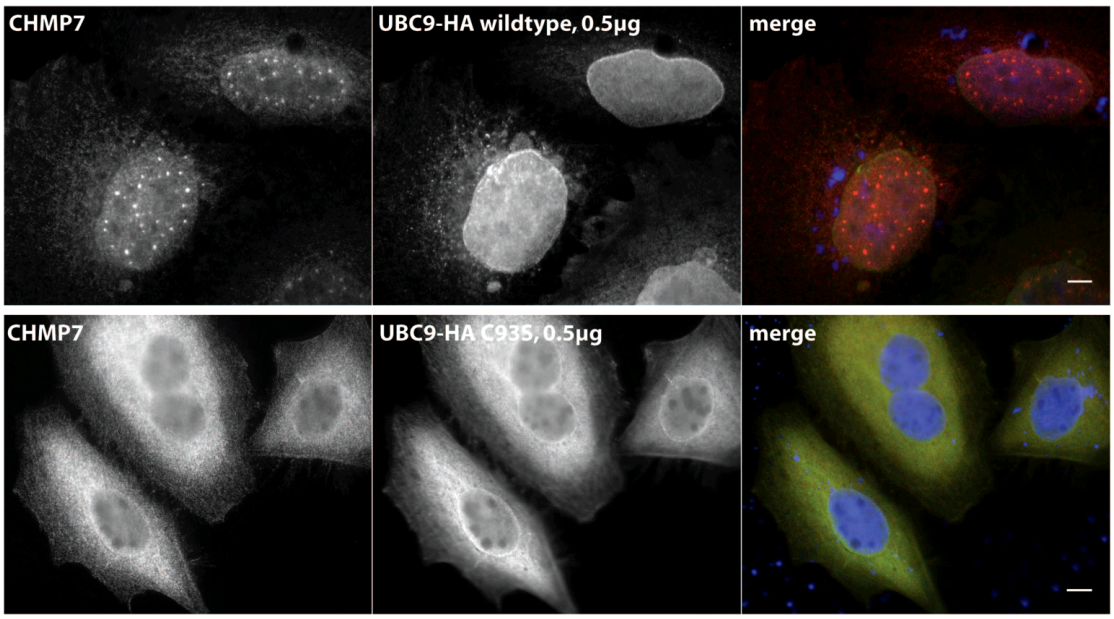

Figure 19 Cells transfected with either 0.5 µg UBC9-HA wildtype or 0.5 µg UBC9-HA C93S constructs. Overexpression of UBC9 results in the nuclear re-localisation of CHMP7 (red, Cy3), revealing a phenotype similar to VPS4 RNAi depletion. UBC9-HA C93S does not result in this nuclear phenotype and is not only absent from the nucleus, but results in CHMP7 becoming absent in the nucleus as well. UBC9 was probed using an antibody for HA (green, ALEXA 488 nm) Scale bars equal 10 µm.

These experiments were repeated twice more in order to quantify the nuclear CHMP7 phenotype (figure 20a). Only 0.5% of control cells displayed nuclear CHMP7 (3 or more nuclear CHMP7 spots). When the inactive UBC9 was overexpressed alone the percentage of cells displaying CHMP7 nuclear spots increased to 5.4%, indicating some remaining enzymatic activity. Strikingly, overexpression of the active UBC9 alone had the greatest effect on CHMP7, with 71.8% of cells displaying the nuclear phenotype (figure 20b). In comparison, the simultaneous overexpression of GFP-SUMO1 and UBC9 wildtype did not increase this percentage further, but actually it decreased to 53%. These data suggest that the effect of both proteins being overexpressed together pushes

a)

Treatment			% of cells with 3, or more, nuclear CHMP7 spots
GFP SUMO	HA-UBC9 WT	HA-UBC9 C93S	
-	-	-	0.5
+	-	-	38.8
+	+	-	53
+	-	+	25.2
-	+	-	71.8
-	-	+	5.4

b)

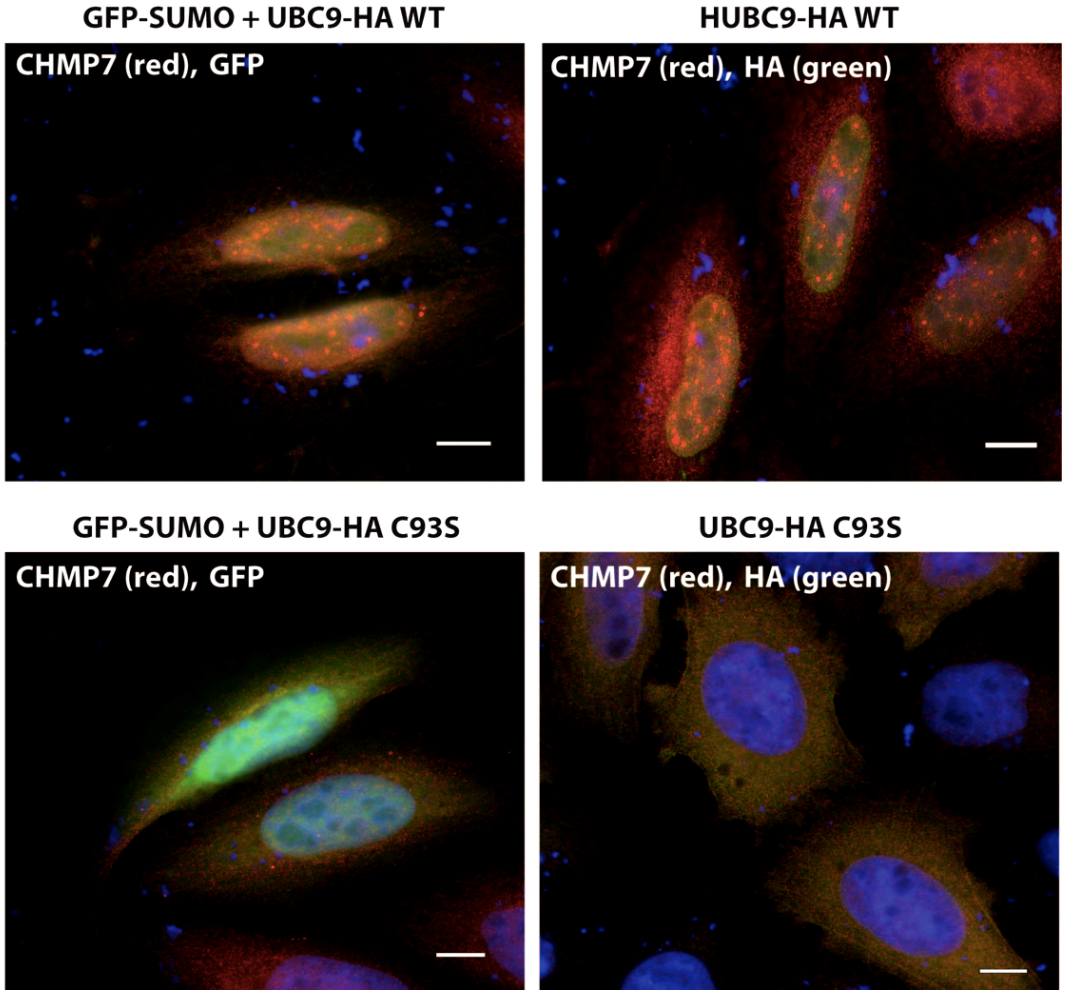

Figure 20 a) Table showing the percentage of cells displaying a nuclear CHMP7 (red, Cy3) distribution, upon different treatments; GFP-SUMO, UBC9-HA WT (wildtype), UBC9-HA C93S or a combination of these (HA, green, ALEXA 488 nm). This scoring was based on 3 independent experiments, with 100 cells counted each time. The number of CHMP7 spots per nucleus was raised from the previous '1 or more' to '3 or more' to take into account the number of control cells that have one CHMP7 spot. (approx 36%) b) examples of CHMP7 distribution displayed upon the following treatments: transfection of both GFP-SUMO1 and UBC9-HA WT, UBC9=HA WT alone, both GFP-SUMO1 and UBC9-HA C93S and UBC9-HA C93S alone. Scale bars equal 10 µm.

CHMP7 distributions too far into the nucleus that any phenotype revealing specific localisation is masked by an excess of CHMP7 or potentially unable to even localise to structures anymore (figure 21a).

GFP-SUMO overexpression alone increases the occurrence of the nuclear phenotype to 38.8% (compared to the control), demonstrating that it does have an effect on CHMP7 localisation –one that is clearly enhanced by UBC9.

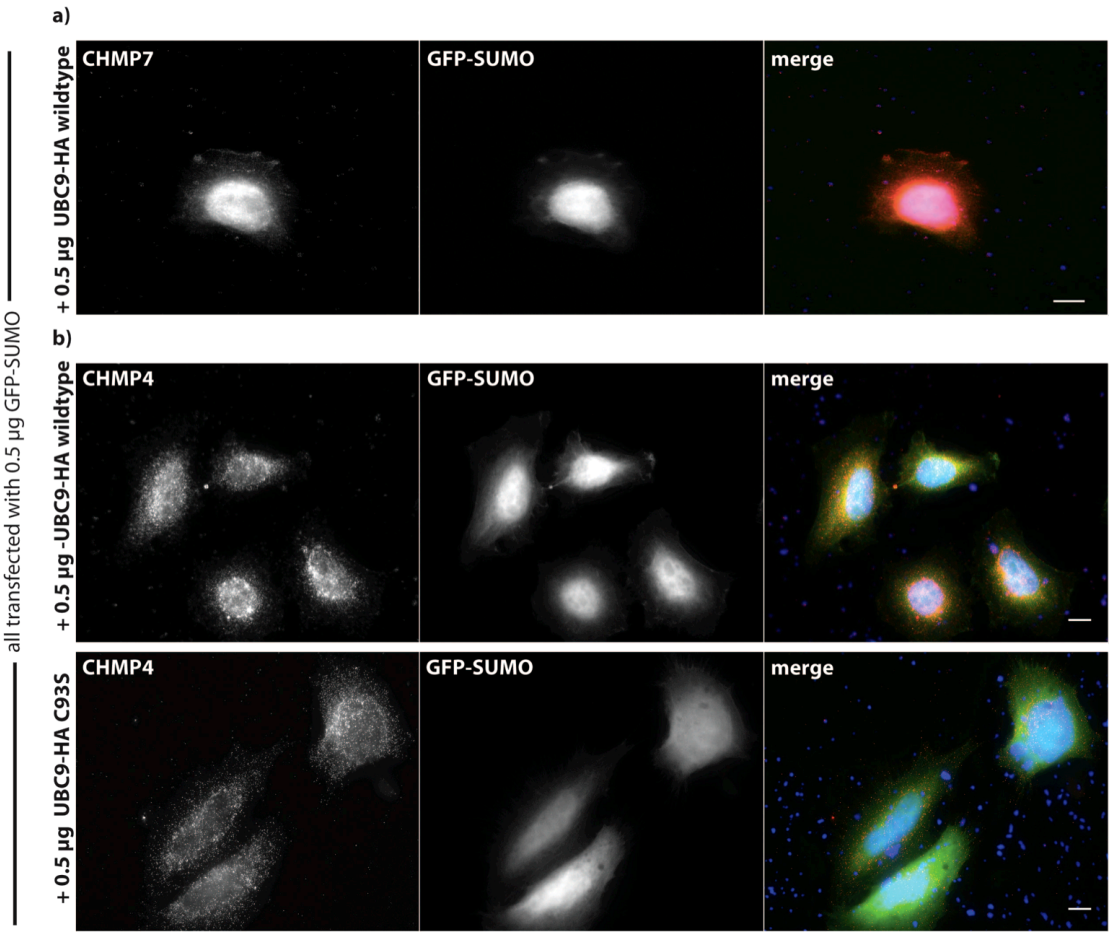

Figure 21 a) example of nuclear CHMP7 (red, Cy3) observed upon transfection of both GFP-SUMO1 and UBC9-HA wildtype. b) CHMP4 (red, Cy3) did not localise to the nucleus upon transfection with GFP-SUMO and UBC9-HA WT (CHMP4C antibody recognises all CHMP4 isoforms, but no other CHMPs). Scale bars equal10 µm.

When SUMO1 is overexpressed with inactive UBC9, the percentage of cells displaying nuclear CHMP7 decreased to 25.2% displaying the competition between inactive UBC9 in excess and the endogenous active enzyme. In contrast to the effects on CHMP7, overexpression of neither UBC9 nor SUMO1 (or both) resulted in any nuclear localisation of CHMP4 or CHMP1B (figure 21b). CHMP4B and CHMP1B are predicted to be sumoylated and interaction between

CHMP4B and UBC9 was shown by yeast two hybrid assay[111] and fluorescence quenching assays (this thesis). One possibility is that sumoylation does not trigger the nuclear localisation of CHMP4B and 1B, but actually triggers their localisation back to the cytoplasm. Sumoylation of CHMP4B and CHMP1B could occur in the nucleus (at PML bodies) and be a signal to send these proteins back to the cytoplasm. If ESCRTs do localise to sites of DNA damage, sumoylation could act to release them from the repair site once it is completed. A known role of sumoylation is to alter the protein distribution and localisation within a cell[135]. Therefore, 'pushing' sumoylation of proteins could potentially drive sumoylated proteins, i.e. CHMP4B and CHMP1B, out of the nucleus. CHMP7 itself would remain unaffected as it binds to SUMO *via* the SIM site and not sumoylation.

5.3 Discussion

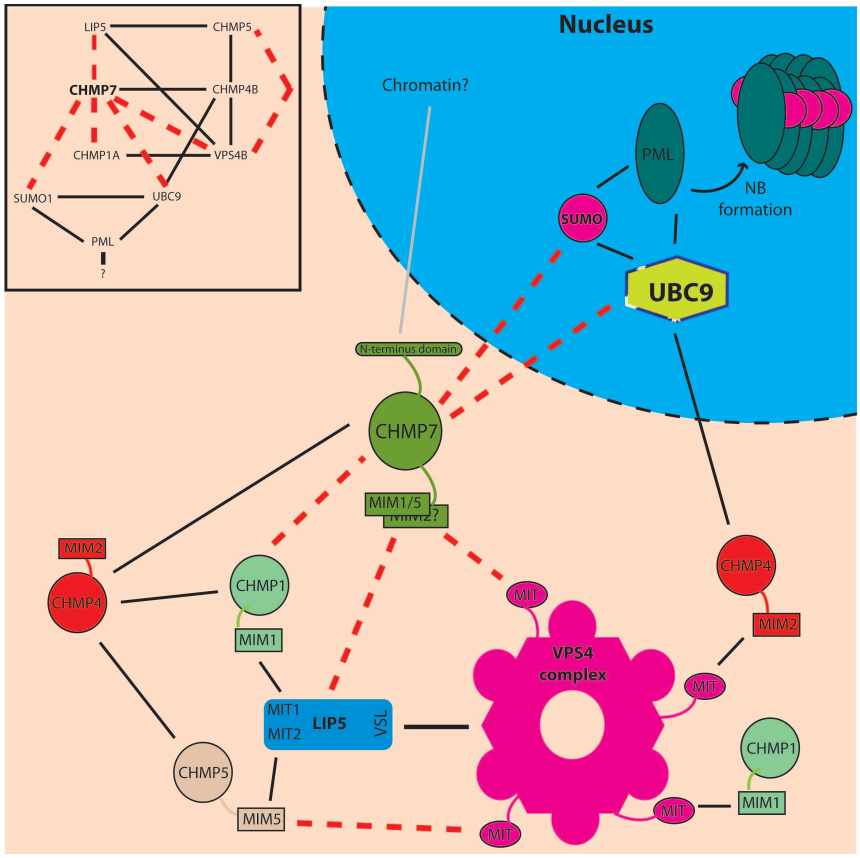

Figure 22 Scheme from chapter 3 with additional interactions added, i.e. those between SUMO, UBC9, CHMP7 and CHMP4B. New interactions are connected with a dashed red line, whereas established interaction are indicated by a solid black line. Using a grey line we suggest the N terminal of CHMP7 might bind chromatin –potentially as a result of DNA damage.

The results in this chapter allow us to expand the protein interaction network outlined at the end of chapters 3 and 4. This network now includes UBC9 and SUMO1 (figure 22). New interactions have been established between CHMP7 and SUMO, potentially *via* a SIM, and also with UBC9.

Figure 23 shows a proposed cartoon of CHMP7 domains and motifs as a result of this work, where previously only the SNF7 domain and phosphorylation sites in black were determined. To expand on this link between ESCRT-III and the SUMO pathway, SUMO2/3 should be explored in future work. This could clarify if CHMP7 can interact with all SUMO isoforms or just SUMO1. SUMO 2/3 is implicated in response to cellular stress, so an interaction between them and CHMP7 may favour the idea of nuclear ESCRT-III resulting from DNA damage and localising to damaged chromatin.

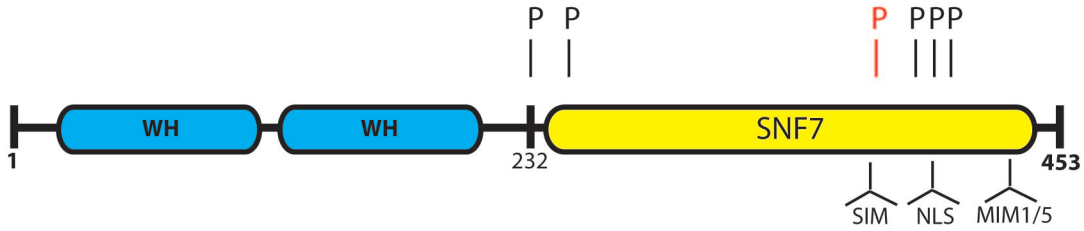

Figure 23 Cartoon of CHMP7 indicating the new motifs (and phosphorylation sites) suggested in this work. Fold threading predicted a double winged helix (WH) domain for the N terminal half. The SNF7 present in all ESCRT-III subunits resides in the C terminal half, with three putative domain in the acidic region around the 4 and 5th helices. Here, evidence suggests, there is a SUMO interacting motif (SIM), a nuclear localisation signal (NLS) and MIT interacting domain (MIM) –potentially similar to the MIM5 found in CHMP5. Phosphorylation sites in black have been established by MS, in red is a further site predicted that may aid and influence the SIM.

The question of whether nuclear localisation of CHMPs is a direct or indirect effect of VPS4 depletion is still debatable. Overexpression of UBC9 recreates the nuclear phenotype, but only for CHMP7. This phenotype in only partially recreated by overexpression of SUMO1 and UBC9 together, indicating it is potentially independent of SUMO.

UBC9 has many functions independent of sumoylation and SUMO, such as regulation of transcription and in nuclear transport[162,163]. UBC9 is frequently upregulated in tumours, this is seen in the literature in lung adenocarcinoma, ovarian carcinoma, melanoma and breast cancer lines[164,165,166,167]. The expression levels of UBC9 are partly regulated by breast cancer type 1 protein (BRCA1)[168]. BRCA1 is commonly found mutated in many cancers, and the

resultant deregulation of UBC9 has been linked to tumour growth and metastasis [165]. This suggests that nuclear CHMP7 could be a signal of cellular stress and feature in tumours. Furthermore, it is possible UBC9 activity in nuclear import allows it to act as a nuclear chaperone for CHMP7 explaining the nuclear CHMP7 phenotype upon UBC9 overexpression. However, if SUMO-independent functions of UBC9 were the case a sumoylation defective mutant UBC9 would have resulted in the same nuclear CHMP7 phenotype. UBC9-HA C93S resulted in only 5.4% of cells displaying nuclear CHMP7 and itself was largely cytoplasmic. Therefore, the combination of SUMO and UBC9, or at least a catalytically active UBC9, may be more important than previous studies have thought.

Some preliminary work (not shown) was conducted to test if a link between the nuclear CHMP phenotype and cellular stress existed. Methods used to stress cells included; heat shock (42°C, 1 hour), oxidative stress (by hydrogen peroxide titration) and the addition of cisplatin. These methods proved to be either too harsh (and killed the majority of cells) or too mild (no effect on cell population or appearance) and did not reproduce the nuclear CHMP phenotype. Future work now aims to probe further the link between response to cellular damage and CHMP nuclear phenotype by introducing specific DNA damage such as by ionising radiation or UV. Further to this the subcellular localisation of CHMP7 in cancer cell lines where UBC9 is upregulated could be an intriguing avenue to explore.

A link between ESCRT-III assembly and function and SUMO/UBC9 activity has been established. However, the link between ESCRT-III and PML nuclear bodies is not as strong. PML and CHMP7 are found adjacent, preferentially in cells where CHMP7 is larger and fewer in numbers. An interesting observation is the lack of PML rings and filaments when CHMP7 is absent –this indicates it is the presence of nuclear CHMPs that cause the changes in PML conformation and not VPS4 depletion itself. Potentially future research could make use of live cell imaging in order to better understand the order of recruitment, localisation and conformational changes occurring between both PML NBs and nuclear ESCRT-

III assembly formation. Based on the data we propose three working hypotheses for the relationship observed between CHMP7 and PML.

1. CHMP accumulations are an aberrant phenotype and are toxic to cells.

The ESCRT assembly localises to a nuclear site driven and selected by CHMP7 and this site is likely chromatin. When in the active conformation CHMPs display a high affinity for each other and so without the regulation of VPS4 they accumulate forming possibly harmful aggregates. The perceived relationship between PML and CHMP7 could be PMLs response to toxic protein aggregates. PML sequesters these aggregates by surrounding them in a ring-like 'cage'. This action protects the cell from further harm and increases the capacity of the nucleus to degrade specific proteins. PML has been shown demonstrating this function in the cell with aggregates of misfolded proteins relating to neurodegenerative disorders[169]. Janer et al refer to these PML structures as clastosomes to reflect their enriched proteasomal content. The proteasome is a protein complex that functions in a protein degradation pathway separate from lysosomal degradation.

2. Specific CHMP complexes (including CHMP7) localise to sites of DNA damage.

Our first hypothesis is not mutually exclusive with the second, but may represent the end result of a disrupted DNA repair process. VPS4 depletion has a disruptive effect on many cellular functions and as result causes high cellular stress and potentially DNA damage. CHMPs localise to damage either to stabilise damaged chromatin or act as a signal for further DNA repair proteins. In particular they could act as a signal to PML, which in turn forms NBs in the vicinity of DNA damage. Further DNA repair proteins can use PML NBs as sites of PT modification and this generally allows PML to regulate the DNA damage response and repair cascade. According to this hypothesis large PML structures, such as the rings observed, could be aiding the stabilisation of damaged chromatin recruited by CHMP assembly.

3. CHMPs allow PML to recognise viral proteins

Ring-like structures of PML have been previously observed encapsulating viral proteins in response to infection. By infecting skin cells and neurons with Varicella-Zoster virus, PML was observed encapsulating newly assembled nucleocapsids[150]. Nucleocapids are the basic structures of a virus, its nucleic acid enclosed in a protein coat. Given the ESCRT machinery's link to viral infection it is possible ESCRT components are involved in this encapsulation. ESCRT-III subunits could act as the recognition site for PML to form 'cages', with ESCRT-III proteins themselves recognising viral components. Therefore, the accumulation of nuclear CHMP proteins caused by VPS4 depletion could effectively be simulating a viral infection response in PML.

PML expression is regulated post-transcriptionally through alternative splicing, resulting in the production of seven PML protein isoforms, labelled PML-I through to PML-VII. These isoforms all contain the same N terminal motifs such as the RBCC domain and it is only in the C terminal additions that these isoforms differ. Apart from PML-VII, which does not contain an NLS, all isoforms are predominantly nuclear[125]. The different C terminal ends are proposed to alter PML specificity -both functionally and through different binding partners. For example, PML-III interacts with the centrosome, whereas PML-IV can bind p53 to promote cellular senescence[170]. Interestingly, where PML has been observed forming ring and filamentous structures the same isoform was responsible –PML IV[150,169]. The ability of PML to sequester harmful proteins, such as aggregates of misfolded protein and viral proteins, is therefore isoform specific. The anti-PML antibody used in this work (abcam ab53773) recognises all endogenous PML protein and cannot specify between isoforms. Thus, CHMP7 may interact with a specific isoform resulting in the appearance of a 'partial co-localisation' phenotype. Future work directed towards establishing if CHMP7 is linked to specific isoforms of PML could be explored. Furthermore, distinguishing between the three possible causes of PML sequestering nuclear CHMP is needed. Observing CHMP behaviour upon viral infection could help discern the validity of the third theory. However, the distinction between CHMP toxicity and CHMPs playing a role in DNA damage is more complicated as the CHMP accumulations could be aiding in DNA damage before they become harmful to the cell.

Interaction with SUMO and UBC9, *via* sumoylation or SIM-binding does not necessarily confine CHMPs to association with PML. Sumoylation is a facet of other nuclear body functions and could be indicative of ESCRT protein involvement with other nuclear proteins. Further investigation in this area could start by probing VPS4 depleted cells with a wide range of nuclear body antibodies. These experiments could serve to confirm the relationship observed with PML or potentially provide an alternative explanation for a nuclear ESCRT-III complex and its partial co-localisation with PML. Examples of SUMO/UBC9 function away from PML NBs include; UBC9 was found to co-localise with splicing factor, arginine/serine-rich 2 (SFRS2) a subunit of nuclear speckles in HeLa S3 and HEK (human embryonic kidney) 293T cells, as well as in mouse oocytes[171]. Nuclear speckles are subnuclear structures involved in transcription *via* mRNA splicing and export. Another example is E3 sumo-protein ligase, aka polycomb 2 homolog (Pc2). Pc2 facilitates sumoylation as part of the sumo cycle shown in figure 4. However, as the name suggests Pc2 is also a component of polycomb group bodies[172]. The function of these bodies was discussed briefly in the chapter introduction, but in particular their role in chromatin remodelling could provide a link to CHMPs. Chromatin remodelling acts as a method of controlling gene expression, but also occurs during the end of mitosis as chromosomes relax once the nuclear envelope reforms. As mentioned briefly in chapter 4, filaments of CHMP4B and CHMP7 (often linking nuclei) were observed upon VPS4 depletion. This phenotype could indicate a role for the ESCRT-III assembly in mitotic events, such as chromosome alignment and segregation or their de-condensation during telophase. ESCRT function during mitosis will be further explored in chapter 6.

CHAPTER 6 ESCRT-III FUNCTIONS DURING ANAPHASE LAG AND DNA DAMAGE

6.1 Introduction

Nuclear defects arise due to impairment of either mitosis or cytokinesis. Mitosis lasts for approximately one hour of a HeLa cells' cell cycle (figure 1). Beginning with prophase, which lasts up to fifteen minutes, chromatin compacts forming visible chromosomes and the nuclear envelope breaks down. Metaphase is the longest stage taking around thirty-five minutes. In early metaphase, or 'prometaphase', kinetochores form on the chromosomes. Microtubules, originating from the centrosomes attach to these kinetochores. Metaphase is complete when all the kinetochores of chromosomes are attached and the chromosomes are aligned in the centre of the cell.

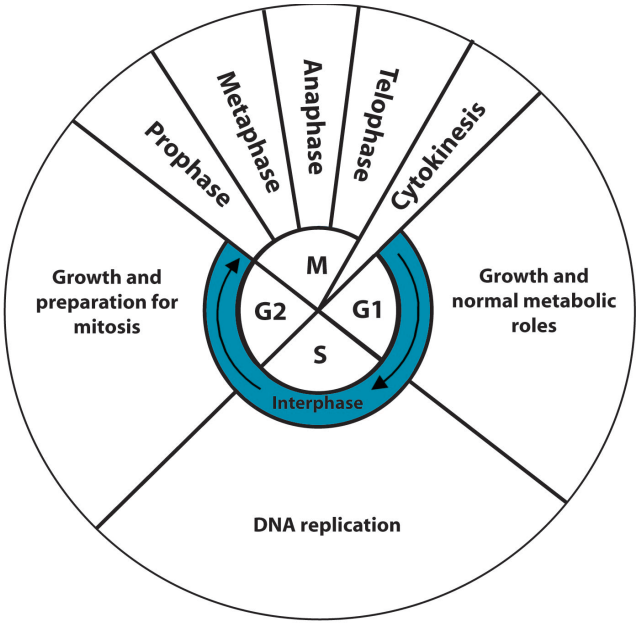

Figure 1 Basic diagram illustrating the stages of the cell cycle.

Anaphase is the shortest stage, lasting up to three minutes and is the point where the chromatids split at their centromeres to form sister chromosomes. During telophase, lasting ten minutes, the nuclear envelope reforms around the chromosomes and they start to unwind. Cytokinesis can begin as early as anaphase, with the specification of the cleavage site and furrow ingression occurring. Late cytokinesis and abscission occur just as telophase ends. During the abscission process, myosin II and actin filaments contract and depolymerise to cleave the cell in two. Correct abscission is largely dependent upon ESCRT machinery components, such as VPS4, CHMP4 and CHMP1.

The entire processes of mitosis and cytokinesis are very tightly regulated; this is aided by checkpoints that verify the progress of each stage is completed properly before allowing progression to the next stage. Checkpoints can slow down or arrest the cell cycle, allowing the cell to fix any damage before proceeding. Mistakes at these checkpoints can have severe consequences for the cell, progressive cycles and the fidelity of future cell generations. Cancer is often a result when cells fail to regulate their growth and division accurately.

Different types of nuclear defect are indicative of specific cell cycle failures. This allows the frequency of a certain defect, upon RNAi depletion, to act as a indicator of where a protein's function lies. ESCRT-III subunits are required for centrosome and spindle maintenance and their individual depletions have demonstrated mitotic defects[45,116]. This chapter focuses on exploring this concept and connecting it with phenotypes observed in chapters 4 and 5.

Some common nuclear defects are briefly outlined below. Firstly, cells with multiple nuclei is a strong signal that cytokinesis has failed. The reformation of the nuclear envelope occurs during telophase to result in two new nuclei. When cytokinesis fails, the cleavage furrow eventually regresses to give the appearance of a multinuclear cell. Secondly, aberrant crescent shaped nuclei have been designated a mitotic defect, specifically during metaphase when chromosomes fail to align properly[173]. Thirdly, the appearance of micronuclei is a good indicator of defects during anaphase. Micronuclei form when a

chromatid either doesn't attach properly to a microtubule or else is drawn too slowly to its pole, referred to as a 'lagging chromosome'. If the anaphase checkpoint fails to correct this, in telophase a nuclear envelope forms around this lagging chromosome. Nucleoplasmic bridges have a similar appearance to micronuclei. They are thought to occur due to telomere end fusions or defective separation of sister chromatids[174]. Lastly, fragmented nuclei are often a sign of highly stressed or apoptotic cells. Apoptosis serves, effectively, as another form of cellular checkpoint and is the initiation of cell death when a cell is damaged beyond repair. During apoptosis endonucleases are released which cleave chromatin resulting in abnormal nuclear morphology and fragmentation. Nuclei can also appear fragmented when there are multiple centrosomes to form around. Figure 3a shows examples of these kinds of defects observed by IF from this body of work.

6.2 Results

6.2.1 ESCRT-III subunit depletion causes nuclear defects

Work carried out by Morita at el used flow cytometry to assay for changes in DNA copy number when ESCRT subunits were depleted using siRNA[45]. DNA copy number can double where cells have gone through mitosis, but failed cytokinesis. They found that depletion of any CHMP or VPS4 isoform resulted in a higher DNA copy number compared to controls and therefore inhibited abscission. This observation included CHMP7, although was most dramatic for ALIX, CEP55, VPS4B, CHMP3 and CHMP4C. Their work concluded that VPS4 and ESCRT-III proteins localised at centrosomes during mitosis to aid in maintenance and chromosome segregation and then later re-localised at the midbody during cytokinesis. It was proposed in a previous chapter that CHMP7 involvement at the midbody may be masked by VPS4 depletion causing cells to fail at an earlier point. The results from Morita et al indicate that CHMP7 is involved in cytokinesis, although not essential. Therefore taken together CHMP7 *is* likely to localise to midbodies, but at a late stage of cytokinesis

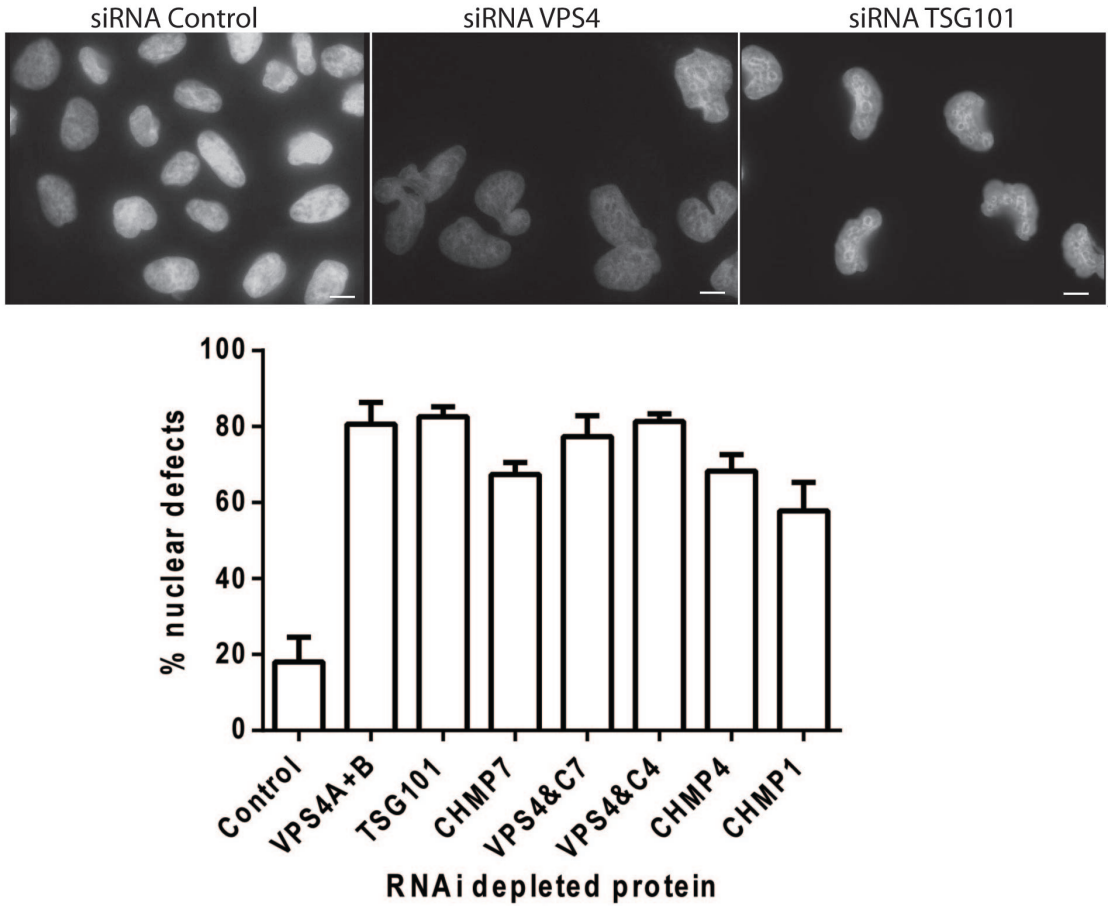

Figure 2 Graph shows the percent nuclear defective cell population across various RNAi knockdowns, where CHMP4 and CHMP1 includes all isoforms and VPS4&C4/C7 represents the double RNAi depletion. Experiments are treated with 5nM RNAi of each isoform (except VPS4 where 3nM of each isoform is used**)** for seventy two hour**.** This is based on three independent experiments, counting 100 cells from each with 'nuclear defect' including all cells displaying any of the above mentioned defects - see figure 3a for examples. The standard error of the mean is shown. P values were calculated on Graphpad Prism 6 using a one-way anova (tukey method). All depletions differed significantly from the control ($P \leq 0.0001$). There was significantly more defects in TSG101 and VPS4 and when compared to CHMP1 ($P \leq 0.001$), CHMP4 and CHMP7 (both $p \leq 0.1$). Above is shown an example of the nuclei of three of these conditions, control, VPS4 isoforms and TSG101 depletions.

RNAi depletion of individual CHMP proteins, 1 4 and 7 (all isoforms) resulted in a statistically significant increase in nuclear defects (figure 2) compared to the control RNAi (18%).The graph shows CHMP7 depletion displayed 67% deformed nuclei and CHMP4 displayed 68%, with CHMP1 slightly less at 58%. There was no significant difference between nuclear defects in individual CHMP depletions. However, deformed nuclei in only the CHMP1 depletion were significantly less than TSG101 and VPS4 knockdowns (including VPS4 double knockdowns).

Double knockdown of either CHMP4 or 7 with VPS4 made no significant difference to the percentage of deformed nuclei when compared to VPS4 alone. This indicates either the inhibitive effect they have is masked by VPS4 depletion or it is at later stages of cytokinesis that the cell fails to reach.

It is not uncommon for proteins involved in endocytosis to have some nuclear function, for example, some subunits of ESCRT-II act as transcription regulators[19]. Proteins equivalent to the CHMP subunits are found in archeal thermophilic bacteria, where they act exclusively in cellular division[175]. The nuclear defect data was next broken down to reflect the different type(s) of defect each depletion caused (figure 3).

VPS4 displayed significantly more micronuclei and multinucleated cells compared to the control and TSG101 depletions. This shows the differing pathway in which they are inhibiting during mitosis and cytokinesis. TSG101 localises to midbodies, but its presence is not crucial for cytokinesis completion, unlike VPS4.

In figure 3 ‘other abnormal shapes’ includes fragmented and odd nuclear morphology. As previously mentioned these are both symptoms of cellular stress or an aberrant number of centrosomes. The centrosome is a tiny organelle (1µm diameter) that initiates and organises microtubules[176]. It is associated with the nucleus during interphase and when the nuclear envelope breaks down during prophase microtubules can begin to interact with chromosomes to build the mitotic spindle. Centrosomes also regulate cell cycle progression and when duplicated incorrectly are common in cells associated with cancer. The centrosome should only replicate once during the cell cycle in S phase. When this doesn’t occur or occurs more than once it has been linked to aneuploidy. Aneuploidy is a cell with an abnormal number of chromosomes and when the nuclear envelope reforms abnormal nuclei are the result. Therefore the crescent and abnormal shaped nuclei resulting from TSG101 depletion could indicate centrosomal defects. This fits with TSG101 as a known tumour suppressor gene and indicates TSG101 inhibits mitosis, rather than cytokinesis.

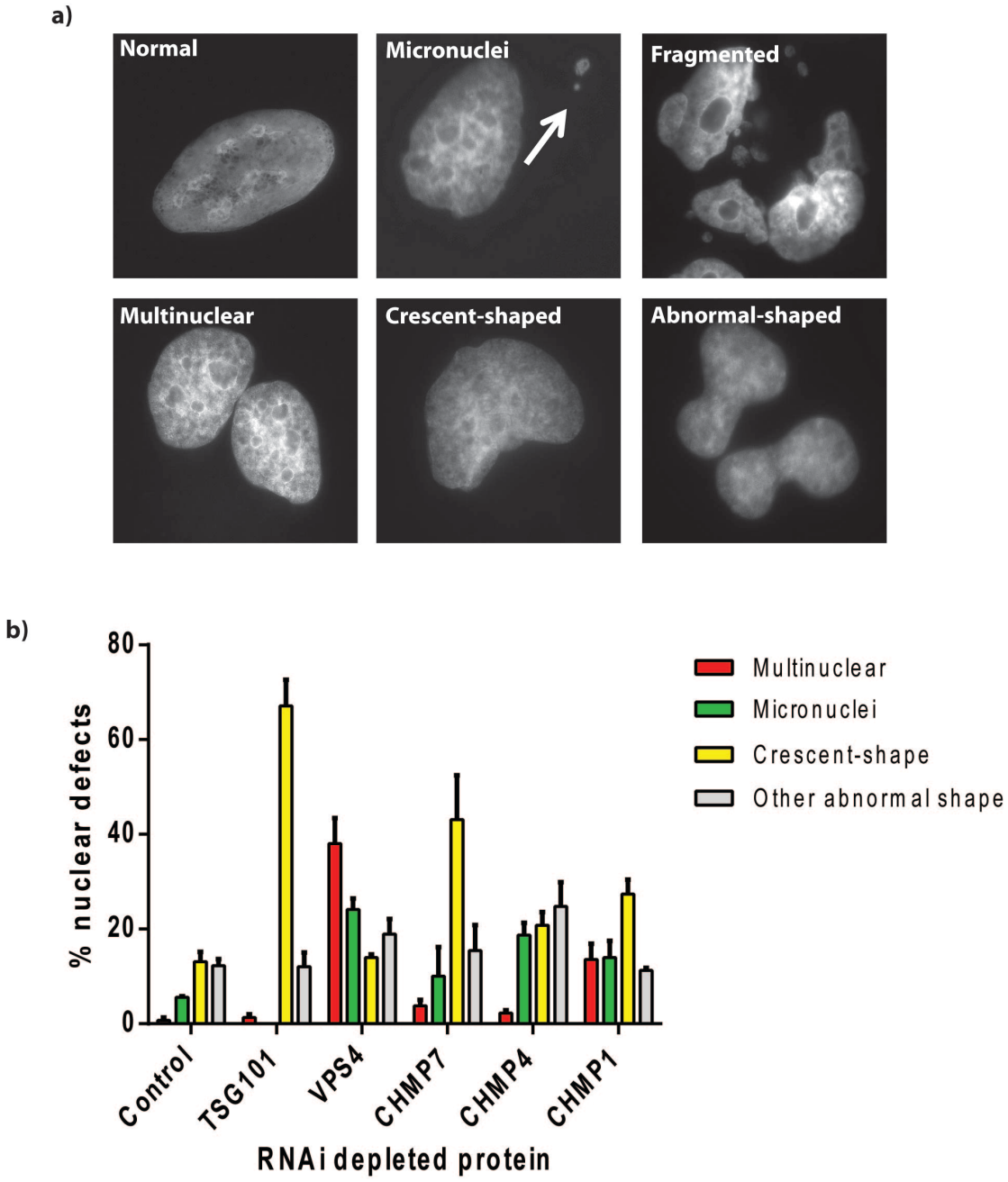

Figure 3 a) Examples of nuclear defects scored for in the cell population upon various depletions b) Graph showing breakdown of nuclear defect data to demonstrate the type of defects observed upon each knockdown: multinuclear (red), micronuclei (green), crescent shaped (yellow) and other abnormal shape (grey). This allows the protein depletion to be related to a stage in mitosis or cytokinesis. Standard error of mean is shown. Note; fragmented nuclei is scored under 'other abnormal shape'.

Statistical analysis was conducted using a two way anova that compared each defect across the different depletions. VPS4 displayed a statistically higher frequency of multinuclear cells than all other conditions ($P \leq 0.001$,

except between CHMP1 where also P≤0.001). Although not statistically significant, CHMP1 depletion resulted in more multinuclear cells than CHMP4 and CHMP7. This is interesting since CHMP4B appeared to spend more time at the midbody than CHMP1B and it could be assumed is more important in cytokinesis. However, CHMP1B recruits spastin through a MIM-MIT interaction. Spastin is a microtubule severing enzyme and is required at the midbody to break the microtubules so cleavage can occur. This explains the increase in multinuclear cells in the CHMP1 depleted population.

In terms of micronuclei, only VPS4 was deemed statistically significant compared to the control. This agrees with Morita et al who proposed that VPS4 first functions in mitosis before re-localising to the midbody later[45]. The similar number of micronuclei for CHMP1, 4 and 7 (14, 18.7 and 10 % respectively) indicates a similar function for them during mitosis. Based on the increase in crescent shaped nuclei this function could likely be in metaphase. Only TSG101 and CHMP7 differed statistically in regard to crescent shaped nuclei compared to all other depletions. Previously CHMP7 had been suggested as a bridging ESCRT with the idea that the N terminal emulates ESCRT-II subunit functions. ESCRT-II subunit, EAP45, interacts with the ESCRT-I complex through VPS28. Therefore CHMP7 could interact with ESCRT-I subunits, such as TSG101, which could result in similar defects when either is depleted. Although data from chapter 4 showed that depletion of TSG101 had no effect on CHMP7, which we would expect if they interacted. Overexpression of a GFP-labelled CHMP7 has been shown to suppress the release of virus-like particles[46]. TSG101 is largely involved in the process of virus budding and is the earliest protein from the ESCRT family to be hijacked by viral proteins. Interestingly, CHMP7 is the only CHMP depletion that showed a statistically significant increase in a nuclear defect (crescent-shaped in this case) indicating a more prevalent role of CHMP7 during mitosis.

6.2.2. CHMP7 localises to micronuclei upon VPS4 depletion.

We wondered if different defects affected the number of nuclear ESCRT-III spots. However, when scoring for individual nuclear defects no noticeably relationship was observed between the number and size of CHMP7 spots and the type of nucleus, deformed or not. Another striking observation was made: CHMP7 localised to 70% of the micronuclei observed (figure 4a).

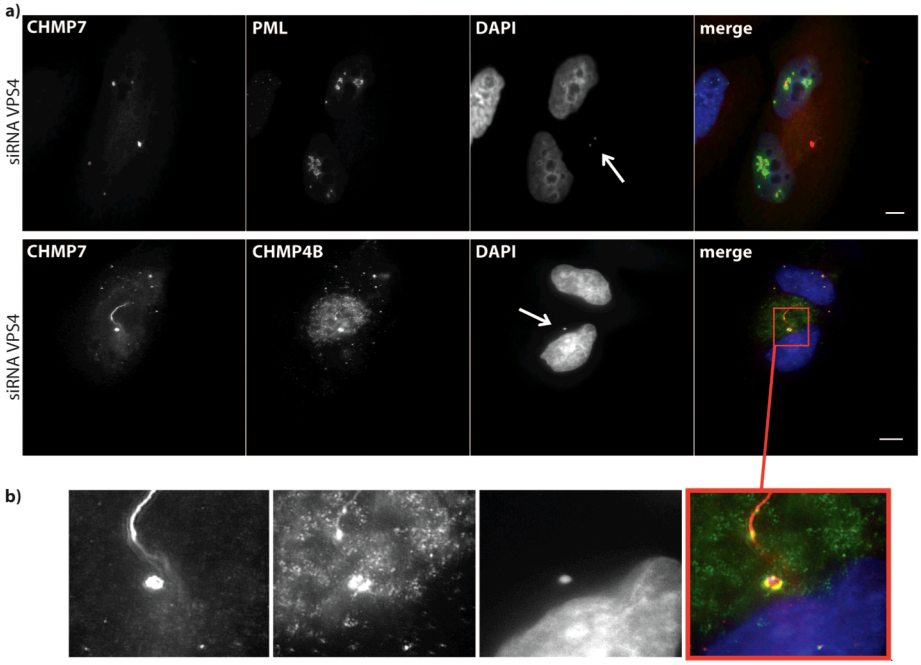

Figure 4 Cells RNAi depleted of VPS4 for seventy-two hours displaying both multinuclear and micronuclei nuclear defects. a) CHMP7 (red, Cy3) is seen localising to micronuclei (stained with DAPI) as indicated by the arrows. CHMP4B and PML (green, ALEXA 488nm) are also shown. PML was not observed localising to micronuclei, whereas CHMP4B was. Scale bars equal 10 μm b) shows a zoomed in view of the localisation of CHMP4B and CHMP7 to micronuclei.

CHMP4B co-localised with CHMP7 in micronuclei in 48% of cells displaying this defect and CHMP1B co-localised in 27.3%. CHMP4B and CHMP1B were never observed in the micronuclei without CHMP7 also being present. As figure 4a shows PML was unaffected and was not observed in micronuclei. Figure 4b shows a zoomed in view of this co-localisation between CHMP4B and CHMP7. Similar to the nuclear phenotype displayed by the CHMPs upon VPS4 depletion, CHMP7 is again the key member that localisation relies on. This localisation to micronuclei indicates a clear relationship between CHMP7 function and lagging chromosomes. One role of CHMP7 likely lies in

chromosome segregation. Lagging chromosomes have been linked to defects in kinetochore proteins or in kinetochore assembly itself[177]. Borealin, a protein involved in the anaphase checkpoint and known to interact with CHMP4C, is also involved in kinetochore assembly[98,178]. Borealin depletion promotes kinetochore-spindle mis-attachment[179]. The outer kinetochore binds microtubules that control chromosome movement and so issues with its assembly and attachment can lead to lagging chromosome and micronuclei. CHMP depletions don't significantly increase the formation of micronuclei and so are likely recruited as a preventative measure or once the anaphase lag has occurred. This suggests their depletion does not cause damage, but they could be recruited to help repair it.

The development of nuclear defects was followed during VPS4 depletion at twenty-four, forty-eight and seventy-two hours after siRNA treatment. After twenty-four hours the majority of cells will have attempted cytokinesis (only cells in early G1 may not have reached this stage yet). However, after twenty-four hours the RNAi knockdown is not fully effective (figure 5b). The graph shown in figure 5 is reflective of this displaying a low number of multinucleated cells after twenty-four hours with a large increase after forty-eight hours.

The significant increase in the amount of crescent and abnormal shaped nuclei after twenty-four hours indicates how VPS4 action in mitosis is more sensitive to changes in VPS4 gene expression when compared to its role in cytokinesis. After forty-eight hours the amount of crescent/abnormal nuclei observed decreases as the majority of cells display evidence of failed cytokinesis. This is because cell defects resulting in crescent and abnormal shaped nuclei are still able to attempt cytokinesis. The depletion of VPS4 isoforms is toxic to cells and as a result their population reduces over time due to cell death. VPS4 depletion disrupts many cellular processes and the accumulation of these defects is mirrored by the range and proportion of nuclear defects. The appearance of micronuclei steadily increases from 4.5%, 12% to 24% in twenty-four, forty-eight and seventy-two hour cell populations respectively.

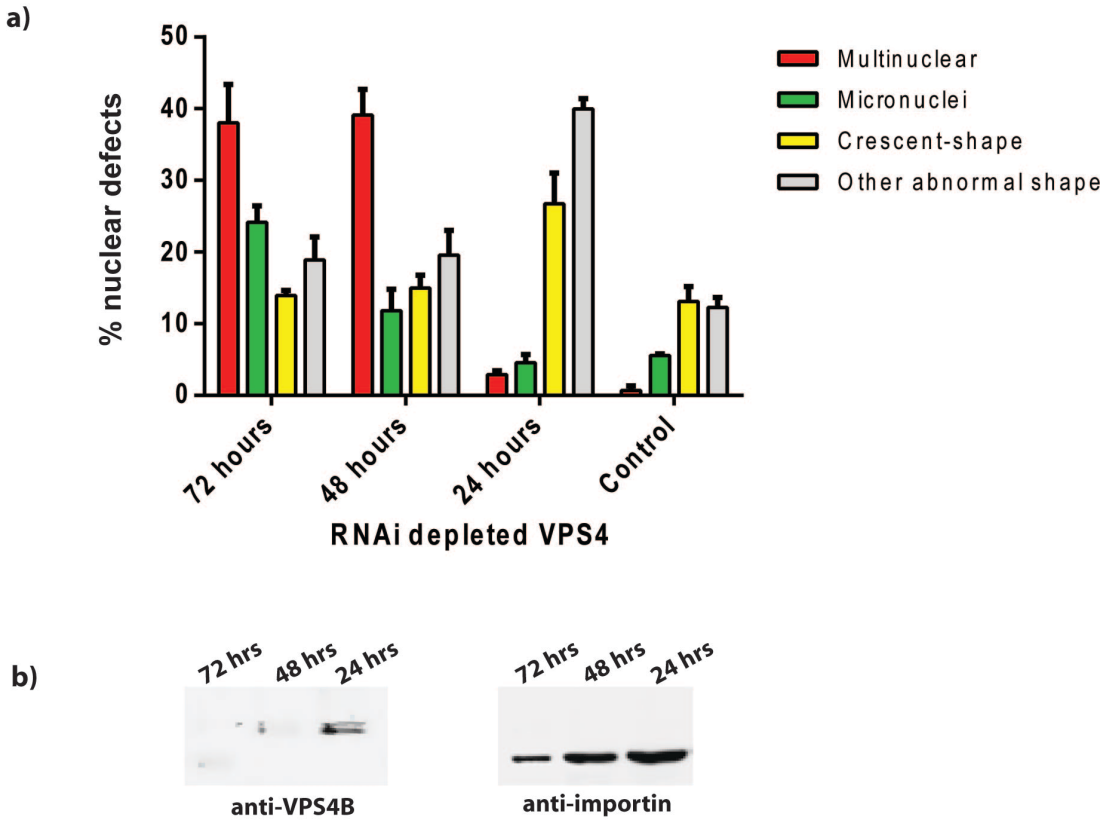

Figure 5 a) Graphing show RNAi depletions of VPS4 lasting twenty-four, forty-eight or seventy-two hours before cell fixation. Different nuclear defects are represented; multinuclear (red), micronuclei (green), crescent shaped (yellow) and abnormally shaped (grey) nuclei. b) Western blot demonstrating VPS4B presence over time, and importin beta as a loading control.

Often micronuclei are observed in cells that are also multinucleated. This indicates the anaphase checkpoint is inhibited by VPS4 depletion resulting in the cell continuing mitosis and attempting cytokinesis.

6.2.3. CHMP7 and CHMP4B form filaments in cells blocked in cytokinesis.

A further observation in VPS4 depleted cells is the appearance of CHMP filaments. This phenotype was seen in 13.7% of VPS4 depleted cells and is scored based on the number of CHMP7 filaments, since they were the most frequent (figure 6). CHMP4B and CHMP1B filaments co-localised with CHMP7 filaments and were not observed in the absence of CHMP7. This

phenotype agrees with the behaviour observed in previous chapters regarding these ESCRT proteins and the likely direction of their recruitment to nuclear structures. CHMP4B showed 72% localisation to CHMP7 filaments, while CHMP1B showed 12% localisation. Interestingly, this phenotype was specific to VPS4 depleted cells since CHMP filaments were not observed in either TSG101 or CHMP depletions. However, double knockdown of VPS4 and CHMP1B reduced the amount of filaments observed to 9.4% and

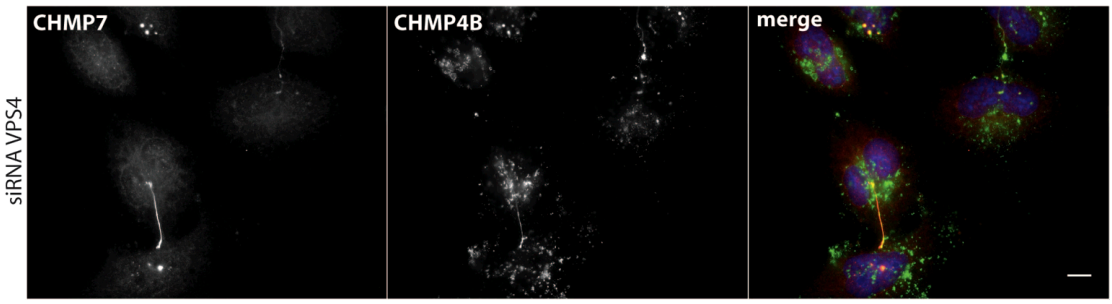

Figure 6 RNAi depletion of VPS4 probed with anti-CHMP7 (red, Cy3) and anti-CHMP4B (green, ALEXA 488 nm). Images shows a CHMP7 filament passing through the midbody and connecting the sister nuclei. To a lesser extent CHMP4B is also observed forming this filament and localising to the midbody. Scale bars equal 10 μm.

VPS4/CHMP4 RNAi depletion reduced the amount to 4.3%. The co-depletion of CHMP7 and VPS4 resulted in 0.5% filaments in the cell population and was observed using the CHMP4B antibody, indicating either that CHMP7 isn't essential to filament formation or that the CHMP7 knockdown was not 100% effective in this case.

These filaments largely originated from the nucleus, including deformed nuclei and micronuclei. In cells blocked in cytokinesis, these filaments were also often observed travelling through the midbody to connect the nucleus with either micronuclei or the daughter nuclei (figure 7). Moreover in multinuclear cells, the filaments linked both nuclei. Taken together, these data suggest CHMP7 functions in chromosome segregation.

The majority of CHMP7 filaments were observed in cells attempting cytokinesis (i.e. containing a visible midbody) and appeared to then persist in cells that had already failed, i.e. displaying multinucleated/micronuclear defects. This implies VPS4 may be involved in dismantling CHMPs from

chromosomes and microtubules during either anaphase or telophase before it re-locates to the nucleus. In VPS4 depleted cells fixed after twenty-four hours, no CHMP7 filaments were observed, whereas after forty-eight hours an average of 22.95% of cells displayed this phenotype.

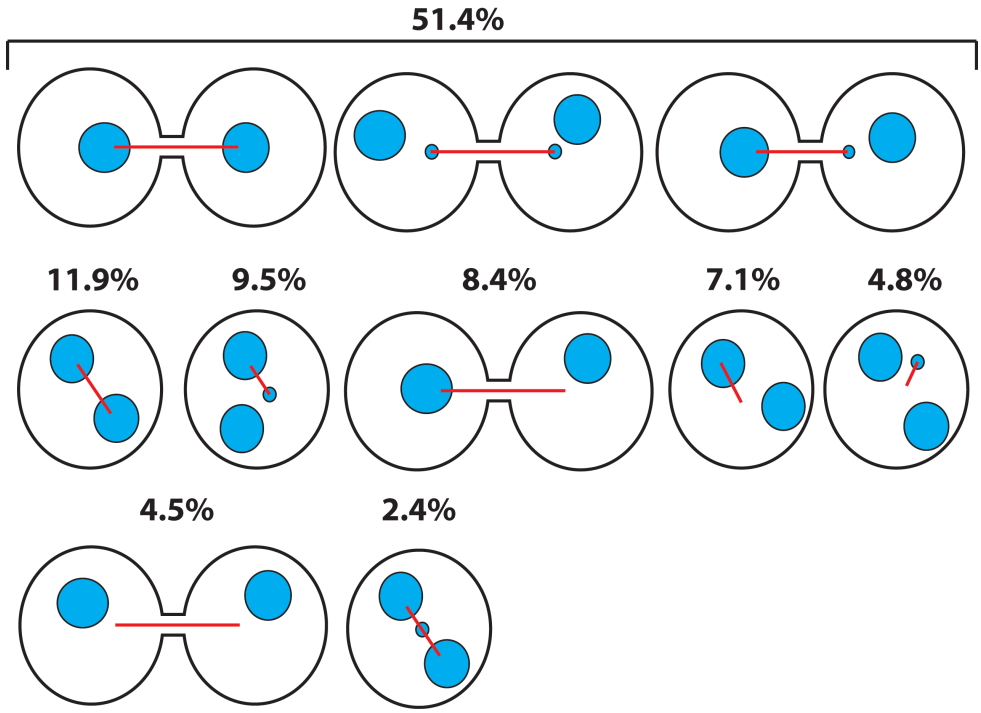

Figure 7 Cartoon represents the variety of CHMP7 filaments phenotypes observed VPS4 depleted cells. Red lines represent CHMP7 filaments and blue circles represent both nuclei and micronuclei. There filaments were always associated with either nuclear material or midbodies and generally linked sister nuclei or micronuclei. This indicates a role in chromosome segregation and trafficking during anaphase and telophase. CHMP7 is potentially concerned with ensuring the midbody is free of genetic material before abscission occurs.

Filament appearance after seventy-two hours is reduced to 13.7% suggesting that post cytokinesis, successful or not, these CHMP filaments are resolved. The process itself appears to be highly dynamic and it is suggested that filaments draw back from the nuclei/micronuclei towards the midbody as they are resolved (figure 8). The disassembly of these filaments likely requires VPS4 since no filaments were observed at midbodies or nuclei in cells depleted with another protein, i.e. TSG101.

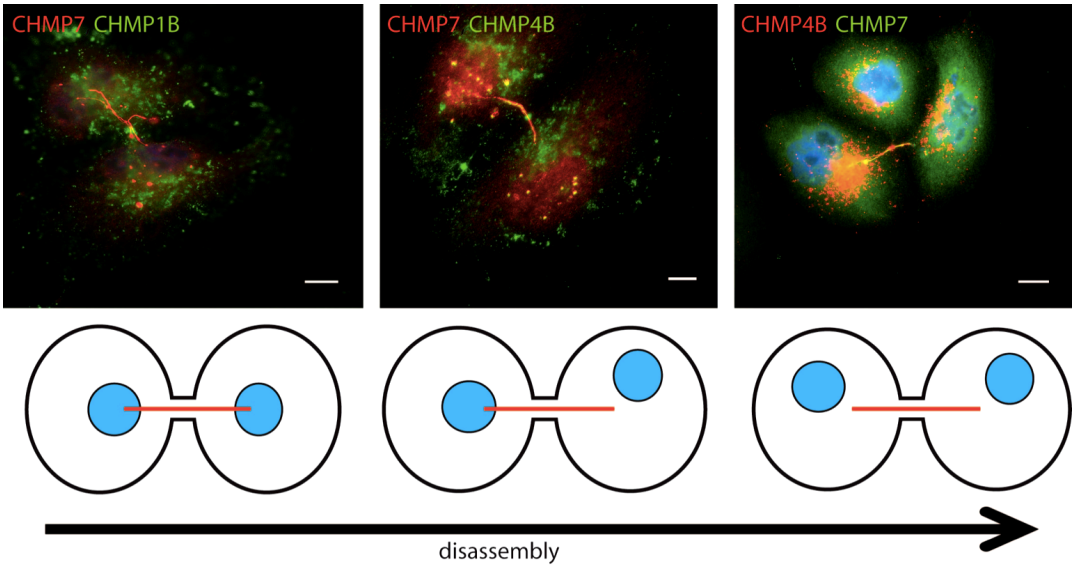

Figure 8 Scheme proposing a direction for CHMP7 filament events. During cytokinesis they attach sister chromatids and 'shrink' back towards the midbody, where potentially VPS4 would normally act to disassemble them. In VPS4 depleted cells this disassembly is severely delayed. Images show VPS4 depleted cells displaying CHMP7/4B filaments in differing stages of their function. Secondary antibodies used were Cy3 and ALEXA 488 nm. Scale bars equal 10 μm.

The scheme in figure 8 proposes how the CHMP7 filaments would normally disassemble in cells undergoing cytokinesis, this is accompanied by images that may capture each stage of this. Other than cells in cytokinesis, filaments are only observed in multinucleated cells, this demonstrates the importance of VPS4 in filament resolution. Interestingly, figure 8 reveals an example of multiple filaments passing through the midbody: two in the nucleus of the upper cell, whereas a third localises to a micronuclei (see figure 9 for an enlarged view). The filaments appear to emerge from CHMP7 nuclear spots. It is suggested that filaments nucleate from CHMP bodies when chromosomes are aligning, likely during metaphase. Moreover, one could speculate that the role of CHMP7 (and partially 4B) works to ensure that no genetic material is at or near the midbody before abscission begins. CHMP4C is important at this stage as it interacts with proteins at the anaphase checkpoint[98]. At this stage VPS4 is localised to the midbody and can disassemble the ESCRT-III subunits, including CHMP7/4B filaments.

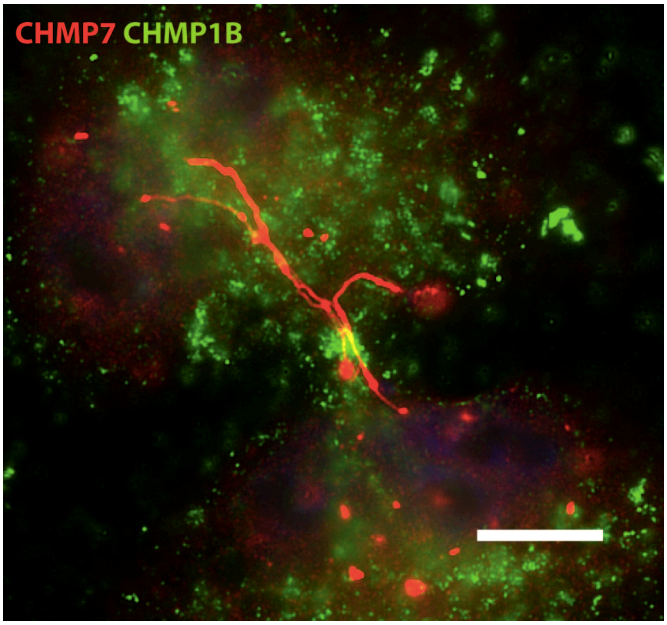

Figure 9 Multiple CHMP7 filaments running through a midbody in a VPS4 depleted cell population. CHMP1B is observed localising at the midbody, but in this case not to CHMP7 filaments. Scale bar equals 10 µm.

The subcellular localisation of a sample of proteins known for their involvement in mitosis and cytokinesis were probed in order to determine their relationship with CHMP filaments (figure 10). This information is important as it allows us to perform an initial screening for partner proteins coordinating CHMP7 and 4B chromatin-related functions.

The first ESCRT shown is, ALIX, which is involved in cytokinesis and localises to the midbody where it recruits CHMP4[180]. Even though ALIX localised to midbodies, it did not localise to CHMP filaments.

Secondly, we decided to probe for endogenous SUMO given the established interaction between CHMP7 and SUMO1 (see chapter five). A recent review by Dasso examines the role of human SUMO in mitosis and cytokinesis. This paper draws links between the sumoylation pathway and kinetochore function and mitotic chromosome structure[181].

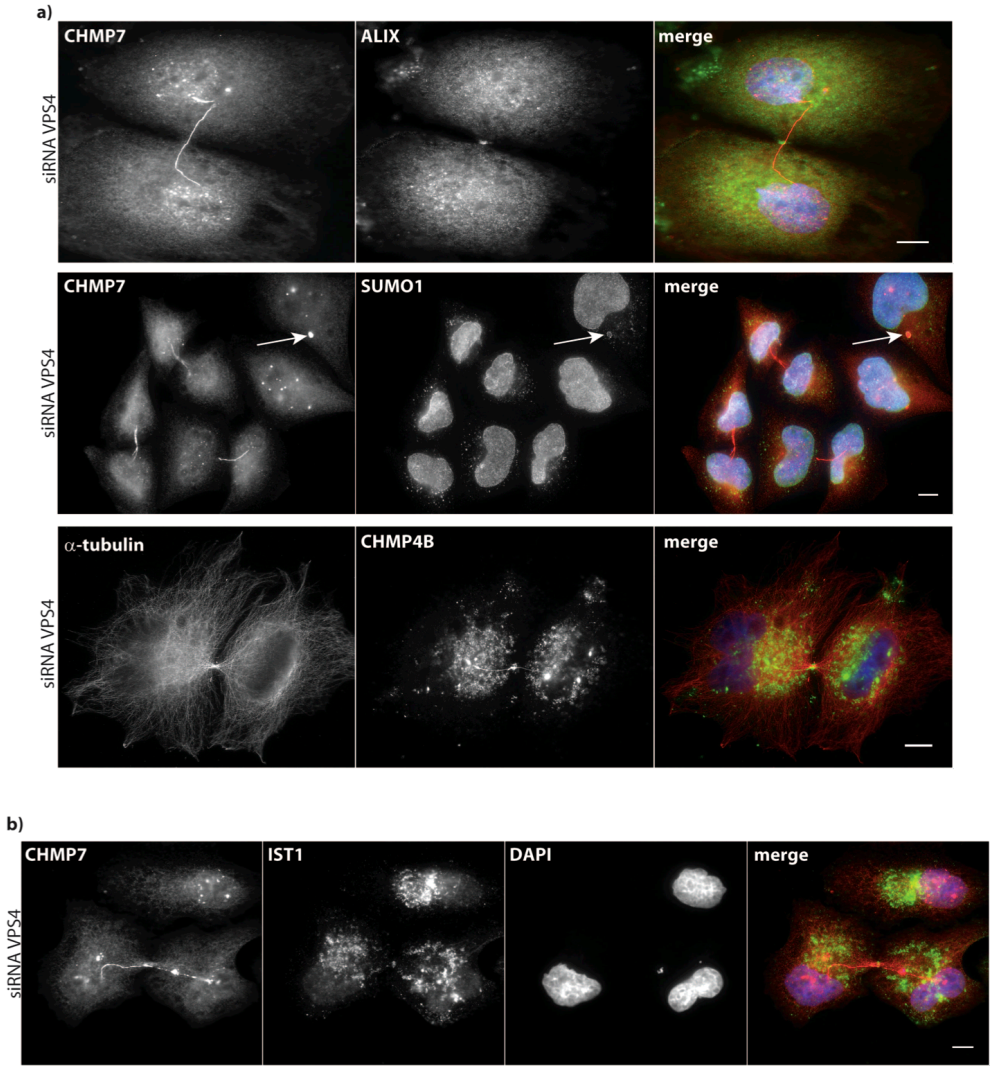

Figure 10 VPS4 depleted cells (seventy-two hours) probed with a variety of antibodies involved in cytokinesis; anti-ALIX (green, ALEXA 488 nm), anti-SUMO1 (green ALEXA 488 nm, DM1A (red, Cy3) and anti-IST1 (green, ALEXA 488 nm) and co-stained with CHMP7 (red, Cy3) or CHMP4B (green, ALEXA 488 nm). White arrows indicate co-localisation between SUMO1 and CHMP7 at a micronucleus. Scale bars equal 10 μm.

Additionally, SUMO specific protease, SENP5, which controls maturation of SUMO1 and removes it from substrates, has been implicated in cell division. RNAi depletion of SENP5 resulted in upregulation of SUMO1 and an increase in multinucleated cells –indicating cytokinesis failure[182]. In chapter five, it was shown that overexpression of SUMO1 (and UBC9) resulted in nuclear CHMP7, although an increase in multinuclear cells was not observed. This implies upregulation of SUMO1 does not itself cause the increase in multinucleated cells or cytokinesis failure. Moreover, this suggests a mechanism by which upregulation of SUMO1 is a response to

mitotic/cytokinetic defects and this partly drives the nuclear localisation of CHMP7.

Our findings link CHMP filament formation with multinucleated cells. Upon VPS4 depletion SUMO1 was mainly nuclear, but did not localise to CHMP filaments. However, SUMO1 was observed co-localising with CHMP7 in micronuclei (figure 10, indicated by white arrows). SUMO1 is normally observed surrounding the periphery of nuclei. This observed co-localisation may just be SUMO1 displaying its normal behaviour of surrounding the nuclear envelope (a micronuclear envelope in this case) and therefore not a real indication of a SUMO/CHMP7 interaction in vivo.

Thirdly, we looked at alpha tubulin (DM1A antibody), which is the main component of microtubules. No noticeable colocalisation was observed between CHMP filaments and microtubules fluorescent signals, except at the midbody region (known to be rich in microtubules filaments) (figure 10).

Lastly, we probed for IST1 (figure 10). As discussed in the introduction IST1 is a regulator of VPS4 enzyme activity. IST1 has been classed as an ESCRT-III protein since 2009 and is known to interact with CHMP1B whilst also proving essential in cytokinesis[69]. Upon VPS4 depletion, the appearance of IST1 is similar to that of CHMP4B and 1B. IST1 appeared clustered on enlarged endosomes and localised to midbodies. Unlike CHMP4B and 1B, however, IST1 did not appear nuclear or to localise to CHMP7 spots or filaments. Furthermore, IST1 did not localise at micronuclei either.

In order to test if CHMP7 localised to kinetochores, we looked at the localisation of centromere protein F (CENPF) in VPS4 depleted cells. CENPF is a nuclear protein associated with the centromere-kinetochore complex. It localises to the kinetochores and spindle midzone during mitosis and has been implicated in chromosome segregation[183]. Figure 11 shows that the distribution of CENPF varied little between control and VPS4 depleted cells – remaining largely nuclear. No localisation was observed between CENPF and CHMP4B or CHMP1A (anti-CHMP1A antibody recognises CHMP4 isoforms) in either control or VPS4 depleted cells. The anti-CENPF and anti-CHMP

antibodies preferred different fixation methods, therefore not many sharp, well defined images could be obtained when probing for them in unison. Interestingly, figure 11 shows the only example observed of a CHMP filament occurring in control cells. This indicates that the CHMP7 filament phenotype is not solely a response to VPS4 depletion, but rather is exaggerated by it.

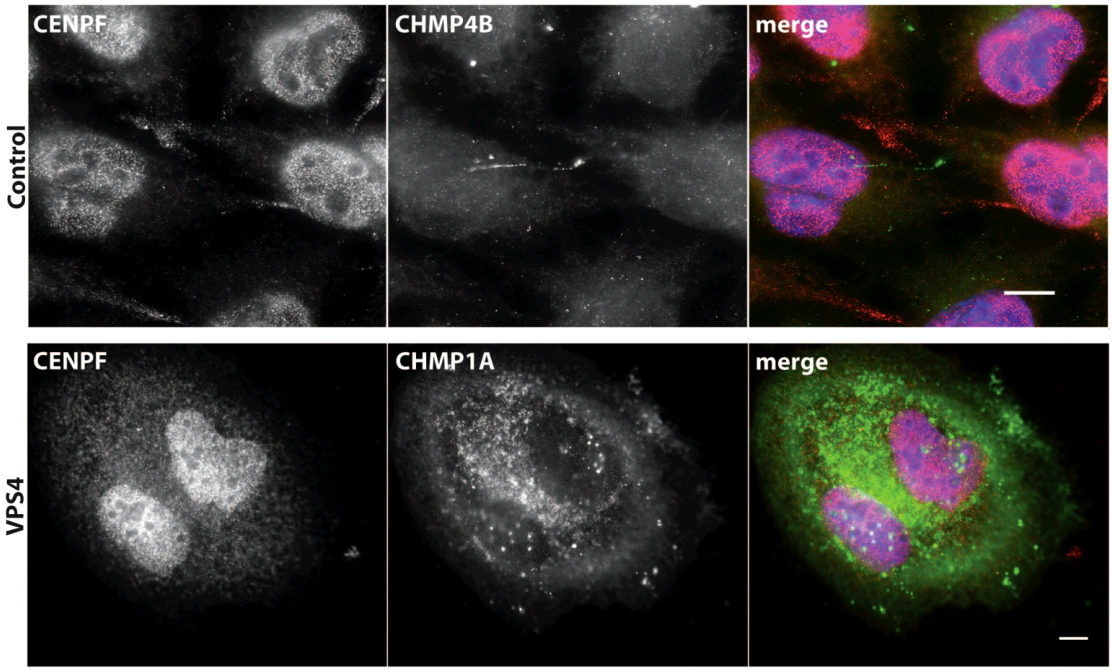

Figure 11 Control and VPS4 depleted cells probed with anti-CENPF (red, Cy3) and CHMP4B and 1A (green, ALEXA 488 nm) antibodies. CENPF is exclusively nuclear, but does not localise to nuclear spots or filaments. Scale bars equal 10 μm.

6.2.4 Nuclear CHMPs localise to sites of DNA damage upon VPS4 depletion

Preliminary experiments aimed to examine the link between nuclear CHMPs and DNA damage. Double strand break (DSB) formation in cells immediately triggers the recruitment of DNA damage, signalling and repair proteins to the damaged area, where these proteins form discrete nuclear bodies. The order and timing of the recruitment of DNA damage repair proteins is critical for detection and repair of DSBs. DSB repair is necessary to maintain genomic stability and if left unrepaired can lead to cancer. H2AX, from the histone family of proteins becomes phosphorylated upon detection of DSBs.

Phosphorylated H2AX localises to these sites of DNA damage and acts as a signal (through ubiquitination) to other DNA damage repair proteins.

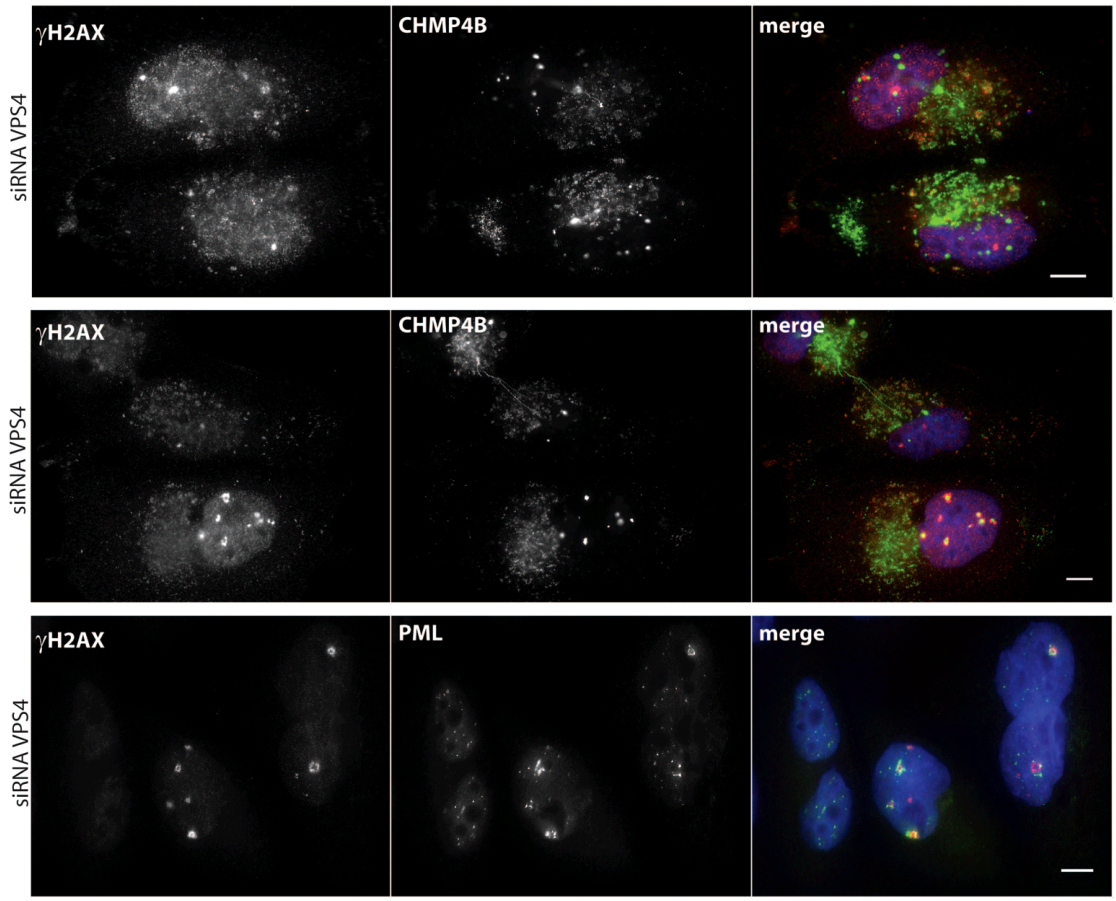

Figure 12 VPS4 depleted cells probed with anti-γH2AX (red, Cy3) and either anti-CHMP4B or anti-PML (green, ALEXA 488 nm). H2AX is a histone protein that is phosphorylated upon detection of double strand breaks (DSB). Once phosphorylated H2AX localises to DSBs, here it acts as a signal to DNA damage repair proteins. Images show here some co-localisation with CHMP4B in the nucleus and also with PML nuclear bodies. Scale bars equal 10 μm

As a result antibodies against the phosphorylated form of H2AX are widely used as DNA damage markers. Nuclear CHMP spots seem likely to be involved with chromatin, a phenotype that extends through mitosis where chromosome segregation can occur with the aid of CHMP filaments. Therefore, it seems sensible to begin exploring the link between DNA damage, likely increased by VPS4 depletion, and the CHMP nuclear and filamentous phenotype. While in the majority of cells there was no clear localisation, strong γH2AX staining was observed around nuclear CHMP4B in some cells (figure 12).

Co-localisation between γH2AX and PML was also observed when PML bodies were large or beginning to form filaments/rings[184]. This phenotype has been previously observed and shows that PML nuclear bodies nucleate near to sites of DNA damage and may have some involvement in apoptosis[184,185]. PML has previously been linked to DNA damage response, where it has been observed forming large supramolecular complexes that recruit and dispatch the appropriate proteins to sites of damage[186]. The relationship between CHMP7 and PML may be a reflection of CHMP7 functions at sites of DNA damage. It seems likely CHMP7 does have some direct contact with PML due to its absence in the VPS4/CHMP7 co-depletion removing PML body maturation. It could be suggested that CHMP7 triggers a DNA damage response function in PML

A second marker of DNA damage utilised was the breast cancer type 1 protein (BRCA1). BRCA1 is a DNA repair protein found in a range of cell tissues, as well as breast cells. It is a ubiquitin ligase that marks sites of DNA damage[187].

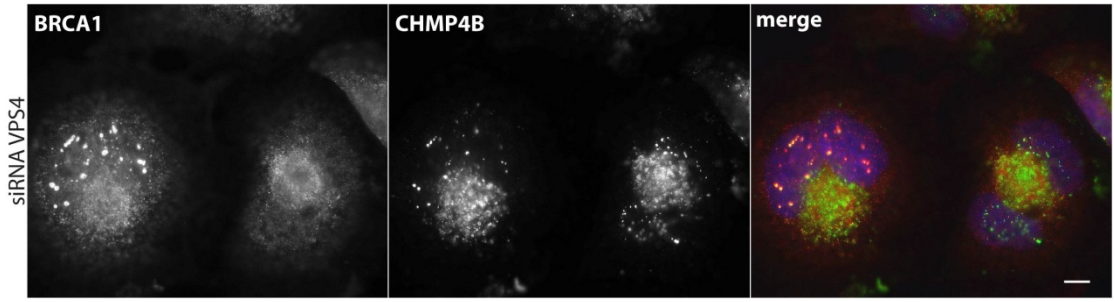

Figure 13 VPS4 depleted cells probed with anti-BRCA1 antibody (MS110, red, Cy3) and anti-CHMP4B (green, ALEXA 488 nm). BRCA1 co-localises to CHMP4B nuclear spots –but not all the time. Scale bar equals 10 μm.

In VPS4 depleted cells, BRCA1 was adjacent to nuclear CHMP4B, in a similar fashion to γH2AX (figure 13). This localisation in a small sample of cells could be a reflection of a cell cycle-dependent process. In these experiments we cannot determine the timing of DNA damage, therefore, a mix of DNA damage at different stages of detection, signalling and repair would be present. This could explain why in some cells co-localisation is high whereas in others only CHMP4B spots are observed. Moreover, this implies CHMP4B

is present at DSBs before the BRCA1 complex. It was previously mentioned that VPS4 depletion is exaggerating 'normal' CHMP behaviour. Based on this assumption it could be proposed that the excess of nuclear CHMPs localised, to chromatin, and trapped by VPS4 depletion, could be causing DNA breaks. This hypothesis was earlier proposed (chapter five) to explain the tendency of PML to co-localise next to and surround toxic CHMP accumulations. This also agrees with the partial co-localisation observed between DNA damage markers and CHMP4B.

6.3 Discussion

The data presented in this chapter is the most recent work from this thesis and provides new information regarding CHMP7, CHMP4B and CHMP1B function during mitosis.

Individual CHMP depletions confirmed work by Morita et al indicating their absence results in metaphase defects such as crescent shaped nuclei[45]. Furthermore, depletion of VPS4 blocks cytokinesis generating a significant number of multinucleated cells after the RNAi is in full effect.

In the previous chapter data were presented corroborating how structural changes in CHMP7 size increase their adjacency with PML NBs and promote PML conformational changes. This localisation was unaffected by the type of nuclear defect present and agrees with either of two theories provided in chapter five. First, mature CHMP bodies act as a nucleation point for PML NB formation nears sites of DNA damage. Or second, an excess of CHMPs causes cellular stress and DNA damage that leads to PML recruitment and body formation to remove toxic protein aggregates.

It seems likely a combination of these two ideas could take place with PML acting as a 'clean-up' for excess CHMP proteins accumulating on chromatin. Here, the initial role of CHMPs (before they become harmful to the cell) is to help regulate chromosome segregation and separation during metaphase. Partial co-localisation of CHMP4B with BRCA1 and γH2AX could be

distinguishing between CHMP complexes causing DNA damage and ones that are not yet big enough to cause damage.

The relationship between ESCRT-III and DNA damage response could be further explored by introducing DNA damage in a regulated quantified and timed manner -such as using exposure to ionising radiation. These experiments as time lapse studies would allow us to determine whether DNA damage markers localise before or after CHMPs accumulate in the nucleus. Furthermore, other cell lines could be explored to examine CHMP behaviour across different tissues where its basal level of expression may differ.

The appearance of CHMP filaments occurred only in cells undergoing cytokinesis or multinucleated cells that had already failed cytokinesis. Filaments appear to nucleate from CHMP spots and linked genetic material from sister nuclei and micronuclei. CHMP7 also localised to micronuclei, whereas PML NBs were never observed here. Micronuclei are the result of fragments or whole chromosomes lagging behind during anaphase. They can persist for generations and their occurrence is used as an indicator in genotoxicity[188].

Based on the initial data obtained we propose that a CHMP complex could have the dual function of trafficking chromosomes during mitosis and aiding lagging chromosomes as they arise. Chromosomal trafficking is disrupted by VPS4 depletion, which jointly causes DNA damage and an exaggerated amount of lagging chromosomes. When these CHMP accumulations reach a certain size they initiate a DNA damage response resulting in recruitment of BRCA1, γH2AX and PML (figure 14).

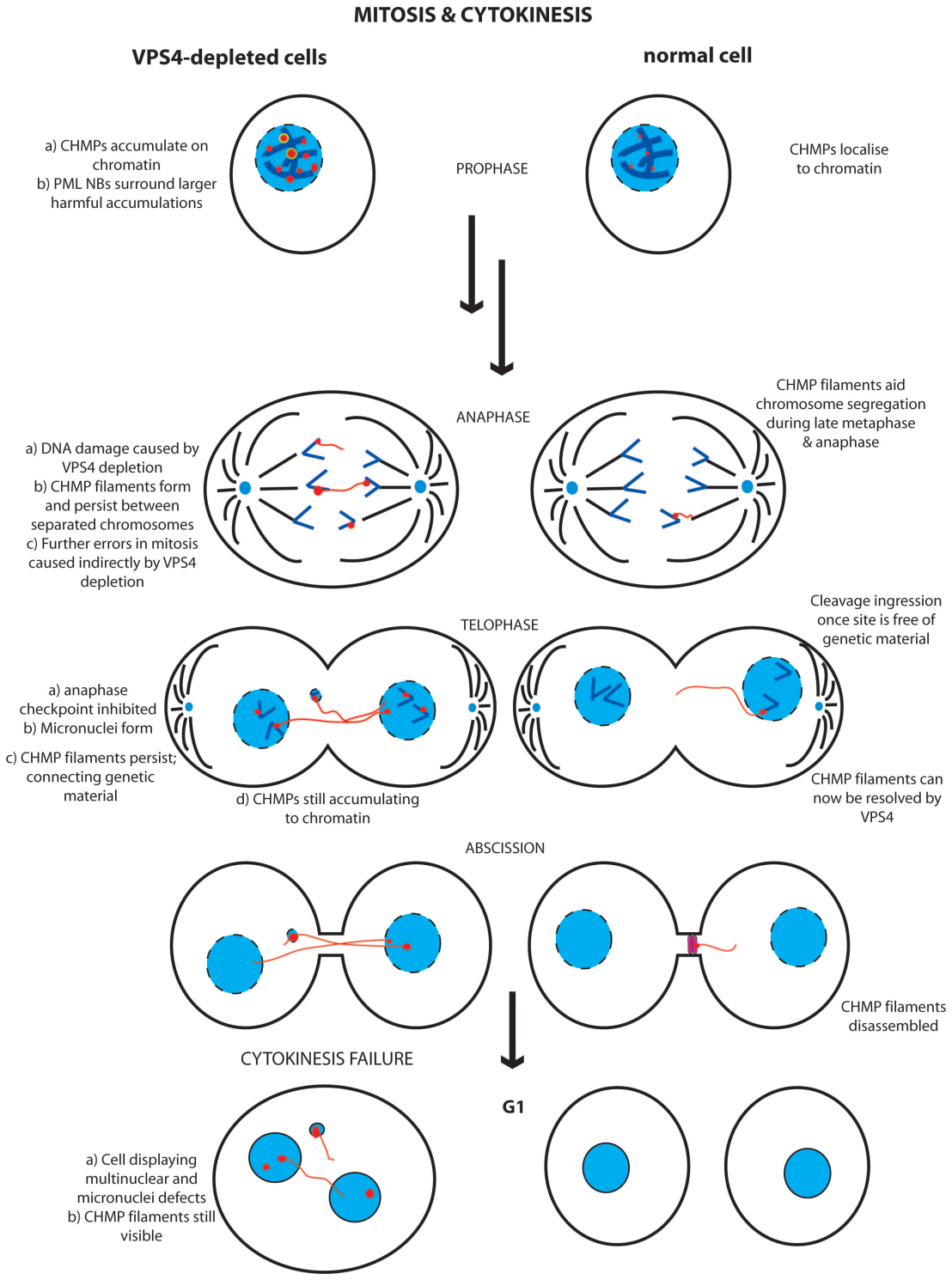

Figure 14 Scheme proposing how CHMP filaments and bodies (red) function during mitosis and cytokinesis in normal cells and also compared to VPS4-depleted cells. We suggest that VPS4 depletion exaggerates and therefore reveals a nuclear CHMP function in chromosome segregation and trafficking damaged chromosomes through mitosis. In VPS4-depleted cells this function is severely disrupted as CHMP spots and filaments are not able to be disassembled and recycled by VPS4. Further to this, accumulation of CHMPs on chromatin causes DNA damage that initiates a DNA repair response and promotes the formation of large PML NB complexes that act to sequester and degrade harmful CHMP aggregates.

The DNA damage response system in attenuated during mitosis and full activity only resumes once cells enter G1 phase post cytokinesis[189]. The system itself is highly regulated, comprised of initial DNA break sensing and signalling followed by a cascade of events that lead to cell cycle arrest, repair and cell cycle continuation. In contrast, breaks that occur during mitosis are not immediately repaired. Once mitosis has reached a certain stage it is committed to complete despite DNA damage[190]. DSBs do not hinder mitosis and are, whilst not repaired, still sensed by signalling proteins such as γH2AX, which localise to the site of damage. Therefore, it could be proposed that in its 'normal' function the nuclear CHMP complex could form filaments that localise preferentially to damaged chromosomes and aid their progression through mitosis, especially during chromosome segregation when an anaphase lag is most likely to occur. During cytokinesis normally these filaments would be disassembled by VPS4 from its location at the midbody. However, in VPS4 depleted cells not only do these filaments persist and micronuclei form, but the knockdown itself further increases DSBs due to trapped CHMPs on chromatin and thereby 'enhancing' the nuclear CHMP phenotype. CHMP filaments in control cells (HeLa M) are rare and hard to capture an image of due to their formation only in the presence of damaged and lagging chromosomes. This theory implies that CHMP7 would appear localised to the midbody in a small fraction of cases as VPS4 disassemblies it from this location. Disassembly would likely occur in the late stages of cytokinesis, which VPS4 depletion blocks.

We found that PML filaments and rings localised to γH2AX (similar in appearance to its localisation with CHMPs). This has been previously observed by Bøe et al[191]. Several DNA damage repair proteins transit through PML NBs, confirming a regulatory role for PML in DNA damage. The mechanisms, partition and progression of nuclear bodies through mitosis is unclear. Dellaire et al proposes that PML protein is not degraded during mitosis, but forms mitotic accumulations that are recycled and reform PML NB in the new nuclei[192]. PML may still function in a limited capacity during mitosis, triggered by accumulation of CHMPs. PML NBs forming near and surrounding

these accumulations may also act to prepare damaged loci for the resumption of DNA repair post cytokinesis.

Further to this, we demonstrated (chapter 5) that a non-covalent interaction between CHMP7 and SUMO1/UBC9 does exist. Overexpression of SUMO1 and UBC9 led to a recreation of the nuclear CHMP7 phenotype, but no filaments were observed. Based on this evidence we propose that sumoylation of CHMP4B and CHMP1B is regulated through the CHMP7 SIM-SUMO interaction and this signals the redistribution of the CHMPs to chromatin. ESCRT-III subunits can likely associate with chromatin regardless of whether it is damage or not, but possibly they migrate towards sites of damage upon certain signals, such as phosphorylation. As proposed earlier when this accumulation reaches a critical level CHMPs cannot function properly during mitosis resulting in an increase of mitotic defects.

Further work is required to substantiate this hypothesis, but so far these results are cohesive and provide a promising explanation highlighting a novel function for ESCRT-III subunits dependent upon CHMP7 and exaggerated when disrupted by VPS4 depletion.

CHAPTER 7 FINAL DISCUSSION AND CONCLUSIONS

This thesis has built upon the existing knowledge regarding CHMP7 to reveal new domains, motifs and interactions partners. Furthermore, through depletion of the ATPases VPS4A and B, we have revealed a CHMP7-dependent nuclear assembly consisting of CHMP7, 4B and 1B. The existence of a nuclear ESCRT complex is complimented by evidence from literature implicating CHMP proteins in nuclear events, such as gene silencing, tumour suppression, abscission checkpoint regulation, cell cycle regulation and mitosis[42,43,45,98]. We propose that the nuclear ESCRT assembly outlined in this work has novel functions in chromatin maintenance and chromosome trafficking during mitosis. The need for this maintenance function is increased by DNA damage, but significantly enhanced by VPS4 depletion, where CHMPs become 'trapped' on chromatin and can accumulate.

The data outlined in chapter three support a nuclear function for CHMP7 through protein domain structure and motif predictions. Moreover, it identifies further interactions between CHMP7 and other nuclear CHMPs (figure 1). Using fragments of CHMP proteins it has been shown that CHMP7 interacted with CHMP4B, CHMP1A and VPS4B. CHMP4B forms part of the nuclear assembly, and it is likely CHMP1A may as well. Due to lack of an isoform specific CHMP1A antibody we could not confirm this. However, CHMP1A is already known to have many nuclear functions and, like CHMP1B, contains an NLS. Future work in this area could focus on a complete analysis of CHMP

isoforms to determine if any other CHMP isoforms form a part of the nuclear assembly. Moreover, pull down assays which employ full length CHMP proteins could provide further confidence in the CHMP7 interactions revealed.

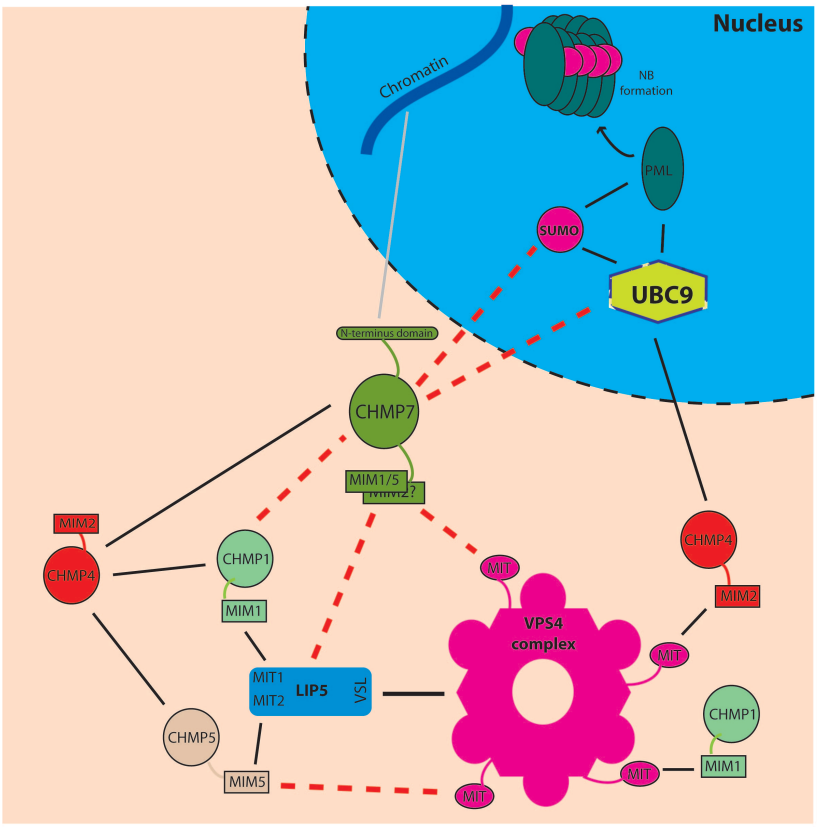

Figure 1 Final scheme highlighting CHMP7 protein-protein interaction network.

We propose the N terminal half (1-222) of CHMP7 comprises a double winged helix domain, a prediction made based upon protein threading analysis. The presence of nucleic acid binding domains supports a nuclear function for CHMP7 and further indicates that the presence of this domain could be the basis for a CHMP7-dependent re-localisation of CHMPs to chromatin structures.

The C terminal of CHMP7 contains an SNF7 domain[46]. Sequence alignment and protein modelling revealed that CHMP7 is predicted to contain both a MIM1 and MIM2 (similar to IST1). Peptide fragments spanning these MIT-interacting motifs both revealed interaction with VPS4B, although the interaction between CHMP7 MIM2 and VPS4B was less reproducible when

prey and bait protein were reversed in pull down assay. This could imply the affinity between VPS4B and the MIM2 is less than with the MIM1. MIM1 containing CHMP proteins generally bind VPS4 with greater affinity than MIM2[61]. However, the His pull down could be a false positive result due to the histidine residue present in the CHMP7 MIM2 fragment causing unspecific binding.

We also revealed an interaction between CHMP7 and LIP5, a positive regulator of VPS4 activity and oligomerisation. This interaction was specific to a region of CHMP7 (4th-5th alpha helices) containing the MIM1. Protein modelling indicated that CHMP7 could bind LIP5 through a MIM5 binding motif, previously found only in CHMP5. This implied some similarity of function between CHMP7 and CHMP5

CHMP1 isoforms contain nuclear localisation signals and sequence alignment indicates that CHMP7 might also contain this signal allowing it to access the nucleus upon certain triggers, such as phosphorylation[146]. CHMP7 also contains a classical nuclear export signal in the same region as the MIM1 motif. This could imply a dual function for this region in recognising VPS4 through its MIM1 and then being recycled back to the cytoplasm upon release from chromatin by VPS4 action.

To summarise, the data presented in chapter 3 revealed common CHMP characteristics for CHMP7 such as interaction with VPS4 *via* a MIM (possibly both MIM1 and MIM2). Furthermore, it expanded CHMP7 function to include the N terminal domain and suggested nuclear targeting and potential chromatin binding properties.

Chapter 4 provides perhaps the most important data that CHMP7 reproducibly displays a unique phenotype upon VPS4 depletion by localising exclusively to discrete nuclear structures, likely chromatin. CHMP4B and CHMP1B partially localise with CHMP7 in the nucleus, whilst still being observed upon aberrant endosomes and at the midbody of dividing cells. Furthermore the localisation of CHMPs to chromatin was largely dependent upon CHMP7. Only VPS4 depletion caused this localisation implying it is the 'freezing' of CHMPs on

chromatin that allows these structures to be visualised. Some nuclear localisation of CHMP7 to discrete structures is observed in control cells (34% of cells contained 2 or less CHMP7 bodies) agreeing with the hypothesis that VPS4 depletion only exaggerates this effect and does not cause it. Other methods that could be expected to reveal nuclear CHMPs such as monitoring CHMP7 through the cell cycle (*via* cell synchronisation) or overexpression of dominant negative VPS4 isoforms did not show the same nuclear phenotype. Similar to other regulatory CHMPs, depletion of CHMP7 did not show any significant disruption to the MVB pathway[2,6]. However, the overexpression of the VPS4 dominant negative mutant resulted in CHMP7 clustering on endosomes and partially co-localised with VPS4B. This could indicate that, although VPS4 isoforms in many respects are functionally redundant, in some cases one isoform performs a specific role primarily over the other. For example, VPS4A could be primarily involved in dismantling a nuclear assembly and, therefore, can continue in this function despite overexpression of a VPS4B mutant, as a result nuclear CHMPs would not be observed. Alternatively, in both cases of individual VPS4 isoform depletion endogenous VPS4 isoforms are still present in cells and may still be able to recycle the nuclear complex. It was observed both in our IF imaging and literature that the VPS4 EQ mutants are largely absent from the nucleus, whereas endogenous VPS4 is evenly distributed between the nucleus and cytoplasm[51,193]. Overexpression of wildtype VPS4B saw it dispersed between the cytoplasm and nucleus. Therefore, it is sensible to propose that mutations disrupting VPS4 ATP hydrolysis block VPS4 itself from localising in the nucleus. Mutant VPS4 is unable to disassemble nuclear CHMPs, allowing endogenous VPS4 to dismantle any nuclear CHMP complexes. This hypothesis provides the intriguing possibility that VPS4 isoforms require their ATPase function in order to localise within the nucleus. The nuclear CHMP complex is only seen upon depletion of both isoforms simultaneously, indicating their ability to function independently and also goes some way to discounting the idea that VPS4A plays a more dominant role in nuclear CHMP functions. Further work here could be to ‘rescue’ VPS4 depleted cells with wildtype and mutant VPS4 constructs and see if nuclear CHMP bodies are recycled. A series of VPS4

point mutations could help locate further residues important for VPS4 nuclear import. Also, designing a truncated VPS4B, removing the MIT domain (1-82 residues) would confirm the interaction between CHMPs and VPS4, *via* the MIT-MIM motifs, is crucial for their recycling:- this construct when overexpressed would be expected to result in an increase of nuclear CHMP accumulations, due to MIT-less VPS4B being unable to recycle CHMPs efficiently.

The phenotype of nuclear CHMP7 appeared similar to the nuclear pattern created by PML NBs, furthermore an interaction between UBC9 (an enzyme vital to PML formation) and CHMP4B had been observed by yeast two hybrid assay[111]. Given the relationship between PML and sumoylation, we started by looking at PML NBs to determine if these were the nuclear structures CHMP7 was localising to. Interestingly, CHMP7 and PML were observed adjacent to each other and the frequency of this increased when CHMP7 accumulations were larger in size (>1.25 μm). PML and PML NBs normally range in size between 0.2-0.8μm[127]. Large PML structures were observed likened to filaments and rings, surrounding CHMP7. When CHMP7 was co-depleted with the VPS4 isoforms large PML filamentous or ring-like structures were no longer observed, indicating that they are a direct response to large accumulations of CHMPs in the nucleus. PML behaves this way in response to viral infection and also accumulation of misfolded harmful proteins. In both cases, PML sequesters the harmful/viral proteins by surrounding them effectively in a 'cage'[150,169]. Furthermore, a specific PML isoform was responsible for this sequestration, PML-IV. Further work is this area could source isoform specific PML antibodies in order to validate if PML-IV is responsible for the large PML structures we observed.

The other instances of PML filaments and cage structures led us to formulate three hypotheses regarding the relationship between CHMPs and PML.

1. CHMP accumulations are toxic to the cell and PML functions to isolate them and reduce their damaging effects.

2. CHMPs localise to DNA damage and recruit PML to aid in DNA repair and possibly to stabilise sites of damage.

3. CHMPs regulates PML response to viral infection and their accumulation initiates a viral infection response in PML

CHMPs could localise to sites of DNA damage through the CHMP7 subunit. Viral infection causes DNA damage so CHMP accumulation could recruit PML to sites of both viral protein and damage. We propose that nuclear CHMP accumulations are likely to be toxic to cells when they progress un-regulated past a certain size. In the absence of VPS4 a nuclear complex could accumulate unchecked to a state where it not only causes further DNA damage, but hinders the repair of damage it initially localised to. Nuclear CHMP7 is observed in control cells localising in a more dispersed fashion and in significantly reduced numbers. Therefore, VPS4 depletion could be simply exaggerating a normal function of CHMP7 by causing DNA damage. Observing CHMP behavior upon viral infection could help discern the validity of the third hypothesis. However, the first two ideas are likely connected and pinpointing the exact moment that nuclear CHMPs turn from beneficial to harmful would be difficult to determine. Live cell imaging and time lapse studies could be useful tools in monitoring CHMP migration to the nucleus and the time at which PML or other DNA repair proteins are recruited. This would also allow us to follow PML conformational changes.

We next explored the relationship between CHMP7 and proteins vital to PML NB formation. Positive pull down assays revealed direct interactions between CHMP7 with SUMO1 and UBC9. Sumoylation sites were predicted in both CHMP4B, CHMP1B and CHMP5, but no other CHMPs. In contrast, CHMP7 contained no sumoylation sites, but instead a SUMO-interacting motif (SIM). Many proteins that are sumoylated have a SIM to aid in their recognition by SUMO[135]. Therefore, it is possible CHMP7 contains a novel sumoylation site or that its SIM regulates and aids CHMP4B and 1B sumoylation. To expand on this link between ESCRT-III and the SUMO pathway, SUMO2/3 should be explored in future work. This could clarify if CHMP7 can interact with all

SUMO isoforms. SUMO2/3 is implicated in response to cellular stress so an interaction between them and CHMP7 could act as the molecular switch that drives CHMP7 to localise to damaged chromatin.

Other knockdowns or methods of inducing toxicity did not recreate the nuclear phenotype of CHMPs, indicating that it isn't just the DNA damage caused by VPS4 depletion that results in nuclear CHMPs -VPS4 itself is essential for recycling these CHMPs. We were able to partially recreate the nuclear phenotype of CHMP7 by overexpression of wildtype UBC9, and to a lesser extent by overexpression of UBC9 with SUMO1 and also SUMO1 alone. Noticeably, this overexpression had no significant effect on the nuclear localisation of CHMP4B and CHMP1B. This could either indicate that sumoylation is not important in CHMP4B and 1B nuclear localisation or that potentially these CHMPs are sumoylated in order to remove them from the nucleus.

UBC9 has many functions independent of sumoylation and SUMO, such as regulation of transcription and in nuclear transport[162,163]. UBC9 acts as a nuclear chaperone for proteins involved in DNA damage, such as BRCA1[194]. If the NLS predicted for CHMP7 is incorrect, UBC9 represents an alternative method for the nuclear import of CHMP7. The fact that overexpression of UBC9 resulted in nuclear CHMP7 strongly suggests that UBC9 does mediate CHMP7 entry to the nucleus (figure 2). An enzymatically active site in UBC9 must be necessary, as an inactive UBC9 mutant didn't result in significant nuclear localisation of CHMP7. UBC9 RNAi depletion results in predominantly cytoplasmic BRCA1, therefore UBC9 depletion could be an experiment used to determine if CHMP7 nuclear import is also blocked[194]. UBC9 is frequently upregulated in tumours, so future work could explore CHMP7 expression and localisation in a variety of UBC9-upregulated cell lines as well as investigating the effect of UBC9 depletion and also VPS4/UBC9 co-depletion. This could suggest nuclear CHMP7 is a marker for cellular stress and features in tumours. Further to this, future work is now probing the link between DNA damage and nuclear CHMPs by introducing specific DNA damage by different methods, such as ionising radiation and UV, whilst also employing a wider

range of cell lines for analysis. Disruption to chromatin structures by UV, for instance, would be expected to affect nuclear CHMP structures.

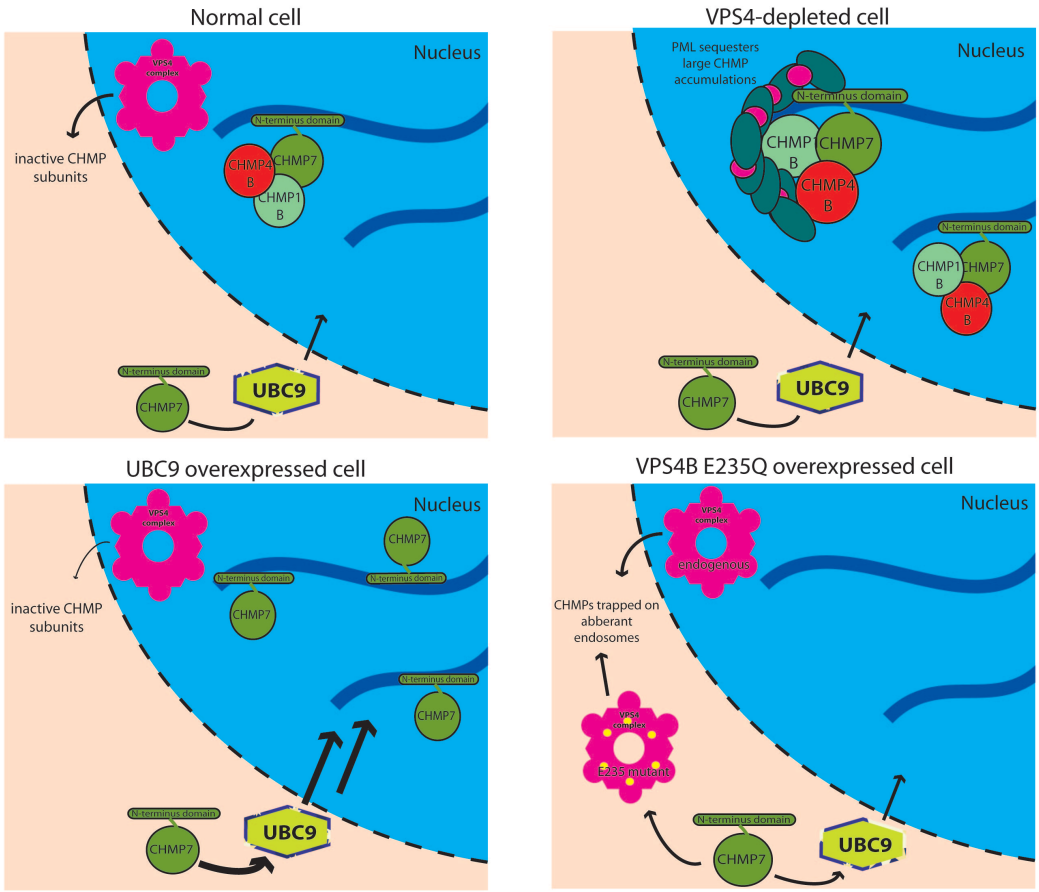

Figure 2 Scheme comparing the different CHMP phenotypes observed upon various treatments; VPS4 depletion, wildtype UBC9 overexpression and VPS4B E235Q overexpression. We propose that UBC9 aids nuclear localisation of CHMP7 -CHMP1 and CHMP4 are likely already nuclear as they weigh 25kDa and in the case of CHMP1 isoforms contains an NLS. The minor role that CHMP7 may play in the MVB sorting pathway is exaggerated by VPS4 E235Q trapping CHMPs onto endosomal membranes.

Just as UBC9 can act independently of its sumoylation function, SUMO and sumoylation is also often independent of PML NB formation. It is possible nuclear CHMPs are associated with other nuclear bodies and this provides a further area for future work by probing VPS4 depleted cells with a wide range of nuclear body antibodies. These experiments could serve to confirm the relationship observed with PML or potentially provide an alternative explanation for a nuclear ESCRT-III complex, for example we have not explored any relationship between CHMPs and polycomb group bodies, which

are already linked by an indirect relationship between CHMP1A and a subunit of these bodies, BMI-1[89]. Polycomb group bodies are associated with chromatin remodelling and gene silencing, therefore a CHMP complex localising to chromatin could function in a similar capacity.

VPS4 depleted cells undergoing cytokinesis (visible midbody) or having already failed cytokinesis (multinuclear) occasionally displayed CHMP filaments connecting the genetic material of each nuclei. This phenotype indicates a role for the ESCRT-III assembly in mitotic events, such as chromosome alignment and segregation or their de-condensation during telophase.

VPS4 depletion blocks cells in cytokinesis, therefore an increase of nuclear defects is observed, largely multinuclear cells and micronuclei. Morita et al suggested CHMPs function during mitosis is in spindle maintenance and our data agreed resulting in similar nuclear defects upon CHMP depletion.

Taking a step further, we propose CHMPs function in chromosome trafficking and segregation between metaphase and anaphase. This mechanism protects against genetic damage during abscission by ensuring the site is free of genetic material (potentially through CHMP4C involvement in abscission inhibition). The DNA damage response is reduced during mitosis, therefore, where damage occurs a higher chance of lagging chromosomes and incorrect abscission can occur. CHMP proteins, particularly CHMP7, could aid damaged chromosomes through mitosis where they can then be repaired once in G1 phase. This hypothesis still allows for the need of PML to sequester an excess of CHMP protein, where their disrupted function becomes a hindrance and filaments, that originally aided chromosome trafficking, persist and connect sister chromatids. In normal cells, these filaments would be resolved by VPS4 action, likely situated at the midbody, which would allow for the appearance of CHMP7 at the midbody only in the final stages before abscission. In contrast, CHMP1B and CHMP4B localise here earlier as they function in abscission -for this reason they were observed at the majority of midbodies, whereas CHMP7 was not.

Partial co-localisation of CHMP4B with BRCA1 and γH2AX was observed, which suggest that this could be a combination of CHMPs localising to damaged chromatin and CHMPs themselves damaging chromatin. The partial co-localisation could be distinguishing between harmful CHMP accumulations and smaller ones that have not yet caused damage. Furthermore, it is possible CHMPs can localise to undamaged chromatin and the complex is able to migrate to damaged regions as they arise.

PML filaments and rings localised to γH2AX and BRCA1 (similar in appearance to its localisation with CHMPs), as observed previously[195,196]. Several DNA damage repair proteins transit through PML NBs and this confirms the role of large PML structures in DNA repair. Whilst resulting in nuclear CHMP7, overexpression of UBC9 did not result in CHMP7 filaments. This is likely because UBC9 overexpression does not affect cytokinesis and so there is no increase in cells blocked or failing cytokinesis, in which all the CHMP7 filaments were observed.

To summarise, this thesis reveals a novel nuclear CHMP assembly, dependent upon CHMP7 and exaggerated by VPS4 depletion. Furthermore we have expanded the protein-protein interaction network of CHMP7 providing some promising avenues for further investigation into CHMP7 functions. In particular, this thesis presents a novel function for a specific CHMP assembly in chromosomal trafficking and segregation; a function which is regulated by VPS4 activity and interceded by PML when left unregulated. Further work is required to define the molecular mechanisms that regulate the multiple actions of ESCRT-III centred around CHMP7, nonetheless the data presented provide a solid framework for investigating additional new functions of the ESCRT machinery.

REFERENCES

1. Hurley, S., Hurley, J. & Emr, S. The ESCRT Complexes: Structure and Mechanism of a Membrane-Trafficking Network. *Annual review of biophysics and biomolecular structure* **35,** 277–298 (2006).
2. Raiborg, C. & Stenmark, H. The ESCRT machinery in endosomal sorting of ubiquitylated membrane proteins. *Nature* **458,** 445–452 (2009).
3. Iwaki, T. *et al.* Essential roles of class E Vps proteins for sorting into multivesicular bodies in Schizosaccharomyces pombe. *Microbiology* **153,** 2753–2764 (2007).
4. Babst, M. A protein's final ESCRT. *Traffic* **6,** 2–9 (2005).
5. Wollert, T., Wunder, C., Lippincott-Schwartz, J. & Hurley, J. Membrane scission by the ESCRT-III complex. *Nature* **458,** 172–177 (2009).
6. Williams, R. & Urbé, S. The emerging shape of the ESCRT machinery. *Nature reviews Molecular cell biology* **8,** 355–368 (2007).
7. Huotari, J. & Helenius, A. Endosome maturation. *The EMBO journal* **30,** 3481–3500 (2011).
8. Lodish, H. *Molecular Cell Biology*. **8,** 731–41 (W.H. Freeman, 2012).
9. Wollert, T. *et al.* The ESCRT machinery at a glance. *Journal of cell science* **122,** 2163–2166 (2009).
10. Raiborg, C., Malerød, L., Pedersen, N. & Stenmark, H. Differential functions of Hrs and ESCRT proteins in endocytic membrane trafficking. *Experimental Cell Research* **314,** 801–813 (2008).
11. Ren, X. & Hurley, J. VHS domains of ESCRT-0 cooperate in high-avidity binding to polyubiquitinated cargo. *The EMBO Journal* **29,** 1045–1054 (2010).
12. Lu, Q., Hope, L. W., Brasch, M., Reinhard, C. & Cohen, S. N. TSG101 interaction with HRS mediates endosomal trafficking and receptor down-regulation. *Proceedings of the National Academy of Sciences* **100,** 7626–7631 (2003).
13. Hicke, L., Schubert, H. L. & Hill, C. P. Ubiquitin-binding domains. *Nature reviews Molecular cell biology* **6,** 610–621 (2005).
14. Bache, K. *et al.* Hrs regulates multivesicular body formation via ESCRT recruitment to endosomes. *The Journal of Cell Biology* **162,** 435–442 (2003).
15. Garrus, J. *et al.* Tsg101 and the Vacuolar Protein Sorting Pathway Are Essential for HIV-1 Budding. *Cell* **107,** 55–65 (2001).
16. Carlton, J., Agromayor, M. & Martin-Serrano, J. Differential requirements for Alix and ESCRT-III in cytokinesis and HIV-1 release.

in *Proceedings of the National Academy of Sciences* **105,** 10541–10546 (2008).
17. Teis, D., Saksena, S., Judson, B. & Emr, S. ESCRT-II coordinates the assembly of ESCRT-III filaments for cargo sorting and multivesicular body vesicle formation. *The EMBO Journal* **29,** 871–883 (2010).
18. Hierro, A. *et al.* Structure of the ESCRT-II endosomal trafficking complex. *Nature* **431,** 221–225 (2004).
19. Kamura, T. *et al.* Cloning and characterization of ELL-associated proteins EAP45 and EAP20 a role for yeast EAP-like proteins in regulation of gene expression by glucose. *Journal of Biological Chemistry* **276,** 16528–16533 (2001).
20. Teo, H., Perisic, O., González, B. & Williams, R. ESCRT-II, an Endosome-Associated Complex Required for Protein SortingCrystal Structure and Interactions with ESCRT-III and Membranes. *Developmental Cell* **7,** 559–569 (2004).
21. Slagsvold, T. Eap45 in Mammalian ESCRT-II Binds Ubiquitin via a Phosphoinositide-interacting GLUE Domain. *Journal of Biological Chemistry* **280,** 19600–19606 (2005).
22. Im, Y., Wollert, T., Boura, E. & Hurley, J. Structure and Function of the ESCRT-II-III Interface in Multivesicular Body Biogenesis. *Developmental Cell* **17,** 234–243 (2009).
23. Agromayor, M. Interaction of AMSH with ESCRT-III and Deubiquitination of Endosomal Cargo. *Journal of Biological Chemistry* **281,** 23083–23091 (2006).
24. Shim, S., Kimpler, L. A. & Hanson, P. I. Structure/Function Analysis of Four Core ESCRT-III Proteins Reveals Common Regulatory Role for Extreme C-Terminal Domain. *Traffic* **8,** 1068–1079 (2007).
25. Hurley, J. H. & Hanson, P. I. Membrane budding and scission by the ESCRT machinery: it's all in the neck. *Nature reviews Molecular cell biology* **11,** 556–566 (2010).
26. Lenz, M., Crow, D. & Joanny, J.-F. Membrane Buckling Induced by Curved Filaments. *Physical Review Letters* **103,** 1–4 (2009).
27. Lata, S. *et al.* Structural Basis for Autoinhibition of ESCRT-III CHMP3. *Journal of Molecular Biology* **378,** 818–827 (2008).
28. Grigoryan, G. & Keating, A. E. Structural specificity in coiled-coil interactions. *Current opinion in structural biology* **18,** 477–483 (2008).
29. Bajorek, M. *et al.* Structural basis for ESCRT-III protein autoinhibition. *Nature structural & molecular biology* **16,** 754–762 (2009).
30. Lata, S., Schoehn, G., Solomons, J. & Pires, R. Structure and function of ESCRT-III. *Biochemical Society* **37,** 156–160 (2009).
31. Zamborlini, A. *et al.* Release of autoinhibition converts ESCRT-III components into potent inhibitors of HIV-1 budding. in *Proceedings of the National Academy of Sciences* **103,** 19140–19145 (2006).
32. Yorikawa, C. *et al.* Human CHMP6, a myristoylated ESCRT-III protein, interacts directly with an ESCRT-II component EAP20 and regulates endosomal cargo sorting. *Biochem. J* **387,** 17–26 (2005).
33. Usami, Y. *et al.* Regulation of CHMP4/ESCRT-III Function in Human Immunodeficiency Virus Type 1 Budding by CC2D1A. *Journal of*

Virology **86,** 3746–3756 (2012).
34. Skalicky, J. J. *et al.* Interactions of the human LIP5 regulatory protein with endosomal sorting complexes required for transport. *Journal of Biological Chemistry* **287,** 43910–43926 (2012).
35. Hurley, J. H. & Yang, D. MIT domainia. *Developmental cell* **14,** 6–8 (2008).
36. Babst, M., Katzmann, D., Estepa-Sabal, E., Meerloo, T. & Emr, S. Escrt-III: An endosome-associated heterooligomeric protein complex required for mvb sorting. *Developmental Cell* **3,** 271–282 (2002).
37. Teis, D., Saksena, S. & Emr, S. Ordered Assembly of the ESCRT-III Complex on Endosomes Is Required to Sequester Cargo during MVB Formation. *Developmental Cell* **15,** 578–589 (2008).
38. Hanson, P. I., Roth, R., Lin, Y. & Heuser, J. E. Plasma membrane deformation by circular arrays of ESCRT-III protein filaments. *The Journal of cell biology* **180,** 389–402 (2008).
39. Hanson, P., Shim, S. & Merrill, S. Cell biology of the ESCRT machinery. *Current Opinion in Cell Biology* **21,** 568–574 (2009).
40. Lata, S. *et al.* Helical Structures of ESCRT-III Are Disassembled by VPS4. *Science* **321,** 1354–1357 (2008).
41. Fabrikant, G. *et al.* Computational Model of Membrane Fission Catalyzed by ESCRT-III. *PLoS Comput Biol* **5,** e1000575 (2009).
42. Li, J., Belogortseva, N., Porter, D. & Park, M. Chmp1A functions as a novel tumor suppressor gene in human embryonic kidney and ductal pancreatic tumor cells. *Cell cycle* **7,** 2886–2893 (2008).
43. Stauffer, D., Howard, T., Nyun, T. & Hollenberg, S. CHMP1 is a novel nuclear matrix protein affecting chromatin structure and cell-cycle progression. *J Cell Sci* **114,** 2383–2393 (2001).
44. Shim, J. CHMP5 is essential for late endosome function and down-regulation of receptor signaling during mouse embryogenesis. *The Journal of Cell Biology* **172,** 1045–1056 (2006).
45. Morita, E. *et al.* Human ESCRT-III and VPS4 proteins are required for centrosome and spindle maintenance. *Proceedings of the National Academy of Sciences* **107,** 12889–12894 (2010).
46. Horii, M. *et al.* CHMP7, a novel ESCRT-III-related protein, associates with CHMP4b and functions in the endosomal sorting pathway. *Biochemical Journal* **400,** 23 (2006).
47. Vale, R. D. Aaa proteins lords of the ring. *The Journal of cell biology* **150,** F13–F20 (2000).
48. Dougan, D., Mogk, A., Zeth, K., Turgay, K. & Bukau, B. AAA+ proteins and substrate recognition, it all depends on their partner in crime. *FEBS Letters* **529,** 6–10 (2002).
49. Latterich, M. & Patel, S. The AAA team: related ATPases with diverse functions. *Trends in Cell Biology* **8,** 65–71 (1998).
50. Iyer, L., Leipe, D., Koonin, E. & Aravind, L. Evolutionary history and higher order classification of AAA+ ATPases. *Journal of Structural Biology* **146,** 11–31 (2004).
51. Bishop, N. & Woodman, P. ATPase-defective Mammalian VPS4 Localizes to Aberrant Endosomes and Impairs Cholesterol Trafficking. *Molecular Biology of the Cell* **11,** 227–239 (2000).

52. Fujita, H. *et al.* A dominant negative form of the AAA ATPase SKD1/VPS4 impairs membrane trafficking out of endosomal/lysosomal compartments: class E vps phenotype in mammalian cells. *J Cell Sci* **116,** 401–414 (2003).
53. Morita, E. *et al.* Human ESCRT and ALIX proteins interact with proteins of the midbody and function in cytokinesis. *The EMBO Journal* **26,** 4215–4227 (2007).
54. Scott, A. *et al.* Structural and mechanistic studies of VPS4 proteins. *The EMBO Journal* **24,** 3658–3669 (2005).
55. Lee, S. *et al.* The Structure of ClpB. *Cell* **115,** 229–240 (2003).
56. Vajjhala, P., Wong, J., To, H.-Y. & Munn, A. The β domain is required for Vps4p oligomerization into a functionally active ATPase. *FEBS Journal* **273,** 2357–2373 (2006).
57. Scott, A. *et al.* Structure and ESCRT-III protein interactions of the MIT domain of human VPS4A. *Proceedings of the National Academy of Sciences* **102,** 13813–13818 (2005).
58. Takasu, H. *et al.* Structural characterization of the MIT domain from human Vps4b. *Biochemical and Biophysical Research Communications* **334,** 460–465 (2005).
59. Stuchell-Brereton, M. *et al.* ESCRT-III recognition by VPS4 ATPases. *Nature* **449,** 740–744 (2007).
60. Obita, T. *et al.* Structural basis for selective recognition of ESCRT-III by the AAA ATPase Vps4. *Nature* **449,** 735–739 (2007).
61. Kieffer, C. *et al.* Two Distinct Modes of ESCRT-III Recognition Are Required for VPS4 Functions in Lysosomal Protein Targeting and HIV-1 Budding. *Developmental Cell* **15,** 62–73 (2008).
62. Yu, Z., Gonciarz, M., Sundquist, W., Hill, C. & Jensen, G. Cryo-EM Structure of Dodecameric Vps4p and Its 2:1 Complex with Vta1p. *Journal of Molecular Biology* **377,** 364–377 (2008).
63. McDonald, B. & Martin-Serrano, J. No strings attached: the ESCRT machinery in viral budding and cytokinesis. *Journal of cell science* **122,** 2167–2177 (2009).
64. Ward, D. The Role of LIP5 and CHMP5 in Multivesicular Body Formation and HIV-1 Budding in Mammalian Cells. *Journal of Biological Chemistry* **280,** 10548–10555 (2005).
65. Shim, S., Merrill, S. & Hanson, P. Novel Interactions of ESCRT-III with LIP5 and VPS4 and their Implications for ESCRT-III Disassembly. *Molecular Biology of the Cell* **19,** 2661–2672 (2008).
66. Azmi, I. F. *et al.* ESCRT-III family members stimulate Vps4 ATPase activity directly or via Vta1. *Developmental cell* **14,** 50–61 (2008).
67. Dimaano, C., Jones, C., Hanono, A., Curtiss, M. & Babst, M. Ist1 Regulates Vps4 Localization and Assembly. *Molecular Biology of the Cell* **19,** 465–474 (2007).
68. Rue, S., Mattei, S., Saksena, S. & Emr, S. Novel Ist1-Did2 Complex Functions at a Late Step in Multivesicular Body Sorting. *Molecular Biology of the Cell* **19,** 475–484 (2007).
69. Agromayor, M. *et al.* Essential Role of hIST1 in Cytokinesis. *Molecular Biology of the Cell* **20,** 1374–1387 (2009).
70. Xiao, J. *et al.* Structural Basis of Ist1 Function and Ist1-Did2

Interaction in the Multivesicular Body Pathway and Cytokinesis. *Molecular Biology of the Cell* **20,** 3514–3524 (2009).

71. Chen, B. & Lamb, R. Mechanisms for enveloped virus budding: Can some viruses do without an ESCRT? *Virology* **372,** 221–232 (2008).
72. Pornillos, O., Garrus, J. & Sundquist, W. Mechanisms of enveloped RNA virus budding. *Trends in Cell Biology* **12,** 569–579 (2002).
73. Morita, E. Differential requirements of mammalian ESCRTs in multivesicular body formation, virus budding and cell division. *FEBS Journal* **279,** 1399–1406 (2012).
74. Levine, B. & Klionsky, D. Development by Self-Digestion: Molecular Mechanisms and Biological Functions of Autophagy. *Developmental Cell* **6,** 463–477 (2004).
75. Lee, J.-A., Beigneux, A., Ahmad, S., Young, S. & Gao, F.-B. ESCRT-III Dysfunction Causes Autophagosome Accumulation and Neurodegeneration. *Current Biology* **17,** 1561–1567 (2007).
76. Rusten, T. *et al.* ESCRTs and Fab1 Regulate Distinct Steps of Autophagy. *Current Biology* **17,** 1817–1825 (2007).
77. Prekeris, R., Gould, G., Prekeris, R. & Gould, G. Breaking up is hard to do - membrane traffic in cytokinesis. *J Cell Sci* **121,** 1569–1576 (2008).
78. Ilievska, J., Bishop, N. E., Annesley, S. J. & Fisher, P. R. The roles of ESCRT proteins in healthy cells and in disease. *Cell Biology* (2011).
79. Carmena, M., Wheelock, M., Funabiki, H. & Earnshaw, W. The chromosomal passenger complex (CPC): from easy rider to the godfather of mitosis. *Nature reviews Molecular cell biology* **13,** 789–803 (2012).
80. Steigemann, P. *et al.* Aurora B-Mediated Abscission Checkpoint Protects against Tetraploidization. *Cell* **136,** 473–484 (2009).
81. Lee, H. H., Elia, N., Ghirlando, R., Lippincott-Schwartz, J. & Hurley, J. H. Midbody targeting of the ESCRT machinery by a noncanonical coiled coil in CEP55. *Science* **322,** 576–580 (2008).
82. Elia, N., Sougrat, R., Spurlin, T. A., Hurley, J. H. & Lippincott-Schwartz, J. Dynamics of endosomal sorting complex required for transport (ESCRT) machinery during cytokinesis and its role in abscission. *Proceedings of the National Academy of Sciences* **108,** 4846–4851 (2011).
83. Yang, D. *et al.* Structural basis for midbody targeting of spastin by the ESCRT-III protein CHMP1B. *Nature structural & molecular biology* **15,** 1278–1286 (2008).
84. Connell, J. W., Lindon, C., Luzio, J. P. & Reid, E. Spastin couples microtubule severing to membrane traffic in completion of cytokinesis and secretion. *Traffic* **10,** 42–56 (2009).
85. Samson, R., Obita, T., Freund, S., Williams, R. & Bell, S. A Role for the ESCRT System in Cell Division in Archaea. *Science* **322,** 1710–1713 (2008).
86. Carlton, J. G. & Martin-Serrano, J. Parallels between cytokinesis and retroviral budding: a role for the ESCRT machinery. *Science* **316,** 1908–1912 (2007).
87. Li, G. *et al.* Chromatin modifying protein 1A (Chmp1A) of the

endosomal sorting complex required for transport (ESCRT)-III family activates ataxia telangiectasia mutated (ATM) for PanC-1 cell growth inhibition. *Cell cycle* **10,** 2529–2539 (2011).
88. You, Z. *et al.* Chmp1A acts as a tumor suppressor gene that inhibits proliferation of renal cell carcinoma. *Cancer Letters* **319,** 190–196 (2012).
89. Pasini, D., Bracken, A. P. & Helin, K. Polycomb group proteins in cell cycle progression and cancer. *Cell Cycle* **3,** 394–398 (2004).
90. Kammerer, R. A. *et al.* Tenascin-C hexabrachion assembly is a sequential two-step process initiated by coiled-coil α-helices. *Journal of Biological Chemistry* **273,** 10602–10608 (1998).
91. Dong, H., Nilsson, L. & Kurland, C. Co-variation of tRNA Abundance and Codon Usage inEscherichia coliat Different Growth Rates. *Journal of Molecular Biology* **260,** 649–663 (1996).
92. Sambrook, J. & Russell, D. *The Condensed Protocols*. (Cold Spring Harbor Laboratory Press, 2005).
93. Studier, F. W. Protein production by auto-induction in high-density shaking cultures. *Protein Expression and Purification* **41,** 207–234 (2005).
94. Laemmli, U. K. Cleavage of structural proteins during the assembly of the head of bacteriophage T4. *Nature* **227,** 680–685 (1970).
95. Ma, H. & Poon, R. *Synchronization of HeLa Cells*. *Cell Cycle Synchronization* 151–161 (Humana Press, 2011). doi:10.1007/978-1-61779-182-6_10
96. McCullough, J., Fisher, R. D., Whitby, F. G., Sundquist, W. I. & Hill, C. P. ALIX-CHMP4 interactions in the human ESCRT pathway. *Proc. Natl. Acad. Sci. U.S.A.* **105,** 7687–7691 (2008).
97. Peck, J. W., Bowden, E. T. & Burbelo, P. D. Structure and function of human Vps20 and Snf7 proteins. *Biochem. J* **377,** 693–700 (2004).
98. Carlton, J., Caballe, A., Agromayor, M., Kloc, M. & Martin-Serrano, J. ESCRT-III Governs the Aurora B-Mediated Abscission Checkpoint Through CHMP4C. *Science* **336,** 220–225 (2012).
99. Cuff, J. A. & Barton, G. J. Evaluation and improvement of multiple sequence methods for protein secondary structure prediction. *Proteins: Structure, Function, and Bioinformatics* **34,** 508–519 (1999).
100. Cole, C., Barber, J. & Barton, G. The Jpred 3 secondary structure prediction server. *Nucleic Acids Research* **36,** 197–201 (2008).
101. Lupas, A. Predicting coiled-coil regions in proteins. *Current Opinion in Structural Biology* **7,** 388–393 (1997).
102. Kelley, L. & Sternberg, M. Protein structure prediction on the Web: a case study using the Phyre server. *Nature Protocols* **4,** 363–371 (2009).
103. Wu, S. & Zhang, Y. LOMETS: A local meta-threading-server for protein structure prediction. *Nucleic Acids Research* **35,** 3375–3382 (2007).
104. Blom, N., Gammeltoft, S. & Brunak, S. Sequence and structure-based prediction of eukaryotic protein phosphorylation sites. *Journal of Molecular Biology* **294,** 1351–1362 (1999).
105. Langelier, C. *et al.* Human ESCRT-II Complex and Its Role in Human

Immunodeficiency Virus Type 1 Release. *Journal of Virology* **80,** 9465–9480 (2006).
106. Gajiwala, K. & Burley, S. Winged helix proteins. *Current Opinion in Structural Biology* **10,** 110–116 (2000).
107. Sievers, F. *et al.* Fast, scalable generation of high-quality protein multiple sequence alignments using Clustal Omega. *Molecular Systems Biology,* **7,** 1–6 (2011).
108. Kalderon, D., Roberts, B., Richardson, W. & Smith, A. A short amino acid sequence able to specify nuclear location. *Cell* **39,** 499–509 (1984).
109. Makkerh, J., Dingwall, C. & Laskey, R. Comparative mutagenesis of nuclear localization signals reveals the importance of neutral and acidic amino acids. *Current Biology* **6,** 1025–1027 (1996).
110. Cour, T. *et al.* Analysis and prediction of leucine-rich nuclear export signals. *Protein Engineering Design and Selection* **17,** 527–536 (2004).
111. Tsang, H. *et al.* A systematic analysis of human CHMP protein interactions: Additional MIT domain-containing proteins bind to multiple components of the human ESCRT III complex. *Genomics* **88,** 333–346 (2006).
112. Guex, N. & Peitsch, M. C. SWISS-MODEL and the Swiss-Pdb Viewer: An environment for comparative protein modeling. *Electrophoresis* **18,** 2714–2723 (1997).
113. Azmi, I. *et al.* Recycling of ESCRTs by the AAA-ATPase Vps4 is regulated by a conserved VSL region in Vta1. *The Journal of Cell Biology* **172,** 705–717 (2006).
114. Row, P. *et al.* The MIT domain of UBPY constitutes a CHMP binding and endosomal localization signal required for efficient epidermal growth factor receptor degradation. *Journal of Biological Chemistry* **284,** 8207–8207 (2009).
115. Shilatifard, A. Identification and Purification of the Holo-ELL Complex. Evidence for the presence of ELL-associated proteins that suppress the transcriptional inhibitory activity of ELL. *Journal of Biological Chemistry* **273,** 11212–11217 (1998).
116. Bajorek, M. *et al.* Biochemical Analyses of Human IST1 and Its Function in Cytokinesis. *Molecular Biology of the Cell* **20,** 1360–1373 (2009).
117. Bishop, N. & Woodman, P. TSG101/mammalian VPS23 and mammalian VPS28 interact directly and are recruited to VPS4-induced endosomes. *Journal of Biological Chemistry* **276,** 11735–11742 (2001).
118. Boettcher, B., Marquez-Lago, T., Bayer, M., Weiss, E. & Barral, Y. Nuclear envelope morphology constrains diffusion and promotes asymmetric protein segregation in closed mitosis. *The Journal of Cell Biology* **197,** 921–937 (2012).
119. Wong, C. & Stearns, T. Mammalian cells lack checkpoints for tetraploidy, aberrant centrosome number, and cytokinesis failure. *BMC Cell Biol.* **6,** 6 (2005).
120. Stukenberg, P. Triggering p53 after cytokinesis failure. *The Journal of*

Cell Biology **165,** 607–608 (2004).
121. Bache, K. G. *et al.* The ESCRT-III subunit hVps24 is required for degradation but not silencing of the epidermal growth factor receptor. *Molecular biology of the cell* **17,** 2513–2523 (2006).
122. Matera, A., Izaguire-Sierra, M., Praveen, K. & Rajendra, T. Nuclear Bodies: Random Aggregates of Sticky Proteins or Crucibles of Macromolecular Assembly? *Developmental Cell* **17,** 639–647 (2009).
123. Takahashi, Y., Lallemand-Breitenbach, V., Zhu, J. & Thé, H. PML nuclear bodies and apoptosis. *Oncogene* **23,** 2819–2824 (2004).
124. Van Damme, E., Laukens, K., Dang, T. H. & Van Ostade, X. A manually curated network of the PML nuclear body interactome reveals an important role for PML-NBs in SUMOylation dynamics. *International journal of biological sciences* **6,** 51 (2010).
125. Bernardi, R. & Pandolfi, P. P. Structure, dynamics and functions of promyelocytic leukaemia nuclear bodies. *Nature reviews Molecular cell biology* **8,** 1006–1016 (2007).
126. Condemine, W. *et al.* Characterization of endogenous human promyelocytic leukemia isoforms. *Cancer research* **66,** 6192–6198 (2006).
127. Lallemand-Breitenbach, V. PML nuclear bodies. *Cold Spring Harbor perspectives in biology* **2,** (2010).
128. Nisole, S., Stoye, J. & Saib, A. TRIM family proteins: retroviral restriction and antiviral defence. *Nature Reviews Microbiology* **3,** 799–808 (2005).
129. Zhong, S. *et al.* Role of SUMO-1–modified PML in nuclear body formation. *Blood* **95,** 2748–2752 (2000).
130. Ishov, A. M. *et al.* PML is critical for ND10 formation and recruits the PML-interacting protein daxx to this nuclear structure when modified by SUMO-1. *The Journal of cell biology* **147,** 221–234 (1999).
131. Seeler, J.-S., Dejean, A. & Seeler, A. Nuclear and unclear functions of SUMO. *Nature Reviews Molecular Cell Biology,* **4,** 690–699 (2003).
132. Hay, R. SUMO: A History of Modification. *Molecular Cell* **18,** 1–12 (2005).
133. Praefcke, G., Hofmann, K. & Dohmen, R. SUMO playing tag with ubiquitin. *Trends in Biochemical Sciences* **37,** 23–31 (2012).
134. Geiss-Friedlander, R. & Melchior, F. Concepts in sumoylation: a decade on. *Nature reviews Molecular cell biology* **8,** 947–956 (2007).
135. Meulmeester, E. & Melchior, F. Cell biology: SUMO. *Nature* **452,** 709–711 (2008).
136. Wijk, S. *et al.* Shared and unique properties of ubiquitin and SUMO interaction networks in DNA repair. *Genes Dev.* **25,** 1763–1769 (2011).
137. Rodriguez, M. SUMO-1 Conjugation in Vivo Requires Both a Consensus Modification Motif and Nuclear Targeting. *Journal of Biological Chemistry* **276,** 12654–12659 (2000).
138. Johnson, E. Protein Modification By Sumo. *Annual Review of Biochemistry* **73,** 355–82 (2004).
139. Hecker, C.-M., Rabiller, M., Haglund, K., Bayer, P. & Dikic, I. Specification of SUMO1-and SUMO2-interacting motifs. *Journal of*

Biological Chemistry **281,** 16117–16127 (2006).
140. Song, J. Identification of a SUMO-binding motif that recognizes SUMO-modified proteins. *Proceedings of the National Academy of Sciences* **101,** 14373–14378 (2004).
141. Stehmeier, P. & Muller, S. Phospho-Regulated SUMO Interaction Modules Connect the SUMO System to CK2 Signaling. *Molecular Cell* **33,** 400–409 (2009).
142. Shen, T., Lin, H.-K., Scaglioni, P., Yung, T. & Pandolfi, P. The Mechanisms of PML-Nuclear Body Formation. *Molecular Cell* **24,** 331–339 (2006).
143. Rajasekhar, V. K. & Begemann, M. Concise review: roles of polycomb group proteins in development and disease: a stem cell perspective. *Stem Cells* **25,** 2498–2510 (2007).
144. Mochida, G. H. *et al.* CHMP1A encodes an essential regulator of BMI1-INK4A in cerebellar development. *Nature genetics* **44,** 1260–1264 (2012).
145. Grande, M. A. *et al.* PML-containing nuclear bodies: Their spatial distribution in relation to other nuclear components. *Journal of cellular biochemistry* **63,** 280–291 (1996).
146. Dephoure, N. *et al.* A quantitative atlas of mitotic phosphorylation. *Proceedings of the National Academy of Sciences* **105,** 10762–10767 (2008).
147. Li, J. *et al.* The Molecule Pages database. *Nature* **420,** 716–717 (2002).
148. Everett, R. *et al.* PML Contributes to a Cellular Mechanism of Repression of Herpes Simplex Virus Type 1 Infection That Is Inactivated by ICP0. *Journal of Virology* **80,** 7995–8005 (2006).
149. Takahashi, J. *et al.* PML nuclear bodies and neuronal intranuclear inclusion in polyglutamine diseases. *Neurobiology of Disease* **13,** 230–237 (2003).
150. Reichelt, M. *et al.* Entrapment of Viral Capsids in Nuclear PML Cages Is an Intrinsic Antiviral Host Defense against Varicella-Zoster Virus. *PLoS Pathog* **7,** e1001266 (2011).
151. Rual, J.-F. *et al.* Towards a proteome-scale map of the human protein–protein interaction network. *Nature* **437,** 1173–1178 (2005).
152. Dou, H., Huang, C., Van Nguyen, T., Lu, L.-S. & Yeh, E. T. SUMOylation and de-SUMOylation in response to DNA damage. *FEBS letters* **585,** 2891–2896 (2011).
153. Saitoh, H. Functional Heterogeneity of Small Ubiquitin-related Protein Modifiers SUMO-1 versus SUMO-2/3. *Journal of Biological Chemistry* **275,** 6252–6258 (2000).
154. Ren, J. & Xue, Y. GPS-SBM Manual. (2009).
155. Kim, E., Kim, K., Matunis, M. & Ahn, J.-H. Enhanced SUMOylation of proteins containing a SUMO-interacting motif by SUMO-Ubc9 fusion. *Biochemical and Biophysical Research Communications* **388,** 41–45 (2009).
156. Anckar, J. & Sistonen, L. SUMO: getting it on. *Biochemical Society Transactions* **35,** 1409–1413 (2007).
157. Bossis, G. & Melchior, F. SUMO: regulating the regulator. *Cell Div* **1,**

13 (2006).
158. Vethantham, V. & Manley, J. In Vitro Sumoylation of Recombinant Proteins and Subsequent Purification for Use in Enzymatic Assays. *Cold Spring Harbor Protocols*, (2009).
159. Waardenburg, R., Duda, D., Lancaster, C., Schulman, B. & Bjornsti, M.-A. Distinct functional domains of the SUMO Ubc9 conjugating enzyme regulate cell resistance to genotoxic stress. *AACR Meeting Abstracts* **2006,** 578 (2006).
160. Kerscher, O. SUMO junction—what's your function? New insights through SUMO-interacting motifs. *EMBO reports* **8,** 550–555 (2007).
161. Kolesar, P., Sarangi, P., Altmannova, V., Zhao, X. & Krejci, L. Dual roles of the SUMO-interacting motif in the regulation of Srs2 sumoylation. *Nucleic Acids Research* **40,** 7831–7843 (2012).
162. Kurtzman, A. L. & Schechter, N. Ubc9 interacts with a nuclear localization signal and mediates nuclear localization of the paired-like homeobox protein Vsx-1 independent of SUMO-1 modification. *Proceedings of the National Academy of Sciences* **98,** 5602–5607 (2001).
163. Kaul, S., Blackford, J. A., Cho, S. & Simons, S. S. Ubc9 is a novel modulator of the induction properties of glucocorticoid receptors. *Journal of Biological Chemistry* **277,** 12541–12549 (2002).
164. McDoniels-Silvers, A. L., Nimri, C. F., Stoner, G. D., Lubet, R. A. & You, M. Differential gene expression in human lung adenocarcinomas and squamous cell carcinomas. *Clinical cancer research* **8,** 1127–1138 (2002).
165. Mo, Y.-Y. & Moschos, S. Targeting Ubc9 for cancer therapy. *Expert Opinion on Therapeutic Targets* **9,** 1203–1216 (2005).
166. Moschos, S. *et al.* SAGE and antibody array analysis of melanoma-infiltrated lymph nodes: identification of Ubc9 as an important molecule in advanced-stage melanomas. *Oncogene* **26,** 4216–4225 (2007).
167. Lu, Z., Wu, H. & Mo, Y.-Y. Regulation of bcl-2 expression by Ubc9. *Experimental Cell Research* **312,** 1865–1875 (2006).
168. Qin, Y. *et al.* BRCA1 proteins regulate growth of ovarian cancer cells by tethering Ubc9. *American Journal of Cancer Research* **2,** 540 (2012).
169. Janer, A. *et al.* PML clastosomes prevent nuclear accumulation of mutant ataxin-7 and other polyglutamine proteins. *The Journal of cell biology* **174,** 65–76 (2006).
170. Xu, Z.-X., Zou, W.-X., Lin, P. & Chang, K.-S. A Role for PML3 in Centrosome Duplication and Genome Stability. *Molecular Cell* **17,** 721–732 (2005).
171. Ihara, M., Stein, P. & Schultz, R. M. UBE2I (UBC9), a SUMO-conjugating enzyme, localizes to nuclear speckles and stimulates transcription in mouse oocytes. *Biol. Reprod.* **79,** 906–913 (2008).
172. Melhuish, T., Kagey, M., Yang, S.-H., Sharrocks, A. & Wotton, D. A Role for Non-Covalent SUMO Interaction Motifs in Pc2/CBX4 E3 Activity. *PLoS ONE* **5,** 8794 (2010).
173. MacQueen, A. Nuclear reorganization and homologous chromosome

pairing during meiotic prophase require C. elegans chk-2. *Genes Dev.* **15,** 1674–1687 (2001).
174. Fenech, M. *et al.* Molecular mechanisms of micronucleus, nucleoplasmic bridge and nuclear bud formation in mammalian and human cells. *Mutagenesis* **26,** 125–132 (2010).
175. Makarova, K., Yutin, N. & Bell, S. Evolution of diverse cell division and vesicle formation systems in Archaea. *Nature Reviews* **8,** 731–41 (2010).
176. Doxsey, S. The centrosome—a tiny organelle with big potential. *Nature Genetics* **20,** 104–06 (1998).
177. Thompson, S. L. & Compton, D. A. Chromosome missegregation in human cells arises through specific types of kinetochore-microtubule attachment errors. *Proc. Natl. Acad. Sci. U.S.A.* **108,** 17974–17978 (2011).
178. Emanuele, M. *et al.* Aurora B kinase and protein phosphatase 1 have opposing roles in modulating kinetochore assembly. *The Journal of Cell Biology* **181,** 241–254 (2008).
179. Gassmann, R. *et al.* Borealin a novel chromosomal passenger required for stability of the bipolar mitotic spindle. *The Journal of cell biology* **166,** 179–191 (2004).
180. Guizetti, J. *et al.* Cortical Constriction During Abscission Involves Helices of ESCRT-III–Dependent Filaments. *Science* **331,** 1616–1620 (2011).
181. Dasso, M. Emerging roles of the SUMO pathway in mitosis. *Cell Div* **3,** (2008).
182. Bacco, A. *et al.* The SUMO-Specific Protease SENP5 Is Required for Cell Division. *Molecular and Cellular Biology* **26,** 4489–4498 (2006).
183. Varis, A., Salmela, A.-L. & Kallio, M. Cenp-F (mitosin) is more than a mitotic marker. *Chromosoma* **115,** 288–295 (2006).
184. Carbone, R., Pearson, M., Minucci, S. & Pelicci, P. G. PML NBs associate with the hMre11 complex and p53 at sites of irradiation induced DNA damage. *Oncogene* **21,** 1633 (2002).
185. Bernardi, R., Papa, A. & Pandolfi, P. P. Regulation of apoptosis by PML and the PML-NBs. *Oncogene* **27,** 6299–6312 (2008).
186. Dellaire, G. & Bazett-Jones, D. P. PML nuclear bodies: dynamic sensors of DNA damage and cellular stress. *BioEssays* **26,** 963–977 (2004).
187. Henderson, B. The BRCA1 Breast Cancer Suppressor: Regulation of Transport, Dynamics, and Function at Multiple Subcellular Locations. *Scientifica* **2012,** 1–15 (2012).
188. Xu, B. *et al.* Replication Stress Induces Micronuclei Comprising of Aggregated DNA Double-Strand Breaks. *PLoS ONE* **6,** e18618 (2011).
189. Giunta, S., Belotserkovskaya, R. & Jackson, S. DNA damage signaling in response to double-strand breaks during mitosis. *The Journal of Cell Biology* **190,** 197–207 (2010).
190. Rieder, C. L. & Cole, R. W. Entry into mitosis in vertebrate somatic cells is guarded by a chromosome damage checkpoint that reverses the cell cycle when triggered during early but not late prophase. *The*

Journal of cell biology **142,** 1013–1022 (1998).
191. Bøe, S. O. *et al.* Promyelocytic leukemia nuclear bodies are predetermined processing sites for damaged DNA. *Journal of cell science* **119,** 3284–3295 (2006).
192. Dellaire, G. *et al.* Mitotic accumulations of PML protein contribute to the re-establishment of PML nuclear bodies in G1. *J Cell Sci* **119,** 1034–1042 (2006).
193. Bruce, E. *et al.* Budding of filamentous and non-filamentous influenza A virus occurs via a VPS4 and VPS28-independent pathway. *Virology* **390,** 268–278 (2009).
194. Qin, Y. *et al.* Ubc9 mediates nuclear localization and growth suppression of BRCA1 and BRCA1a proteins. *Journal of Cellular Physiology* **226,** 3355–3367 (2011).
195. Luciani, J. J. *et al.* PML nuclear bodies are highly organised DNA-protein structures with a function in heterochromatin remodelling at the G2 phase. *Journal of cell science* **119,** 2518–2531 (2006).
196. Xu, Z., Timanova-Atanasova, A., Zhao, R. & Chang, K. PML Colocalizes with and Stabilizes the DNA Damage Response Protein TopBP1. *Molecular and Cellular Biology* **23,** 4247–4256 (2003).

GLOSSARY OF ABBREVIATIONS

AAA:	ATPases associated with diverse cellular activities
ADP:	Adenosine diphosphate
AEC:	Anion exchange chromatography
ALG:	Apoptosis-linked gene
ALIX:	ALG-interacting protein X
AMSH:	Associated molecule with SH3 domain of STAM
ATM:	Ataxia telangiectasia mutated
ATP:	Adenosine triphosphate
BCA:	Bicinchoninic acid
BLAST:	Basic local alignment search tool
BME:	Beta mercaptoethanol
BMI-1:	B lymphoma Mo-MLV insertion region 1
BRCA-1:	Breast cancer type 1
BRO:	BCK1-like resistance to osmotic shock
CBD:	Clathrin binding domain
CD:	Circular dichroism
CHMP:	Charged multivesicular body protein/Chromatin modifying protein
CPC:	Chromosomal passenger complex
DAPI:	4′6-diamidino-2-phenylindole
DAXX:	Death domain associated protein
DDM:	*n*-Dodecyl β-D-maltoside
DMEM:	Dulbecco's modified eagle medium
DMSO:	Dimethyl sulfoxide
DNA:	Deoxyribonucleic acid
DSB:	Double strand break
DTT:	Dithiothreitol
EAP:	ELL-associated protein
EDTA:	Ethylene diamine tetraacetic acid
EGF:	Epidemal growth factor
EGFR:	Epidemal growth factor receptor
EGTA:	Ethylene glycol tetraacetic acid
ESCRT:	Endosomal sorting complex required for transport
FBS:	Fetal bovine serum

FRT:	Flp recombinant target
GFP:	Green fluorescent protein
GLUE:	GRAM-like Ubiquitin-binding in EAP45
GRAM:	Glucosyltransferases, Rab-like GTPase activators and Myotubularins
GST:	Glutathione S-transferase
GTP:	Guanosine triphosphate
HA:	Hemagglutinin
HDPTP:	His-domain protein tyrosine phosphatase
HEK:	Human embryonic kidney
HEPES:	Hydroxyethyl piperazineethanesulfonic acid
HGF:	Hepatocyte growth factor
HIV:	Human immunodeficiency virus
HSE:	Has symptoms of class E mutants
HRS:	HGF-regulated tyrosine-kinase substrate;
IF:	Immunofluorescence
ILV:	Intraluminal vesicle
IPTG:	Isopropyl β-D-1-thiogalactopyranoside
IST1:	Increased Sodium tolerance 1
LB:	Luria-Bertani
LIP5:	LYST-interacting protein 5
LYST:	Lysosomal trafficking regulator
MEAA:	Modified essential amino acids
MESG:	7-Methyl-six-thioguanosine
MIM:	MIT-interacting motif
MIT:	Microtubule interacting and trafficking
MVB:	Multivesicular body
NB:	Nuclear bodies
NES:	Nuclear export signal
NLS:	Nuclear localisation signal
OD:	Optical density
PBS:	Phosphate buffered saline
PC2:	Polycomb 2 homolog
PCR:	Polymerase chain reaction
PFA:	Paraformaldehyde
PIPES:	Piperazine-N,N′-bis(2-ethanesulfonic acid)
PML:	Promyelocytic Leukemia protein
POD:	PML oncogenic domains
PSAP:	proline, serine, alanine and proline
PtdIns(3)P:	Phosphatidylinositol 3-phosphate
PVDF:	Polyvinylidene fluoride
RBCC:	Ring box coiled-coil
RNA:	Ribonucleic acid
RNAi:	Ribonucleic acid interference
SIM:	SUMO interacting motif

SFRS2:	Splicing factor arginine(R)/serine rich 2
SOB:	Super-optimal broth
SDS PAGE:	Sodium dodecyl sulphate polyacrylamide gel electrophoresis
siRNA:	Short interfering ribonucleic acid
SNF7:	Sucrose non-fermenting 7
STAM:	Signal transducing adaptor molecule
SUMO:	Small Ubiquitin-like modifier
TAE:	Tris-acetate-EDTA
TBP:	Tata binding protein
TGS:	Tris glycine SDS
TRIM:	Tripartite motif
TBS:	Tris-buffered saline
TSG101:	Tumour suppressor gene 101
UBC9:	Ubiquitin-conjugating enzyme 9
UBD:	Ubiquitin binding domain
UBPY:	Ubiquitin-specific protease Y
UEV:	Ubiquitin E2 variant
VPS:	Vacuolar protein sorting
VTA-1:	VPS-twenty-associated- 1

APPENDICES

CHAPTER 2

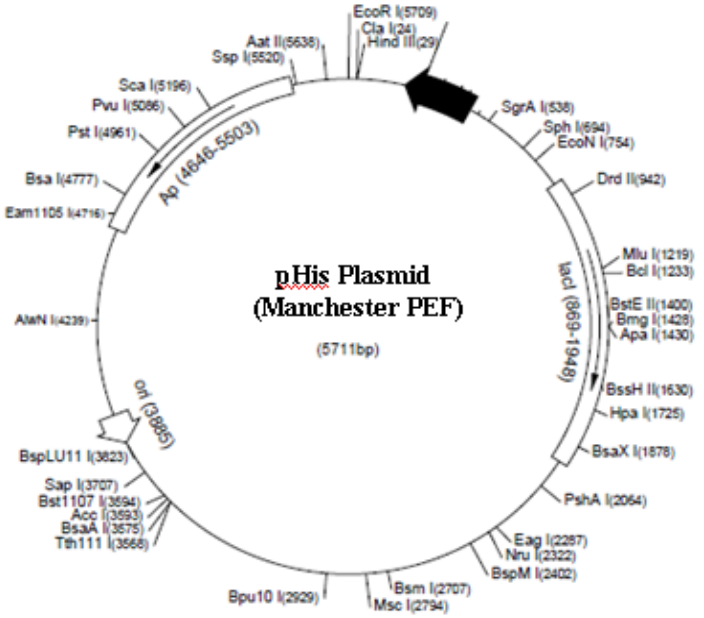

Appendix 1: pHis vector map modified from pET32

His_6-TrxA tag amino-acid sequence

HHHHHHGSGMSDKIIHLTDDSFDTDVLKADGAILVDFWAEWCGPCKMIAPILDEIADEYQGKLTVAKLNID
QNPGTAPKYGIRGIPTLLLFKNGEVAATKVGALSKGQLKEFLDANLAGSGSGLVPRGS-(Insert)

pHisTrx2 DNA sequence

CATCACCATCACCATCACGGTTCTGGT**ATG**AGCGATAAAATTATTCACCTGACTGACGACAGTTTTGACAC
GGATGTACTCAAAGCGGACGGGGCGATCCTCGTCGATTTCTGGGCAGAGTGGTGCGGTCCGTGCAAAATGA
TCGCCCCGATTCTGGATGAAATCGCTGACGAATATCAGGGCAAACTGACCGTTGCAAAACTGAACATCGAT
CAAAACCCTGGCACTGCGCCGAAATATGGCATCCGTGGTATCCCGACTCTGCTGCTGTTCAAAAACGGTGA
AGTGGCGGCAACCAAAGTGGGTGCACTGTCTAAAGGTCAGTTGAAAGAGTTCCTCGACGCTAACCTGGCCG
GTTCTGGTTCTGGCCTGGTTCCGCGTGGATCCGAATCC

Appendix 2: pHis.trx2 vector sequence (from Kammerer et al, see reference 90)

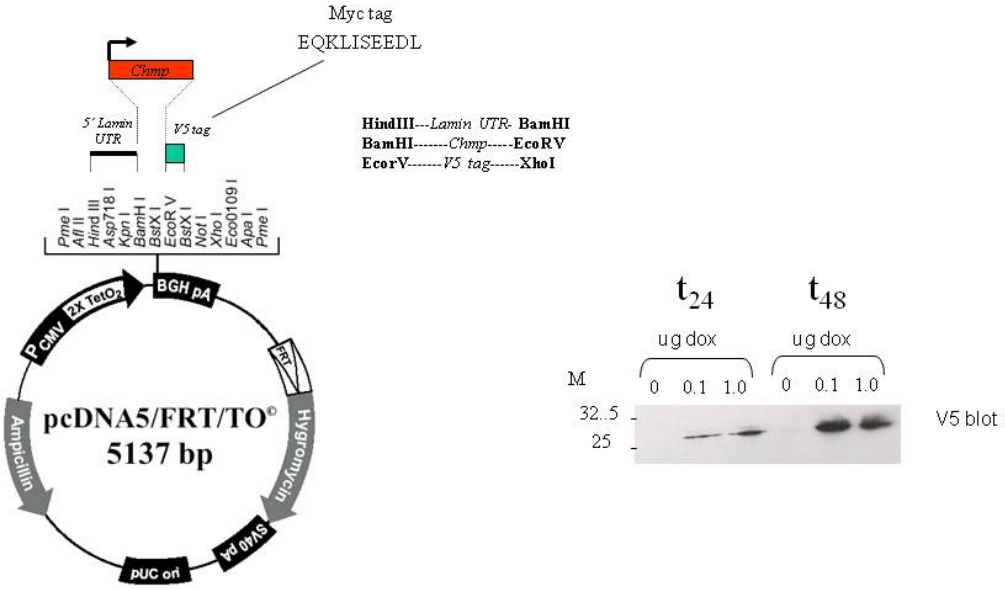

Appendix 3: pcDNA5 FRT vector map, used to generate doxycycin-inducible cell lines of CHMP-MYC tagged constructs and kindly gifted by Prof. P. Woodman. Provided blot shows protein expression after 24 and 48 hours with varying concentrations of doxycyclin (dox) -using a MYC antibody. This thesis used CHMP4B-MYC and CHMP7-MYC inducible cell lines.

RNAi oligos	Sequence
CHMP1A Thermo Scientific *(SMARTpool)*	CCGAGAACGCCAUCCGCAA GGUGUUGAGUUUCUGCAAA GGUUCGAGCAGCAGGUGCA GGUGGUAUUUACAAUGACA
CHMP1B Thermo Scientifc *(SMARTpool)*	CAAAUUCGAGCACCAGUUU GUCGAUGGCUGGUGUGGUU CCUUCGGGAUCAAGUGUGA CAUGGAAGUUGCGAGGAUA
CHMP4A Thermo Scientific *(SMARTpool)*	GGCACAAACUGACCGGGACA UGUUAAAUGUGGGCGACAA GGAAGAAAAGAUUCGAACA CCCUGGAGUUUCAGCGUGA
CHMP4B Thermo Scientific *(SMARTpool)*	CCAUCGAGUUCCAGCGGGA AGAAGAGUUUGACGAGGAU CGGAAGAGAUGUUAAGCAA UGGAAAGGGUCGACUGGUU
CHMP4C Thermo Scientific *(SMARTpool)*	UGUUAUUUGGUAUGCGAUU GCAGCUUGGGCUACCUAAA GGAUAUCGCCCAAGAAAUC AAGCACGGCACGCAGAAUA
CHMP7 Thermo Scientific *(SMARTpool)*	CAGAAGGAGAAGAGGGUCA GGGAGAAGAUUGUGAAGUU GCAGAGAGGUGUAAAGAAG GGGCAUGCCGAGCAGGAAA
TSG101 Thermo Scientific CUSTOM	CGAUGGCAGUUCCAGGGAA
VPS4A Thermo Scientific *(SMARTpool)*	CCACAAACAUCCCAUGGGU CCGAGAAGCUGAAGGAUUA
VPS4B Thermo Scientific *(SMARTpool)*	GGGCAAAGUGUACAGAAUA CGAUAGAUCUGGCUAGCAA

Appendix 4: siRNA oligo sequences for RNA depletion from Dharmacon, Thermo Scientific (5' to 3'). Random sequence non-targeting oligo called 'control' was used as a negative control.

CHMP7 412-438 **MIM1** (29 residues) changes/additions to sequence

```
ccg aac ccg agg atc tca gac gct gaa ctg gaa gct gaa ctg gag aaa ctg
P   N   P   R   I   S   D   A   E   L   E   A   E   L   E   K   L
tcc ttg tca gaa ggt ggt ttg gta ccg ttc taa taa
S   L   S   E   G   G   L   V   P   S   STOP STOP
```

CHMP7 389-416 **MIM2** (30 residues)

```
caa gac acc acc aaa gaa ccg ctg gac ctg ccg gac aac ccg cgc aac cgt cat ttc
Q   D   T   T   K   E   P   L   D   L   P   D   N   P   R   N   R   H   F

acc aac tcc gtt ccg aac ccg cgt atc taa taa
T   N   S   V   P   N   P   R   I   STOP STOP
```

Appendix 5: Sequence of proposed CHMP7 MIM1 and MIM2 motifs. Highlighted yellow shows changes to codons to optimise expression, plus the addition a two stop codons. Highlighted in grey shows the leucine residues (MIM1) known to be critical in binding to the VPS4 MIT domain.

CHMP7 N term

```
          10         20         30         40         50         60
MWSPEREAEA PAGGDPAGLL PPEWEEDEER MSFLFSAFKR SREVNSTDWD SKMGFWAPLV

          70         80         90        100        110        120
LSHSRRQGVV RLRLRDLQEA FQRKGSVPLG LATVLQDLLR RGELQRESDF MASVDSSWIS

         130        140        150        160        170        180
WGVGVFLLKP LKWTLSNMLG DNKVPAEEVL VAVELLKEKA EEVYRLYQNS PLSSHPVVAL

         190        200        210        220        230
SELSTLCANS CPDERTFYLV LLQLQKEKRV TVLEQNGEKI VKFARGPRAK VSP
```

CHMP7 C term

```
         240
VNDVDVG

         250        260        270        280        290        300
VYQLMQSEQL LSRKVESLSQ EAERCKEEAR RACRAGKKQL ALRSLKAKQR TEKRIEALHA

         310        320        330        340        350        360
KLDTVQGILD RIYASQTDQM VFNAYQAGVG ALKLSMKDVT VEKAESLVDQ IQELCDTQDE

         370        380        390        400        410        420
VSQTLAGGVT NGLDFDSEEL EKELDILLQD TTKEPLDLPD NPRNRHFTNS VPNPRISDAE

         430        440        450
LEAELEKLSL SEGGLVPSSK SPKRQLEPTL KPL
```

Appendix 6: Amino acid sequence of CHMP7. Light blue indicates serine residues predicted to be phophorylated. Red shows the residues spanning the CHMP7 fragment designed to encompass the 1st and 2nd alpha helical regions. Purple shows the residues spanning the CHMP7 fragment designed to encompass the 4th and 5th alpha helical regions -including MIM motifs. Highlighted grey indicates the location of the predicted NLS and NES respectively.

CHAPTER 3

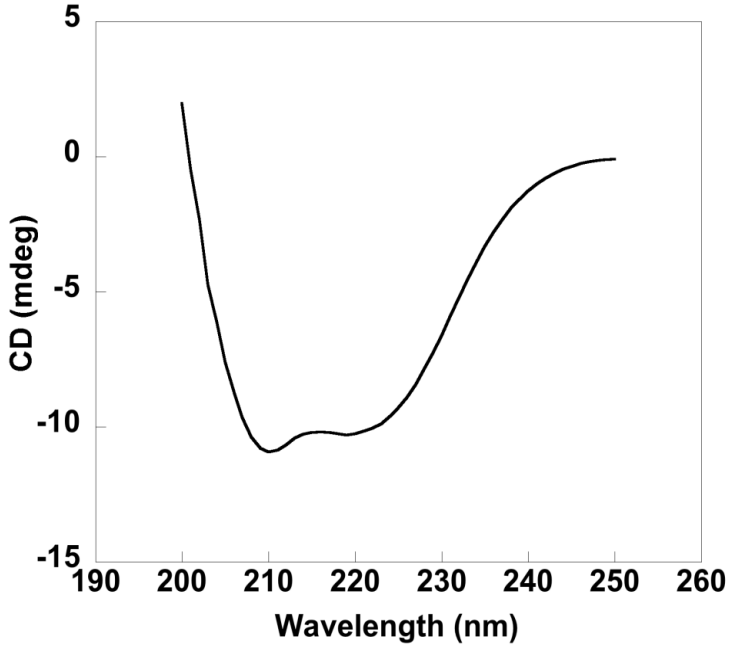

Appendix 7: CD spectrum of VPS4B showing that the purified protein was still correctly folded by the presence of characteristic peaks for alpha helical secondary structure. The correct folding of the protein is critical for further experiments investigating protein-protein interactions. Spectrum recorded at room temperature using protein from -80 °C storage in 5 mM TRIS-HCl, 150 mM NaCl, pH 7.4. His-tagged protein sample was 18.77μM (0.94mg/ml) before snap freezing and approximately 0.2 mg/ml was used for each CD spectrum. Spectrum collected between 260 to 190 nm.

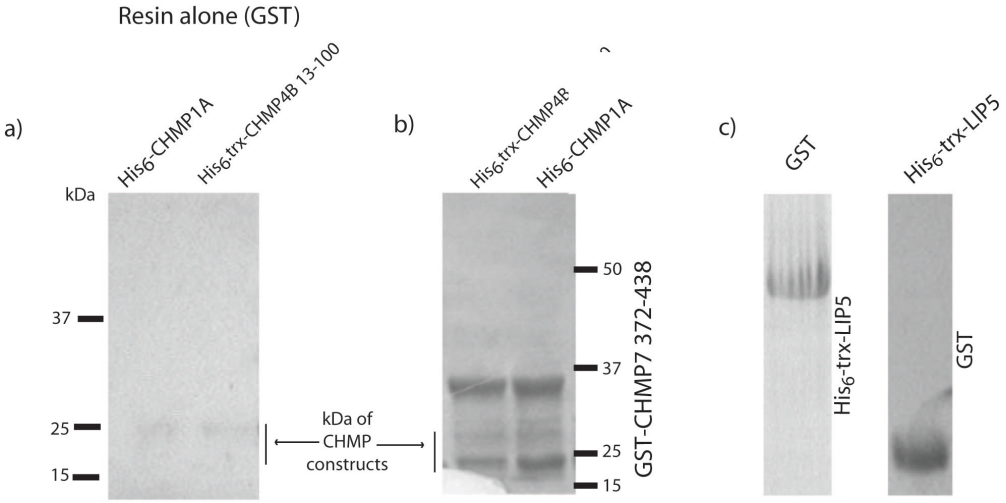

Appendix 8: Control pull downs not shown in body of thesis. a) His-tagged constructs were tested for aspecific binding to the glutathione sepharose beads. b) the pull down assays between GST-CHMP7 372-438 and both CHMP1A and CHMP4B 13-100 were reversed, using GST-CHMP7 372-438 preloaded GST beads incubated with either His-tagged CHMP1A or CHMP4B 13-100. c) GST was incubated with nickel charged chelating sepharose preloaded with his-tagged LIP5 and alternatively, his-tagged LIP5 was incubated with GST beads preloaded with GST –to demonstrate no interaction is observed with the GST tag and LIP5.

CHAPTER FOUR

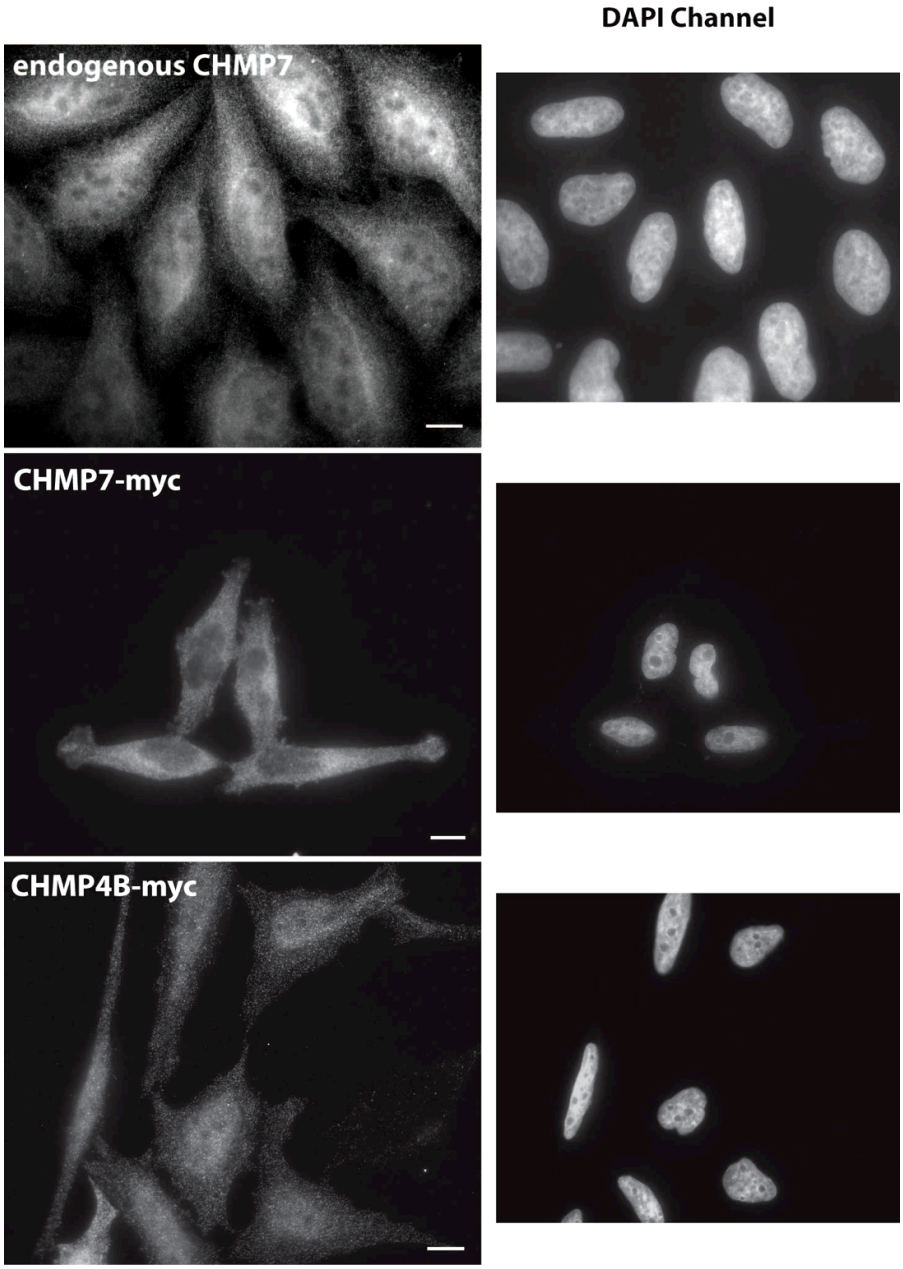

Appendix 9: (top) endogenous CHMP7 (probed using the custom sheep anti-CHMP7 antibody) –show an even distribution of CHMP7 with slight accumulation in the peri-nuclear region. (middle) Using an inducible CHMP7-myc cell line, this image shows cells treated with 100ng/ml of doxycyclin to induce expression of CHMP7-myc. The distribution of CHMP7-myc appears absent from the nucleus, unlike endogenous CHMP7. (bottom) Using an inducible CHMP4B-myc cell line, this image shows cells treated with 20ng/ml of doxycyclin to induce expression of CHMP4B-myc. To the right shows the DAPI channel for these images to indicate the location of the nucleus. Scale bars equal 10 μm.

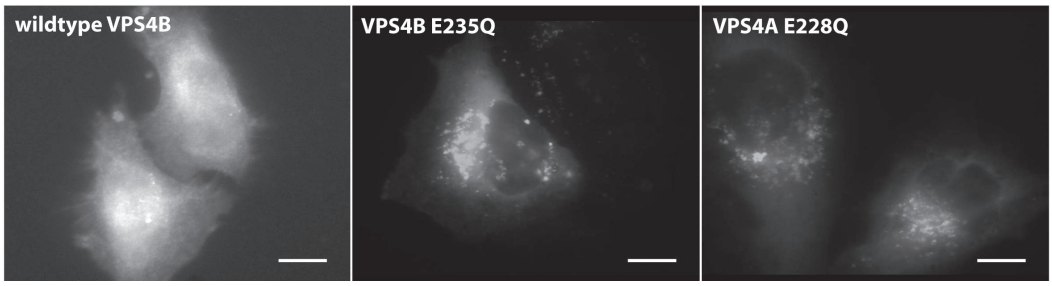

Appendix 10: Overexpression of various GFP-labelled VPS4 constructs (all 0.5 µg); including VPS4B wildtype and both dominant negative mutants VPS4A (E228Q) and VPS4B (E235Q), where ATP hydrolysis is impaired. These mutants are largely absent from the nucleus, either because they are blocked or accumulate rapidly with CHMPs on aberrant endosomes. Wildtype VPS4B resembles endogenous VPS4 displaying an even distribution across the cytoplasm and nucleus. We suggest endogeneous VPS4 is still able to recycle nuclear CHMPs when a dominant negative VPS4 mutant is overexpressed resulting in no nuclear CHMP accumulating. Scale bars equal10 µm.

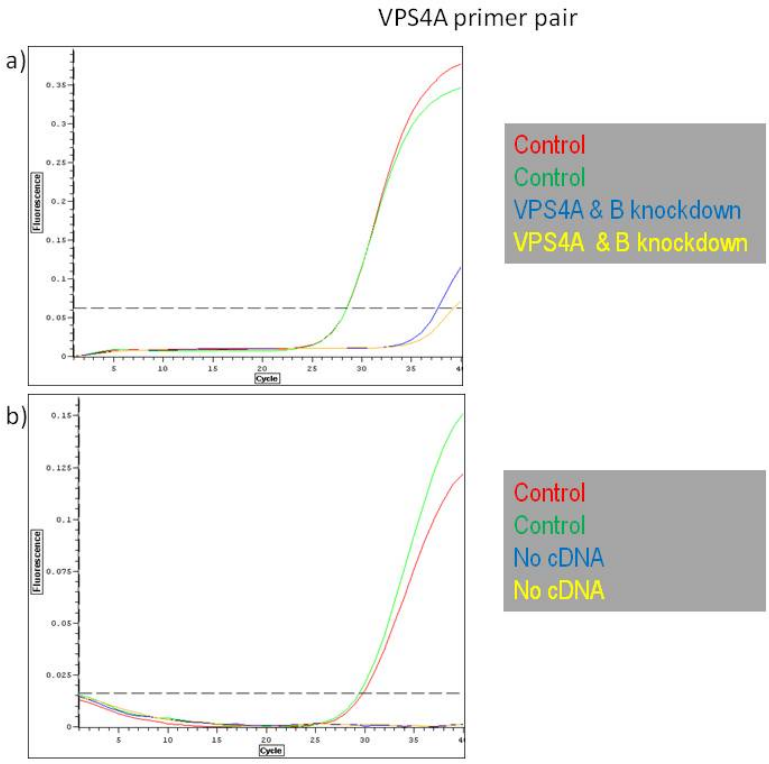

Appendix 11: a) control and VPS4 depleted cells after 72 hours showing the significant decrease in VPS4A gene expression (blue and yellow) when compared to control cells (green and red); as demonstrated by reduced DNA content and an increase in PCR cycles required to achieve DNA amplification. b) One control conducted was between control cell samples and samples with no cDNA, i.e. water instead; showing that no false positives are observed due to problems with the VPS4A primers or the fluorescence.

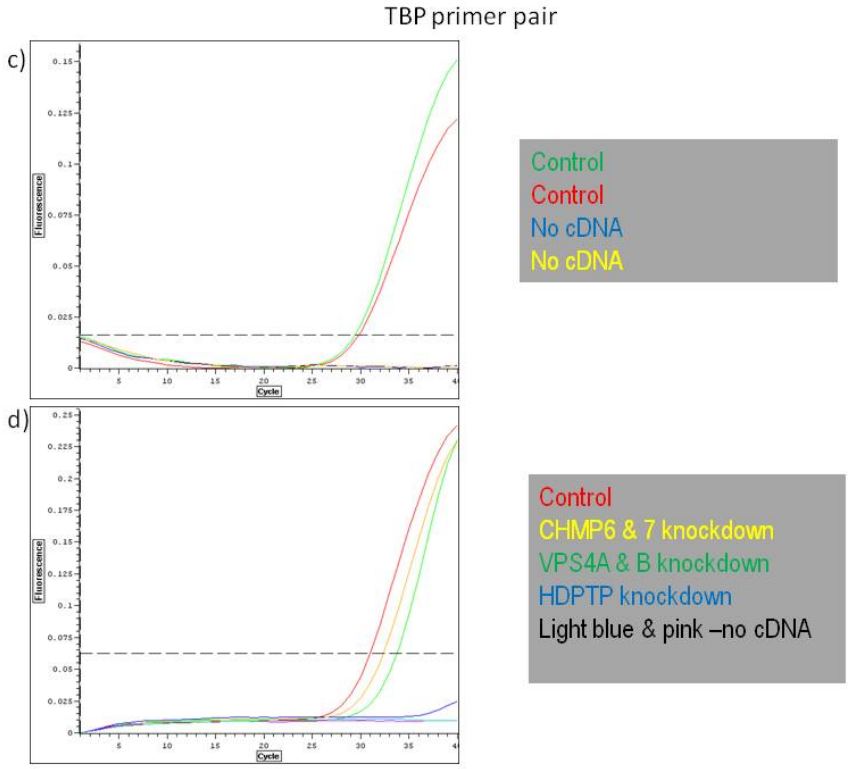

Appendix 12: A further control shows TBP (an unrelated protein) expression is unaffected by RNAi as no significant difference is observed between VPS4 depleted, CHMP7 depleted or control cells. Again a sample absent of cDNA shows no fluorescent signal. Knockdown of HDPTP, an accessory protein in the ESCRT machinery did appear to affect the expression of TBP.